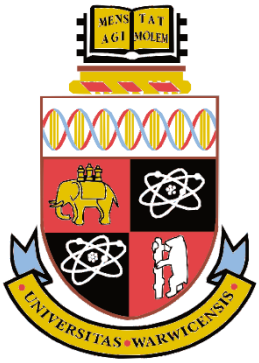

The electrophysiological impact of oligomeric alpha-Synuclein on thick-tufted layer 5 pyramidal neurons in the neocortex of mice

by

Timothy John Kaufmann

Thesis

Submitted to the University of Warwick

for the degree of

Doctor of Philosophy

in

Life Sciences

Supervisors: Dr Mark J. Wall and Dr Teresa J. T. Pinheiro

University of Warwick, School of Life Sciences
September 2015

Contents

List of figures

List of tables

Acknowledgments

First and foremost I would like to thank my supervisors, Dr Mark Wall and Dr Teresa Pinheiro, for their continued support and advice throughout my PhD. This work would not have been possible without their invaluable contributions and collaborative efforts. I wish to thank Dr Narinder Sanghera for my training in protein expression and purification but more importantly for her vital teachings on patience and persistence in those difficult first few months. I give my deepest thanks to Dr Paul Harrison for my training in experimental neuroscience and data analysis. I would also like to thank Dr Magnus Richardson for his insights on neuron modelling and the theoretical neuroscience group for their stimulating discussions. I would also like to extend my gratitude to the Biotechnology and Biological Sciences Research Council for funding this research.

My thanks to Mr Ian Hands-Portman for training and assistance on the confocal and electron microscopes. I also thank Mrs Rosemary Parslow and Dr Sarah Lee at the Biophysical Characterisation Facility, University of Birmingham, for operating the Analytical Ultracentrifuge. I would also like to acknowledge the Genomics Facility and Mass Spectrometry Facility in the School of Life Sciences, University of Warwick, for DNA sequencing and mass spectrometry analysis.

Thanks to all the members of the structural biology and neuroscience labs for their encouragement and friendship; it has been an honour and a joy to have worked alongside them.

I would like to thank all my friends both inside and outside the University of Warwick and from afar I wish to thank Arin, Suzy, John, Barry, Danny, Brian, Ross, Holly and Kevin for making me laugh every single day. Whatever your futures may hold, never stop being who you are.

Finally, and from the bottom of my heart, I give thanks to my parents Polly and Mike and to my sister Annie for their lifelong support and to Rebecca Bailey; whose incredible motivation and character has kept my mind intact these past few years.

Declaration

I, Timothy John Kaufmann, hereby declare that, to the best of my knowledge, the material contained in this thesis is original and my own work unless otherwise indicated, cited, or commonly known. I confirm that this thesis has not been previously submitted for any degree at this or any other institution.

Abstract

Parkinson's disease (PD) is one of the most prevalent movement disorders in the world. A clinical hallmark of PD is the appearance of proteinaceous Lewy Bodies throughout the brain that are predominantly formed from aggregation of the presynaptic protein alpha-Synuclein (αSyn). Increasing evidence, however, suggests that the soluble annular αSyn oligomers, formed during early stages of aggregation, are more toxic and pathologically relevant than the larger fibrils which form at later stages of aggregation. The underlying mechanism(s) through which αSyn oligomers exert their toxicity is still largely unknown.

This thesis investigates how the toxic nature of αSyn oligomers may affect the electrophysiological properties of neurons. A population of soluble oligomers, termed *mOligomers,* were isolated from the early stages of *in vitro* aggregation. In addition, a separate oligomeric species was recovered from the fragmentation of large fibrils; termed *fOligomers*. Structural characterisation of these two species revealed them to be similar in size and ring-like in shape but showed subtle differences in their secondary structure.

Purified, oligomeric αSyn was injected directly into the somata of thick-tufted layer 5 pyramidal neurons in mouse neocortical brain slices during whole-cell patch clamp recording and compared to the effects of equivalent concentrations of αSyn monomer. Using a combined experimental and modelling approach, a wide range of neuronal parameters were extracted and demonstrated oligomer-specific changes in neuronal electrophysiology that were time dependent. Perfusion with αSyn oligomers markedly reduced input resistance, enhanced the current required to trigger an action potential and reduced the firing rate illustrating a reduction in excitability that has the potential to impact both neural circuitry and cognitive output.

Abbreviations

αSyn	Alpha-Synuclein
αSyn$^{Y39W, E46K}$	Alpha-Synuclein with a tryptophan residue at position 39 and a lysine residue at position 46
βSyn	Beta-Synuclein
γSyn	Gamma-Synuclein
Aβ	Amyloid-beta
aCSF	Artificial cerebrospinal fluid
AD	Alzheimer's disease
AFM	Atomic force microscopy
AMPA	Alpha-amino-3-hydroxy-5-methyl-4-isoxazolepropionic acid
ANOVA	Analysis of variance
APase	Alkaline phosphatase
AS	Ammonium sulphate
ATP	Adenosine 5' triphosphate
AUC	Analytical ultracentrifugation
BSA	Bovine serium albumin
CA	*Cornus Ammonis* (hippocampus)
CC	Corticocortical
CD	Circular dichroism
CM	Centromedian
CMA	Cingulate motor area
CNS	Central nervous system
CT	Corticothalamic
CV	Column volume
DA	Dopamine
DAPI	4',6-diamidino-2-phenylindole
DC	Direct current
DLB	Dementia with Lewy bodies
EGCG	Epigallocatechin gallate
EGTA	Ethylene glycol tetraacetic acid
EIF	Exponential integrate-and-fire
ER	Endoplasmic reticulum

ESI-MS	Electrospray ionisation mass spectrometry
FT	Flow through
GABA	Gamma-aminobutyric acid
GF	Gel filtration
GPe	Globus palidus external
GPi	Globus palidus internal
GTP	Gianosine 5’ triphosphate
HEPES	4-(2-hydroxyethyl)-1-piperazineethanesulfonic acid
HH	Hodgkin-Huxley
IEx	Ion exchange
IF	Integrate-and-fire
IgG	Immunoglobulin G
$\mathbf{I_H}$	Hyperpolarisation activated current
IPD	Idiopathic Parkinson’s disease
IPTG	Isopropyl beta-D-1-thiogalactopyranoside
IR-DIC	Infra-red differential interference contrast
ISI	Inter-spike interval
$\mathbf{I_{spike}}$	Spike-initiation current
ITN	Intratelencaphalic neurons
I-V	Current-voltage
L-dopa	Levodopa
LB	Lysogeny broth
LIF	Leaky integrate-and-fire
LRRK2	Leucine-rich-repeat-kinase 2
LTP	Long-term potentiation
M1	Primary motor cortex
MAM	Mitochondrial associated endoplasmic reticulum membrane
MPTP	1-methyl-4-phenyl-1,2,3,4-tetrahydropyridine
MSA	Multiple system atrophy
MSN	Medium spiny neurons
NAC	Non amyloid-beta component
NACP	Non amyloid-beta component precursor
NHS	N-hydroxysuccinimide

NIF	Non-linear integrate-and-fire
NMDA	N-methyl-D-aspartate
NMR	Nuclear magnetic resonance
PARK	Parkinson's disease gene locus
PBS	Phosphate buffer saline
PC	Principle cell
PD	Parkinson's disease
PFA	Paraformaldehyde
PINK1	PTEN-induced kinase 1
PMA (PMC)	Pre-motor area (Pre-motor cortex)
PMSF	Phenylmethanesulfonylfluoride
PPN	Pedunculopontine nucleus
PTEN	Phosphatase and tensin homolog
rEIF	Refractory exponential integrate-and-fire
REM	Rapid eye movement
R_{in}	Input resistance
SDS-PAGE	Sodium dodecyl sulphate – polyacrylamide gel electrophoresis
SMA	Supplementray motor area
SNARE	Soluble NSF attachment protein receptor
SNc	Substantia nigra pars compacta
SNr	Substantia nigra pars reticulate
SPN	Subcerebral projection neurons
STN	Subthalamic nucleus
TB	Terrific broth
TBS	Tris buffer saline
TBST	Tris buffer saline + Tween20
TEM	Transmission electron microscopy
TH	Tyrosine hydroxylase
ThT	Thioflavin-T
TSE	Transmissible spongiform encephalopathy
TTL5	Thick-tufted layer 5
UPR	Unfolded protein response
VA/VL	Ventral anterior/ventrolateral nuclei

1 Introduction

Parkinson's disease is one of the most prevalent movement disorders in the world and is clinically characterised by the appearance of Lewy Bodies made predominantly from the protein alpha-Synuclein. However, increasing evidence produced within the last few decades strongly suggests that soluble, oligomeric species are more neurotoxic than the large fibrillar aggregates that form later. The exact mechanism through which oligomers exert their toxicity is still unknown. The aims of this thesis are twofold: to provide in-depth structural characterisation of alpha-Synuclein oligomers and to investigate their impact on the electrophysiological properties of neurons. Such goals will help to develop our understanding of the cellular mechanisms through which oligomers exert their toxicity.

This introduction reviews the aspects of structural biology and neurobiology relevant to this body of work. Firstly, I provide an overview on the origin, clinical staging and pathology of Parkinson's disease and related neurodegenerative disorders. In addition to motor dysfunction, I draw attention to the wide range of non-motor symptoms that are prevalent throughout the disease and describe the microcircuitry of pyramidal neurons in the neocortex; a region severely affected in late stages of the disease. The second half of this introduction is dedicated to the structure and function of both native and pathological alpha-Synuclein. Discussed here are the speculated physiological roles ascribed to this protein, the evidence for its association with Parkinson's disease, the variety of oligomeric intermediates formed during aggregation, and the leading theories on the mechanism of toxicity. Lastly, this introduction shall conclude with a brief outline of the research carried out in this thesis.

1.1 History of Parkinson's disease

Parkinson's disease (PD) was first characterised in 1817 by James Parkinson, who analysed the collective symptoms of six case studies (two of whom he met in the street and one he observed from a distance) in which the patients suffered from a vague motor disorder. He describes:

'Involuntary tremulous motion, with lessened muscular power, in parts not in action and even when supported; with a propensity to bend the trunk forward, and to pass from a walking to a running pace: the senses and intellects being uninjured.'

This constituded the first clinical description of a motor disorder refered to then as *paralysis agitans* or 'shaking palsy' *(Parkinson, 1817)* but was later renamed in 1877 by Jean-Martin Charcot *(Charcot, 1877; Lees, 2007)* in honour of the original discoverer. Charcot helped to refine and expand upon the description of PD; particularly in defining bradykinesia as a fundimental symptom *(Charcot, 1877)*. Around the same time, Armand Trousseau described muscle rigidity and a displaced centre of gravity in patients with PD *(Trousseau, 1867; Pearce, 1989)*. Although these pioneers are accredited as the first to medically examine the disease, several early sources, including 1200 B.C. Egyptain papyrus, Hindu texts and Bible passages give accounts of people suffering from PD-like symptoms *(Ruiz, 2004)*.

The end of the 19th century marked the first anatomical insight into PD and other movement disorders. The general role of the basal ganglia in the brain at effecting motility had already been proposed in relation to Wilson's disease *(Gowers, 1888)*. However, it was Edouard Brissaud that proposed a connection between motor dysfunction and the specific *substantia nigra* region within the basal ganglia *(Brissaud, 1899)*. This was proven in 1919 by Tretiakoff who noted a reduction in the number of pigmented cells in the *substantia nigra* in PD patients *(Trétiakoff, 1919)*. A few years earlier, a key pathological finding was made by Frederic Lewy who discovered large concentric inclusion bodies, that he named Lewy bodies, in the brains of Alzheimer's patients *(Lewy, 1912)*. The detection of Lewy bodies throughout the brain is still regarded as a clinical hallmark of PD *(Braak et al., 2003b)*. These aggregates were also found by Tretiakoff in the cytoplasm of neurons in the *substantia nigra pars compacta (Trétiakoff, 1919)*. However, the loss of neurons in this region of the brain was not generally accepted as a critical pathological lesion in PD until the much later neuropathological studies carried out by *Hassler (1938)* and then *Greenfield and Bosanquet (1953)* which led to an almost universal acceptance *(Lees, 2007)*.

During the 1950s, Arvid Carlsson showed that dopamine functioned as a neurotransmitter in the brain and was not simply the precursor to noradrenalin, as was the dominant opinion at the time *(Bertler and Rosengren, 1959; Carlsson, 1959)*. In 1957, he revealed that depleting the otherwise abundant supply of dopamine in the basal ganglia, using the drug reserpine, resulted in a loss of movement control reflecting the symptoms of PD *(Carlsson et al., 1957)*. It was soon after establised that

the motor dysfunction observed in PD did indeed stem from a loss of dopaminergic innervation within the basal ganglia *(Ehringer and Hornykiewicz, 1960; Hornykiewicz, 1963)*. Importantly, the administration of levodopa (L-dopa) reversed the immobilising effects of reserpine in animals *(Carlsson et al., 1958)* and was even able to successfully, albeit temporarily, aleviate the symptoms of PD patients *(Cotzias et al., 1967; Cotzias et al., 1969; Yahr et al., 1969)*. For this work, Carlsson was awarded the 2000 Nobel prize in medicine and has since been considered one of the poineers of L-dopa treatment *(Lees et al., 2015)*.

1.2 Pathology of Parkinson's disease

1.2.1 Clinical stages

The pathological development of PD is a slow process that can take several years before accumulative damage in the brain produces symptoms. In the course of the disorder, specific regions of the brain become increasingly affected in a predictable, ascending pathology. As such, neuron degeneration commonly occurs in areas of the brainstem prior to the onset of classical PD motor dysfunction; this is known as the presymptomatic phase. The spread of pathology to the *substantia nigra pars compacta* (SNc) region of the basal ganglia marks the beginning of the symptomatic phase of PD as loss of these predisposed neurons is exclusively responsible for loss of motor control. The later stages of PD are fraught with secondary, non-motor symptoms as pathology reaches the higher centres of the brain includng the hippocampus and neocortex. This pathological topology is closely complemented by the prevalence of Lewy bodies in the same neuronal regions during presymptomatic and symptomatic phases of PD (figure 1.1) *(Braak et al., 2002)*. This finding, by Braak and colleagues, now defines the six clinical stages of PD progression *(Braak et al., 2002; Braak et al., 2003b)*.

1.2.2 Stages 1 and 2: the presymptomatic phase

The earliest appearances of inclusion bodies in the brainstem denote the first stages of PD and precede the onset of motor symptoms. In stage 1, Lewy bodies appear in the dorsal motor nucleus of the vagus nerve and surrounding areas of the medulla and pons (figure 1.1a) *(Del Tredici et al., 2002)*. Curiously, Lewy bodies also appear at this stage in the olfactory bulb and related portions of the anterior olfactory nucleus *(Barz et al., 1997; Braak et al., 2002)*. However, since the pathology does not advance

out from the olfactory bulb into the neocortex or subcortical structures, it is the dorsal nucleus that is considered the main starting point for disease ascention *(Del Tredici et al., 2002; Braak et al., 2003b).*

In stage 2, Lewy bodies are still confined to the medulla and pons however the lesions within the dorsal vagal region become increasingly severe, and portions of the caudal raphe nuclei and locus coeruleus become involved (figure 1.1a) *(Braak et al., 2002).* Diagnosis of PD during these two early stages, which collectively comprise the presymptomatic phase, is difficult and non – definitive. Olfactory loss occurs in up to 90 % of patients with PD and has thus become a reliable indicator in the presymptomatic phase *(Sommer et al., 2004; Haehner et al., 2007; Ross et al., 2008a; Silveira-Moriyama et al., 2009).* A variety of other non-motor symptoms are often seen in patients with early untreated PD including rapid eye movement (REM) sleep behavioural disorder, constipation, autonomic dysfunction, and mood/behavioural disorders *(Wu et al., 2011).* Such non-motor symptoms are less universal during the early stages but become increasingly dominant in cases of advanced PD *(Chaudhuri et al., 2006).*

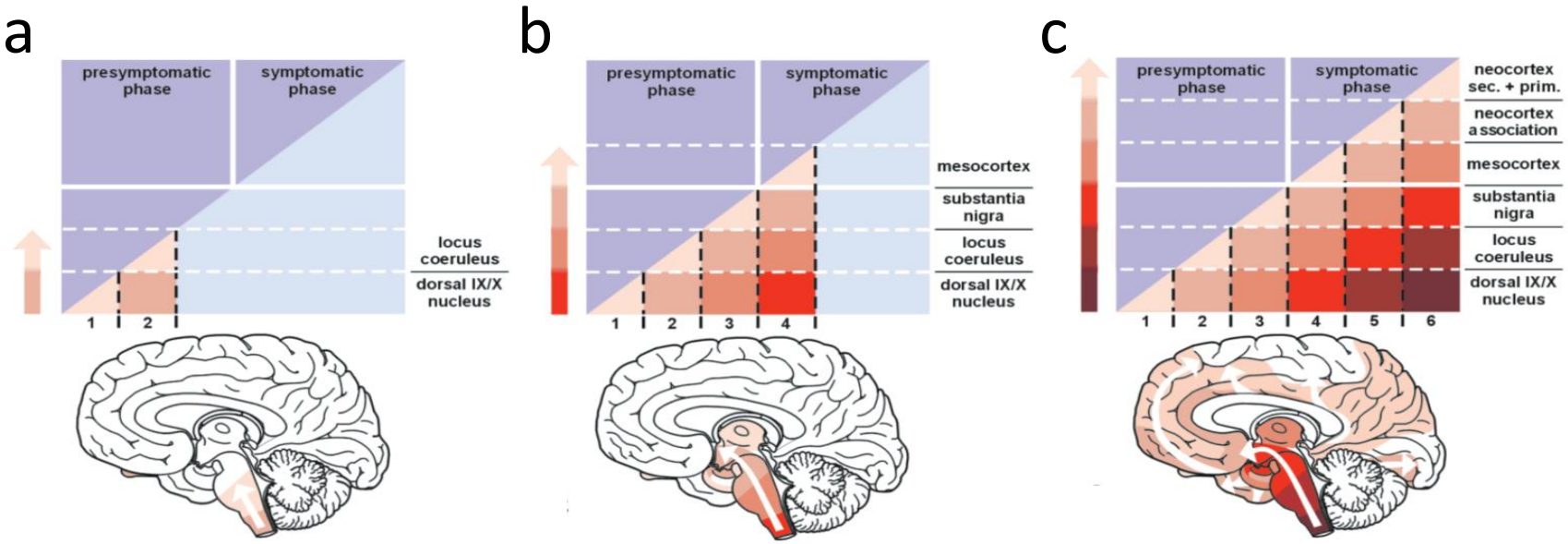

Figure 1.1 Schematic diagram illustrating the ascending pathology underlying PD. (a) Presymptomatic stages 1 and 2; inclusion bodies are confined to the medulla oblongata, pons and olfactory bulb. (b) In stages 3 and 4 motor dysfunction appears as the substantia nigra and other midbrain areas become affected. (c) The later stages 5 and 6; Lewy bodies spread throughout the cerebral cortex and non-motor symptoms appear *(Braak et al., 2002)*.

1.2.3 Stages 3 and 4: the symptomatic phase

Stages 3 and 4 are the most well established in PD pathology as Lewy bodies spread to the basal ganglia and are detected specifically in the dopaminergic neurons of the SNc (figure 1.1b). It is during these stages that we enter the symptomatic phase and the main clinical characteristics of PD including muscle rigidity, bradykinesia, and tremours at rest begin to appear *(Eriksen et al., 2009)*. Although destruction in the subsequent stages is assured, the SNc in stage 3 appears macroscopically intact with no detectable reduction in neuromelanin within the dopamine-containing neurons *(Braak et al., 2003b)*. Lewy bodies, however, typically develop close to the neuromelanin accumulations in the SNc neurons. Importantly, non-dopaminergic neurons from the nigral subnuclei (particularly the *substantia nigra pars reticulata*) refrain from developing Lewy bodies or lesions *(Braak et al., 2003b)*. Other areas in stage 3 that begin to accumulate Lewy bodies include the magnocellular nuclei of the basal forebrain, which is involved in sleep/wake regulation and projects throughout the neocortex *(Divac, 1975; Szymusiak, 1995)*, and the CA2/3 region of the hippocampus *(Dickson et al., 1991)*.

In stage 4, the SNc becomes strikingly impaired; showing a significant decrease in the number of dopamine-containing neurons *(Braak et al., 2003b)*. Disease severity is also elevated in the basal forebrain which spreads Lewy bodies up through the mesocortex (figure 1.1b). Stage 4 Lewy bodies and lesions in the mesocortex become less dense following the cortex either medially to the entorhinal region or laterally to the high order sensory areas of the neocortex *(Braak et al., 2003b)*.

1.2.4 The underlying mechanism of motor dysfunction: basal ganglia circuitry

The basal ganglia represents a collection of subcortical nuclei that are involved in the regulation of movement. Within the basal ganglia lies the neostriatum (caudate nucleus and putamen), the external and internal segments of the globus palidus (GPe and GPi), the subthalamic nucleus (STN), and the substantia nigra pars reticulata (SNr) and pars compacta (SNc) (figure 2.1a). Other projections in basal ganglia reach the centromedian (CM) thalamic nucleus and lower brainstem regions including the pedunculopontine nucleus (PPN) involved in the reticular activating system. When preparing to carry out a desired movement, the striatum and STN receive glutamatergic transmission from specific motor areas of the neocortex (M1, PMA and

SMA) and also from the thalamus. Information is transferred from the striatum to the basal ganglia output nuclei, GPi and SNr, through two separate pathways; a 'direct' (monosynaptic) connection, and an 'indirect' projection via the GPe and STN. The inhibitory γ-aminobutyric acid (GABA) output from GPi/SNr is received by the ventral anterior and ventrolateral nuclei of the thalamus (VA/VL), which, in turn, project back to the cerebral cortex.

As such a 'striatal' loop exists; travelling from the neocortex to the basal ganglia and back again, that ensures fine tuning of neurons to carry out the intended movement (figure 1.2b). Thus, the key motor function of the basal ganglia is the selection and implimentation of willed movements.

Importantly, the striatum receives vital dopaminergic input from the SNc; forming the nigrostriatal pathway. The SNc neurons form synapses with striatal medium spiny output neurons (MSNs) which are also the recipients of corticostriatal projections carrying the raw motor planning signal *(Nicola et al., 2000; Wang et al., 2006; Surmeier et al., 2007).* This anatomical arrangement places the dopaminergic inputs in a position to regulate corticostriatal transmission (figure 1.2b). MSNs in the 'direct' and 'indirect' pathways carry different dopamine receptors that produce opposing effects on the basal ganglia output nuclei *(Gerfen et al., 1990).* Activation of the 'direct' pathway by dopamine D1-receptors inhibits the GPi/SNr, thereby disinhibiting thalamocortical interactions, while reduction of the 'indirect' pathway by D2-receptors creates the opposite effect (figure 1.2) *(DeLong and Wichmann, 2007; Galvan and Wichmann, 2008; Keeler et al., 2014).*

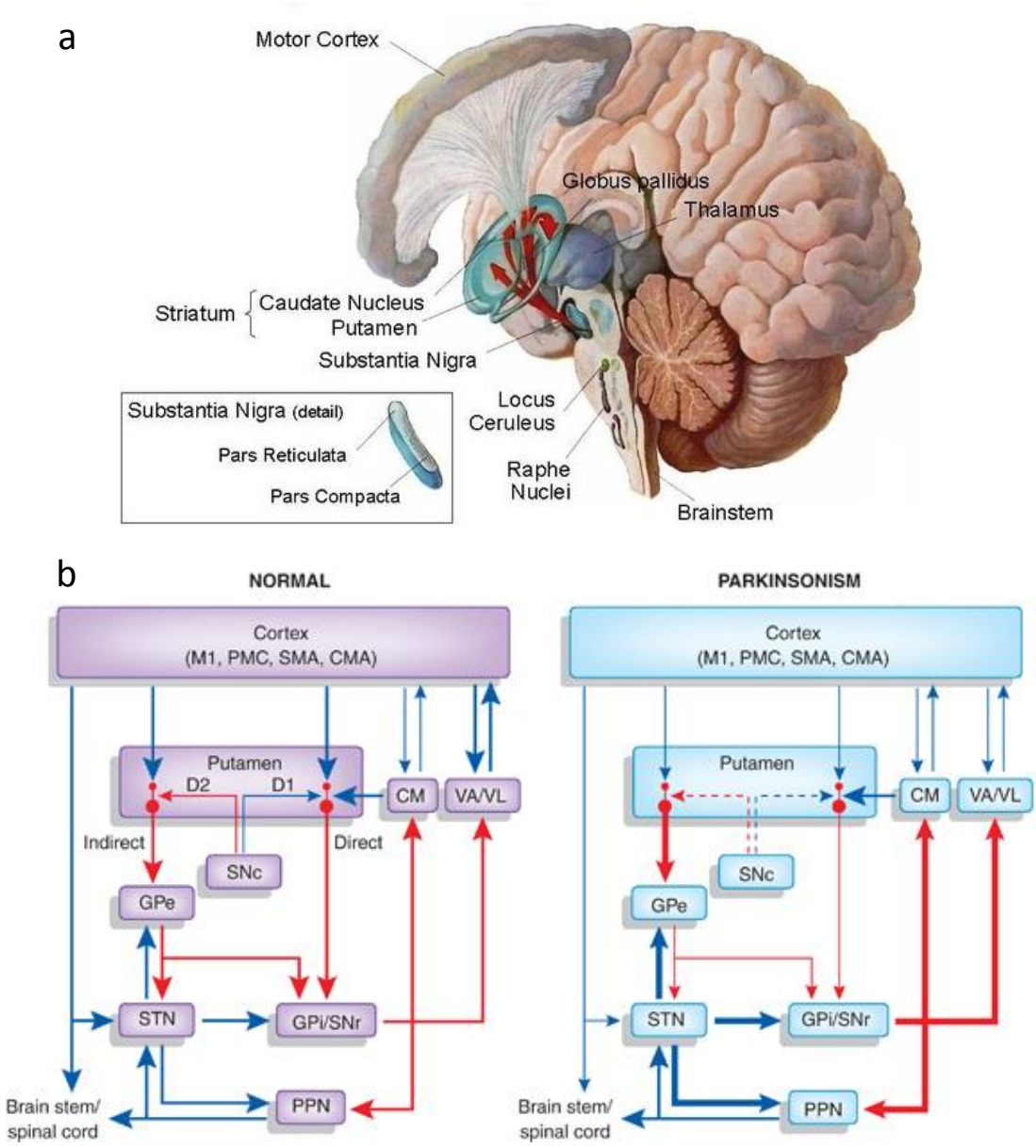

Figure 1.2 Schematic diagram of the direct and indirect pathways of the basal ganglia motor circuits in normal and PD states. (a) Anatomic layout of the areas affected in Parkinson's disease. In addition to the areas that comprise the basal ganglia, the brain stem, thalamus and cortex are shown. (b) Red arrows indicate inhibitory projections and blue arrows indicate excitatory projections. Changes in arrow thickness between normal and PD states denotes an increase (larger arrow) or decrease (thinner arrow) in the firing activity of specific projections. The dashed arrow in the PD state illustrates the lesioning of dopaminergic neurons that make up the nigrostriatal pathway. CM, centromedian nucleus; CMA, cingulate motor area; GPe, globus pallidus, external segment; GPi, globus pallidus, internal segment; M1, primary motor cortex; PMC, pre-motor cortex; PPN, pedunculopontine nucleus; SMA, supplementary motor area; SNc, substantia nigra pars compacta; SNr, substantia nigra pars reticulata; STN, subthalamic nucleus; VA/VL, ventral anterior/ventral lateral nucleus *(Smith et al., 2012)*.

Overall, the net action of the SNc is to reduce GPi/SNr activity which in turn upregulates glutamatergic output from the thalamus back to the neocortex. In Parkinson's disease, the eventual loss of SNc neurons and their dopaminergic innervation of the striatum results in unregulated GPi/SNr inhibition of the thalamus, a subsequent loss of excitation to the neocortex (figure 1.2b) and impaired motor control.

1.2.5 Stages 5 and 6: non-motor symptoms

The later stages of PD mark the most severe and wide spread pathology in the brain. In addition to the areas affected in the earlier stages, the hippocampus and neocortex become increasingly damaged (figure 1.1c). In stage 5, Lewy bodies extend from the mesocortex into adjoining prefrontal and sensory areas of the neocotrex. Of the layers of pyramidal neurons that make up the neocortex structure, layers 5 and 6 in particular develop Lewy bodies and a thick band of neuritic filaments appear in layers 2/3 *(Braak et al., 2000; Braak et al., 2002)*. Within the hippocampus, Lewy bodies are detected in all CA sections with increasing prevalence. Stage 6 signifies the most advanced topography for the distribution of Lewy bodies and neuron degeneration, with the entirity of the neocortex becoming affected (figure 1.1c).

Secondary, non-motor symptoms of PD correlate with advancing age and disease progression into stages 5 and 6 *(Braak et al., 2005)*. As described above some non-motor symptoms can appear in the early stages of PD *(Wu et al., 2011)*, however in the later stages these become more prevalent. A wide variety of non-motor symptoms have been described in patients with PD including; dementia, cognitive impairments such as apathy, depression, anxiety and hallucinations, as well as sleep disorders, sexual dysfunction, gastrointestinal problems and many more that are listed in table 1.1 *(Chaudhuri et al., 2006)*. In a 15 year follow up study of non-levodopa responsive patients, non-motor symptoms were noted as the most debilitating feature of the disease *(Hely et al., 2005)*. Other surveys have similarly found that sleep distubances, episodic confusion/memory loss, and dribbling of saliva were rated by PD patients to be the most disabling features *(Gulati et al., 2004)*. Many non-motor symptoms, including dementia and hallucinations, are now recognised as leading causes of patient morbidity and institutionalisation *(Goetz and Stebbins, 1993; Guttman et al., 2003)*,

and can effectively quadruple the cost of care *(Findley et al., 2003; Chaudhuri et al., 2005)*.

The non – motor symptom complex of Parkinson's disease					
Neuropsychiatric symptoms	**Seelp disorders**	**Autonomic symptoms**	**Gastrointestinal symptoms**	**Sensory symptoms**	**Other symptoms**
Depression, apathy, anxiety Anhedonia Attention deficit Hallucinations, illusion, delusions Dementia Obsessional behaviour*, repetitive behaviour Confusion Delirium* Panic attacks	Restless legs and periodic limb movements Rapid eye movement (REM) sleep behaviour disorder Non – REM – sleep related disorders Excessive daytime somnolence Insomnia Sleep disordered breathing	Bladder disturbances (urgency, nocturia, frequency) Sweating Orthostatic hypotension (falls, coat – hanger pain) Sexual dysfunction (hypersexuality*, erectile impotence) Dry eyes (xerostomia)	Dribbling of saliva Ageusia Dysphagia and choking Reflux, nausea and vomiting Constipation Faecal incontinence	Pain Paraesthesia Oflactory distrubance	Fatigue Diplopia Seborrhoea Weight loss Weight gain*

Table 1.1 The range of non-motor symptoms reported in patients with Parkinson's disease. * indicates symptoms that may be drug induced *(Chaudhuri et al., 2006)*.

1.3 The microcircuitry of the neocortex

While denervation of the dopaminergic nigrostriatal pathway is the cause of traditional motor symptoms, many of these non-motor symptoms are the result of dysruption to cholinergic systems in higher functioning centres of the brain *(Bohnen and Albin, 2011)*. Loss of cholinergic input to the cerebral cortex from the basal forebrain, along with the presence of cortical Lewy bodies, is recognised as a key pathological cause of dementia in both Alzheimer's and Parkinson's disease *(Müller and Bohnen, 2013)*.

The neocortex is the most evolutionarily recent part of the brain and is vital for higher cognitive functions including perception, motor command, semantic memory, language, social interactions and emotional processing. Developmental abnormalities within the neocortex form the basis for several neurophysiological disorders; such as schizophrenia, autism and epilepsy, while pathological damage results in cognitive

dysfunction witnessed in many neurodegenerative diseases including Alzheimer's disease (AD), PD, dementia with Lewy bodies (DLB) and multiple system atrophy (MSA) *(Sugiyama et al., 1994; Bierer et al., 1995; Armstrong et al., 2005).*

The neocortex is generally divided into six layers (figure 1.3) although the distinction between individual layers is dependent on the cortical region of interest. Despite their functional diversity, different regions of the neocortex all share a distinctly standardised neuronal morphology, columnar organisation and interlayer connectivity *(Kozloski et al., 2001; Silberberg et al., 2002).* The preservation of certain patterns of connectivity between layers throughout the neocortex has led to the development of a canonical microcircuit (figure 1.3) that is now a well established concept for experimental and theoretical neuroscientists alike *(Thomson and Lamy, 2007).*

The topmost layer of the neocortex, layer 1, is primarily composed of dendritic tufts from pyramidal neurons in the lower layers that are synapsed by a sparse population of GABAergic neuronal somata *(Cauller and Connors, 1994).* Layer 1 is believed to provide top-down 'contextual' information from cortical areas to bottom-up sensory signals arriving via the thalamus and other subcortical regions *(Cauller, 1995; Petreanu et al., 2012).*

With the exception of the primary visual cortex, layers 2 and 3 are generally considered to be a single layer *(Gur and Snodderly, 2008).* Layer 2/3 receives strong feed-forward excitation from layer 4 that converges with input from other layers to provide an integrated signal that is relayed to layer 5; the crucial output layer that projects to the thalamus and other subcortical regions *(Feldmeyer et al., 2002; Kampa et al., 2006).*

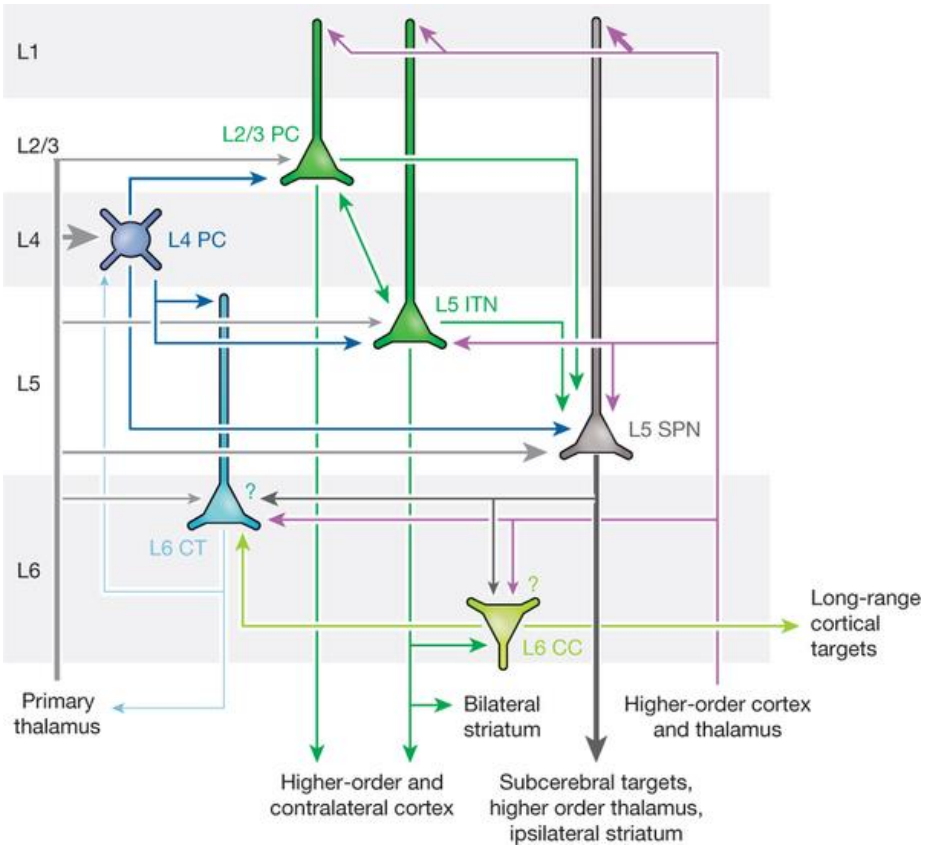

Figure 1.3 Simplified diagram of the canonical microcircuit of the neocortex. The locations and connectivity of excitatory cells are illustrated *(Harris and Mrsic-Flogel, 2013)*.

Although all layers of the neocortical sensory areas receive thalamic inputs, the strongest is in layer 4. One of the principle cells (PCs) in layer 4, in addition to pyramidal neurons, are spiny stellate neurons. Spiny stellate neurons are the main excitatory neurons that target the pyramidal neurons in layer 2/3 *(Feldmeyer et al., 2002)*. Layer 4 is absent from the motor cortex, however the organisation of this area remains poorly understood *(Shepherd, 2009; Hooks et al., 2011)*.

Layer 5 pyramidal neurons are subdivided into two classes of excitatory cells. Slender-tufted pyramidal cells, also referred to as intratelencephalic neurons (ITNs), are situated higher in the layer, have a regular spiking pattern and project to intra-cortical targets. Thick-tufted pyramidal cells, also referred to as subcerebral projection neurons (SPNs), are located deeper in the layer (layer 5b) and represent the major output to subcortical targets, often firing bursts of action potentials.

The deepest layer of the neocortex, layer 6, is possibly the least well understood although it has been shown to offer gain control to layers 5a and 4 *(Kim et al., 2014)*. Layer 6 contains a more heterogenous neuronal population relative to the others *(Chen*

et al., 2009; Thomson, 2010). Corticocortical (CC) cells have a uniquely inverted soma morphology and form long-range horizontal connections with other cortical areas *(Thomson, 2010)*. Corticothalamic (CT) cells send signals along slow conducting fibers *(Swadlow, 1989)* to reticular and primary sensory thalamic nuclei *(Sherman, 2012)*. CT cells also inhibit the principle cells of layer 4 by strongly innervating fast-spiking interneurons *(Watakabe et al., 2012)*.

Since the canonical microcircuit utilises all layers in some manner, especially layers 2/3, 4 and 5, it is possible that neuron degeneration in any of the layers will have pathological consequences. However, as they present the main subcortical output projections of the neocortex, my investigations in this thesis will focus on the thick-tufted pyramidal neurons of layer 5b.

1.4 Electrophysiological modelling of neurons

The electrophysiological properties of a neuron can be captured and recreated through mathematical modelling; an important tool for investigating neuron signalling at the single cell and network levels. In mathematical models, neurons are represented as electrical circuits that vary in complexity from single variable differential equations that can predict the firing times of action potentials, to multi-variable equations that attempt to illustrate the complete spatial arrangement of the neuron membrane.

Complex models are often difficult to accurately fit to experimental data but have been used to examine spike-threshold variability *(Shu et al., 2007)*, the effects of temperature on action potential efficiency *(Yu et al., 2012)* and the influence of dendritic morphology on cell output *(Hay et al., 2011; Hay et al., 2013)*. Simple models, on the other hand, have less biophysical representation in the cell circuit but can reliably fit experimental recordings and are more easily included in network models. The simplest neuron model describes an RC circuit (figure 1.4a) in which the capacitor represents the charge storing ability of the phospholipid bilayer, resistors represent ion channels and batteries represent the ionic reversal potentials. The collective action of all ion channels can be represented by a single resistor or multiple resistors can be added in parallel to show different ion channels, each with their own reversal potential (figure 1.4b). The potential difference across the membrane, *V(t)*, is governed by

$$C\frac{dV}{dt} + I_{ion} = I_{in} \quad (1.1)$$

where C is the membrane capacitance and I_{in} is the input current, either from synapses or injected experimentally. I_{ion} is the ionic current and gives the current passing through the resistor in the RC circuit, which is equivalent to the sum of currents from all ion channels in the model.

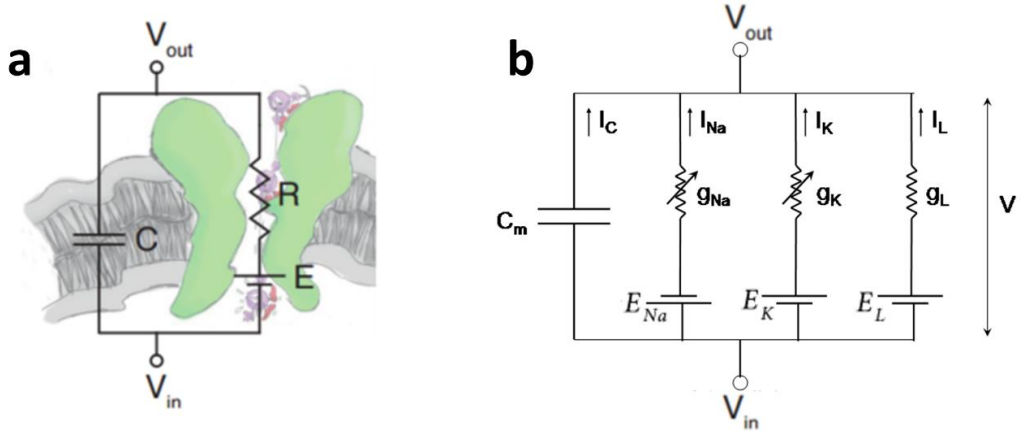

Figure 1.4 The simple neuron model as an RC circuit. (a) The neuron membrane acts as a capacitor *(C)* while embedded ion channels act as a resistor *(R)* with a battery *(E)* to signify their reversal potentials. The summed effects of the ion channels can be represented as a single resistor or can be separated into multiple resistors connected in parallel. The latter signifies the Hodgkin-Huxley model and is illustrated in (b).

In continuous models, designed to capture both subthreshold and action potential behaviour *(Hines and Carnevale, 1997)*, the ionic current is described as a time-dependent conductance in the general form

$$I_{ion}\big(t, V(t)\big) = \sum_i g_i(t)(V(t) - E_i) \quad (1.2)$$

where E_i is the ionic reversal potential of ion i and $g_i(t)$ is the channel conductance, which is dependent on the dynamics of gating variables. The Hodgkin-Huxley (HH) model of the squid giant axon, for example, was the first continuous model to describe the three principle ion-channels underlying subthreshold and action potential dynamics *(Hodgkin and Huxley, 1952a, b, c; Hodgkin et al., 1952)*. Hodgkin and Huxley found that the generation of action potentials was the coordinated result of leak conductances, due to passive ion channels, sodium conductance and potassium conductance (figure 1.4b). The ionic current from equation (1.1) is then given as

$$I_{ion} = g_L(V - E_L) + \bar{g}_{Na}m^3h(V - E_{Na}) + \bar{g}_K n^4(V - E_K) \quad (1.3)$$

where the gating variables *m*, *h* and *n* are responsible for the activation and deactivation of sodium channels and the activation of potassium channels, respectively; g_L is the leak conductance, $\bar{g}_{Na}$ and $\bar{g}_K$ the maximal sodium and potassium conductance; and E_L, E_{Na}, and E_K are their respective reversal potentials. The HH model is regarded as one of the most important models in modern neuroscience and has been developed in many ways to vary the amount of physiological detail *(Wang and Buzsaki, 1996; Pospischil et al., 2008).*

Integrate-and-fire (IF) neuron models are simplified forms of the continuous model that focus on accurate prediction of spike times rather than detailing the properties of the action potential. The leaky integrate-and-fire (LIF) model, which has been used extensively to study the activity of single cells *(Burkitt, 2006a, b),* describes the neuron as a capacitor, equation (1.1), with the leak conductance from equation (1.3) to illustrate the passive membrane response:

$$C\frac{dV}{dt} = g_L(E_L - V) + I_{in} \tag{1.4}$$

The IF models focus on the subthreshold activity of a neuron and register a spike when the membrane potential reaches a pre-defined threshold value, after which the value is reset *(Fourcaud-Trocme et al., 2003).* This can be extended to better describe spike dynamics by introducing a non-linear forcing function, *F(V),* to produce non-linear IF (NIF) models in the form:

$$\frac{dV}{dt} = F(V) + \frac{I_{in}(t)}{C} \tag{1.5}$$

The exponential IF (EIF), is a NIF model in which the non-linear forcing function includes an exponential component for describing the fast activation of voltage-gated sodium channels needed for the sharp rise in membrane potential at spike onset *(Fourcaud-Trocme et al., 2003).* The forcing function is given as

$$F(V) = \frac{1}{\tau_m}\left(E_m - V + \Delta_T exp\left(\frac{V - V_T}{\Delta_T}\right)\right) \tag{1.6}$$

with the four parameters being: the membrane time constant (τ_m), the resting potential (E_m), the spike-onset sharpness (Δ_T) and the spike-initiation threshold (V_T). The EIF model has been experimentally verified in a variety of cell types including thick-tufted layer 5 pyramidal neurons *(Badel et al., 2008).* Furthermore, previous work by *Badel*

et al. (2008) introduced post-spike dynamics in which the parameters of equation (1.6) become shifted and then relax back over time to pre-spike conditions with either a single (τ_m and V_T) or double (E_m) exponential fit; yielding the refractory EIF (rEIF) model. The EIF and rEIF models provide an efficient method for accurately extracting several neuronal parameters from experimental data. As such, they will be used in this thesis for the novel purpose of investigating cortical electrophysiology under pathological conditions relating to PD.

1.5 Risk factors in Parkinson's disease

1.5.1 Parkinson's disease epidemiology

The biggest risk factor for many neurodegenerative disorders is age *(Hindle, 2010; Niccoli and Partridge, 2012)*. PD is well recognised as an age-related disease *(Morgan and Finch, 1988; Eriksen et al., 2009)* with a high prevalence in the elderly; the average age of onset being ~60 years *(Samii et al., 2004)*. However, juvenile-onset (initial symptoms presenting before 21 yrs) and young-onset PD (between 21-39 yrs) do occur *(Muthane et al., 1994)*. Young-onset PD comprises 5-10 % of all patients *(Golbe, 1991)*.

PD is currently the second most common neurodegenerative disorder in humans, after AD, and is the most common movement disorder; with a prevalence of ~1 % in adults over the age of 60 years, rising to as high as ~4 % in those over 80 years *(de Lau and Breteler, 2006)*. The incidence of PD is consistently greater in men than in women *(Mayeux et al., 1992; Lyons et al., 1998; Van Den Eeden et al., 2003; Haaxma et al., 2007; Shulman, 2007)* which has been attributed to oestrogen activity in women promoting higher levels of physiological striatal dopamine *(Haaxma et al., 2007)*. People of all ethnicities can be affected by idiopathic PD *(Van Den Eeden et al., 2003)*.

A variety of occupational and environmental risk factors have been associated with the development of PD. The chronic exposure to pesticides and herbicides used in agriculture has been shown to correlate with higher risk of PD development in farmers *(Lai et al., 2002)*. The precise mechanism of toxicity varies depending on product although many are believed to induce mitochondrial dysfunciton. The insecticide rotenone, for example, is a non-competitive inhibitor of complex 1 *(Li et al., 2003)*

that induces progressive, PD-like motor dysfunction in animal models *(Sherer et al., 2003)*.

Increased risk of PD is connected to long-term exposure to metals such as manganese, copper, mercury, lead, iron, zinc and aluminium *(Lai et al., 2002)*. This was originally observed when a high prevalence of PD mortality was found among workers in heavy metal industries *(Rybicki et al., 1993)*. Iron and copper have been shown to bind to several PD-associated proteins such as alpha-Synuclein *(Bush, 2000; Binolfi et al., 2006; Brown, 2010b)* and DJ-1 *(Bjorkblom et al., 2013)*. In addition, the SNc extracellularly accumulates high levels of heavy metal ions during PD *(Dexter et al., 1991)*. A loss of heavy metal ion homeostasis, typically seen in patients with PD *(Dexter et al., 1989; Gorell et al., 1999)*, is therefore a likely contributor to the specific denervation of the nigrostriatal pathway *(Brown, 2010b)*.

Curiously, from an epidemiological perspective, there is strong, consistent evidence that cigarette smoking is connected to a lower risk of PD *(Checkoway et al., 2002; Hernan et al., 2002)*. In support of this, nicotine has been shown to have potential neuroprotective properties for PD *(Quik et al., 2012)*. There is also evidence for caffeine consumption lowering the risk of PD *(Checkoway et al., 2002; Ross et al., 2008a)*, as well as the intake of alcohol *(Hernan et al., 2003)*, vitamin C *(Zhang et al., 2002)*, vitamin E *(Morens et al., 1996)* and unsaturated fatty acids *(de Lau et al., 2005)*. However, the inconsistency of these findings makes their association less certain *(de Lau and Breteler, 2006)*.

1.5.2 Molecular mechanisms of idiopathic Parkinson's disease

Several molecular mechanisms have been proposed to play a role in PD pathology: protein aggregation, oxidative stress, mitochondrial dysfunction, protein degredation pathway dysruption, membrane permeabilisation and synaptotoxicity to name a few. Many of these mechanisms are directly connected to one another or develop in tandem and are also found in other neurodegenerative disorders. However, the precise underlying mechanism of toxicity is still unknown.

Protein aggregation and inclusion body formation is a shared pathological trait for many neurodegenerative diseases (figure 1.5a) *(Ross and Poirier, 2004)*. The subsequent identification of the molecular content of these inclusions was a vital step in differentiating these diseases from one another (figure 1.5b). Despite their

differences in protein composition, the amyloid fibrils that make up inclusion bodies are generally filamentous with a cross-β structure; in which the β-sheets align almost perpendicular to the long axis of the fibril (figure 1.5c). The conversion of disease proteins from their native, often unfolded, structure into an aggregating subunit is an important and complex mechanism underpinning the development of pathology. Following investigations into the aggregation process, there is increasing evidence that several intermediate species, oligomeric and protofibrilar, exist prior to the completed

a

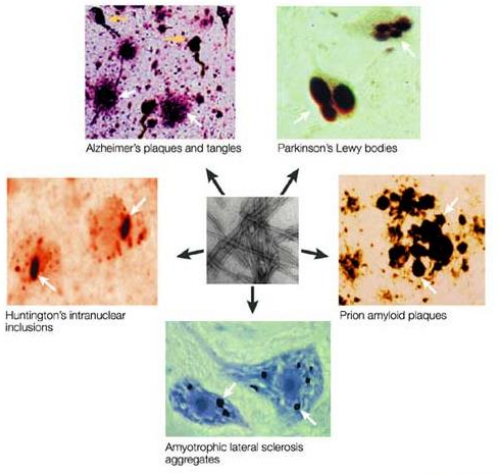

b

Disease	Protein involved
Alzheimer's	Amyloid – β and Tau
Huntington's	Huntingtin
Parkinson's	α – Synuclein
Multiple system atrophy	α – Synuclein
Prion diseases (TSE, Kuru, etc)	Prion protein
Amyotrophyic lateral sclerosis	Superoxide dismutase

c

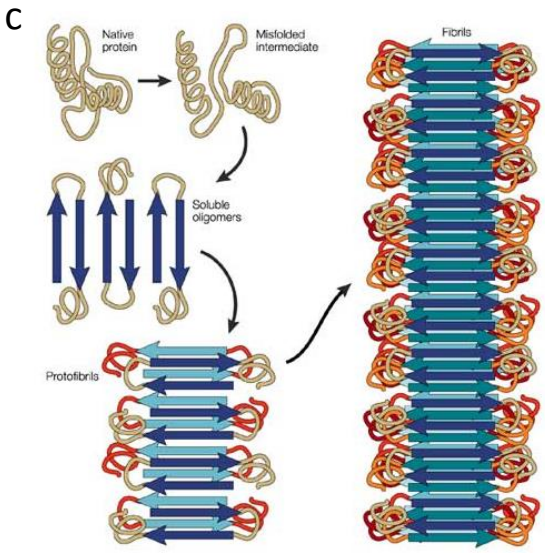

Figure 1.5 Protein aggregation in neurodegenerative diseases. (a) Proteinaceous inclusions are detected by histochemical staining in many neurodegenerative diseases. (b) Identifying the main protein component in these aggregates helps to distinguish between the diseases. (c) Protein aggregation is the result of misfolding and assimilating into long fibrils that are rich in β-sheet structure *(Soto, 2003)*.

fibrillar state. Although Lewy Bodies are still regarded as a clinical hallmark for neurodegenerative diseases, the timing of Lewy Body formation throughout the brain poorly correlates with the onset of symptoms *(Terry et al., 1991)*. Oligomeric intermediates are now believed to be the most neurotoxic element in protein aggregation *(Kayed et al., 2003; Outeiro et al., 2008; Brown, 2010b; Winner et al., 2011)* although their precise mechanim of toxicity is still under investigation (see later sections on alpha-Synuclein aggregation). Conversely, fibrils are more inert and may be neuroprotective as oligomers are removed from the cell *(Conway et al., 2000a)*.

The oxidation of cytosolic dopamine has been shown to contribute to PD through the production of free radicals *(Greenamyre and Hastings, 2004)*. The oxidative stress from dopamine may help to explain why the dopaminergic nigrostriatal pathway is specifically affected in PD. However, the lack of destruction of dopamine-containing neurons in the nearby ventral tegmental area suggests that dopamine stress cannot be solely responsible for the specialised susceptability of the SNc. Furthermore, the administration of L-dopa to patients does not accelerate disease progression *(Fahn 2005)*. Regardless of the contributions from dopamine, oxidative stress from other sources and cellular components appears to be an important factor in PD. The mitochondria are regarded as significant contributors to cellular ageing as they are a major source of reactive oxygen species; a toxic by-product of their respiratory function. It has been well established that oxidative stress resulting from mitochondrial dysfunction plays a role in PD *(Henchcliffe and Beal, 2008; Vila et al., 2008)*. The first evidence of this arose following the hospitilisation of drug abusers intravenously exposed to self-administered meperidine contaminated with 1-methyl-4-phenyl-1,2,3,4-tetrahydropyridine (MPTP), an inhibitor of the mitochondrial complex 1 machinery *(Nicklas et al., 1987; Gluck et al., 1994)*, that resulted in chronic, irreversible parkinsonian symptoms almost indistinguishable from PD *(Langston et al., 1983)*. The pathology of MPTP, similar to that of rotenone, has since become a widely accepted model for PD *(Przedborski et al., 2001; Dauer and Przedborski, 2003)* that has been studied in both human and non-human primates *(Porras et al., 2012)*, as well as a variety of other animals *(Hallman et al., 1985; Tieu, 2011)*.

Neurotoxin based models, such as MPTP, provide useful means for investigating idiopathic PD. However, there is debate surrounding the reliability of MPTP modeling *(Porras et al., 2012)* and whether or not the environment plays a role in PD aetiology

(Tanner, 1989; Hardy, 2006). As such, models based on changes in PD-associated genes, that give insight into hereditary forms of PD, are of great interest as they may hold the key to further understanding the molecular pathways involved in neurodegeneration.

1.5.3 Genetic risk factors in familial Parkinson's disease

While the majority of PD cases are idiopathic, an estimated 10 % are hereditary *(de Lau and Breteler, 2006)*; displaying clear mendelian inheriance of disease symptoms *(Hardy et al., 2003)*. Thus far, twenty one genetic loci have been described in various families with inherited PD (table 1.2), although the function of many of them is largely unknown *(Gasser, 2007)*. From these PARK loci, at least ten genes have been identified, mainly through positional cloning strategies, that contribute to the genetic aetiology of familial PD *(Saiki et al., 2012)*. Many of these genes, such as PTEN-induced kinase 1 (*PINK1*) *(Valente et al., 2004)*, DJ-1 *(Bonifati et al., 2003)*, and parkin *(Kitada et al., 1998)* are autosomal recessive; with their pathogenicity theorised to stem from a loss-of-function mechanism *(Gasser, 2007)*. Autosomal dominant genes include leucine-rich-repeat kinase 2 (*LRRK2*) *(Zimprich et al., 2004)*, and *SNCA* which codes for alpha-Synuclein (αSyn); the first PD-associated gene to ever be identified *(Polymeropoulos et al., 1997)*.

Gene mutations involved in familial PD					
Gene (loci)	**Locus**	**Inheritance**	**Clinical features**	**Protein**	**Protein function**
SNCA (PARK1 & PARK4)	4q21	AD	Similar to IPD, young onset, rapid progression	α - Synuclein	Primary component of Lewy bodies
Parkin (PARK2)	6q25·2–27	AR	Young onset, slow progression, early dystonia and dyskinesia	Ubiquitin ligase	component of ubiquitin proteasome system (UPS)
Omi/HrtA2 (PARK3 & PARK13)	2p13	AD	Similar to IPD, levodopa-responsive	Omi/HtrA2	Nuclearly encoded mitochondrial protein.
UCHL-1 (PARK5)	4p14	AD	Similar to IPD	UCHL-1	UPS component
PINK1 (PARK6)	1p35–36	AR	Young onset, benign course, levodopa-responsive	PTEN-induced kinase	Protection against mitochondrial dysfunction
DJ-1 (PARK7)	1p36	AR	Young onset, levodopa-responsive	DJ-1	Protection against oxidative stress
LRRK2 (PARK8)	12p11·2–q13·1	AD	Similar to IPD	Dardarin	Unknown
ATP13A2 (PARK9)	1p36	AR	Kufor – Rakeb syndrome, early onset PD with spasticity and dementia	P5 – type ATPase	Regulates cation homeostasis. Localises with lysosomes
PARK10	1p32	Sporadic	-	Unknown	-
PARK11	2q37.1	AD	-	Unknown	-
PARK12		Sporadic	-	Unknown	-
PLA2G6 (PARK14)	22q13.1	AR	Young onset PD	Calcium independent phospholipase A2	Generating free fatty acids
FBXO7 (PARK15)	22q12.3	AR	Juvenile onset (10 – 19 years old)	Fbox7	Molecular scaffold; still unknown
PARK16	1q32	Sporadic	-	Unknown	-
VPS35 (PARK17)	16q11.2	AD	Similar to IPD	Vacuolar protein sorting 35	Endosome – trans – Golgi trafficking
EIF4G1 (PARK18)	3q27.1	AD	Similar to IPD	Translation initiation factor	Translation machinery
DNAJC6 (PARK19)	1p31.3	AR	Juvenile onset PD	Auxilin	Clathrin – mediated endocytosis
SYNJ1 (PARK20)	21q22.11	AR	Early onset PD	Synaptojanin 1	Clathrin – mediated endocytosis
DNAJC13 (PARK21)	3q22.1	AD	Similar to IPD	HSP40 homolog	Vesicle formation and trafficking

Table 1.2 Genetic and clinical characteristic of familial Parkinson's disease. AD – autosomal dominant, AR – autosomal recessive, IPD – idiopathic PD (modified from *Saiki et al., (2012)*).

Regardless of the manner of inheritance, the translated products of the above mentioned genes have been shown to either directly or indirectly influence the apoptotic state of mitochondria *(Vila et al., 2008).* In addition, many of these proteins have been found to interact with each other and play important roles in several cellular functions including synaptic transmission (αSyn), lysosomal degradation pathway (αSyn, parkin, PINK1, Omi/HtrA2), axonal transport (LRRK2) and ubiquitin proteasome systems (αSyn, parkin, DJ-1, UCH-L1).

1.6 Alpha-Synuclein

1.6.1 Native structure

In humans, the protein alpha-Synuclein (αSyn) is encoded by the single gene SNCA which is located on chromosome 4 (4q21) and made up of seven exons *(Chen et al., 1995).* This protein was first identified in neurons; localising to both the presynaptic nerve terminals and nucleus, and was accordingly named *synuclein (Maroteaux et al., 1988).* Since then, αSyn has been found at high concentrations in both the soluble and membrane bound fractions of brains, and has been estimated to comprise as much as 1 % of the total soluble protein content in cytosolic brain fractions *(Iwai et al., 1995).*

The 140 amino acid sequence of αSyn can be divided into three distinct regions (figure 1.5a). The N-terminal (residues 1-60) is a highly conserved domain in all Synuclein proteins that is unordered in solution but can form an α-helical conformation in the presence of lipids *(George, 2002).*The N-terminal includes four imperfect 11-subunit repeats, each containing a conserved hexameric motif (KTKEGV) that is capable of forming amphipathic alpha helixes when bound to lipid membranes *(Davidson et al., 1998; Jo et al., 2000; Bussell and Eliezer, 2003).*

The central region (residues 61-95) contains a 12 amino acid sequence (^{71}VTGVTAVAQKTV^{82}) that is necessary and sufficient for fibrillisation *(Giasson et al., 2001).* This stretch of hydrophobic and amyloidogenic amino acids was originally identified as a peptide, known as the Non Amyloid-β Component (NAC), that strongly associated with the amyloid plaques found in Alzheimer's disease; *(Ueda et al., 1993).* The precursor (NACP), from which the NAC peptide is derived, was found soon after to be the full length αSyn protein *(Chen et al., 1995).* The NAC represents a key structural determinant of αSyn fibrillisation based on the following evidence:

- The NAC enables αSyn to undergo a conformational change from random coil to β-sheet structure *(Serpell et al., 2000)*
- The NAC sequence is resistant to proteolytic digestion and forms the core in αSyn filaments *(Giasson et al., 2001).*
- The rate of αSyn fibrilisation *in vitro* decreases with the insertion of charged residues into the NAC sequence *(Giasson et al., 2001).*
- Synthetic peptides that contain the NAC are able to self polymerise and promote fibrillisation of full length αSyn *in vitro (Giasson et al., 2001).*
- Human β-Synuclein (βSyn) and γ-Synuclein (γSyn) both lack the 12 residue sequence (figure 1.6) and thereby fail to assemble into filaments *in vitro* or form coploymers with αSyn *(Biere et al., 2000).*

The NAC region also contains three more KTKEGV repeats that, combined with those in the N-terminal region, collectively form a lipid-binding domain *(Perrin et al., 2000)* that consists of two extended α-helices interupted by a short break *(Chandra et al., 2003)* (figure 1.6a). This lipid-binding domain is similar to those found in apolipoproteins *(Clayton and George, 1998)* and fatty acid binding proteins *(Sharon et al., 2001).* The conservation of this domain, accounting for over half the sequence of each Synuclein protein, suggests that all three Synucleins share lipid binding activity as part of their native function.

In comparison, the C-terminal (residues 96-140) is predominantly unfolded in structure *(Hoyer et al., 2002)* and does not associate with lipid membranes *(Eliezer et al., 2001).* The C-terminal region is rich in acidic amino acids and has greater variation between members of the synuclein family than the rest of the primary sequence (figure 1.7) *(Clayton and George, 1999),* suggesting the specific funcitons of each Synuclein protein is derived from this area. The C-terminal of αSyn is critical for chaperone – like activity *(Kim et al., 2000; Souza et al., 2000; Kim et al., 2002)* and offers a neuroprotective function against oxidative stress factors *(Albani et al., 2004).* Forms of αSyn with a truncated C-terminal (residues 1-120) show enhanced vulnerability to oxidative stress *(Kanda et al., 2000)* and are more prone to fibrilisation that the full-length protein *(Crowther et al., 1998).* The C-terminal is believed to play a role in regulating αSyn transport into the nucleus where it can bind to histones *(Goers et al., 2003b; Cherny et al., 2004).* Importantly, this region is responsible for numerous sites of interaction with other proteins *(Jensen et al., 1999; Giasson et al., 2003),* metal ions

(Paik et al., 1999; Rasia et al., 2005; Bisaglia et al., 2009; Brown, 2009) and natural ligands (e.g. dopamine and polyamines) *(Goers et al., 2003a; Illes-Toth et al., 2013)* (figure 1.6b).

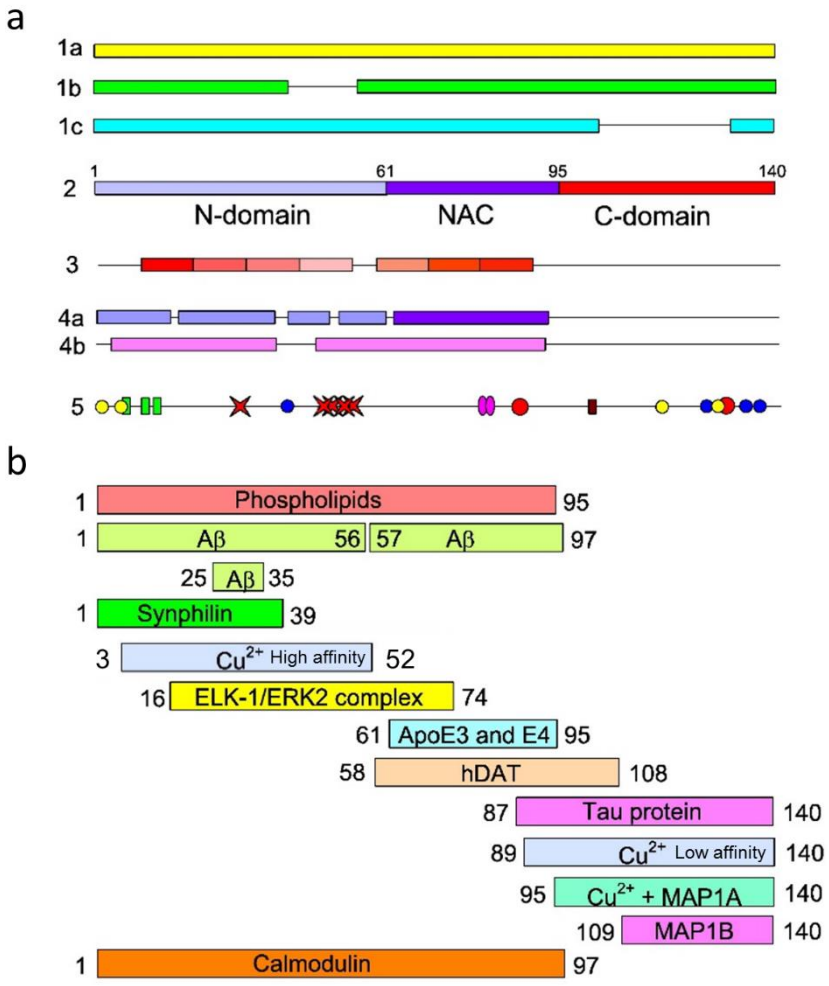

Figure 1.6 Schematic representation of alpha-Synuclein (αSyn) primary sequence indicating: (a) structural information and (b) putative interaction domains. Depicted from the top down are the three isoforms of αSyn (1a-b); the three structural domains (2); seven imperfect repeats (3); predicted (4a) and experimentally determined α – helixes (4b); sites of posttranslational modification (methionine – yellow circles, tyrosine – blue circles, phosphorylation sites – red circles, ubiquitination – green boxes, SUMOylation – brown box, transglutaminase crosslinking sites – pink ovals) and PD-related mutations – red stars (5). The interaction domains responsible for binding of several ligands and proteins are indicated in (b). The N-terminal high affinity Cu(II) binding site, involving His-50 *(Rasia et al., 2005)*, is indicated in addition to the low affinity C-terminal binding site. The numbers on the bars correspond to the residues in αSyn sequence *(image adapted from Breydo et al., 2012)*.

Figure 1.7 ClustalW2 alignment of α, β and γ – Synuclein primary sequence. Under each aligned residue: * indicates homology between all three sequences, **:** indicates 2/3 homology but all residues share similar properties, whereas **.** indicates 2/3 homology with residues showing different properties. Note the preservation of the N-terminal domain across the whole Synuclein family. The NAC domain is either missing or mutated in β and γ – Synuclein respectively and variation in the C-terminal may provide functional specificity. red – small/hydrophobic residues, blue – acidic residues, magenta – basic residues, green – hydroxyl/sulphydryl/amine residues

1.6.2 Conformational behaviour of native αSyn

Since its discovery, native αSyn has been widely regarded as an unfolded, monomeric species capable of forming α-helixes when bound to membranes (figure 1.8a) *(Weinreb et al., 1996; Fauvet et al., 2012)*. The abundance of acidic residues near the C-terminal produces a high net charge (pl = 4.7) and low overall hydrophobicity that is common for unstructured proteins *(Hoyer et al., 2002)*. Increasing the temperature or decreasing the pH of the protein environment can counter these two structural parameters and induce partial folding of αSyn *(Uversky et al., 2001a)* into an intermediate state that facilitates aggregation *(Li et al., 2001)*.

Recent evidence has shown that αSyn also exists physiologically as a helically folded tetramer (figure 1.8b) *(Bartels et al., 2011; Wang et al., 2011a)*. This soluble tetramer has been purified from both endogenous *(Bartels et al., 2011)* and recombinant sources *(Wang et al., 2011a)*, and forms unassisted by lipid membranes. Unlike other oligomeric states that are pathologically-linked to neurodegenerative diseases, the tetramer is non-toxic and does not readily aggregate into amyloid fibrils *(Wang et al., 2011a)*. The insertion of PD-associated point mutations into αSyn destabilises the tetrameric structure; providing a potential mechanism for disease initiation *(Wang et al., 2011a; Dettmer et al., 2015)*. Similar to other proteins with a tertiary structure, the stability of the αSyn tetramer is likely to be dependent on subunit concentration and environmental factors *(Wang et al., 2011a)*. It is predicted therefore that the tetramer

formation constitutes a small percentage of the total αSyn content *(Bartels et al., 2011)*, which occurs predominantly in cell as an unfolded monomer *(Fauvet et al., 2012)*, and that tetramer disassembly precedes the fibrillisation process.

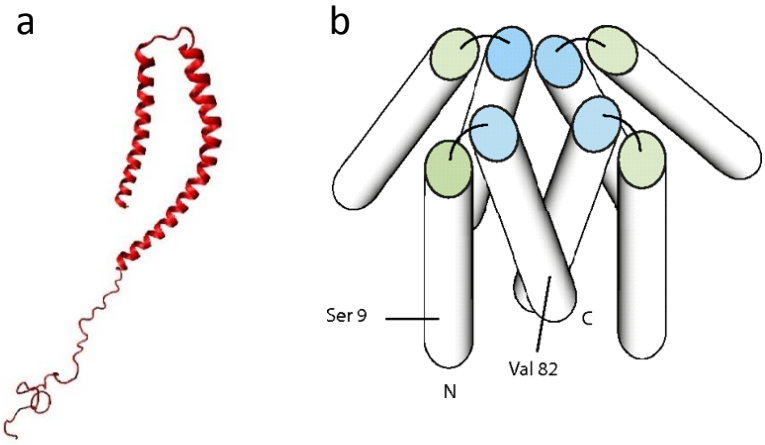

Figure 1.8 Physiological structures of αSyn. (a) 3D structure of αSyn bound to membrane (protein database ID: 2KKW) *(Ulmer et al., 2005)*. (b) Model structure of αSyn helically folded tetramer based on electron microscopy reconstruction. *(Wang et al., 2011a)*.

1.6.3 Function of native αSyn

The physiological role of αSyn has been the subject of many investigations and is still not entirely understood. Increasing evidence shows that αSyn may function as a cellular ferrireductase *(Brown, 2013)*. For this activity, αSyn is able to bind both copper and iron simultaneously *(Davies et al., 2011a)*. Similar to the metal ion cofactors found in other proteins, the copper bound to the N-terminal of αSyn is likely to catalyse the reduction of cellular iron from Fe(III) to Fe(II) *(Davies et al., 2011a; Davies et al., 2011b)*. Metal-binding activity has been proposed for numerous proteins associated with neurodegenerative disorders including: DJ-1, prion and Aβ *(Brown, 2010a)*.

The localisation of αSyn at presynaptic nerve terminals (figure 1.9a-b) *(Jakes et al., 1994; Iwai et al., 1995; Withers et al., 1997)* as well as its interaction with SNARE complexes *(Burre et al., 2010)* and the distal reserve pool of synaptic vesicles *(Murphy et al., 2000; Lee et al., 2008b)*, suggests that αSyn is important for regulating neurotransmitter release, healthy synaptic function and plasticity (figure 1.9c). The association between αSyn and vesicles has been demonstrated *in vitro* while investigating the helical structure of the lipid-binding domain *(Davidson et al., 1998;*

Jo et al., 2000). This interaction is implicated in regulating the size of the presynaptic vesicular pool in cultured hippocampal neurons *(Murphy et al., 2000)*. Mice lacking αSyn show depleted vesicle reserves and impaired vesicle mobilisation at the nerve terminals *(Cabin et al., 2002)*.

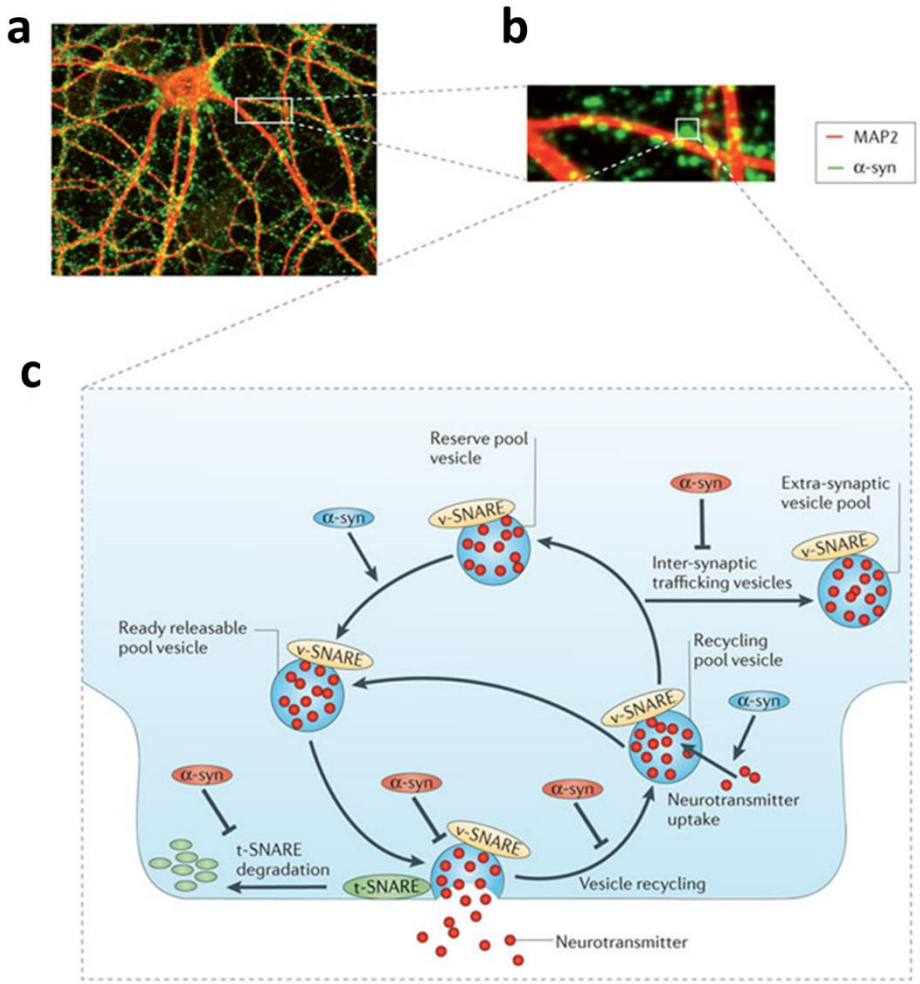

Figure 1.9 Physiological role of αSyn in regulating vesicle trafficking and neurotransmission. (a) Wide field image (magnified in b) of cultured neurons. MAP2 reveals neuronal dendrites (red); αSyn (green) localises presynaptically. (c) The functions of αSyn in the presynaptic terminal include vesicle refilling (αSyn; blue), interaction with target membrane – associated SNARE (t-SNARE) and vesicle-associated SNARE (v-SNARE) proteins. Accumulation of αSyn (αSyn; red) impairs neurotransmitter release, vesicle recycling and vesicle trafficking *(Lashuel et al., 2013)*.

Despite its general abundance throughout the brain *(Vivacqua et al., 2011)*, song learning in zebra finches requires a reduced expression of Synelfin (the avian homologue to αSyn/NACP) in specific areas during the critical stage of development *(George et al., 1995)*. In αSyn-knockout mice, however, only mild, inconsistent changes in cognitive/learning behaviour are observed *(Chen et al., 2002; Kokhan et al., 2012)*. The fact that single, double and even triple Synuclein knockouts (α-, β- and γ- Synuclein) remain viable *(Chandra et al., 2004; Drolet et al., 2004; Senior et al., 2008; Greten-Harrison et al., 2010)* suggests that these proteins are not essential for healthy synaptic function but may contribute to the regulation of the neurotransmitter release mechanism *(Lashuel et al., 2013)*.

In particular, dopamine-dependent behavioural changes are often seen in αSyn-knockout mice *(Maries et al., 2003; Drolet et al., 2004; Senior et al., 2008)*; linking αSyn to healthy neurotransmission. It has been shown that αSyn is involved in regulating dopamine (DA) neurotransmission by interacting with DA vesicles *(Lotharius and Brundin, 2002a)*. In addition, αSyn has been shown to have an inhibitory effect on the activity of tyrosine hydroxylase (TH), the rate-limiting enzyme in DA biosynthesis *(Perez et al., 2002)*, and regulates the insertion of DA transporters into the membrane *(Lee et al., 2001; Lehmensiek et al., 2002)*. The ability to rapidly sequester DA, a function that is impaired by familial PD mutations in αSyn *(Lotharius et al., 2002)*, provides a protective mechanism against the oxidative damage caused by dopamine breakdown products *(Lotharius and Brundin, 2002b)*. This may explain why specific dopaminergic pathways in the brain are more susceptible than others in PD pathology *(Xu et al., 2002)*.

1.6.4 Pathological αSyn

Although its native function remains elusive, αSyn has a well established pathological role in a number of neurodegenerative disorders, collectively termed Synucleinopathies. Since its initial discovery as a non-Aβ component of amyloid plaques in Alzheimer's disease patients *(Ueda et al., 1993)*, a pathological function was always suspected for αSyn. Research interest grew rapidly when, a few years later, a missense mutation in the SNCA gene was found in familial cases of early-onset PD *(Polymeropoulos et al., 1997)*. At the same time it was discovered, through immunohistochemistry, that αSyn fibrils form the main component in Lewy bodies *(Spillantini et al., 1997; Baba et al., 1998)*. Over the last few decades, the involvment

of αSyn aggregation in PD pathogenesis has become increasingly well established. The strongest evidence linking the two is summarsied below:

- In several cases of familial PD, point mutations in αSyn (A53T, A30P, E46K, H50Q and G51D) *(Polymeropoulos et al., 1997; Kruger et al., 1998; Zarranz et al., 2004; Lesage et al., 2013; Proukakis et al., 2013)* and gene multiplications *(Singleton et al., 2003; Chartier-Harlin et al., 2004; Ibanez et al., 2004; Fuchs et al., 2007; Ross et al., 2008b)* promote the early onset of symptoms *(Conway et al., 1998; Narhi et al., 1999)*.
- The main protein component of Lewy bodies was found to be amyloid αSyn fibrils *(Spillantini et al., 1997; Spillantini et al., 1998)*.
- The expression of human αSyn (both WT and mutants) in transgenic mice *(Masliah et al., 2000; Kirik et al., 2002; Lo Bianco et al., 2002; Chen et al., 2015)*, flies *(Feany and Bender, 2000)*, and nematode worms *(Kuwahara et al., 2006)* resulted in age-dependent dopaminergic neuron loss, motor dysfunctions and inclusion body formation comparable to those found in PD.
- Conversely, αSyn-null mice display resistance to MPTP-induced degeneration of DA neurons as the toxin becomes unable to inhibit complex 1 *(Dauer et al., 2002)*.
- Expression of αSyn in cell cultures led to increased oxidative stress, calcium influx and mitochondrial-associated cell death *(Hsu et al., 2000; Ko et al., 2000)*.
- Animal models that induce Parkinsonism by exposure to pesticides (rotenone, paraquat) and neurotoxins (MPTP) aquire Lewy bodies containing αSyn *(Betarbet et al., 2000; Sherer et al., 2003; Drolet et al., 2004; Feng and Maguire-Zeiss, 2011)*.

1.6.5 Pathology of extracellular αSyn

Initially, the aggregation of αSyn was believed to be a largely intracellular trait *(McNaught and Olanow, 2006)* with evidence for Lewy Bodies ending up in the extracellular space as a result of host cell destruction *(Katsuse et al., 2003)*. However, the release and uptake of αSyn aggregates from the extracellular space appears to play an important role in disease progression *(Lee, 2008; Brown, 2010b)*. Implications of extracellular αSyn arose following the detection of αSyn oligomers in the cerebrospinal fluid of PD patients *(El-Agnaf et al., 2003; El-Agnaf et al., 2006)* and soluble protein fractions from the brains of DLB patients *(Paleologou et al., 2009)*.

Subsequently, αSyn release has been shown to occur via a calcium-dependent exocytosis mechanism *(Emmanouilidou et al., 2010)*. Whilst in the extracellular space, αSyn is chaperoned by Hsp70 *(Outeiro et al., 2008; Danzer et al., 2011)* which plays a neuroprotective role against aggregation *(Auluck et al., 2002)*. However, the extracellular accumulation of high levels of heavy metal ions in the SNc *(Dexter et al., 1991)* could promote αSyn aggregation through binding to the C-terminal *(Bush, 2000; Binolfi et al., 2006; Brown, 2010b)*. A loss of heavy metal ion homeostasis, typically seen in patients with PD *(Dexter et al., 1989; Gorell et al., 1999; de Lau and Breteler, 2006)*, is therefore a likely promoter of extracellular αSyn toxicity.

The extracellular release of αSyn in neurons is thought to be mediated from presynaptic terminals, which become enriched in αSyn aggregates *(Schulz-Schaeffer, 2010)*, and may impact upon postsynaptic elements. Complementing the release of αSyn, all major brain cell types (neurons, astrocytes, and microglia) are also capable of clearing extracellular αSyn *(Lee et al., 2008a)* and that, once internalised, αSyn can be retrogradely transported from the axon to the cell soma *(Danzer et al., 2011)*. The transmission of αSyn in this manner has been recorded directly from neuron to neuron *(Desplats et al., 2009)* and from neuron to astroglia *(Lee et al., 2010)* emphasising the likelihood of synaptically-released extracellular αSyn being an important factor in the spreading of synucleinopathic diseases.

The accumulation of αSyn has been associated with a reduction in pre- and post-synaptic markers *(Kramer and Schulz-Schaeffer, 2007)* and in the actin-binding protein, debrin; involved in the formation and maintenance of dendritic spines *(Takahashi et al., 2003)*. Dendritic spine retraction in striatal MSNs is hypothesised to underlie late-stage motor complications in PD *(Zaja-Milatovic et al., 2005)* and contribute to executive dysfunction in patients with DLB *(Zaja-Milatovic et al., 2006)*, while the dendritic spines of the hippocampus have been shown to regulate long-term potentiation (LTP) *(Engert and Bonhoeffer, 1999)* associated with memory and learning. These changes in dendritic spine morphology are accountable as a result of increased impairment of neurotransmitter release brought about by the presynaptic accumulation of αSyn aggregates *(Kramer and Schulz-Schaeffer, 2007)*. Consequently, the disease pathology for many neurodegenerative disorders may stem from neurotransmitter deficiencies and synaptic dysfunction instead of being a direct result of cell death *(Linazasoro, 2007; Nikolaus et al., 2009)*.

1.6.6 Aggregation of αSyn

The mechanism of αSyn aggregation is a nucleation-dependent process *(Wood et al., 1999)*; characterised by a slow phase in which the protein unfavourably associates into an ordered nucleus, followed by a growth phase in which the nucleus rapidly polymerises, and a steady state phase in which the aggregate and monomer are in equilibrium *(Harper and Lansbury, 1997)*. This process follows first-order kinetics with respect to αSyn concentration *(Wood et al., 1999)*. The aggregation of αSyn into fibrils, however, is preceded by oligomeric and protofibrillar intermediate states (figure 1.5). Increasing evidence suggests that soluble oligomeric αSyn is more neurotoxic and better correlates with PD pathology than the larger insoluble aggregates that form later *(Haass and Selkoe, 2007; Winner et al., 2011)*. In cell models, toxicity and cell death often precede the appearance of insoluble aggregates *(Gosavi et al., 2002)*. Additionally, many familial mutations in αSyn accelerate oligomerisation rather than fibrilisation *(Conway et al., 2000b)*.

1.6.7 Oligomeric αSyn

Oligomers of αSyn are highly diverse with regard to size, shape, structure, aggregation kinetics and toxicity. The secondary structure of αSyn oligomers is varied with some describing a predominantly β-sheet structure *(Giehm et al., 2011)* while others propose a greater α-helical content *(Apetri et al., 2006)*. Oligomers have been used to seed aggregation indicating that they are on pathway to fibrils *(Lee et al., 2002; Danzer et al., 2007; Danzer et al., 2009; Hansen et al., 2011)*. Competing evidence, however, shows that some forms of oligomer can impede the aggregation process; suggesting that they are off pathway to fibril formation *(Hong et al., 2011; Lorenzen et al., 2014c)*.

Soluble oligomers have been reported to be amorphous, globular, tubular, stellate, spherical and annular in shape *(Lashuel et al., 2002a; Lashuel et al., 2002b; Lowe et al., 2004; Pountney et al., 2005; Danzer et al., 2007; Hong et al., 2008; Giehm et al., 2011)*. Annular oligomers (figure 1.10) in particular are a commonly seen species and their pore-like morphology has been compared with that of the cytolytic, β-barrel pore-forming bacterial toxin; α-hemolysin *(Lashuel et al., 2002b)*. However, the dimensions of ring-like oligomers are also subject to variability with some demonstrating external diameters as small as 10-12 nm *(Lashuel et al., 2002a)*, while

others report them to be 40-45 nm *(Danzer et al., 2007)* and even as big as 70-90 nm *(Lowe et al., 2004)*. It is unclear whether these different sized ring oligomers are an indication of biological/pathological activity, separate stages of oligomer aggregation or simply the result of differences in *in vitro* oligomerisation conditions. Numerous physiological factors have already been implicated in having an effect on aggregation rate, oligomer morphology and toxicity: molecular crowding *(Uversky et al., 2002)*, αSyn concentration *(Wang et al., 2011a)*, divalent metal ions *(Binolfi et al., 2006;*

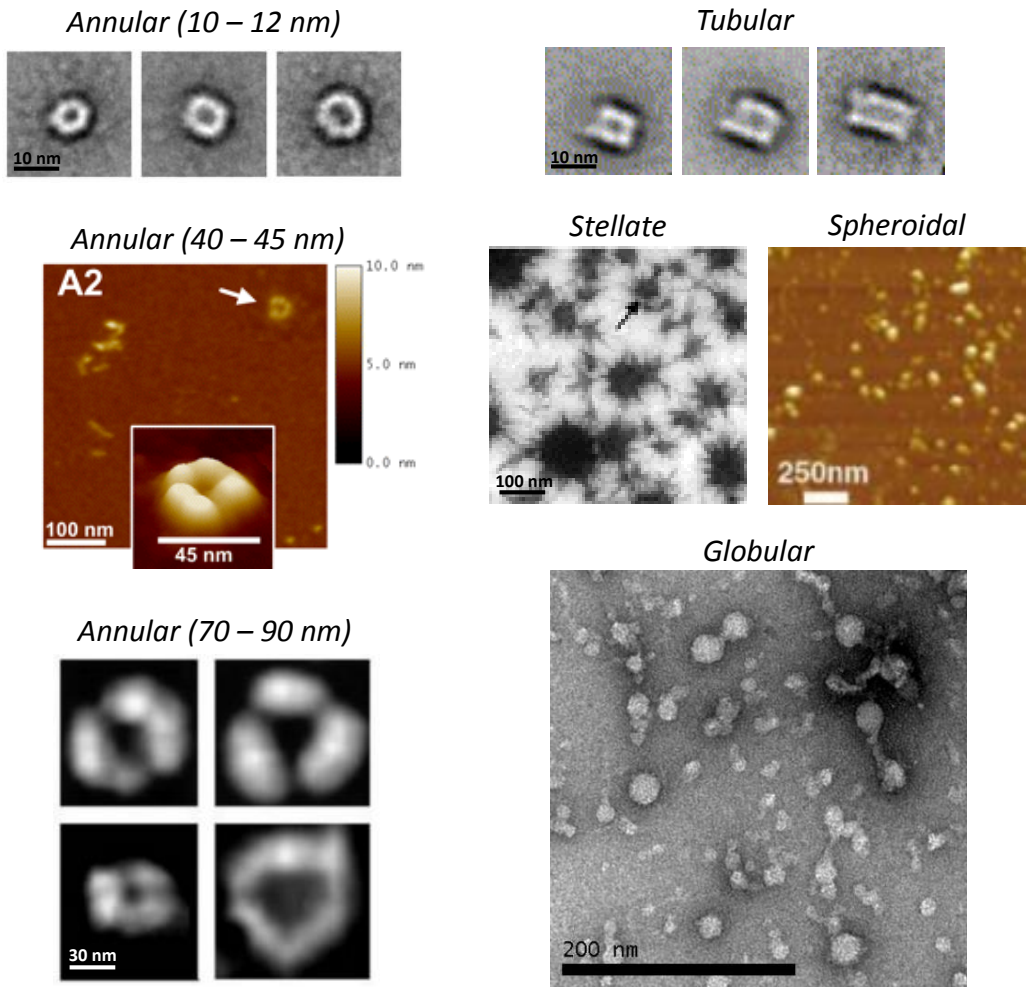

Figure 1.10 Variations in the size and shape of oligomeric αSyn formed under different conditions. Annular oligomers (10-12 nm) are commonly formed under incubation with shaking conditions, although tubular oligomers have also been characterised *(Lashuel et al., 2002b)*. Spheroidal oligomers, with α-helical structure, were seen by atomic force microscopy (AFM) after long incubation under slow aggregation conditions *(Apetri et al., 2006)*. Incubation of αSyn with copper produced large stellate oligomers *(Wright et al., 2009)* while baicalein – stabilised oligomers were more globular *(Hong et al., 2008)*. Annular oligomers with larger diameters were formed from incubation with iron (40-45 nm) *(Danzer et al., 2007)* and with calcium/cobalt (70-90 nm) *(Pountney et al., 2005)*.

Brown, 2009, 2010b), dopamine *(Cappai et al., 2005)*, environmental pH and salt concentrations *(Hoyer et al., 2002)*. Variability in the molecular properties of αSyn oligomers between *in vitro* studies is therefore likely to be, in part, the result of differences in oligomerisation conditions.

1.6.8 Mechanism of toxicity

The permeabilisation of lipid bilayers was one of the first proposed mechanisms through which αSyn oligomers exert their toxicity *(Volles et al., 2001)*. Indeed, permeabilisation of artificial vesicles filled with cations or fluorescent dyes has become a frequent *in vitro* model for measuring oligomer toxicity *(Butterfield and Lashuel, 2010)*. If such a wide variety of oligomeric species exists physiologically for αSyn, then variation in oligomer toxicity is equally plausible. Rod-shaped oligomers containing dopamine, for example, are unable to bind or permeabilise membranes *(Cappai et al., 2005; Pham and Cappai, 2013)* but may be involved in loss-of-function of the SNARE complex *(Choi et al., 2013)*. Copper binding to αSyn forms soluble stellate oligomers but also reduces membrane association *(Wright et al., 2009; Wang et al., 2010)*. The flavonoid epigallocatechin gallate (EGCG) has been shown to redirect αSyn aggregation and remodel fibrils into disordered, non-toxic oligomers *(Bieschke et al., 2010; Lorenzen et al., 2014b)*. The membrane permeabilising activity of αSyn oligomers has been proposed to be dependent on the exposure of the hydrophobic core. Oligomers that have a less compact hydrophobic core and greater structural flexibility are able to insert into membranes and permeabilise vesicles. Non-toxic oligomers on the other hand are more constrained and do not as readily associate with membranes *(Campioni et al., 2010)*.

Increasing evidence proposes that oligomers are able to permeabilise membranes through the formation of a pore complex *(Butterfield and Lashuel, 2010)*. This concept is largely attributed to annular oligomers that are able to span membranes *(Zhang et al., 2013)* and produce discrete stepwise changes in membrane conductance reflecting the electrophysiology of a single channel opening and closing *(Kim et al., 2009; Feng et al., 2010; Schmidt et al., 2012; Tosatto et al., 2012; Mironov, 2015)*. The conformational antibody A11 that specifically targets annular oligomers *(Kayed et al., 2003)* is able to block channel activity and inhibit membrane permeabilisation *(Yoshiike et al., 2007)*. The A11 antibody is also capable of binding Aβ oligomers

(Kayed et al., 2003) and α-hemolysin *(Yoshiike et al., 2007)*; supporting the idea of a shared mechanism of pathology.

Counter to the theory of pore-forming oligomers, however, is the finding that membrane permeabilisation can be induced by a heterogeneous range of αSyn oligomers and is highly sensitive to the charge and content of the bilayer *(van Rooijen et al., 2009a)*. This does not support the insertion of a stable pore complex but rather the transient association of αSyn with the membrane. Membrane 'thinning', in which the hydrophobic barrier is destabilised but not perforated by αSyn, is an alternative theory for describing the membrane permeabilisation mechanism of oligomers *(Stockl et al., 2013; Lorenzen et al., 2014b)*.

The preferential binding to lipid membranes with high lipid-protein ratio *(Auluck et al., 2010)* suggests that αSyn interacts more efficiently with lipid raft-like domains *(Fortin et al., 2004)*. In addition to localisation at synapses, intracellular lipid-rafts, such as those present along mitochondria-associated endoplasmic reticulum membranes (MAM), present vital subcellular targets for αSyn that may be linked to toxicity *(Guardia-Laguarta et al., 2014)*. As described earlier, mitochondrial dysfunction plays a central role in PD pathology. The connection between αSyn and mitochondria is poorly understood *(Nakamura, 2013)*, although interactions with complex 1 have been proposed *(Devi et al., 2008; Vila et al., 2008)*. Oligomer-specific alterations to calcium homeostasis *(Danzer et al., 2007)*, as well as the accumulation of reactive oxygen species *(Junn and Mouradian, 2002)*, are also likely to play a role in mitochondria-linked apoptosis.

A multitude of other toxicity mechanisms have been proposed for oligomeric αSyn, including loss of cytoskeletal integrity *(Prots et al., 2013)*, endoplasmic reticulum stress *(Thayanidhi et al., 2010)*, impaired protein degradation systems *(Xilouri et al., 2013)*, disturbed vesicle-membrane fusion *(Choi et al., 2013)* and neuroinflammation *(Beraud et al., 2013)*. The role of αSyn in these various mechanisms are well reviewed by *Roberts and Brown (2015)* and summarised in figure 1.11. Thus, αSyn oligomer toxicity is likely to be the result of many different structural species acting upon many different cellular systems. However, there still remains much to be understood with regard to oligomers in neurodegenerative diseases.

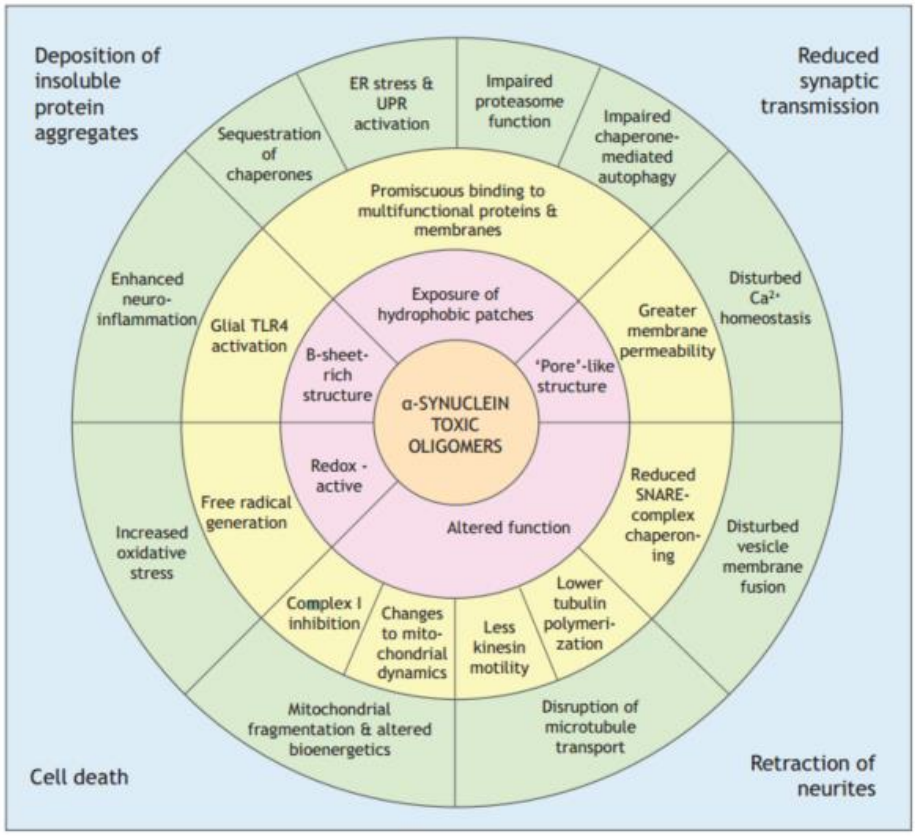

Figure 1.11 Toxicity mechanisms in relation to properties of αSyn oligomers. Pink circle – properties of αSyn oligomers. Yellow circle – molecular effects conferred by toxic oligomers. Green circle – cellular systems disrupted by oligomers. Blue box – pathological outcomes of neuron dysfunction. ER – endoplasmic reticulum. UPR – unfolded protein response *(Roberts and Brown, 2015)*.

1.7 Thesis outline

This thesis aims to develop our understanding of how soluble, annular αSyn oligomers affect the electrophysiology of neurons in mouse neocortical brain slices. The neocortex is an area heavily associated with the non-motor symptoms of PD and other neurodegenerative disorders, yet is often overlooked in studies regarding αSyn oligomer pathology. Furthermore, research into the electrophysiological properties of αSyn oligomers often lack characterisation which is important considering the structural and functional heterogeneity described in the previous sections. The hypotheses of this thesis are that oligomers will produce changes in specific neuronal parameters that are not caused by the monomer. Furthermore, oligomers isolated from separate stages of the aggregation pathway will show structural differences that alter their impact on neuron electrophysiology. This thesis attempts to bridge this gap between structural biology and neurobiology as two well defined

populations of soluble αSyn oligomers are injected directly into thick-tufted layer 5 pyramidal neurons in the neocortex.

Chapter 2 provides an overview of the methods used to express and purify recombinant αSyn. Two point mutations are introduced into the N-terminal region; Y39W provides structural information in the form of tryptophan fluorescence and E46K is a disease-linked mutation that facilitates aggregation.

Chapter 3 examines the aggregation time course of αSyn and the isolation of oligomeric species. In addition to purifying oligomers formed during αSyn aggregation, a separate population of oligomers were recovered from the sonication of fibrils. A range of analytical tools were applied including circular dichroism and fluorescence spectroscopy, transmission electron microscopy, analytical ultracentrifugation and Thioflavin-T binding assays to characterise the structural differences between these two species of oligomeric αSyn.

In Chapter 4 monomeric and oligomeric αSyn are introduced directly into thick-tufted layer 5 pyramidal neurons using the whole-cell patch clamp technique. Neurons with intracellularly injected αSyn remained stable for over half an hour, as determined by the series resistance. Additionally, both monomer and oligomer were observed by immunofluorescence imaging specifically within recorded neurons. The voltage responses to step and naturalistic input currents were used to generate standard and dynamic I-V curves respectively. The dynamic I-V curve can be accurately fitted to an exponential integrate-and-fire neuron model from which a range of electrophysiological parameters can be extracted.

Chapter 5 examines the time course of changes in electrophysiological parameters, derived from standard and dynamic I-V curves, as a result of oligomeric αSyn. Over time, neurons injected with oligomer displayed a significantly reduced input resistance compared to either control or monomer-injected neurons. Consequentially, the amount of current needed for spike initiation was significantly elevated and the firing rate markedly slower.

Finally, a general discussion and conclusion are presented in which the implications of these findings, particularly with regard to the cognitive symptoms prevalent throughout PD, are assessed.

2 Expression and purification of recombinant alpha-Synuclein

2.1 Introduction

While it is possible to extract high yields of endogenous alpha-Synuclein (αSyn) from brain tissues and red blood cells *(Scherzer et al., 2008; Bartels et al., 2011; Fauvet et al., 2012),* this process is expensive, inconsistent and technically challenging. Recombinant expression of αSyn on the other hand has become a more favourable and widely used method as it provides comparably large amounts of protein in a renewable manner. Recombinantly expressed αSyn has been used in countless *in vitro* studies on native structure and function, membrane/protein/small molecule interactions, aggregation kinetics and mechanism of toxicity. The secondary structure of native αSyn purified from human brain tissue, in the unfolded monomeric state, was shown to be identical to that of recombinant αSyn *(Fauvet et al., 2012).* Therefore, recombinant αSyn will be used throughout this thesis as an appropriate model for native αSyn.

The dual focus of this thesis is to combine structural characterisation of purified oligomeric αSyn (chapter 3) with investigations into their electrophysiological impact (chapters 4 & 5) in cortical neurons. To facilitate the aggregation process a point mutation linked to a familial form of PD (position 46; glutamate to lysine) will be inserted into the recombinant human αSyn construct. The E46K mutation has been shown to accelerate aggregation *in vitro (Choi et al., 2004),* produce amyloid-like fibrils faster than the wild type *(Greenbaum et al., 2005),* and cause juvenile onset of disease symptoms *(Zarranz et al., 2004).*

The structural changes exhibited by αSyn during aggregation will be investigated using circular dichroism spectroscopy and tryptophan fluorescence. Intrinsic tryptophan fluorescence is a useful tool for investigating protein structure as the emission spectrum of these residues is highly sensitive to the local environment *(Royer, 2006).* Since αSyn does not have any native tryptophan residues, a folding sensitive mutation can be strategically introduced through site-directed mutagenesis in place of a large aromatic amino acid such as phenylalanine or tyrosine *(Smith et al., 1991).* For all investigations, the tyrosine residue at position 39 will be mutated to

tryptophan (Y39W). This location was chosen as the N-terminal region is known to undergo α-helical folding during lipid binding *(Bussell and Eliezer, 2003)* and may form integral structures in the oligomeric state *(Lorenzen et al., 2014c)*. Three other tyrosine residues exist close to the C-terminal end, however the consistently unfolded nature of this region (see Introduction) makes them impractical for tryptophan insertion. Tryptophan fluorescence has been successfully used to study the native and pathological structures of αSyn. Previous investigations have shown that the Y39W mutation has no effect on the unfolded monomeric structure, does not interfere with protein aggregation or alter the structure of αSyn oligomers *(Dusa et al., 2006; van Rooijen et al., 2009b).*

This chapter details the methods used for mutagenesis, expression, purification and structural characterisation of recombinant αSyn carrying point mutations at Y39W and E46K. The fluorescence spectrum of the solvent exposed tryptophan residue as well as the secondary structure as determined by circular dichroism illustrate recombinant $\alpha Syn^{Y39W, E46K}$ to be in an unfolded, monomeric state.

2.2 Materials and methods

2.2.1 Materials

IPTG, Tris, PMSF were purchased from Melford (Ipswich, UK)

Glycerol, NaCl, KH_2PO_4, K_2HPO_4, $MgSO_4$, $CaCl_2$, $MnCl_2$, potassium acetate, ammonium sulphate, ammonium persulphate, EDTA, 2-mercaptoethanol, were purchased from Fisher Scientific (Loughborough, UK).

Peptone from casein (pancreatically digested) and yeast extract were purchased from Merch (Darmstadt, Germany).

Nitrocellulose membrane filters (0.22 µm diameter) were purchased from Millipore (Ireland), 30 % acrylamide solution from Geneflow (Staffordshire, UK), and SnakeSkin™ Dialysis Tubing (#68035) was purchased from Thermo Scientific (Rockford, IL). All other materials were purchased from Sigma (Poole, UK) unless stated otherwise.

Growth media

Lysogeny Broth (LB) contained (per litre): 10 g peptone, 5 g yeast extract and 10 g NaCl, made up to 1 litre with distilled water and autoclaved.

Terrific Broth (TB) contained (per litre): 12 g Peptone, 24 g yeast extract, 4 ml glycerol, made up with distilled water to 900 ml. After autoclaving, 100 ml of 0.17 M KH_2PO_4 and 0.72 M K_2HPO_4 (autoclaved) was added. Ampicillin (100 µg/ml) and chloramphenicol (20 µg/ml) were added directly, prior to inoculation with starter cultures.

Competence buffers

TBF1 contained (in mM): 30 potassium acetate, 10 $CaCl_2$, 50 $MnCl_2$, 100 RbCl, in 15 % glycerol (pH 5.8).

TBF2 contained (in mM): 10 MOPS, 75 $CaCl_2$, 10 RbCl, in 15 % glycerol (pH 6.5).

Both TBF1 and TBF2 were filtered before use and stored at room temperature.

Purification buffers

Lysis Buffer: 10 mM Tris (pH 8.0), 1 mM EDTA, 1 mM PMSF

Buffer A: 10 mM Tris (pH 8.0)

Buffer B: 10 mM Tris (pH 8.0), 2 M NaCl

Both buffers A and B were passed through nitrocellulose membrane filters (0.22 µm diameter) and degassed either by vacuum pump or sonicating water bath

Buffer C: 10 mM sodium phosphate buffer (pH 7.40). Dibasic sodium phosphate (Na_2HPO_4) was titrated against monobasic sodium phosphate (NaH_2PO_4) to achieve the desired pH.

SDS-PAGE solutions

Resolving Gel: 375 mM Tris (pH 8.8), 15 % acrylamide, 0.1 % SDS, 0.1 % ammonium persulphate, 0.004 % TEMED.

Stacking Gel: 100 mM Tris (pH 6.8), 5 % acrylamide, 0.1 % SDS, 0.1 % ammonium persulphate, 0.001 % TEMED.

Sample Buffer: 62.5 mM Tris-HCl (pH 6.8), 10 % glycerol (v/v), 2 % SDS, 5 % 2-mercaptoethanol, 0.0 5% bromophenol blue.

Running Buffer: 25 mM Tris base, 192 mM glycine, 0.1 % SDS, pH 8.3.

Staining Solution: 10 % ammonium sulphate, 0.1 % Coomassie G250, 20 % ethanol, 3 % phosphoric acid.

Western blotting

Transfer Buffer: 25 mM Tris, 192 mM glycine, 20 % methanol, topped up to 1 Litre.

Tris Buffer Saline (TBS): 10 mM Tris, pH 7.5, 150 mM NaCl

Primary antibody: Mouse anti-αSyn (BD biosciences, Oxford, UK)

Secondary antibody: Anti-mouse IgG conjugated to alkaline phosphatase (APase) (Promega, Southampton, UK).

Phosphate Buffer Saline (PBS)

PBS was prepared and sterilised in-house by the University of Warwick Department of Biological Sciences media preparation staff; containing: 137 mM NaCl, 2.7 mM KCl, 8.1 mM Na_2HPO_4, 1.5 mM KH_2PO_4

2.2.2 Protein expression

2.2.2.1 Expression plasmid

The pGS-21a (6169 bp) plasmid encoding recombinant *Human* αSyn^{Y39W} (400 bp), flanked by *Hin*dIII & *Nde*I restriction sites, was purchased from GenScript. The pGS-21a plasmid (Figure 2.1) contains a T7 promoter sequence that is specific to bacteriophage T7 RNA polymerase *(Studier and Moffatt, 1986)* and located upstream of a *lac* repressor binding site. BL21* Rosetta™(DE3) Competent Cells carry a chromosomal copy of the T7 RNA polymerase gene under control of the *lacUV5* promoter. Consequentially, the addition of IPTG (analogous to allolactose) allosterically inhibits the *lac* repressor enabling both T7 RNA polymerase synthesis and the induction of target gene transcription on the pGS-21a plasmid.

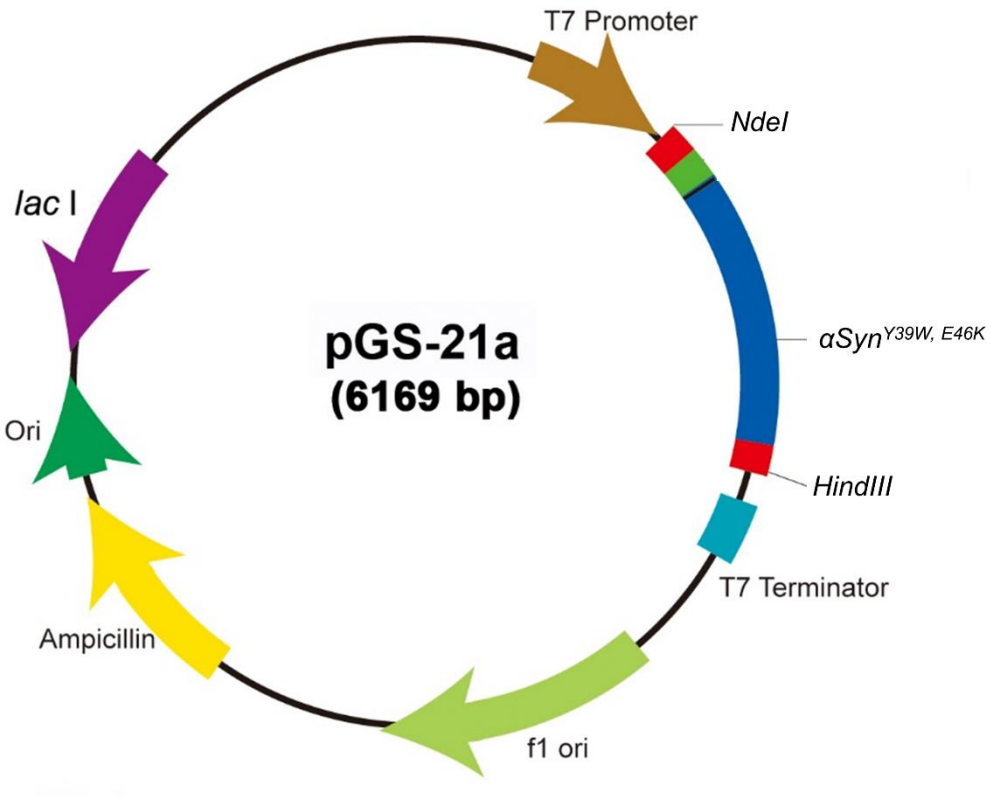

Figure 2.1 Construct of the pGS-21a plasmid encoding αSyn$^{Y39W, E46K}$. The *SNCA* gene was inserted between *Nde*I and *Hin*dIII restriction sites downstream of the T7 promoter. The plasmid also encodes genes for ampicillin resistance and the *Lac I* repressor protein.

2.2.2.2 Site-directed mutagenesis

The pGS-21a-αSyn^{Y39W} plasmid was used as a template for all mutagenesis reactions. Site-directed mutagenesis was performed by Antony Wambua (2011) using a QuikChange® II Site-Directed Mutagenesis Kit (Stratagene, Amsterdam Zuidoost, the Netherlands). The native glutamate residue at position 46 was mutated to lysine using the following primers synthesised by Integrated DNA Technologies:

E46K:
5'- TGG GTG GGC TCT AAA ACG AAA AAA GGC GTG GTG CAT GGC GTG GCG -3'
5'- CGC CAC GCC ATG CAC CAC GCC TTT TTT CGT TTT AGA GCC CAC CCA -3'

The mutagenesis reaction contained 50 ng of template DNA and 300 ng of both the forward and reverse primers, with 5 µl of 10x reaction buffer and 1.5 µl of dNTP mix (both provided by the QuikChange® II Site-Directed Mutagenesis Kit). The reaction

mixture was made up to 50 µl with sterile water after which 1 µl (2.5 units) of PfuUltra® high-Fidelity DNA polymerase was added. PCR mutagenesis was carried out in a thermal cycler under the following conditions:

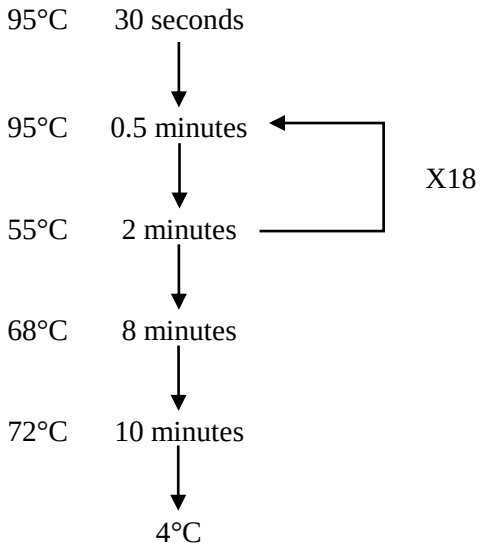

After mutagenesis, a restriction digest assay was performed on 100 ng of the plasmid DNA; digested with 1 µl of both *Hin*dIII *& Nde*I (purchased from New England BioLabs) in 1 µl of 10x NEbuffer4 (New England BioLabs), topped up to 10 µl with sterile water. The plasmid DNA was transformed into competent cells and expressed in starter cultures (as described later in Methods). Plasmid extraction and purification was performed using a QIAprep® Spin miniprep kit (Qiagen, Dusseldorf, Germany) according to the manufacturer's instructions.

2.2.2.3 DNA sequencing

DNA sequencing was carried out by the Warwick Genomics Facility; School of Life Sciences; University of Warwick. For each sequencing reaction, 500 ng of plasmid DNA was mixed with 5.5 pmol of primer in sterile water to a total volume of 10 µl. Plasmids were sequenced in both forward and reverse directions using the T7 promoter and terminator primers.

2.2.2.4 Preparation of competent cells

A single colony of BL21* Rosetta cells (plated on LB) was picked to inoculate 2.5 ml of LB medium; incubated overnight at 37 °C with shaking. This overnight culture was made up to 250 ml with LB medium containing 20 mM $MgSO_4$ and incubated as previous with aeration until the A_{600} reached between 0.4-0.6, at which time the cells

were pelleted by centrifugation at 4,500 x g for 5 minutes, 4 °C. The cells were resuspended in 0.4 volume of ice cold TBF1 and incubated for 5 minutes at 4 °C before re-pelleting using the same centrifugation settings as before. The cells were resuspended in 1/25th of the original culture volume, in ice cold TFB2 and incubated for 15 minutes at 4 °C before dividing into 200 µl aliquots, quick freezing on dry – ice, and storage at -80 °C until use.

2.2.2.5 Transformation of competent cells

E. coli BL21* Rosetta cells were used for expression of all mutagenised constructs of human αSyn. During each transformation: a 200 µl aliquot of competent cells was thawed on ice and 10 ng of plasmid DNA was added. The cell + plasmid mix was incubated on ice for 30 minutes followed by 45 seconds of heat shock at 42 °C. After a further 2 minute incubation on ice, the mix was added to 3 ml of LB medium and incubated for 45 minutes at 37 °C with shaking. A 200 µl aliquot of the transformation reaction was plated onto LB agar containing 100 µg/ml ampicillin and 20 µg/ml chloramphenicol and left at 37 °C overnight.

2.2.2.6 Expression of recombinant alpha-Synuclein

From the overnight plates, single colonies of transformed cells were picked and used to inoculate starter cultures containing 10 ml LB media with 100 µg/ml ampicillin and 20 µg/ml chloramphenicol. After 16-24 hours of incubation at 37 °C, with shaking at 150 rpm, the starter culture was used to inoculate 1 Litre of TB media; incubated at same conditions. Expression of αSyn$^{Y39W,\ E46K}$ was induced when the cells reached OD_{600} of 0.5-0.8 by adding 1 mM IPTG and incubating for 4 hours as prior to induction. Cells were pelleted by centrifugation at 10,000 x g for 15 minutes.

2.2.3 Protein purification

2.2.3.1 Cell lysis

Cell pellets were resuspended on ice in 15 ml lysis buffer and sonicated at 60 % power for 3 x 30 second bursts with 30 second intervals in between. Cellular debris was removed by centrifugation at 10,000 x g for 30 minutes (4 °C).

2.2.3.2 Heat treatment and ammonium sulphate precipitation

The supernatant was topped up to 100 ml with lysis buffer and incubated in boiling water for 10 minutes with continuous stirring. The precipitant formed during the heat treatment was removed by centrifugation at 20,000 x g for 20 minutes (4 °C). The supernatant was kept on ice and solid ammonium sulphate was added slowly over 20 minutes with continuous stirring. As the salt saturation increased to 50%, the protein content became insoluble and was collected by centrifugation as before. The mass of ammonium sulphate needed to bring a solution from 0% to 50% salt saturation was calculated as previously described *(Wingfield, 2001)*. The pellet, containing the precipitated target protein, was dialysed into buffer A using SnakeSkin™ Dialysis Tubing. To ensure complete dialysis, the pellet was resuspended in 5 ml and dialysed against 3 x 5 Litres of buffer A (refreshed after 3 hours with the final run overnight) at 4 °C with slow stirring.

2.2.3.3 Ion exchange (IEx) chromatography

After dialysis, the re-solubilised protein content was loaded onto a 10 ml Source 30Q anion exchange column (GE Healthcare, *product code: 17-1275-01*). The column was prepared with at least one column volume (CV) of buffer A before injecting the protein sample at a flow rate of 2 ml/min. Protein unable to bind to the column due to incorrect charge passed immediately off the column; this was regarded as flow through material. A linear salt gradient (Buffer B) from 0-35 % was applied over 15 CV at a flow rate of 2 ml/min, with 3 ml fractions collected (Figure 2.4a). From the fractions correlating to elution peaks of interest, 20 µl aliquots were removed for analysis by SDS-PAGE. Due to a net charge of -9, αSyn typically eluted from the column at 14-17 % buffer B (280-340 mM NaCl). Thus, the fractions under the peak corresponding to αSyn elution, confirmed by SDS-PAGE (Figure 2.4b), were pooled together and concentrated by overnight freeze drying on a Scanvac Coolsafe™ freeze dryer.

2.2.3.4 Size exclusion chromatography

The lyophilised protein was resuspended in 4 ml buffer A and loaded onto a HiPrep™ 26/60 Sephacryl™ S-300 High Resolution gel filtration column (Amersham Biosciences, Buckinghamshire, UK) equilibrated with buffer A, flow rate 2 ml/min. Fractions (3 ml) were collected across the elution profile and 20 µl aliquots were taken for analysis by SDS-PAGE. The fractions containing purified αSyn were pooled

together, freeze dried overnight, and resuspended in 5 ml buffer C with dialysis (minimum of 3 x 3 hours in 5 L buffer C). The concentration of purified αSyn was determined by A_{280} scan on NanoDrop 1000 (Thermo Scientific). The extinction coefficient of $\alpha Syn^{Y39W,\ E46K}$ was determined from the primary sequence to be 9530 $cm^{-1}M^{-1}$. The αSyn stock solution was divided into 200 µl aliquots, flash frozen and stored at -20 °C for future experimentation.

2.2.4 SDS-PAGE

Aliquots taken from various purification stages were diluted 1:1 with sample buffer and heated at 95 °C for 3 minutes before immediately loading onto a solidified stacking gel solution. The protein content of each aliquot was separated out by electrophoresis at 170 volts in solidified resolving gel solution. Gels containing protein were stained overnight in staining solution and de-stained with repeat washes in distilled water.

2.2.5 Western blot assay

After running samples on SDS-PAGE, the resolving gel was washed in transfer buffer to remove excess SDS. The gel was packed into a Mini Trans-Blot® Cell (Bio-Rad, Hertfordshire, UK) in contact with Hybond-ECL™ nitrocellulose membrane paper (Amersham Biosciences, Buckinghamshire, UK) and submerged in transfer buffer at 4 °C with continuous stirring. Electrophoresis was carried out at 100 volts for 1 hour, after which the nitrocellulose paper was washed with appropriate antibodies. In cases of dot blotting, small aliquots (2 µl) of protein samples were transferred repeatedly (20 µl in total) onto nitrocellulose paper, with each additional aliquot being placed over the last so as to concentrate the protein into a dot.

In western bot assays, the nitrocellulose paper was blocked for 1 hour in TBS + Tween20 (TBST) containing 2 % dried skimmed milk (Marvel, UK), before staining with primary and secondary antibodies. Mouse anti-αSyn antibody (BD biosciences, Oxford, UK) 1/1000 in TBST + 2 % milk was used to detect the presence of αSyn, the secondary for which was Anti-mouse IgG conjugated to alkaline phosphatase (APase) (Promega, Southampton, UK) 1/5000 in TBST+ 2 % milk. Before and after the addition of secondary antibodies, the paper was washed thoroughly in TBST to remove non-specific binding. A final wash in TBS was carried out to remove Tween20

prior to the addition of Western blue™ (Promega), a substrate for APase, that enabled visualisation of the target protein.

2.2.6 Mass spectrometry

The molecular weight of all αSyn constructs was determined using intact molecular mass analysis by means of electrospray ionisation mass spectrometry (ESI-MS), carried out on a Q-Tof Ultima Global instrument operated in positive ion mode and calibrated over a m/z range of 500-4000 using sodium iodide. Prior to analysis, aliquots (200 µl) of αSyn in buffer C were subjected to five desalting steps into 100 mM ammonium bicarbonate using BioMax Ultrafree-0.5 PBCC Centrifugal filter units and diluted to a final concentration of 10 µM in 30 % acetonitrile/1 % formic acid. The spectrum was deconvoluted in cases where multiply charged protein species were observed.

2.2.7 Circular dichroism (CD) spectroscopy

Far-UV CD spectra (190-260 nm) were measured on a JASCO J-815 spectropolarimeter (JASCO, Essex, UK) using 1 mm path length quartz cuvettes. The CD chamber was purged with nitrogen gas and maintained at 20 ± 2 °C by a PFD-425S/15 Peltier temperature controller. The scanning parameters were set as follows: Scanning speed = 100 nm/min, Time constant = 1 second, and bandwidth = 1 nm. Spectra were recorded to a resolution of 0.5 nm and an accumulation of 16 – 32 scans were averaged per spectrum. The corresponding appropriate buffer backgrounds were subtracted from the final spectra. The High Tension (HT) was monitored in parallel to the spectra to make sure that the salt content in the samples did not interfere with CD analysis. Samples were dialysed in distilled water to prevent the HT from exceeding 600 V.

2.2.8 Fluorescence spectroscopy

Fluorescence spectra were recorded on a Photon Technology International spectrofluorometer with a 4mm path length quartz cuvette. The sample was excited at 295 nm (2 nm bandwidth) and the emission spectra were recorded from 300 to 450 nm (2 nm bandwidth) with a resolution of 1 nm and an integration time of 1 second. Each spectrum was the average of 4 scans from which the appropriate buffer background was subtracted.

2.3 Results

2.3.1 Human αSyn containing point mutations at E46K and Y39W

To ensure that only the specified mutations of interest were present, the target gene was sequenced and aligned with the human wild type (wt) αSyn sequence (Accession No. – P37840) using BLASTn and BLASTp online alignment tools (Figure 2.2). Aside from the two intended mutations at E46K and Y39W, no other unwanted mutations were present throughout the primary sequence, thus providing the construct αSyn$^{Y39W, E46K}$.

a

Score	Expect	Identities	Gaps	Strand
682 bits(369)	0.0	403/420(96%)	0/420(0%)	Plus/Plus

```
Query  1    ATGGATGTGTTTATGAAAGGCCTGAGCAAAGCGAAAGAAGGCGTGGTGGCGGCGGCGGAA  60
            ||||||||||||||||||||||||||||||||||||||||||||||||||||||||||||
Sbjct  1    ATGGATGTGTTTATGAAAGGCCTGAGCAAAGCGAAAGAAGGCGTGGTGGCGGCGGCGGAA  60

Query  61   AAAACCAAACAGGGCGTGGCGGAAGCGGCGGGCAAAACCAAAGAAGGCGTGCTGTGGGTG  120
            ||||||||||||||||||||||||||||||||||||||||||||||||||||||| |||
Sbjct  61   AAAACCAAACAGGGCGTGGCGGAAGCGGCGGGCAAAACCAAAGAAGGCGTGCTGTATGTG  120

Query  121  GGCTCTAAAACGAAAAAAGGCGTGGTGCATGGCGTGGCGACCGTGGCGGAAAAAACCAAA  180
            |||   ||||| ||| ||||||||||||||||||||||||||||||||||||||||||||
Sbjct  121  GGCAGCAAAACCAAAGAAGGCGTGGTGCATGGCGTGGCGACCGTGGCGGAAAAAACCAAA  180

Query  181  GAACAGGTGACCAATGTGGGCGGCGCGGTGGTTACCGGTGTGACCGCCGTGGCCCAGAAA  240
            ||||||||||||| |||||||||||||||| ||||| |||||||| ||||| ||||||
Sbjct  181  GAACAGGTGACCAACGTGGGCGGCGCGGTGGTGACCGGCGTGACCGCGGTGGCGCAGAAA  240

Query  241  ACCGTGGAAGGCGCGGGTAGCATTGCCGCCGCCACCGGTTTTGTGAAAAAAGATCAGCTG  300
            |||||||||||||||| |||||||| || || ||||| ||||||||||||||||||||||
Sbjct  241  ACCGTGGAAGGCGCGGGCAGCATTGCGGCGGCGACCGGCTTTGTGAAAAAAGATCAGCTG  300

Query  301  GGCAAAAACGAAGAAGGCGCGCCGCAGGAAGGCATTCTGGAAGATATGCCGGTGGATCCG  360
            ||||||||||||||||||||||||||||||||||||||||||||||||||||||||||||
Sbjct  301  GGCAAAAACGAAGAAGGCGCGCCGCAGGAAGGCATTCTGGAAGATATGCCGGTGGATCCG  360

Query  361  GATAACGAAGCGTATGAAATGCCGAGCGAAGAAGGCTATCAGGATTATGAACCGGAAGCG  420
            ||||||||||||||||||||||||||||||||||||||||||||||||||||||||||||
Sbjct  361  GATAACGAAGCGTATGAAATGCCGAGCGAAGAAGGCTATCAGGATTATGAACCGGAAGCG  420
```

b

Score	Expect	Method	Identities	Positives	Gaps
267 bits(683)	2e-97	Compositional matrix adjust.	138/140(99%)	140/140(100%)	0/140(0%)

```
Query  1    MDVFMKGLSKAKEGVVAAAEKTKQGVAEAAGKTKEGVLWVGSKTKKGVVHGVATVAEKTK  60
            MDVFMKGLSKAKEGVVAAAEKTKQGVAEAAGKTKEGVL+VGSKTK+GVVHGVATVAEKTK
Sbjct  1    MDVFMKGLSKAKEGVVAAAEKTKQGVAEAAGKTKEGVLYVGSKTKEGVVHGVATVAEKTK  60

Query  61   EQVTNVGGAVVTGVTAVAQKTVEGAGSIAAATGFVKKDQLGKNEEGAPQEGILEDMPVDP  120
            EQVTNVGGAVVTGVTAVAQKTVEGAGSIAAATGFVKKDQLGKNEEGAPQEGILEDMPVDP
Sbjct  61   EQVTNVGGAVVTGVTAVAQKTVEGAGSIAAATGFVKKDQLGKNEEGAPQEGILEDMPVDP  120

Query  121  DNEAYEMPSEEGYQDYEPEA  140
            DNEAYEMPSEEGYQDYEPEA
Sbjct  121  DNEAYEMPSEEGYQDYEPEA  140
```

Figure 2.2 BLASTn (a) and BLASTp (b) alignment of αSyn^{Y39W,E46K} template DNA (Query) with Human wild-type αSyn (#P37840) (Sbjct). All non-matching bases have no impact on the transcribed protein sequence aside from the intended point mutations Y39W and E46K (highlighted).

2.3.2 Expression of $\alpha Syn^{Y39W, E46K}$

The expression of αSyn was determined after cell lysis, and monitored throughout purification, using SDS-PAGE (figure 2.3). Due to its unfolded nature, αSyn migrated slower on an SDS-PAGE than the standard protein markers of similar molecular weight. The αSyn band appears closer to 20 kDa on SDS – PAGE despite a Mw of ~14.4 kDa.

2.3.3 Ion exchange (IEx) chromatography

From the IEx chromatogram (figure 2.4a), it is seen that the immediate flow through (FT) contained large amounts of protein corresponding to the portion of the total protein which was unable to bind to the column, as shown by SDS-PAGE (figure 2.4b). Unseen in the FT is the αSyn band, determined by anti-αSyn western blot (figure 2.4c), which has effectively bound to the column. Any αSyn immunoreactivity in the FT is likely the result of column saturation or small amounts of protein degradation. The discrete elution peak for αSyn displacement was at 280-340 mM NaCl (14-17 % buffer B); separate to other bound proteins.

2.3.4 Size exclusion chromatography

The size exclusion column was able to further purify αSyn by separating out proteins of similar ionic strength according to size. In the elution profile (Figure 2.5a), peaks between 50-125 ml were high Mw proteins while peaks after 250 ml were shown by SDS-PAGE to be degradation products (Figure 2.5b). The peak containing αSyn eluted between 90-110 ml, independently of other components.

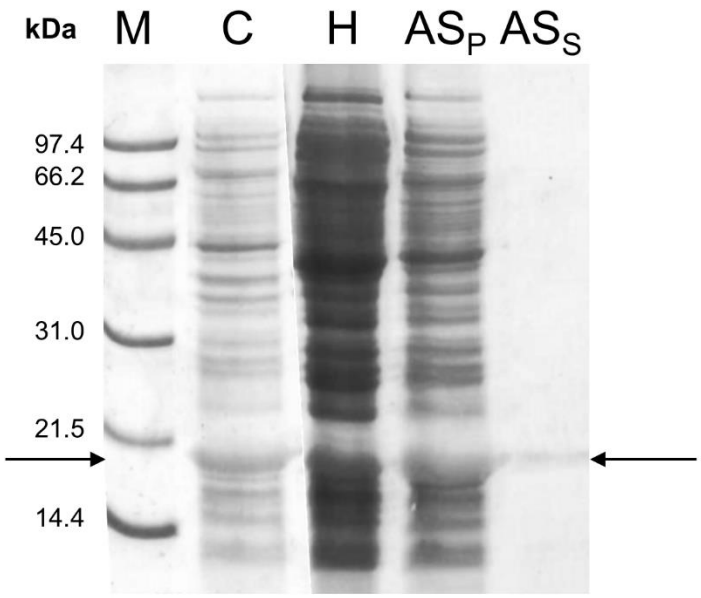

Figure 2.3 Expression, heat treatment and ammonium sulphate precipitation of αSyn. SDS-PAGE analysis of αSyn expression after cell lysis (C). The pellet after heat treatment (H) shows a large amount of cellular protein was removed in this step. During ammonium sulphate precipitation, αSyn was collected in the pellet (AS_P) while the supernatant (AS_S) holds very little. The precipitated αSyn was re-solubilised by dialysis and purified by ion exchange chromatography. Standard molecular weight markers are shown on left side (M). The bands corresponding to αSyn is indicated by the arrows.

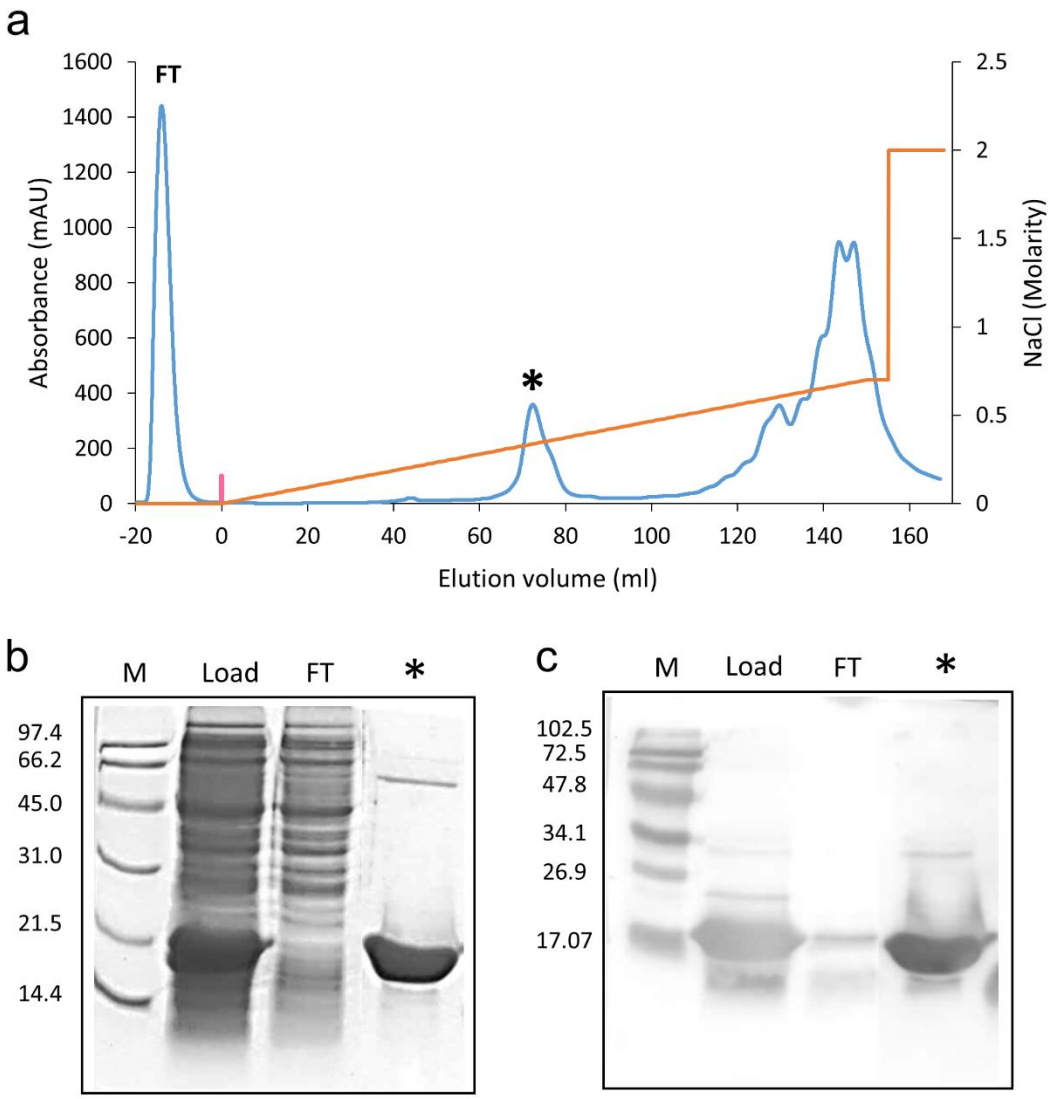

Figure 2.4 Purification of αSyn by ion exchange (IEx) chromatography. (a) The elution profile (blue) shows various bound protein, including αSyn (*), are displaced along the salt gradient (orange, 0-0.7 M). An SDS-PAGE (b) and anti-αSyn western blot (c) of the sample loaded onto the IEx column (Load), the immediate flow through (FT) prior to the beginning of the salt gradient (pink, 0 ml) and pooled fractions containing αSyn; corresponding to peak in (a).

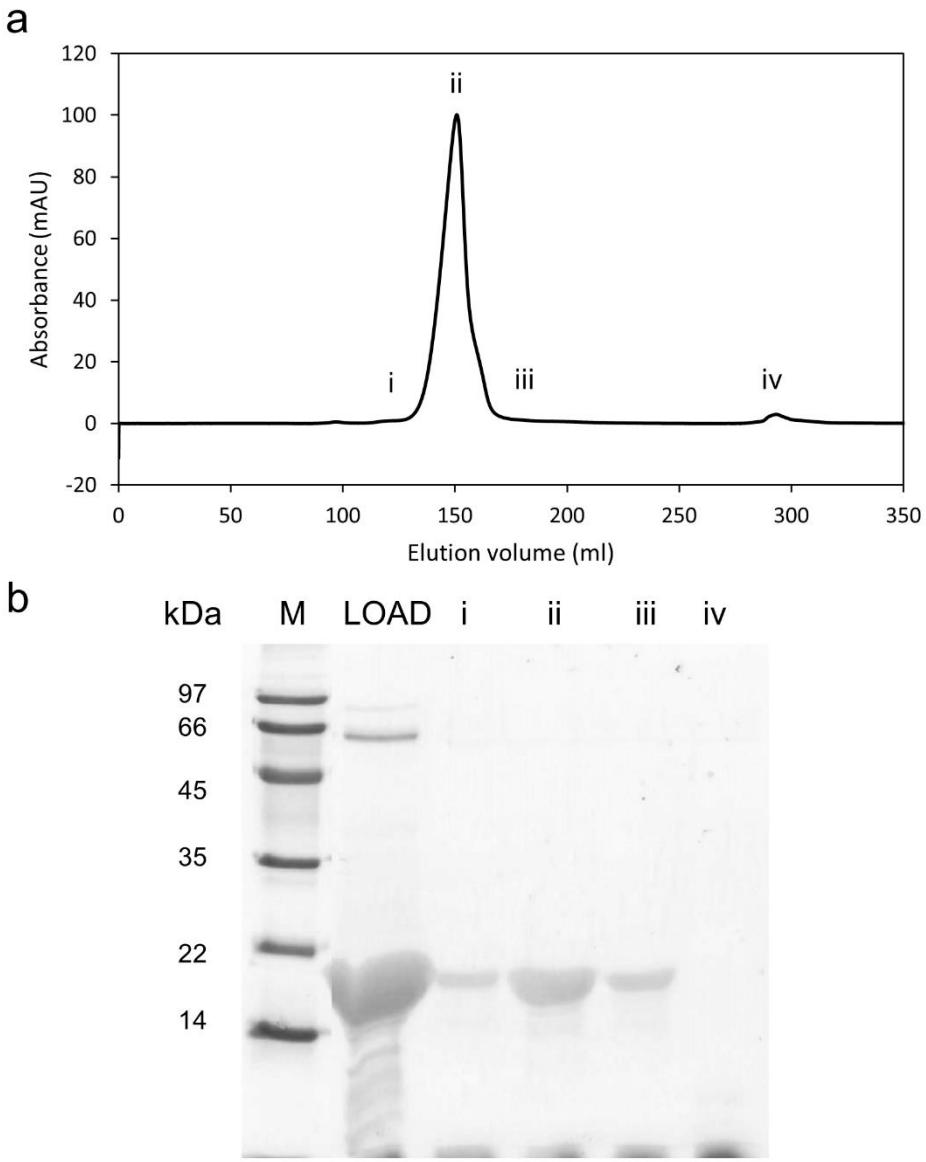

Figure 2.5 Purification of αSyn from proteins of similar ionic strength by size exclusion chromatography. (a) The elution profile for αSyn on size exclusion chromatography. (b) SDS-PAGE illustrating the protein content at various points throughout the elution profile marked by i-iv.

2.3.5 SDS-PAGE and western blot of purified $\alpha Syn^{Y39W, E46K}$

Recombinantly expressed human $\alpha Syn^{Y39W, E46K}$ was run on SDS – PAGE and western blot (figure 2.6) to assess purity. According to SDS-PAGE, αSyn purity was consistently higher than 98 % with no other distinct protein bands detected. Western blot revealed, in addition to the monomeric protein, some heavier αSyn-positive bands that could indicate the formation of dimer, trimer or tetramer. These formations,

however, were not abundant enough to be detected on SDS-PAGE suggesting them to be uncommon formations.

2.3.6 Mass spectrometry

The molecular weight of $\alpha Syn^{Y39W, E46K}$ was confirmed by electrospray ionisation mass spectrometry (ESI-MS) (figure 2.7). Accounting for the two point mutations, $\alpha Syn^{Y39W, E46K}$ has a calculated molecular weight of 14,482 Da which is consistent with the experimentally determined value.

2.3.7 Circular dichroism (CD) spectroscopy

The secondary structure of purified $\alpha Syn^{Y39W, E46K}$ was determined by CD spectroscopy. The far-UV CD spectrum (figure 2.8) shows a gradual negative trend in molar ellipticity between 260 and 220 nm followed by a large negative peak at 195 nm, consistent with the widely accepted belief that the predominating structure of αSyn monomer is unfolded *(Eliezer et al., 2001; Fauvet et al., 2012)*. Previous studies on αSyn have concluded that incorporating tryptophan at residue 39 has no impact on monomer secondary structure, aggregation kinetics or fibril structure *(Dusa et al., 2006; van Rooijen et al., 2009b).*

2.3.8 Fluorescence spectroscopy

In an unfolded state, the tryptophan at position 39 is freely available to the environment producing a fluorescence maxima at ~350 nm *(Pfefferkorn and Lee, 2010).* The fluorescence spectra for $\alpha Syn^{Y39W, E46K}$ (figure 2.9) illustrates the solvent exposed properties of tryptophan-39 in an unfolded protein.

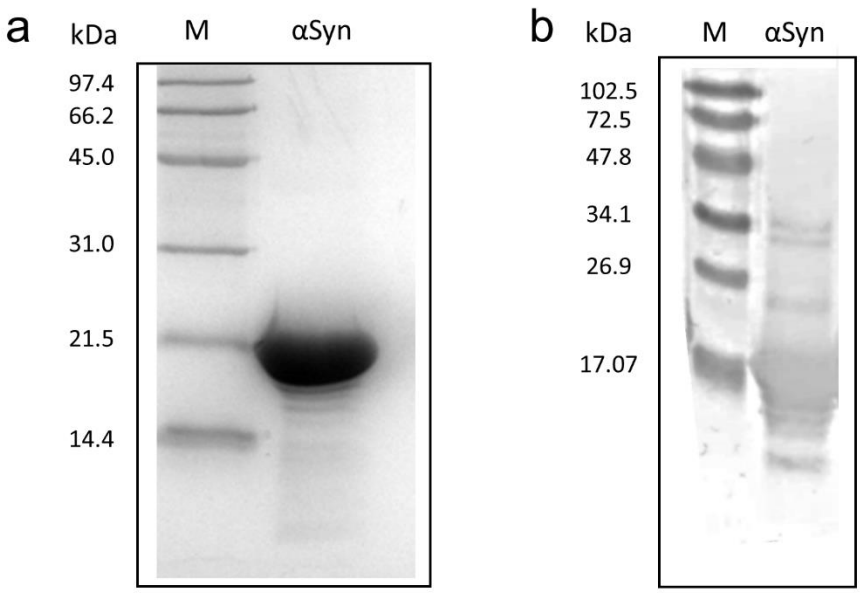

Figure 2.6 SDS-PAGE and western blot of purified human αSyn. Purified $\alpha Syn^{Y39W, E46K}$ as shown by (a) SDS-PAGE and (b) anti-αSyn western blot.

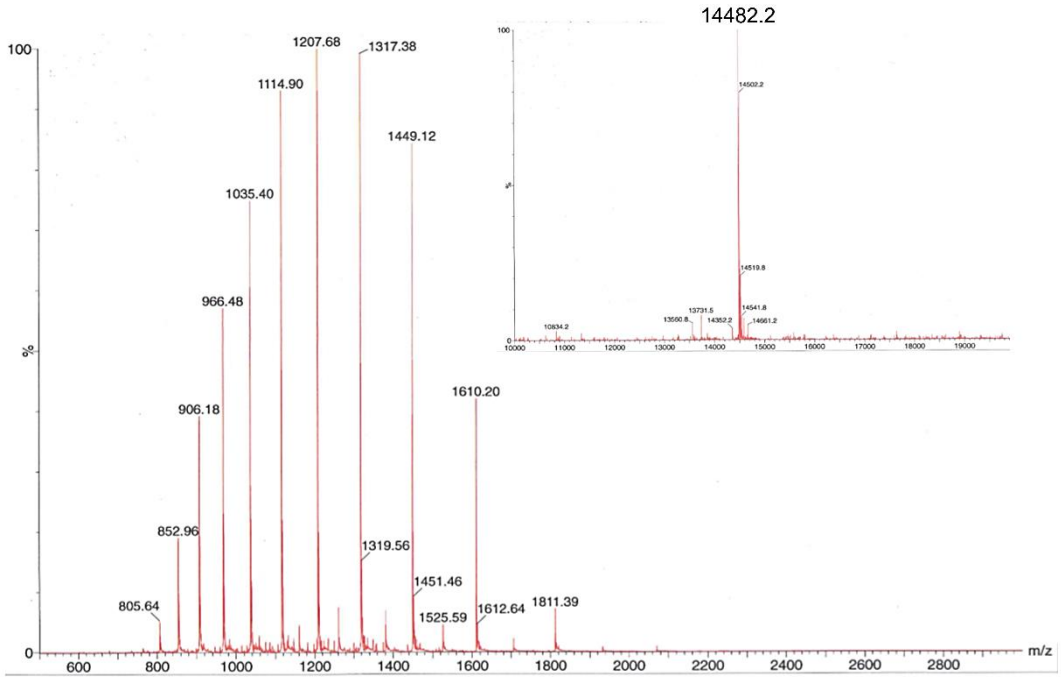

Figure 2.7 ESI-mass spectrum of purified human αSyn. The mass spectrum of $\alpha Syn^{Y39W, E46K}$. The inset shows the deconvoluted spectrum with calculated mass of 14482.2 Da**.**

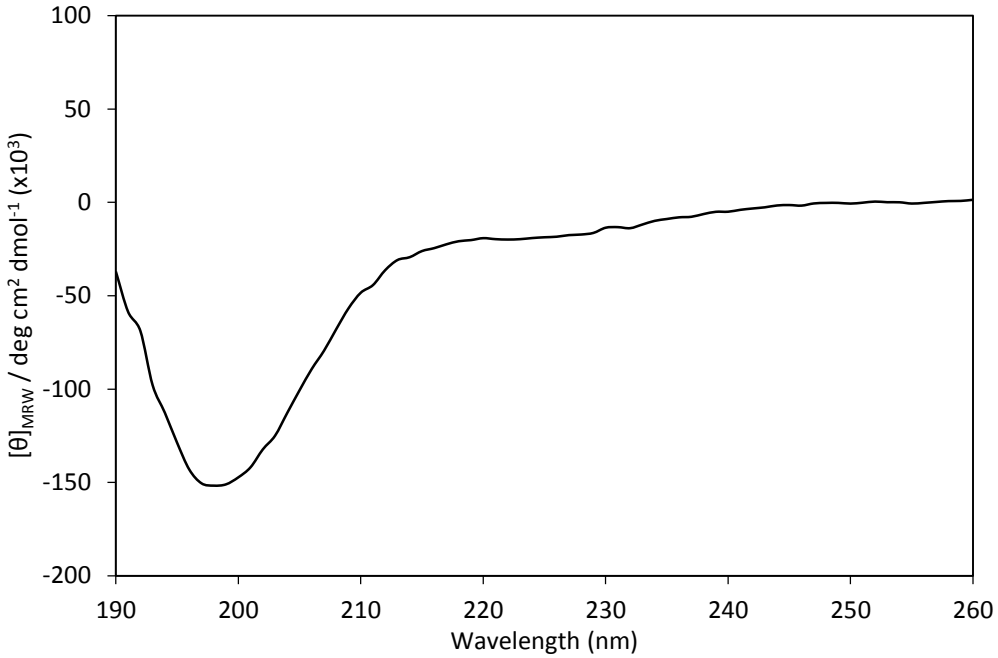

Figure 2.8 The secondary structure of αSyn$^{Y39W, E46K}$. The far-UV CD spectrum of purified αSyn as an unfolded monomer.

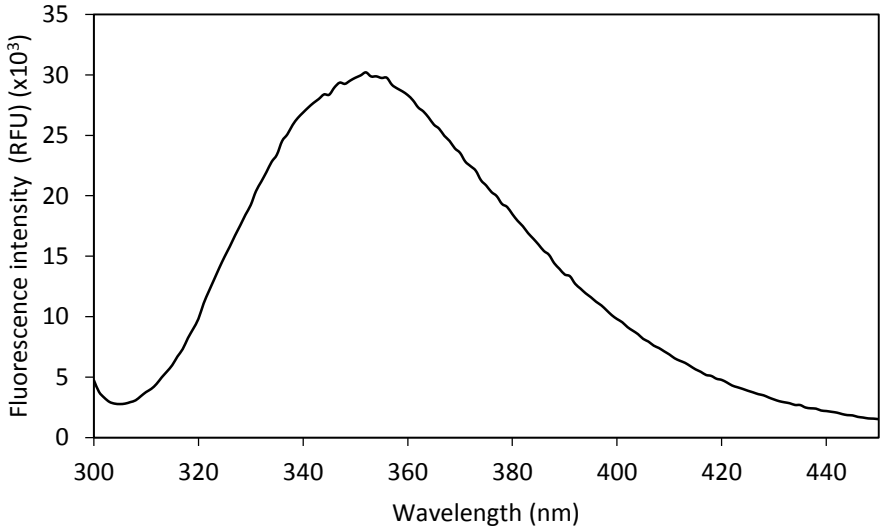

Figure 2.9 Fluorescence properties of αSyn$^{Y39W, E46K}$. The tryptophan at position 39 has a fluorescence maxima at ~350 nm, indicative of a solvent exposed residue. This is in accordance with monomeric αSyn being unfolded.

2.4 Summary

Recombinant human αSyn$^{Y39W,\ E46K}$ has been expressed and purified from BL21* Rosetta cells in preparation for future research. Through site-directed mutagenesis two point mutations were introduced at Try39Trp and Glu46Lys. The replacement of a tyrosine with tryptophan was intended to give intrinsic fluorescence properties within the N-terminal region of the protein, thus enabling one to study changes in the local environment during the aggregation process. This particular region is of great interest as it is believed to play an important physiological role in lipid membrane interaction *(Davidson et al., 1998)* and pathological role in modulating fibril formation *(Kessler et al., 2003; Greenbaum et al., 2005; Vamvaca et al., 2009)*. The second mutation, glutamate to lysine, is a well characterised disease-associated mutation found in familial cases of PD *(Choi et al., 2004; Zarranz et al., 2004)*. The incorporation of a mutation linked to early onset PD will promote αSyn aggregation *(Greenbaum et al., 2005)* and facilitate the production of toxic oligomers *(Fredenburg et al., 2007; Winner et al., 2011)*.

This αSyn construct was expressed and purified for the purpose of structurally characterising oligomers isolated from the aggregation pathway (chapter 3). Isolated and characterised αSyn$^{Y39W,\ E46K}$ oligomers are to be intracellularly injected into pyramidal neurons and electrophysiological recordings taken (chapter 4). Measuring the changes in neuronal parameters over time in the presence or absence of αSyn oligomer (chapter 5) will provide detailed insight into the mechanism of toxicity and potentially link structural elements of αSyn to pathological function. Note; in all future chapters the construct αSyn$^{Y39W,\ E46K}$ will be referred to only as αSyn, since no other constructs are used in this thesis.

3 Development of alpha-Synuclein oligomerisation protocols and structural characterisation of oligomeric species

3.1 Introduction

The association between αSyn and PD came initially from identifying the protein as the main component in Lewy bodies. Indeed, the detection of these αSyn-containing aggregates in various brain regions remains a clinical hallmark for classifying the progression of several neurodegenerative disorders collectively termed Synucleinopathies. In some cases of familial PD, point mutations in αSyn (A53T, A30P, E46K, H50Q and G51D) *(Polymeropoulos et al., 1997; Kruger et al., 1998; Zarranz et al., 2004; Lesage et al., 2013; Proukakis et al., 2013)* and gene multiplications *(Fuchs et al., 2007)* promote the early onset of symptoms. Increasing evidence, however, suggests that soluble αSyn oligomers are more neurotoxic and better correlate with PD pathology than the larger insoluble aggregates into which they form *(Haass and Selkoe, 2007).*

Insoluble fibrils have instead been theorised to provide a neuroprotective function by removing smaller toxic aggregates from the cytosol. In support of this, αSyn mutants that are able to rapidly form fibrils are less toxic than those that rapidly form oligomers *(Winner et al., 2011)*. Fibril fragmentation on the other hand enhances cellular toxicity by increasing the fibril load and seeding further aggregation *(Xue et al., 2009).* Fragmentation can occur *in vivo* as the result of direct mechanical stress, thermal motion or the activity of chaperones such as Hsp104, which is known to fragment fibril samples *(Shorter and Lindquist, 2004)*. Fibril fragmentation may also release soluble oligomeric components, although this concept has yet to be investigated in detail.

There have been many studies on αSyn oligomers, with the oligomerisation protocols varying considerably regarding: protein concentration *(Volles et al., 2001; Danzer et al., 2007),* incubation conditions *(Lashuel et al., 2002b; Lorenzen et al., 2014c),* buffer content *(Hoyer et al., 2002)* and the use of inducers such as metal ions *(Binolfi et al., 2006; Brown, 2009)* or dopamine *(Cappai et al., 2005)*. Unsurprisingly, the oligomers produced from these different conditions show variability in terms of size, structure and toxicity.

Annular oligomers in particular have been shown to form membrane inserting pore-complexes that can induce cell death through various mechanisms including membrane permeabilisation *(Volles and Lansbury, 2002; Schmidt et al., 2012; Tosatto et al., 2012)*, Ca^{2+} influx *(Danzer et al., 2007)*, synaptic alterations *(Diogenes et al., 2012; Pacheco et al., 2015)* and mitochondrial dysfunction *(Guardia-Laguarta et al., 2014)*. However, the precise mechanism of toxicity and its relation to oligomer structure remains unknown and a vital point for understanding αSyn pathology.

In this chapter, I examine the time course of αSyn aggregation under varying incubation conditions and monitor for the appearance of oligomers using dot blot assays. Soluble oligomers, *mOligomers*, were identified and isolated from the early stages of aggregation. As aggregation was allowed to continue for longer, oligomers became undetectable and large amyloid fibrils predominated. Fragmentation of these fibrils by sonication recovered a mixture of soluble aggregates among which was a separate population of soluble oligomers; *fOligomers*. Secondary structure analysis, using CD and fluorescence spectroscopy, suggests that *mOligomers* have a greater helical content than *fOligomers*. Both oligomeric species were found to be ring-like in shape and similar in size, yet had opposing effects on seeding αSyn aggregation.

3.2 Methods

3.2.1 Dot blot assay

Small aliquots (2 µl) of protein were absorbed repeatedly (20 µl in total) onto nitrocellulose paper, with each subsequent aliquot being placed over the last so as to concentrate the protein into a dot. Once dry, the paper was washed with primary and secondary antibodies following the same protocol described previously for western blotting (see chapter 2, methods).

Rabbit polyclonal A11 antibody (Invitrogen, Paisley, UK) 1/1000 in TBST+ 2% milk was used to detect the presence of oligomeric αSyn, the secondary for which was anti-rabbit IgG conjugated to APase (Promega) 1/5000 in TBST+ 2% milk. Rabbit polyclonal A11 antibodies specifically target a structural epitope that is present in oligomeric αSyn but absent in monomeric or fibrillar αSyn *(Kayed et al., 2003; Glabe, 2004)*. Bovine Serum Albumin (BSA) was used as a negative control to test for background levels of non-specific immunoreactivity.

3.2.2 Oligomerisation protocol according to *Lashuel et al. (2002)*

In this protocol lyophilised αSyn was resuspended in PBS (pH 7.4) at a final concentration of 300μM and incubated on ice for 60 minutes. The protein was further stored for four weeks at 4 °C and monitored periodically by A11 dot blot to assay for the appearance of oligomers. At four weeks the sample was centrifuged (16,000 x g; 5 min) and passed through a 0.22 μm nylon filter to remove insoluble components. The supernatant was loaded onto a Superdex 200 HR gel filtration column and the fractions corresponding to oligomers were collected.

3.2.3 Oligomerisation protocol according to *Winner et al. (2011)*

Monomeric αSyn (300 μM in PBS + 0.01 % sodium azide, pH 7.4) was incubated for six days at 37 °C with gentle shaking at 150 rpm. Similar to previous, the aggregation reaction was monitored regularly by A11 dot blot to check for the presence of oligomer. As an alternative to using centrifugal filters, insoluble aggregates were removed by ultracentrifugation at 100,000 x g for 10 minutes and the supernatant loaded onto a Superdex 200 gel filtration column to separate soluble oligomers from monomer.

3.2.4 Oligomerisation protocol according to *Lorenzen et al. (2014)*

Monomeric αSyn (in PBS + 0.01 % azide, pH 7.4) was prepared at the much higher concentration of 12 mg/ml (800-900 μM) and incubated at 37 °C with 900 rpm agitation; using an Eppendorf Thermomixer Compact (Fisher Scientific). With elevated concentration and shaking speed, aggregation is reported to take place within several hours. As such, oligomerisation was monitored every 30 minutes by A11 dot blot over a 6 hour period, after which insoluble aggregates were removed by ultracentrifugation and soluble oligomers purified by Superdex 200 gel filtration.

3.2.5 Fibril preparation, sonication and *fOligomers*

Fibrilisation was carried out under the same conditions described in *Lorenzen et al., (2014)* with the incubation time extended to overnight. Fibrils were pelleted by centrifugation at 16,000 x g for 6 minutes, washed repeatedly in PBS and used for spectroscopic analysis and electron microscopy.

To determine optimal sonication parameters, resuspended fibrils were kept on ice and subjected to probe sonication (VCX 750 sonicator) at either 20, 40, or 60 % power and for 5, 30, or 60 seconds (a total of 9 separate conditions). The resulting fibril fragments were imaged using TEM and assayed by A11 dot blot for the presence of oligomer. The average length of fibril fragments (n = 200 per sonication condition) was determined by blind analysis of TEM images using ImageJ Figi software. Insoluble fragments were pelleted by ultracentrifugation (100,000 x g for 10 minutes) and the supernatant loaded onto Superdex 200 gel filtration column. Oligomers purified from sonicated fibrils were found separate to oligomers purified directly from monomers and thus were termed *fOligomers*.

3.2.6 Ultracentrifugation

Insoluble aggregates were separated from soluble oligomer and monomer by high-speed centrifugation. Mixtures of αSyn aggregates produced from any of the aforementioned protocols were transferred into a TLA-100.3 fixed angle rotor (Beckman Coulter) and placed in a Beckman Optima MAX benchtop ultracentrifuge (Beckman Coulter). Samples were ultracentrifuged for 10 minutes at 100,000 x g, at 4 °C under vacuum. The supernatant was carefully isolated for gel filtration while the pellet was repeat washed in PBS and stored at 4 °C until use.

3.2.7 Superdex 200 high resolution gel filtration

The supernatant from ultracentrifuged samples was loaded onto a Superdex 200 high resolution gel filtration column (Amersham Biosciences, Buckinghamshire, UK) equilibrated with PBS at a flow rate 0.5 ml/min. Fractions (0.5 ml) containing αSyn monomer or oligomer were collected from separate elution peaks. Oligomeric αSyn was concentrated and used within 24 hours of purification. Fractions containing monomeric αSyn were recycled into the αSyn stock (see chapter 2 Methods) for further use in oligomerisation reactions.

3.2.8 Concentration and storage of oligomers

Fractions containing oligomeric αSyn were concentrated using Amicon Ultra – 0.5 ml centrifugal filters (Merck Millipore): centrifugal filtration was carried out at 14,000 x g for 30 minutes and sample concentrate was recovered by a 1,000 x g spin for 2 minutes; in accordance with manual instructions. Concentrated αSyn oligomer

(between 5-20 μM in PBS, pH 7.4) was stored at 4 °C and used for structural and electrophysiological experimentation within 24 hours of purification.

3.2.9 Thioflavin T (ThT) spectroscopic assay

Lyophilised αSyn monomer was resuspended in PBS (pH 7.4) + 0.01 % sodium azide to a final concentration of 10 mg/ml. A stock solution of Thioflavin T (ThT) was added (1/50 dilution) to give a final concentration of 20 μg/ml. The αSyn + ThT sample was passed through a syringe filter (pore size 0.25 μm) to remove aggregates and loaded into a NUNC™ MicroWell™, optical-bottom, 96-well plate (Thermo Scientific). The 96-well plate was loaded into a CLARIOstar microplate reader (BMG Labtech) and incubated at 37 °C with constant orbital shaking (~700 rpm). Fluorescence measurements were taken every 6 minutes over a total of 9 hours using the following optical settings: excitation λ = 444 nm, emission λ = 481 nm, excitation/emission bandwidth = 10 nm, gain = 1000 and focal height = 3.1 mm.

In seeding experiments, either *mOligomer* or *fOligomer* were added to filtered αSyn (final concentration 0.1 mg/ml) immediately prior to the start of recording. All experiments were run in three separate wells with 100 μl total volume per well. Separate wells used for blanking contained equivalent buffer conditions minus αSyn.

3.2.10 Analytical Ultracentrifugation (AUC)

αSyn samples were prepared < 24 hrs in advance and transported on ice to the Analytical Ultracentrifugation (AUC) laboratory based at the University of Birmingham School of Biosciences. Collaborators; Mrs Rosemary Parslow and Dr Sarah Lee, at the Birmingham Biophysical Characterisation Facility, operated a ProteomeLab™ XL-I (Beckman Coulter) protein characterisation system. Samples were diluted in PBS to give a final concentration of 0.1-0.2 mg/ml; as determined by single scan (A_{280}) at 3000 rpm. Sedimentation coefficient was determined from a total of 285 scans per sample. AUC was carried out at 20 ± 0.1 °C in sedimentation velocity mode. The heterogeneity of oligomer samples was assessed by comparing the peak width at 50 % height.

3.2.11 Transmission Electron Microscopy (TEM)

Copper EM grids; 400 mesh with formvar carbon support film (Agar Scientific), were hydrophilised in a K100x Glow Discharger (Quorum Technologies) set to pass a 20

mA current for 30 seconds under vacuum**.** Protein samples, diluted to 75-100 μg/ml in distilled water, were aliquoted (10 μl) onto the prepared grids. Protein was adsorbed over 60 seconds after which excess liquid was removed using filter paper and replaced by an equal volume of 2 % uranyl acetate for a further 60 seconds. After removing the negative stain the grids were stored until use. Images were collected on a JEOL JEM2011 CyroTransmission electron microscope with 200 kV acceleration. Large fibril structures were imaged under low magnification (15-25 k) while small oligomeric structures were imaged at higher magnification (40-120 k) and analysed semi – automatically using ImageJ software.

3.3 Results

3.3.1 Comparing and optimising protocols for αSyn oligomerisation

The starting protocol for αSyn oligomerisation was derived from the Lansbury research group publication in 2002, in which soluble ring-like oligomers were characterised for the first time by single-particle averaging of TEM images *(Lashuel et al., 2002b).* Incubation was carried out over four weeks at 4 °C, during which aliquots were taken periodically and assayed by dot blot using an oligomer-specific antibody (A11). No oligomers were detected for the first three weeks and while a positive blot was seen after four weeks (figure 3.1) the size of the oligomer peak on gel filtration was very small (figure 3.2a). The final oligomer yield was 0.1-0.5 % of total protein; insufficient amounts for electrophysiological experimentation. In addition, the incubation time was inefficiently long to allow for continuous experimentation.

Thus, alternative protocols were sourced to give better yields in a shorter time. Providing evidence for oligomer-specific toxicity *in vivo, Winner et al. (2011)* employed an αSyn aggregation protocol that produced annular oligomers comparable to those from Lansbury's group. This protocol was chosen for comparison as both starting concentration and buffer were held the same as in *Lashuel et al. (2002)* (300 μM in PBS, pH 7.4) with the addition of 0.01 % sodium azide to avoid bacterial contamination. Instead of amending the starting conditions, the incubation environment was altered to improve oligomer yield and reduce waiting time.

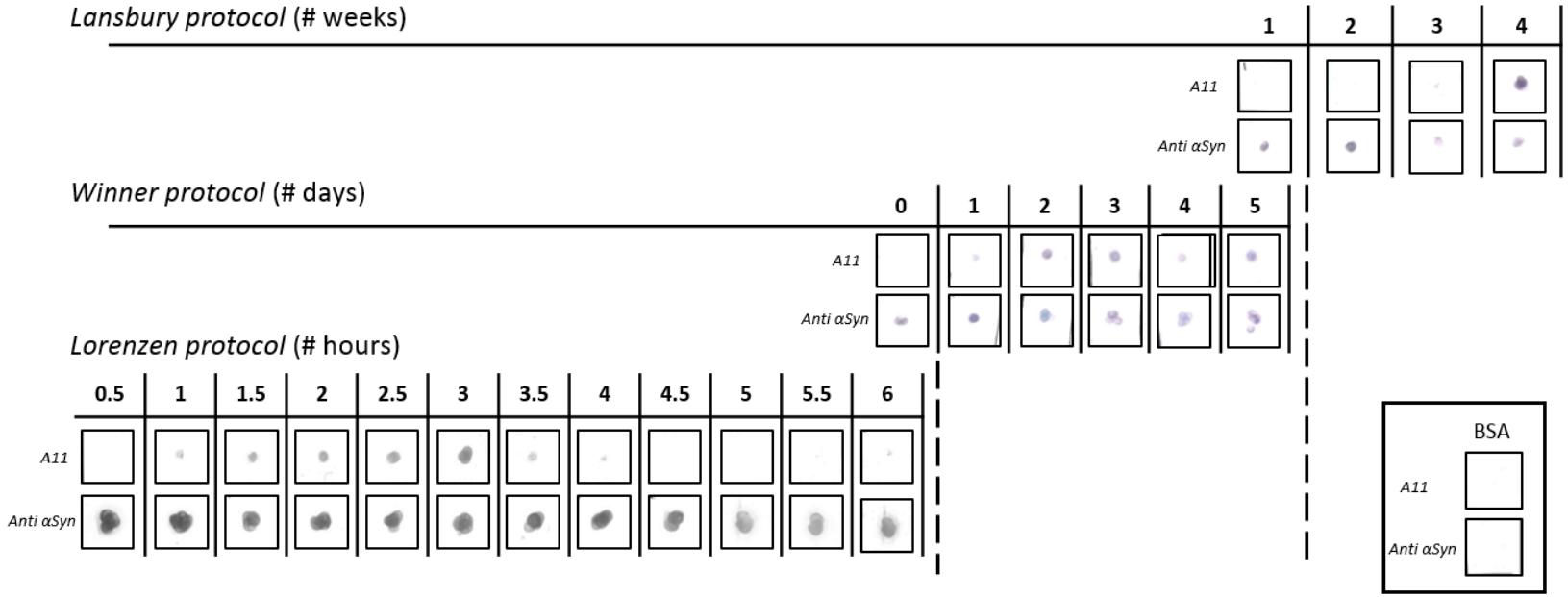

Figure 3.1 Dot blot time course of oligomerisation. Oligomerisation was carried out following protocols from (top) the Lansbury group (*Lashuel et al., 2002*), (middle) *Winner et al., 2011* and (bottom) *Lorenzen et al., 2014*. At the various time points described for each protocol (# weeks/days/hours) the reaction was assayed for the presence of oligomer using A11 antibodies (top row in each time course). In each protocol oligomers appear gradually, however, the speed of oligomerisation is exponentially different depending on the protocol used. To make sure that αSyn had not degraded at any point, reactions were monitored with anti αSyn antibodies (bottom row in each time course); these remained positive for all time points. BSA was used as a negative control for each dot blot to measure background immunoreactivity (inset, bottom right).

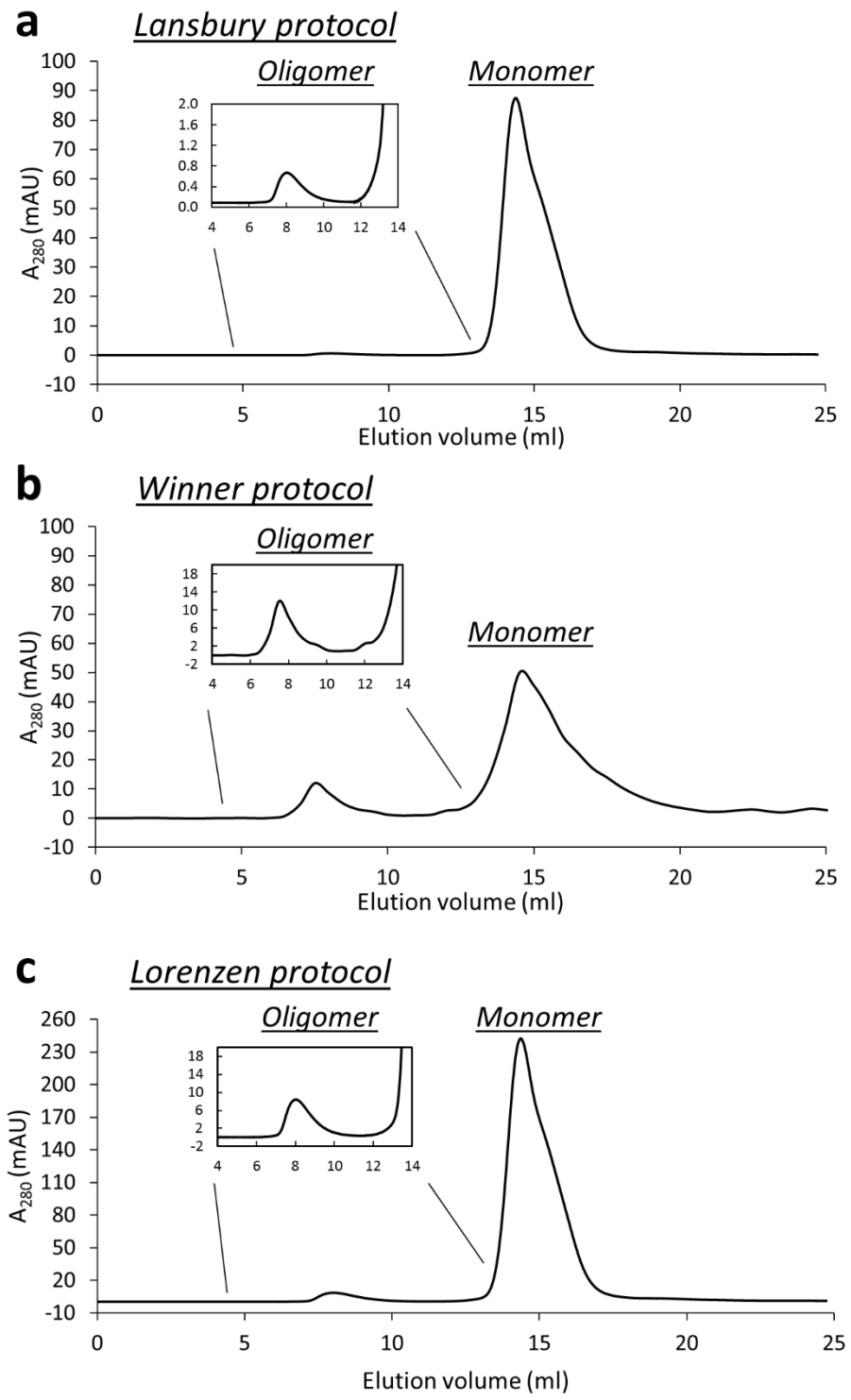

Figure 3.2 Separation of αSyn monomer and oligomer by Superdex 200 gel filtration. Oligomerisation was carried out according to (a) the *Lansbury* group protocol; 4 weeks incubation at 4 °C (b) the *Winner et al.*, protocol; 2 days at 37 °C, 150 rpm or (c) the *Lorenzen et al.*, protocol; 2 hours at 37 °C, 900 rpm.

Monomeric αSyn was incubated at 37 °C with gentle shaking (150 rpm) for 6 days. At this higher temperature and agitation, αSyn aggregation proceeded more rapidly and the reaction mixture turned cloudy with insoluble content; marking the production of fibrils. The aggregation of αSyn from unfolded monomer into β-sheet fibrils was observed directly by CD spectroscopy of the total reaction mixture (figure 3.3a). Similarly, tryptophan fluorescence became progressively blue-shifted over time as the exposed amino acid was internalised; indicating protein folding (figure 3.3b). Amidst these large aggregates, oligomers were detected by A11 dot blot within days rather than weeks (figure 3.1). Soluble oligomers were separated from fibrils by ultracentrifugation and from monomers by gel filtration. Only soluble oligomers, not monomers or fibrils, remained A11 positive once isolated (figure 3.4).

The size of the oligomer peak, and thus the oligomer yield from the *Winner* oligomerisation protocol, was consistently higher (5-10 % of total protein) than from the *Lansbury* protocol (figure 3.2b) and were available within 1-2 days; a fraction of the original incubation time. When the reaction was allowed to proceed for the full 6 days incubation, fibrils predominated in the mixture and the amount of oligomer detected by dot blot and gel filtration was diminished. In figure 3.5, multiple *Winner* oligomerisation reactions were set up at the same time and under the same conditions. After each day of incubation a single reaction was removed, ultracentrifuged and the supernatant run on gel filtration. From the time course of gel filtration chromatograms, the oligomer peak (~8 ml elution volume) appears within the first day and reaches maximum height around day 2, after which it decreases and disappears by day 5/6. As one would expect, the monomer peak (~15 ml elution volume) is in continuous decline over time as it aggregates together to form oligomers and fibrils.

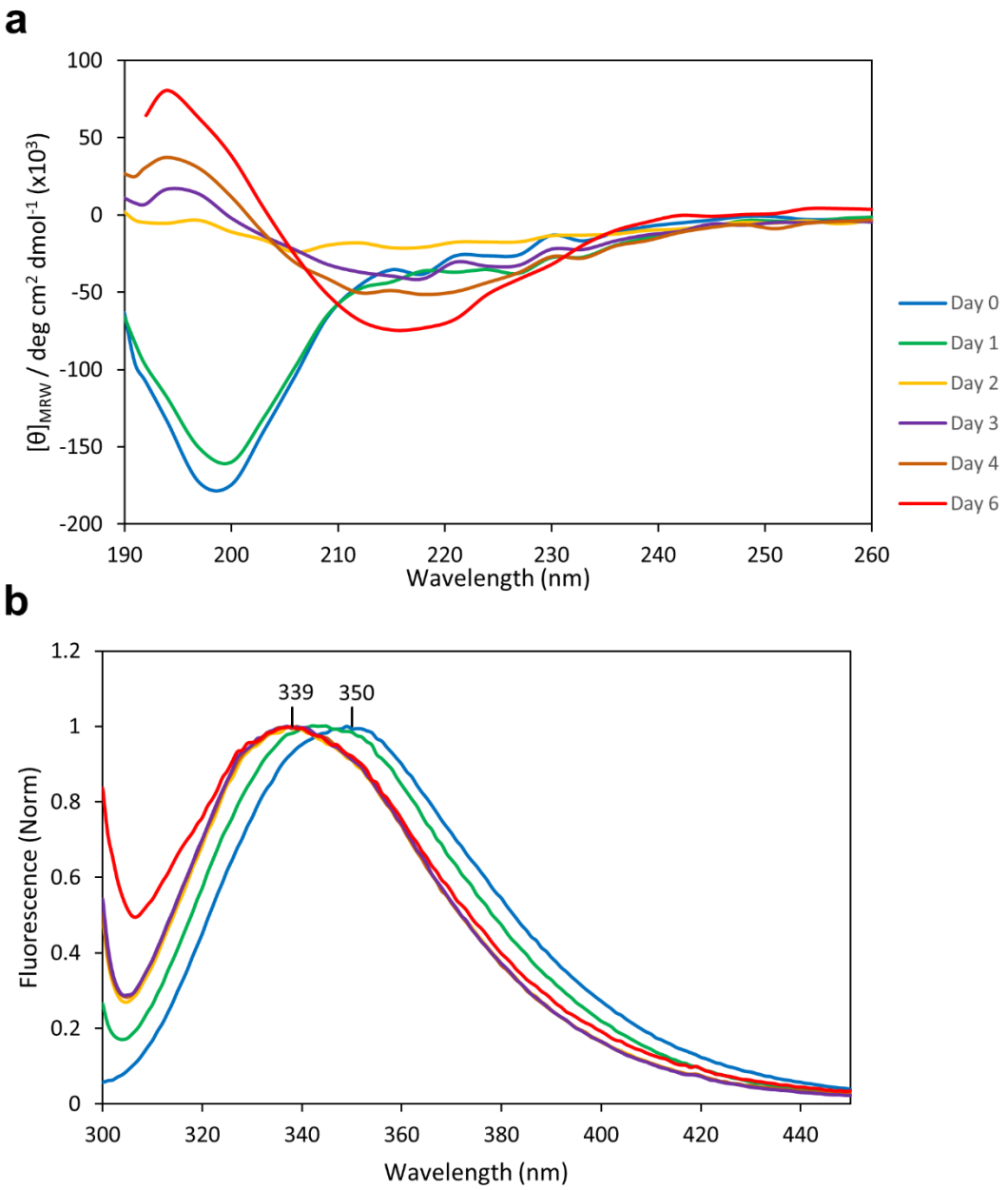

Figure 3.3 CD and fluorescence spectroscopy time course of αSyn oligomerisation according to the *Winner et al. (2011)* protocol. The total reaction mixture was measured each day by (a) circular dichroism, in which the transition from unfolded monomer to β-sheet fibrils is observed, and (b) fluorescence spectroscopy which illustrates the gradual blue-shift of Trp39 as αSyn aggregates.

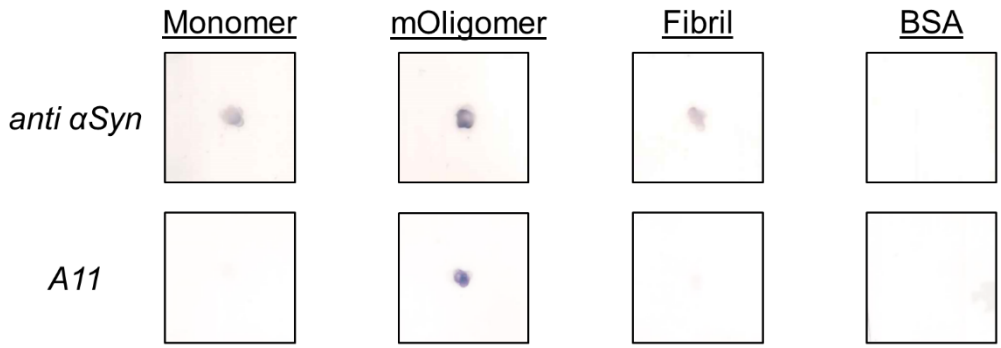

Figure 3.4 Purified *mOligomers*, but neither monomers nor fibrils, are A11 positive. All three samples were assayed with both A11 and anti αSyn antibodies; BSA was negative control.

For many oligomerisation protocols the starting monomer concentration and agitation speed are much higher than those used in the *Winner* protocol *(Diogenes et al., 2012; Lorenzen et al., 2014c)*. To investigate oligomerisation under these conditions, monomeric αSyn was prepared in the same buffer as before (PBS + 0.01 % sodium azide, pH 7.4) but at the higher concentration of 10 mg/ml and incubated at 37 °C with 900 rpm agitation. From this dynamic incubation, A11-positive oligomers appeared within 90 minutes and disappeared after 3-4 hours (figure 3.1). Insoluble aggregates formed quickly and after 6 hours only very small amounts monomer or oligomer could still be detected in the supernatant. As such, oligomers were typically isolated after 2 hours incubation. While the amount of oligomer produced was similar to the *Winner et al.,* protocol, the overall yield of oligomer appeared much lower due to high starting concentration of monomer (~1 % of total protein) (figure 3.2c). However, since the incubation time had now decreased to a matter of hours, coupled with the fact that unaggregated monomer could be easily purified and recycled, this protocol was used consistently for the production of oligomers for structural and electrophysiological experimentation. These oligomers, which were produced directly from monomeric αSyn, are referred to as *mOligomer*.

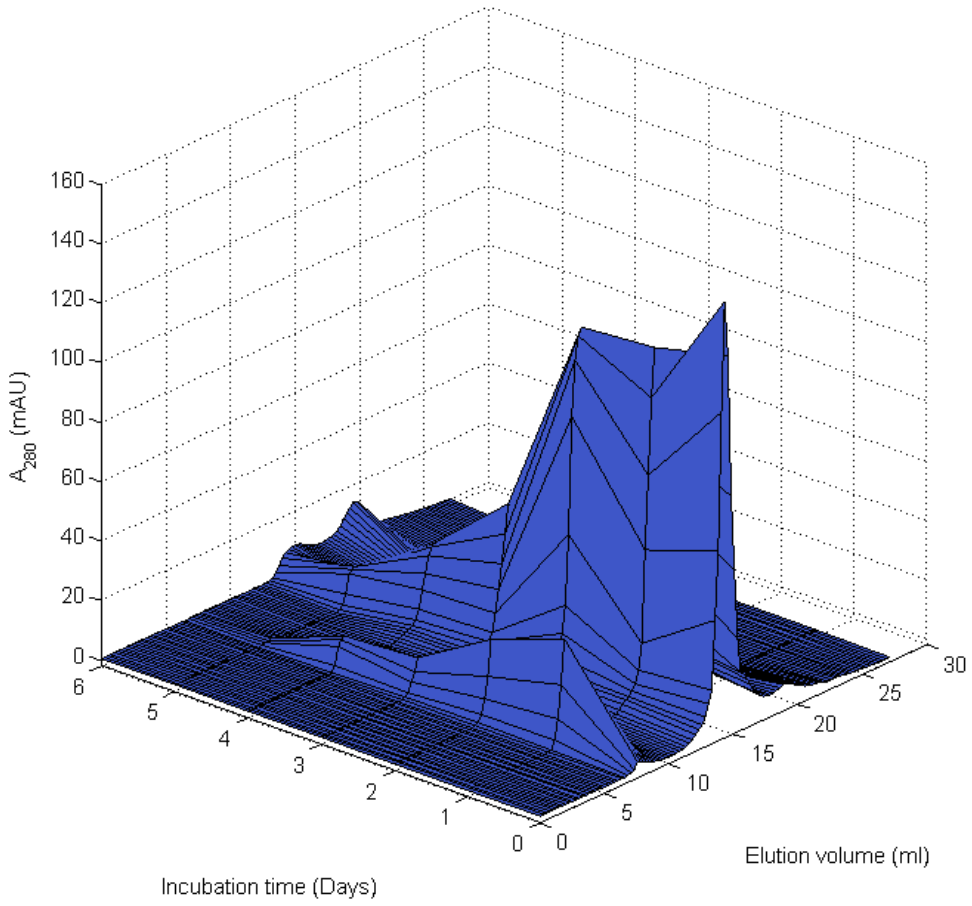

Figure 3.5 Gel filtration time course following the *Winner* oligomerisation protocol. After 0-6 days incubation, the supernatant from ultracentrifugation was loaded onto Superdex 200. The oligomer peak (8 ml elution volume) appears after the first day and gradually declines while the monomer peak (15 ml elution volume) starts high and rapidly falls as it aggregates together.

3.3.2 Recovery of oligomers from fibril sonication

Fibril fragmentation has been shown to enhance cytotoxicity through the production of small fibrillar species that can increase the number of extension sites for new fibril growth, and have greater biological availability for interacting with cellular membranes *(Tanaka et al., 2006; Xue et al., 2010; Wang et al., 2011b)*. To investigate whether soluble oligomers contributed to the mixture of small species produced by fragmentation, intact fibrils (figure 3.6a) were subjected to probe sonication at varying degrees of power and duration (figure 3.6b). As either parameter was increased, the resulting fibril fragments became shorter (figure 3.6c) and A11 immunoreactivity was recovered (figure 3.6d). Prolonged sonication (60 seconds) produced weaker A11 immunoreactivity than shorter durations. Similarly, A11 immunoreactivity was not observed after sonication at 20 % power but became clear at higher settings. Based on these preliminary findings, in all future experiments fibrils were sonicated at 60 % power and for 30 seconds.

Ultracentrifugation of fibril fragments and subsequent gel filtration of the supernatant produced peaks for soluble oligomers and monomer at the same elution volumes as seen for *mOligomers* (figure 3.7a). This separate population of oligomers recovered from fibrils, referred to as *fOligomers*, were similarly found to be A11-positive (figure 3.7b).

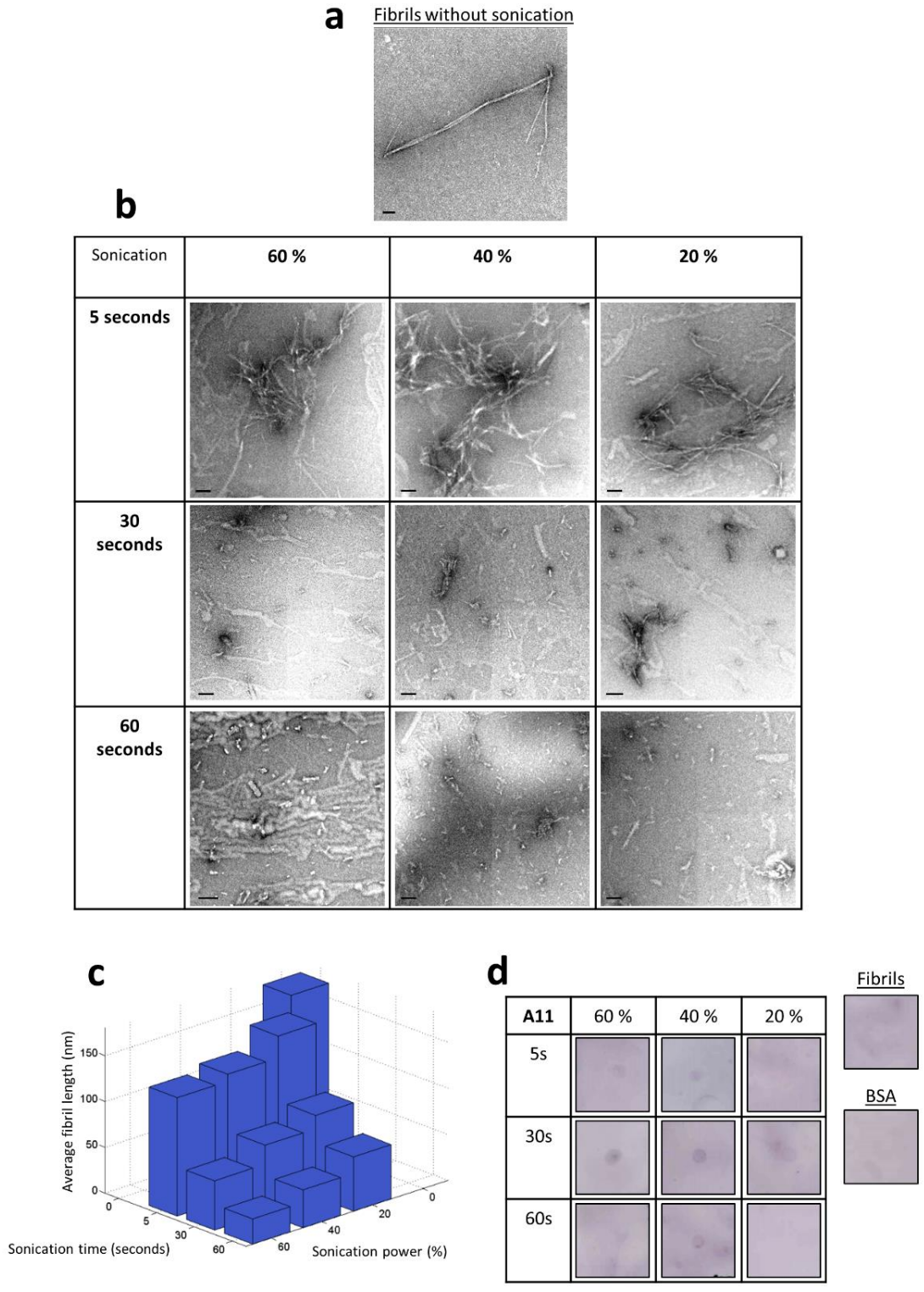

Figure 3.6 Fibrils sonicated under various conditions of power and duration produce different size fragments and recover A11-immunoreactivity. TEM images of fibrils before (a) and after (b) probe sonication at 20, 40 or 60 % power and for 5, 30 or 60 seconds duration, were subject to blind analysis to determine the length of fragments. As either condition was increased, the average fragment length (c) became shorter and samples displayed A11 positive dot blots (d) indicating the presence of oligomers. TEM scale bars = 100 nm.

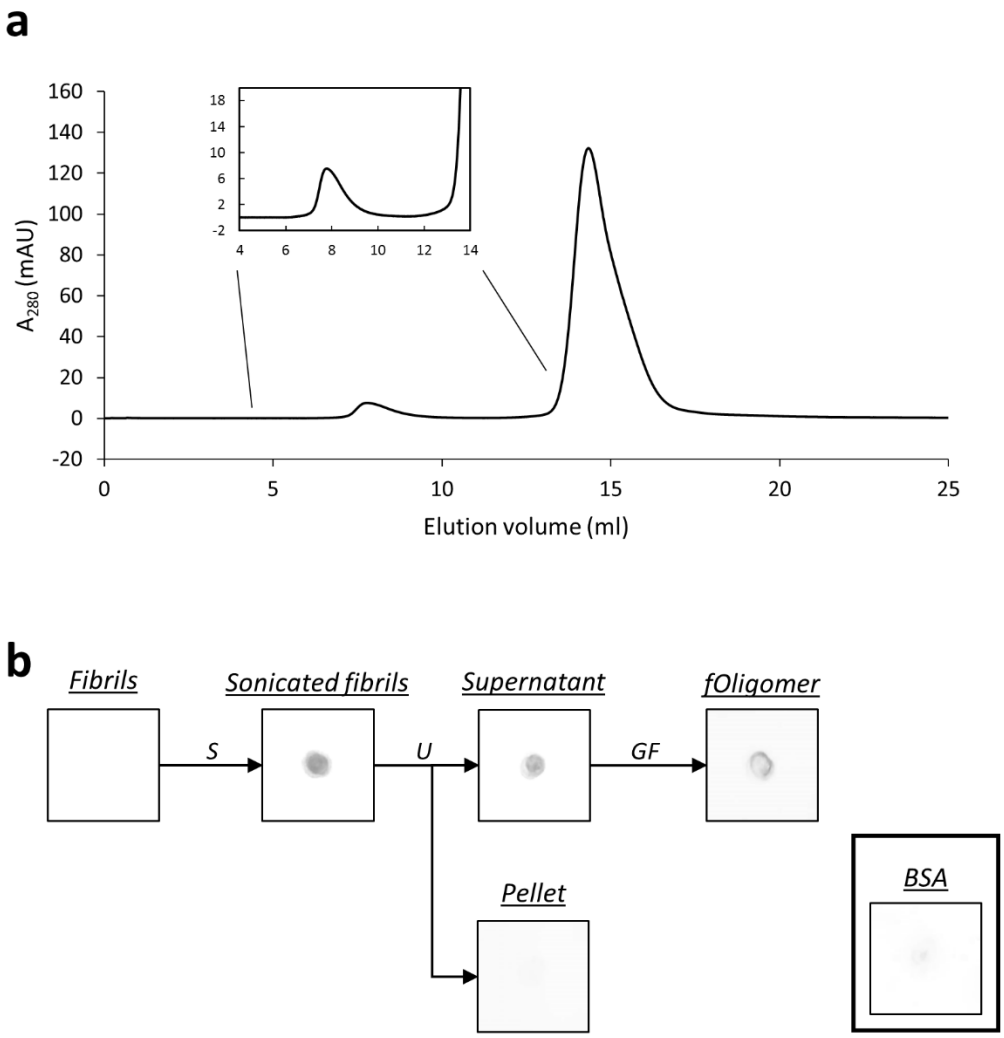

Figure 3.7 Oligomers recovered from sonication of fibrils, *fOligomers*, are A11 positive. The mixture of sonicated fibrils was ultracentrifuged to remove insoluble fragments and the supernatant loaded onto Superdex 200 gel filtration (a). The *fOligomer* peak (inset) is similar in size and elution volume to the peak for *mOligomers*. (b) An A11 dot blot of the steps involved in preparing *fOligomers* from fibrils; *S = Sonication step*, *U = Ultracentrifugation* and *GF = gel filtration*.

3.3.3 Structural differences between oligomers

Using CD spectroscopy (see chapter 2; methods), the secondary structure of *mOligomers* and *fOligomers* were compared to that of monomer and fibrillar αSyn (figure 3.8a). The structure of monomeric αSyn was that of a typically unfolded protein, with a prominent negative band at <200 nm, while fibrillar αSyn had a minimum at 218 nm characteristic of β-sheet. The spectra for *mOligomer* differed from fibrils as the minima is shifted to 212 and the 190 peak was more strongly positive. Similar to *mOligomers*, the spectrum for *fOligomer* clearly diverges from fibrils in wavelength intensity; particularly between 190-210 nm. However, the consistent minimum at 218 nm suggests the presence of β-sheet rather than α-helical structure.

Importantly, neither *mOligomer* nor *fOligomer* spectra could be reconstructed from linear combinations of the monomer and fibril spectra (differences were especially prominent between 200-210 nm), indicating that both oligomers exist as their own distinct species.

The secondary structure composition was estimated by DichroWeb analysis (figure 3.8b) *(Whitmore and Wallace, 2004, 2008)*; comparing spectra to a reference data set (Set 7) using the SELCON3 analysis algorithm *(Sreerama and Woody, 1993)*. This analysis accurately predicts monomeric αSyn to be mainly unfolded *(Fauvet et al., 2012)* but fibrils showed an over estimated percentage of α-helix; amyloid fibrils are well known to be β-sheet in structure *(Heise et al., 2005; Nelson et al., 2005)*. The predicted composition for *fOligomer* was very similar to that of fibrils which, despite their over-estimation, suggests that they share a similar β-sheet secondary structure. In comparison, *mOligomers* showed a surprisingly high percentage of predicted α-helix (~ 82 %) that was significantly (two-tailed t-test; $p < 0.05$) greater than that predicted for *fOligomers* or fibrils. This data suggests that the two oligomer populations display secondary structure characteristics that are different from one another; *mOligomers* are predominantly α-helical while *fOligomers* have more β-sheet.

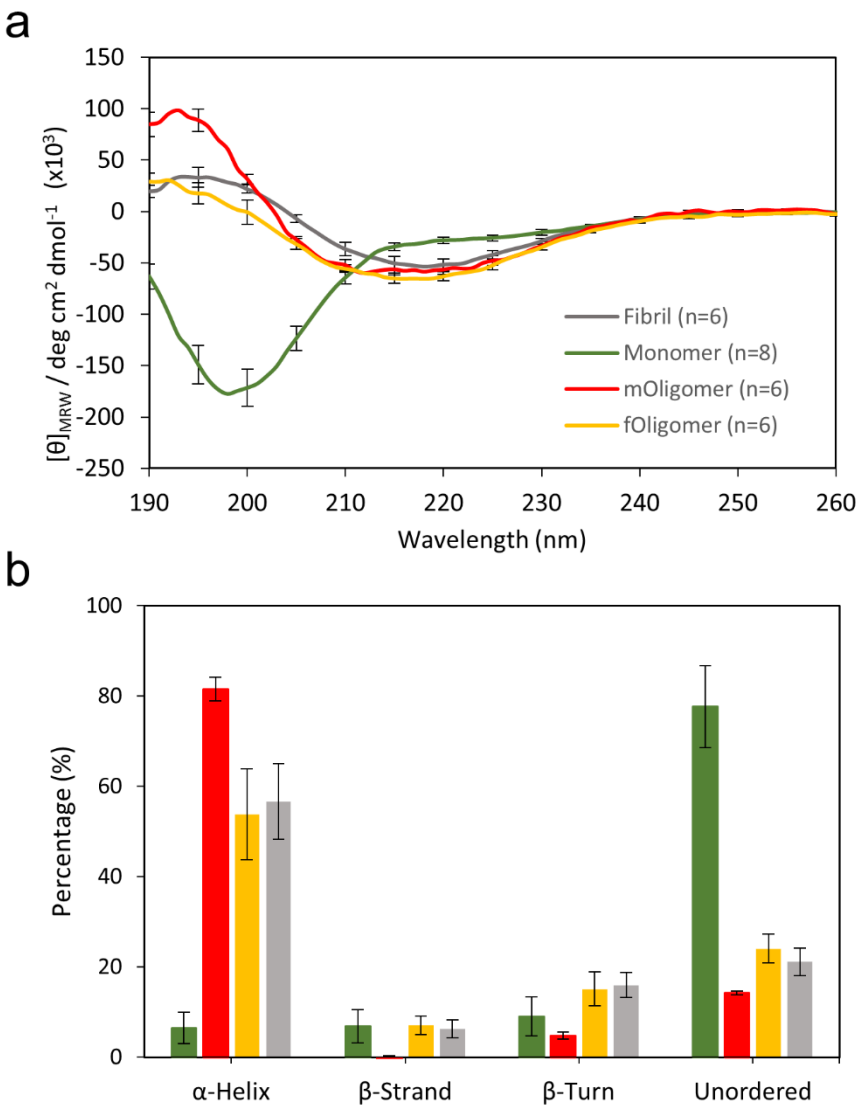

Figure 3.8 Far UV CD spectra of various αSyn species. The secondary structure of αSyn monomer (green), *mOligomer* (red), *fOligomer* (yellow) and fibrils (grey) was analysed by far UV CD spectroscopy (a) and their percentage structure determined using DichroWeb (b).

Fluorescence spectroscopy was used to measure the emission spectrum of tryptophan-39 during aggregation (figure 3.9). The emission wavelength of tryptophan fluorescence is dependent on its exposure to the environment; tryptophan residues that are buried within proteins display a blue-shift compared to solvent-exposed residues. Being structurally unfolded, monomeric αSyn had a freely exposed tryptophan with a fluorescence peak of (mean ± SEM) 350 ± 0.32 nm. Upon oligomerisation, the external tryptophan became buried resulting in a blue-shift of the emission peak to 335 ± 0.31 nm. Interestingly, the shifted peaks for purified fibrils and *fOligomers* were 339 ± 0.97 and 341 ± 1.10 nm respectively; still notably shifted from the monomer but

significantly less than that of the *mOligomer* (two-tailed t-test; $p < 0.005$; figure 3.9 inset); suggesting that fibril fragmentation might recover oligomers with an altered structure.

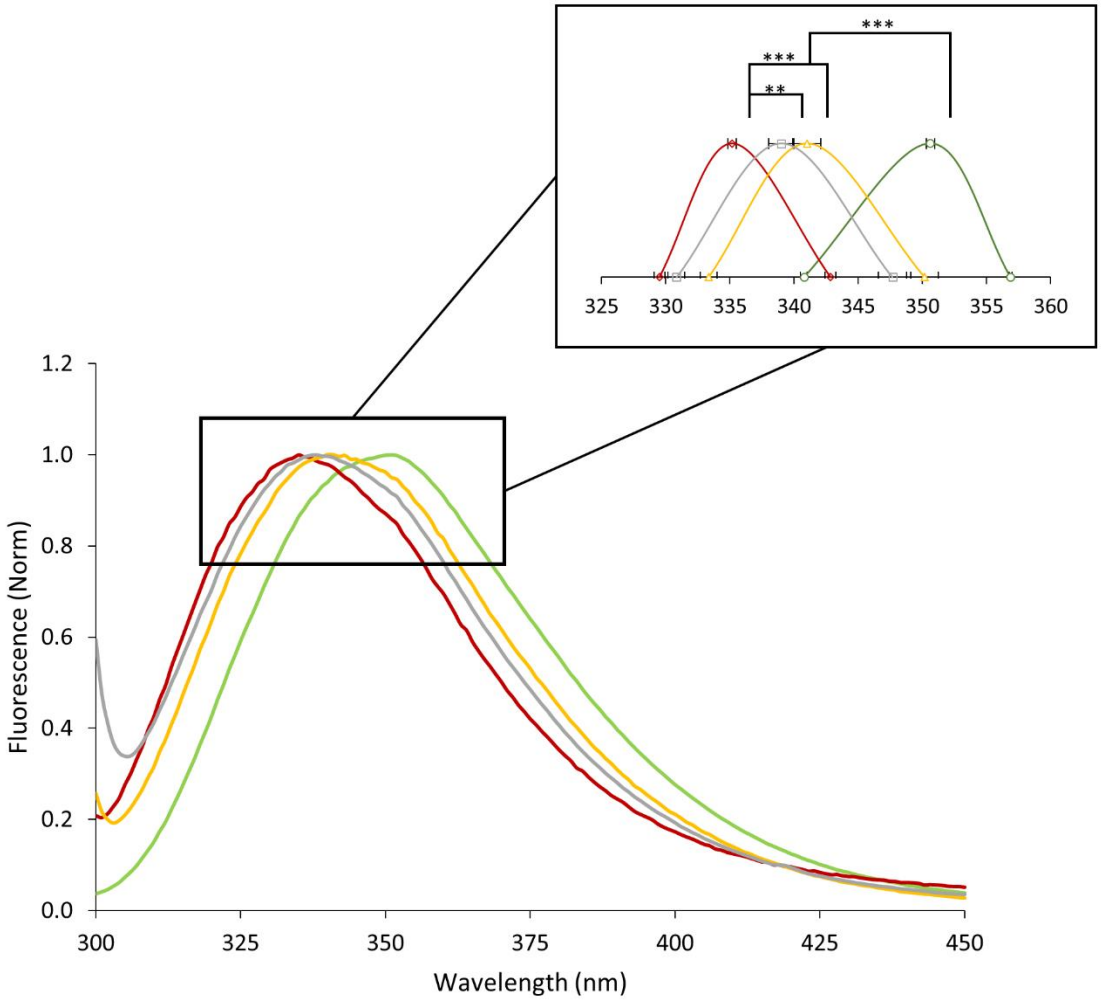

Figure 3.9 Fluorescence spectra of αSyn monomer (green), *mOligomer* (red), *fOligomer* (yellow) and fibrils (grey). Fluorescence spectroscopy quantifies the Trp39 blue – shift and shows that αSyn aggregates are significantly shifted from the monomer by different amounts. Fibrils and *fOligomers* are shifted by 11 and 9 nm respectively, while *mOligomers* have a larger shift of 15 nm. This suggests *mOligomers* to have an altered structure to fibrils that is not seen in *fOligomers*.

3.3.4 Transmission electron microscopy

Transmission electron microscopy (TEM) revealed both species of soluble αSyn oligomers to be ring-like in shape similar to those described previously *(Lashuel et al., 2002b)* (figure 3.10). Both populations had similar size diameter (n = 1000, mean ± std dev: *mOligomer* = 14.2 ± 2.6 nm; *fOligomer* = 13.6 ± 2.5 nm) and central cavity (*mOligomer* = 3.8 ± 1.1 nm; *fOligomer* = 4.3 ± 1.3 nm).

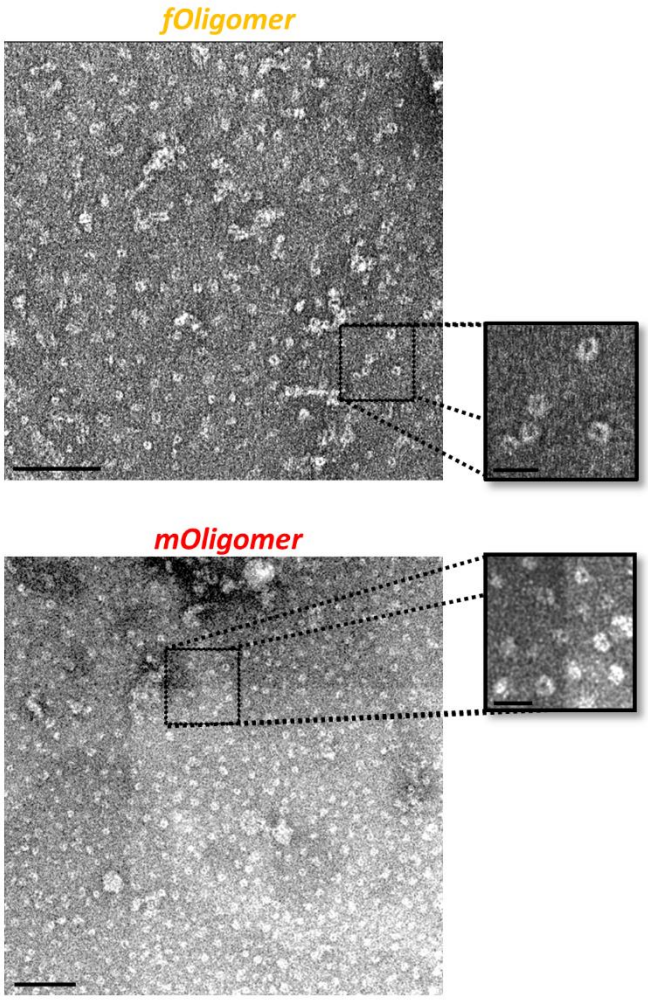

Figure 3.10 TEM images of *mOligomers* and *fOligomers*. Both oligomer species are similar in size and have distinct ring – like shape. Scale bar = 200 nm, inset = 25 nm.

3.3.5 Oligomers with regard to the aggregation pathway

Seeding with sonicated fibrils is commonly used to bypass the nucleation stage and accelerate amyloid formation *(Yagi et al., 2005; Kim et al., 2007; Lorenzen et al., 2012)*. To test whether *mOligomers* and *fOligomers* were able to accelerate the aggregation process in a similar manner to fibril seeds, small amounts (0.1 mg/ml) of either species was added to monomer solution (10 mg/ml) containing ThT and incubated under fibrillising conditions. Figure 3.11 shows the aggregation growth curve produced by ThT fluorescence upon binding to fibrils. Interestingly, the addition of *fOligomers* produced a leftward shift in the curve while adding *mOligomers* shifted the curve right. This parallel shift was the result of either a shortening or lengthening of the lag phase (lag phase for *fOligomers* was ~100 minutes while *mOligomers* were

~150 minutes), implying that *fOligomers* and *mOligomers* are on and off pathway respectively.

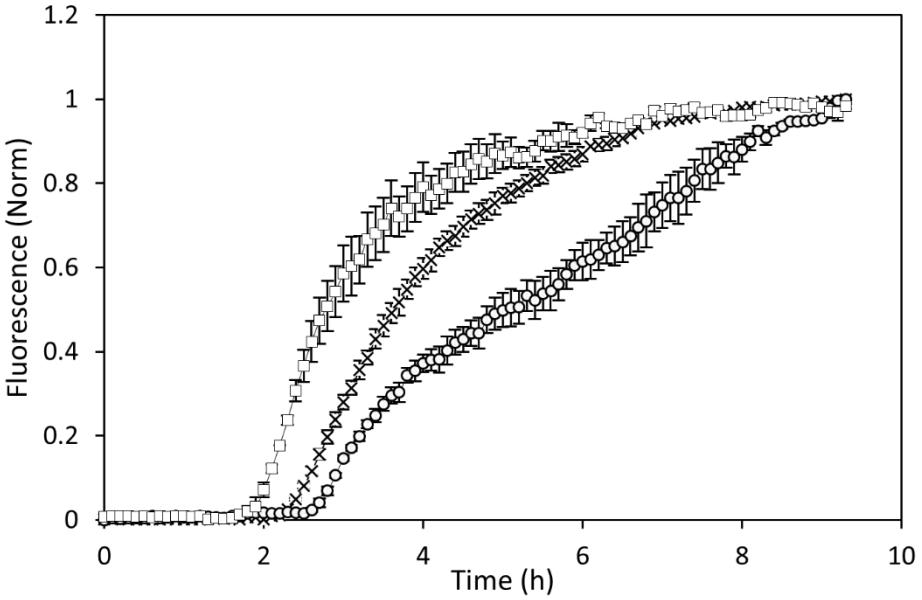

Figure 3.11 ThT assay of αSyn aggregation with seeding from either *mOligomers* or *fOligomers*. ThT experiments were carried out with 10 mg/ml monomer (x) and seeded with 0.1 mg/ml of either *mOligomer* (○) or *fOligomer* (□).

3.3.6 Oligomer size and population heterogeneity

Analytical ultracentrifugation (AUC) of αSyn monomer (figure 3.12a), *mOligomers* and *fOligomers* (figure 3.12b) produced peak sedimentation coefficients of 1.2 S, 11.6 S and 11.3 S respectively. Mass transformation of these peaks gave a predicted molecular mass of 8 kDa for monomer and between 250-260 kDa for both oligomer species; suggesting that the oligomers are comprised of ~30 monomers. The peak width at 50 % height was 0.3 S for monomer, 5.4 S for *mOligomer* and 5.0 S for *fOligomer*. It is worth noting that the native αSyn tetramer *(Bartels et al., 2011)* would be expected to give a peak at ~5 S, which is observed in the *mOligomer* sample but not the *fOligomer*; possibly due to sonication.

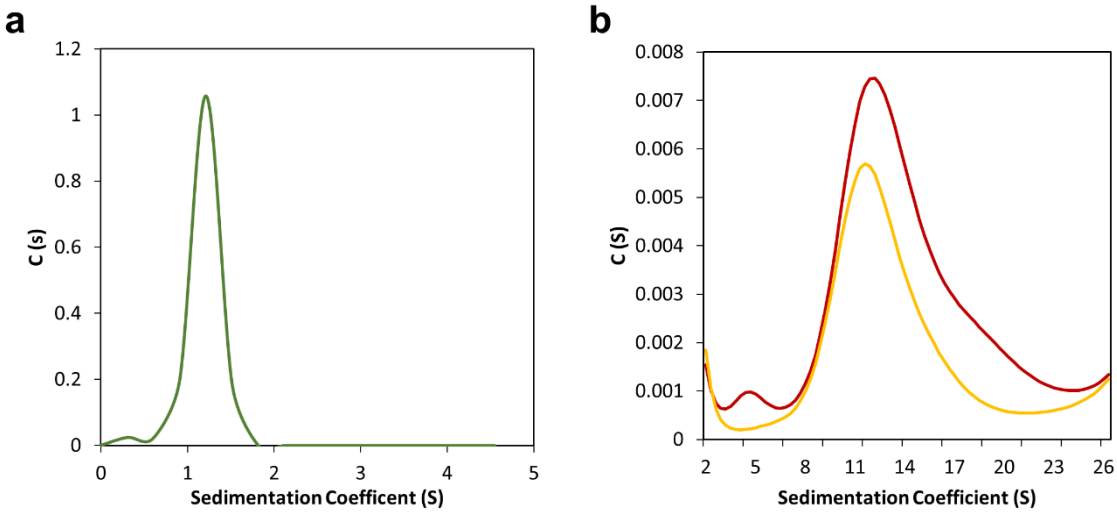

Figure 3.12 AUC experiments to determine oligomer size and heterogeneity. AUC of monomer (a – green) and both mOligomers (b – red) and fOligomers (b – yellow) show peak sedimentation coefficients of 1.2 S, 11.6 S and 11.3 S respectively.

3.4 Discussion

There is increasing evidence that soluble oligomers are the most toxic form of αSyn aggregates in Parkinson's disease *(Giehm et al., 2011; Winner et al., 2011)*. The transient nature and inherent polydispersity of such species *(Uversky, 2010)*, however, limits not only our understanding of their structural properties but of the mechanisms through which they act. Since αSyn has been considered a potential target for drug treatments *(Games et al., 2014)*, characterisation of the oligomeric species will be of great importance for devising new treatments. In this chapter an efficient αSyn oligomerisation protocol was developed to produce oligomers of known size, shape and structure. In addition to isolating oligomers during the aggregation process, referred to as *mOligomers*, a separate species of oligomer was derived from the fragmentation of fibrils by sonication; *fOligomers*. As such, this chapter presents a comparative investigation into these two oligomers with regard to structure and their effect on the aggregation pathway. Any differences in the molecular properties of these two oligomers could convey differences in their pathological efficacy.

3.4.1 Oligomerisation of αSyn is dependent on temperature, agitation speed and concentration

Compared in this chapter are three protocols for αSyn oligomerisation. To begin with oligomerisation was carried out at 4 °C following the protocol described by *Lashuel et al. (2002b)* and after one month of incubation oligomers remained at almost undetectable levels (figure 3.1). With such a long incubation period and low oligomer yields being unsuitable for sustained experimentation, preliminary investigations were intended to develop the oligomerisation protocol to give better yields in a shorter time.

It has been previously found that αSyn folding into an aggregation-prone intermediate state is mediated by an increase in incubation temperature *(Uversky et al., 2001c; Uversky et al., 2001a).* As such, many have reported faster oligomerisation rates at room temperature *(Danzer et al., 2007)* and 37 °C *(Cappai et al., 2005). Uversky et al. (2001c)* originally described oligomer formation only at temperatures higher than 50 °C, although such conditions have not been repeated since. In addition to higher temperatures, many modern protocols follow an incubation-with-shaking method with the speed of agitation ranging from 150 to over 1400 rpm *(Wright et al., 2009; Winner et al., 2011; Diogenes et al., 2012; Ariesandi et al., 2013).* Implementation of this new method (following the protocol from *Winner et al. (2011))* had a profound effect on both the speed of oligomerisation (figure 3.1) and oligomer yield (figure 3.2). On the time scale of days, rather than weeks, αSyn aggregated from monomer to fibrillar (figure 3.3) with A11-positive oligomers being detected at intermediate time points (figures 3.4 and 3.5). As both the shaking speed and starting monomer concentration were increased (following *Lorenzen et al. (2014)*) oligomerisation was accelerated even further and aggregates appeared in a matter of hours. Despite the reduced incubation time, oligomer yield was no different for either protocol at 37 °C. As one might expect, increasing the temperature, shaking and monomer concentration accelerated the overall rate of aggregation without stabilising oligomeric species. In comparison, it is possible to improve oligomer stability through cross-linking *(Bitan et al., 2001; Rosensweig et al., 2012),* protein engineering *(Sandberg et al., 2010)* or with heavy metal ions *(Danzer et al., 2007; Wright et al., 2009).* However these methods can have varying effects on oligomer structure and its molecular properties *(Faendrich, 2012).* The *mOligomers* presented in this work were isolated directly from monomers under aggregation conditions with minimised incubation time.

3.4.2 Fibril fragmentation recovers soluble, ring-like oligomers

Fibril fragmentation is a key determinant of physiological impact for amyloid proteins *(Tanaka et al., 2006; Xue et al., 2010; Wang et al., 2011b)*. In fact, fragmentation may be a more important process than elongation since amyloids with a slow growth rate but increased brittleness are less infectious *(Wang et al., 2011b)* and more cytotoxic *(Xue et al., 2009)*. It was observed by *Xue et al. (2009)* that fibril fragmentation could not only generate new seeds that would rapidly increase the fibril load but also create small fibrillar species of varying dimensions that may have enhanced pathological properties. Still un-investigated, however, is the relation of soluble oligomers to fibril fragmentation.

In this study, fibrils were broken down by probe sonication into fragments and a mixture of small fibrillar species, described previously *(Xue et al., 2009)*, was observed by TEM (figure 3.6). Novel was the finding that sonicated fibrils gave positive results for A11 dot blot; implicating soluble oligomers as a key component of the fragment mixture. After ultracentrifugation and gel filtration of the sonicated sample, a new species of oligomer, termed *fOligomer*, was identified separate to *mOligomers* (figure 3.7). Insoluble fibrils were isolated and thoroughly washed prior to sonication to ensure that *fOligomers* were not contaminated by *mOligomers* during purification. In addition, the fibrils were kept at 4 °C throughout sonication and ultracentrifugation which, in light of the very slow oligomerisation kinetics observed at this temperature, means it is unlikely that *fOligomers* were the result of re-aggregating monomers produced by fragmentation.

3.4.3 Separate species of αSyn oligomer exhibit subtle differences in structure

Two separate species of αSyn oligomer, *fOligomer* and *mOligomer*, were isolated from different stages of aggregation. A range of analytical techniques were employed to compare the structures of these two oligomers and their role in fibrilisation.

With regard to secondary structure, the distinct shift in *mOligomer* CD spectrum (minima = 212 nm) suggests that this species has a lower β-sheet content compared to fibrils and is predicted by DichroWeb to be predominantly α-helical in structure. The shifted spectrum of *mOligomers* was previously seen by *Lorenzen et al (2014)* who describe a degree of β-sheet structure that is intermediate between unfolded monomer and fully structured fibrils, however, the percentage of beta-sheet structure was not

quantified. Previous studies using Raman and AFM microscopy on similar αSyn oligomers *(Apetri et al., 2006)* identified a significant amount of α-helical structure (47% α-helix and 29% β-sheet) that compliments the CD spectrum and illustrates the bias of DichroWeb. The DichroWeb data presented here ascribes a disproportionate percentage of α-helical content to fibrils. The over estimation of α-helix structures may be the result of DichroWeb bias; in which the geometric parameters for recognising helical features are better defined than for β-sheet *(Wallace et al., 2003)*. This can be illustrated when analysing a protein of known structural composition such as lysozyme C (P00698). Lysozyme C has a native secondary structure composition of ~37 % α-helix and ~16 % β-sheet (~34 % unordered and ~13 % turn; *see UniProtKB – LYSC_CHICK*). However, according to DichroWeb analysis Lysozyme C is predicted to have 81 % α-helix and 0 % β-sheet composition. As such, the true structural composition of αSyn oligomers cannot be inferred from these CD spectra alone, but instead can be used in comparison to fibrils and to each other to indicate that they may have subtle differences.

A folding-sensitive tryptophan mutation was positioned in the N-terminal region of αSyn. The N-terminal is naturally capable of forming α-helixes during the interactions of monomers with lipid membranes *(van Rooijen et al., 2009b)*. This region also appears to be folded in *mOligomers* as the fluorescence spectrum from tryptophan-39 was strongly blue shifted; significantly more so than for fibrils. This suggests that the microenvironment in this region may be altered in the oligomeric state and changes during aggregation. Indeed, recovering *fOligomers* from fibrils did not reproduce the same level of blue shift or α-helical content as seen for the *mOligomer*, indicating that *fOligomers* retain elements of the fibril structure that are not present in *mOligomers*.

The impact of the two types of oligomer on the process of amyloid fibril formation was investigated by adding each species separately to a ThT assay (figure 3.11). It was observed that *fOligomers* accelerate aggregation while *mOligomers* are inhibitory; causing a shortening or lengthening of the lag phase respectively. The close correlation between lag phase duration and the first appearance of A11-positive dot blots in the aggregation time course (figure 3.1), indicates that *mOligomers* form in the lag phase of the ThT curve and disappear during the exponential elongation phase *(Giehm et al., 2011)*. Similar to the findings of *Lorenzen et al. (2014)*, the *mOligomers* did not act as seeds for fibril growth. *Lorenzen et al. (2014)* demonstrated oligomer inhibition to be

concentration-dependent with lag phase extension becoming saturated around 0.1 mg/ml of oligomer seeds. Furthermore, this effect was not the result of monomer sequestration by oligomer but rather the inability for oligomers to incorporate into fibrils. The *mOligomers* presented here closely replicate the structural and aggregation findings of *Lorenzen et al. (2014)* and may therefore share these properties as well.

Sonicated fibrils have been found previously to act as seeds for fibril formation *(Kim et al., 2007; Lorenzen et al., 2012)*. Since *fOligomers* were produced by sonication it is possible that this population contains small β-sheet rich fragments, for example soluble tubular protofibrils *(Lashuel et al., 2002b)*, which are present along with the ring-like oligomers. Indeed, the various soluble fibril fragments within the post-sonication supernatant would likely be purified together on gel filtration since soluble oligomers of different sizes elute close to the exclusion limit (~1300 kDa) and cannot be separated on Superdex 200 *(Lorenzen et al., 2014c)*.

This data, therefore, may suggest that fibril fragmentation produces oligomers that are different in structure to those formed prior to fibrils, but could also imply that through sonication a mixture of soluble fragments are recovered; some of which (soluble protofibrils) have β-sheet secondary structure and can seed aggregation, while others (soluble oligomers) have a more helical structure. If this were the case one might expect the heterogeneity of the *fOligomer* population to be greater than the *mOligomer*. According to AUC analysis, however, both oligomer species had similar sedimentation peaks and widths at 50 % height (figure 3.12b), suggesting they have the same size and heterogeneity. According to the transformation ratio of oligomer mass to monomer mass, both *mOligomers* and *fOligomers* are predicted from AUC to contain ~30 monomers. While this ratio is similar to that found previously, the calculated mass (~250 kDa) is much lower than the expected value for an oligomer of this size *(Lorenzen et al., 2014c)*. However, since AUC mass transformation of monomeric αSyn was equally underestimated (8 kDa), the resulting ratio of monomers per oligomer may still be predicted. Were the calculated oligomer mass to be compared to the known mass of αSyn (14.482 kDa), then the ratio falls to ~15 monomers in each oligomer. From the literature, oligomers as small as hexamers, pentamers and octamers have been described previously to form annular, pore-like structure in membranes *(Lashuel et al., 2002b; Tsigelny et al., 2007; Zhang et al., 2013)*. Therefore, while this data, consistent with *Lorenzen et al. (2014)*, suggests

mOligomers and *fOligomers* are large 30 monomer structures, smaller annular oligomers may form under different conditions. Alternatively, annular oligomers may be able to shift between multiple sizes creating stepwise changes in membrane conductance *(Tosatto et al., 2012)*.

Overall, αSyn oligomers were purified from the early stages of aggregation and also recovered from fibril fragmentation. Characterisation of these two oligomer populations suggests them to be similar in size and ring-like shape. Analysis of their secondary structures, however, reveals some subtle differences that may be the cause for their varying effects on seeding aggregation. The following chapters will investigate the effects of αSyn oligomers on neuron electrophysiology and whether differences in oligomer structure equate to differences in toxicity.

4 Intracellular injection of monomeric and oligomeric alpha-Synuclein into thick-tufted layer 5 pyramidal neurons

4.1 Introduction

The pathological spread of αSyn aggregates to the higher regions of the brain, including the hippocampus and neocortex, occurs commonly in the later stages of PD *(Braak et al., 2005)*. The appearance of αSyn-immunoreactive cortical Lewy bodies strongly correlates with the onset of cognitive impairment in PD patients *(Hurtig et al., 2000; Mattila et al., 2000)*. In other neurodegenerative disorders, such as Alzheimer's disease or dementia with Lewy bodies, cortical Lewy bodies can appear without prior loss of motor control; suggesting that they have pathologies distinct from that of PD. Loss of neurons in the neocortex results in a variety of neuropsychiatric symptoms that are severely detrimental to the patient's quality of life *(Braak et al., 2005; Poewe, 2008)*. The neocortex, therefore, presents an important, yet often overlooked, target for studying αSyn toxicity.

The neocortex is responsible for higher cognitive functions including memory, sensory feedback, motor control and emotional/social processing. The preserved interlayer connectivity of pyramidal neurons denotes a canonical microcircuit that forms the basis for signal integration throughout the neocortex *(Thomson and Lamy, 2007)*. The main subcortical output from the neocortex comes from thick-tufted layer 5 (TTL5) pyramidal neurons. The varying morphological and physiological properties of TTL5 neurons, as well as their subcortical projections, help to derive the functional specificity of different cortical regions *(Ramaswamy and Markram, 2015)*. In developing our understanding of cortical function and circuitry, TTL5 neurons have been extensively studied through patch clamp recordings of both *in vitro* brain slices *(Stuart et al., 1993)* and *in vivo* brains of freely moving animals *(Murayama et al., 2007)*, as well as through *in silico* models *(Hay et al., 2011; Ramaswamy et al., 2012; Reimann et al., 2013)*.

Neuronal response properties are typically found from measurements of current-voltage (I-V) relationships constructed from the application of stepwise inputs *(Hodgkin et al., 1952)* or voltage ramps *(Swensen and Marder, 2000)*. Alternatively, injecting a continuous waveform into the cell represents a more naturalistic stimuli

from which I-V curves can be measured during ongoing firing activity. These dynamic I-V curves closely fit to a reduced neuronal model (Exponential Integrate-and-Fire; EIF model) that provides a reliable, in-depth description of electrophysiological properties *(Badel et al., 2008)*. This efficient method is capable of accurately predicting experimental data and has been used previously to assess the heterogeneity of neocortical pyramidal cell populations for use in the modelling of neuronal networks *(Harrison et al., 2015)*.

In this chapter, I develop a system for investigating the electrophysiological effects of αSyn applied intracellularly into TTL5 pyramidal neurons. Monomeric and oligomeric αSyn (purified and structurally characterised as shown in chapters 2 and 3) were injected directly into neurons using the whole-cell patch clamping technique. At regular intervals, the voltage responses to both step and naturalistic currents were recorded and used to construct standard and dynamic I-V curves respectively. Deriving an EIF model from the dynamic I-V curves provides a time course of neuronal parameters.

I assess the integrity of this method by showing that αSyn remains stable throughout recordings and can be detected specifically inside recorded neurons. Furthermore, I demonstrate that the reliability of the reduced neuron model at predicting action potential spike times is not affected by the toxicity-induced changes of αSyn; making this approach suitable for modelling neurons in a pathological state.

4.2 Materials and methods

4.2.1 Materials

Glycerol, NaCl, KCl, $CaCl_2$, KH_2PO_4, $NaHCO_3$, Tris and glucose were purchased from Fisher Scientific (Loughborough, UK) and the $MgCl_2$ was purchased from Merch (Darmstadt, Germany). Compressed gas containing 95 % oxygen and 5 % CO_2 was supplied by BOC gases (Surrey, UK). All other materials were purchased from Sigma (Poole, UK) unless stated otherwise.

Solutions

Artificial Cerebrospinal fluid (aCSF) contained (mM): 127 NaCl, 1.9 KCl, 1 $MgCl_2$, 2 $CaCl_2$, 1.2 KH_2PO_4, 26 $NaHCO_3$, 1 D-glucose (pH 7.4 when bubbled with 95 % O_2 and 5 % CO_2; 290-300 mOSM).

Cutting solution was a high Mg^{2+}, low Ca^{2+} aCSF solution containing (mM): 127 NaCl, 1.9 KCl, 8 $MgCl_2$, 0.5 $CaCl_2$, 1.2 KH_2PO_4, 26 $NaHCO_3$, 1 D-glucose (pH 7.4 when bubbled with 95 % O_2 and 5 % CO_2; 290-300 mOSM), used to reduce synaptic activity and maintain slice integrity.

Intracellular solution contained (mM): 135 potassium gluconate, 7 NaCl, 10 HEPES, 0.5 EGTA, 2 ATP, 0.3 GTP, 10 phosphocreatine (290-300 mOSM, pH 7.2). Aliquots of 500 µl were stored at -20 °C until use. Aliquots (2 µl) of Alexa Fluor® 488 hydrazide, in deionised water, were stored at -20 °C and added to the intracellular solution immediately prior to patch clamp recording; to give a final concentration of 50 µM.

Patch pipettes

Borosilicate glass capillary tubes (1.5 mm, 0.86 mm) were purchased from HARVARD APPARATUS (Kent, UK). Patch pipettes were prepared using a Model P-87 Micropipette puller (Shutter Instrument Co., USA) and fire polished to produce a 2 µm wide tip with 4-5 MΩ resistance.

Immunostaining

Glass slides and coverslips were purchased from Menzel-Gläser (Braunschweig, Germany). Plastic coverslips were purchased from Agar Scientific (Elektron technology, Essex UK) and a square hole was cut out of the middle to make a frame.

VECTASHIELD® mounting media was purchased from Vector Laboratories Ltd. and stored at 4 °C until use.

PFA buffer: 4 % Paraformaldehyde dissolved in distilled water with gentle heating (pH 7.4). Aliquots of 10 ml were stored at -20 °C until use.

Blocking buffer: 0.4 % Triton X-100, and 1 % Bovine Serium Albumin (BSA) in PBS.

Secondary antibodies: All Alexa Fluor® conjugated IgG secondary antibodies, the Alexa Fluor® 488 hydrazide and the 4',6-diamidino-2-phenylindole (DAPI) nuclear stain, were purchased from Molecular Probes™ (Invitrogen, Oregon, USA).

4.2.2 Electrophysiology

4.2.2.1 Slice preparation

All experiments were approved by the local ethic committee. B6CBF1 mice (male, postnatal days P28-35) were killed by cervical dislocation and decapitated in accordance with the UK Animals (Scientific Procedures) Act 1986. Following rapid isolation of the whole brain in cold (2-4 ^{o}C) cutting solution, the two hemispheres were divided with an incision along the midline and glued onto a petri dish with the sagittal plane facing down. The dish was submerged in cold cutting solution and mounted onto a Microm HM 650V microslicer (Carl Zeiss, Welwyn Garden City, UK). With the dorsal side of each hemisphere facing towards the blade, the dish was tilted forwards at an angle of +15 ° so that slicing began in the neocortex and travelled ventrally towards the midline. This method provided parasagittal slices of the neocortex (300 μm thick) containing layer 5 pyramidal neurons with intact apical dendrites. Slices were transferred into normal aCSF with continuous bubbling and incubated for 60 minutes at 34 °C and then stored at room temperature (20-22 °C) for 1-6 hours prior to recording.

4.2.2.2 Intracellular solution with αSyn

Prior to patch clamp recording, all αSyn protein samples were prepared in filtered PBS and added to intracellular solution, with Alexa Fluor® 488, to give a final concentration of 500 nM (5 % v/v). In control recordings, an equivalent volume of PBS was added to the intracellular solution (5 % v/v). The intracellular solution was passed through a Phenex™-RC 4 mm syringe filter (Phenomenex, Cheshire UK) with a pore size of 0.45 μm, before the addition of αSyn, to remove impurities that would otherwise block the flow of solution through the patch pipette tip.

4.2.2.3 Intracellular recording

A brain slice was transferred into the recording chamber, submerged in normal aCSF and perfused at a continuous flow rate of 3 ml/min. Temperature was regulated at 32 ± 0.5 °C using a heated perfusion tube (ALA Scientific Instruments Inc., NY USA) controlled by LinLab software (Scientifica, Bedford UK). Slices were visualised with an Olympus BX51W1 microscope with a Hitachi CCD camera (Scientifica) using IR-DIC optics.

The somatosensory region of the neocortex was located from its position relative to the hippocampus under low magnification. Single or double whole-cell patch clamp recordings were made from thick-tufted layer 5 pyramidal neurons under x630 magnification using patch pipettes filled with intracellular solution and either αSyn or vehicle. As Alexa Fluor® 488 dye quickly diffused intracellularly, neuron morphology could be visualised by excitation from a pE-100 light source (CoolLED, Andover UK). To ensure a complete morphology, only neurons with somata at least 50 μm below the slice surface were recorded from.

Thick-tufted layer 5 pyramidal neurons were identified by their large size and distinct apical dendrite; projecting from layer 5b and bifurcating within layer 2/3. In addition to morphology, pyramidal neurons of the neocortex displayed distinct current-voltage relationships that facilitate identification *(Kasper et al., 1994; Ramaswamy and Markram, 2015)*. Thick-tufted layer 5 neurons exhibit typical burst-firing action potentials and large inward-rectifying currents. Neurons that did not adhere to the aforementioned morphological and electrophysiological features were considered to be either interneurons or thin tufted layer 5 pyramidal neurons and were discarded from analysis.

The voltage responses from current clamped neurons were recorded using an Axon Multiclamp™ 700B amplifiers (Molecular Devices, USA) and digitised at 20 kHz using Axon Digidata® 1440a (Molecular Devices). Data acquisition was carried out using Clampex and analysed using Clampfit; both applications of the pCLAMP™ software (version 10, Molecular Devices).

4.2.2.4 Stimulation protocols

To extract electrophysiological properties over time, both step and dynamic currents were injected at 8 minute intervals (5 minutes recovery time followed by 3 minutes recording) over a 32 minute period and the respective voltage responses used for analysis by standard and dynamic I-V methods.

4.2.2.4.1 Standard I-V method

The standard I-V relationship was produced by the injection of 1 second duration square current sweeps (step currents); starting between -600 and -400 pA (to give a membrane potential of ~ -100 mV), and incrementing by 100-200 pA until a regular

firing pattern (6-12 Hz) was induced. A plot of step current against average voltage response around the resting potential generates the standard I-V curve. The step current needed to generate action potentials was used as an indication of the gain factor required for noisy current injection (see Dynamic I-V section below).

4.2.2.4.2 Dynamic I-V method

In contrast to standard I-V, in which the input current is stepwise, the dynamic I-V curve is generated from the neuronal response to a continuously injected waveform (noisy current) that reflects ongoing synaptic activity *(Badel et al., 2008)*. The dynamic I-V curve, defined by the average transmembrane current as a function of voltage, is able to parameterise single-variable integrate-and-fire models (exponential integrate-and-fire, EIF *(Fourcaud-Trocme et al., 2003),* and refractory exponential integrate-and-fire, rEIF *(Badel et al., 2008)*). The complete method has been described previously *(Badel et al., 2008)* and a brief account is given below.

Injected noisy current traces were constructed from the summed numerical output of two Ornstein-Uhlenbeck processes *(Uhlenbeck and Ornstein, 1930)* with time constants τ_{fast} = 3 ms and τ_{slow} = 10 ms. These stochastic waveforms, with time correlation, are representative of the background post-synaptic activity resulting from activation of AMPA and $GABA_A$ receptor channels. Two sets of variances were applied to the waveform (low; $\sigma_{fast} = \sigma_{slow} = 0.18$ and high; $\sigma_{fast} = 0.36$, $\sigma_{slow} = 0.25$), both with a DC bias of 0.06 (relative units), to give two different current traces (LowV-06 and HighV-06). Each trace had a duration of 40 seconds and was preceded and followed by 5 seconds of zero current (null stimulus). The traces were multiplied by a gain factor (300-800 pA) when injected to give a desired firing frequency of 5-15 Hz.

Between recovery intervals both LowV-06 and HighV-06 noisy currents (and step current sweeps) were injected consecutively into the recorded neuron in the presence of intracellularly applied αSyn constructs or vehicle. When investigating the pre-spike parameters using the EIF model, the dynamic I-V curve was constructed solely from the pre-spike voltage response (subthreshold and run up to spike) with all data falling in a 200 ms window after each spike being excluded from analysis. Pre-spike parameters were collected from both low and high variance traces and averaged. For the post-spike parameters, the previously excluded refractory data (200 ms after each spike) was used to construct dynamic I-V curves to fit the rEIF model. Since the

refractory parameters require a high firing frequency, only the voltage responses to HighV-06 noisy current were used for post-spike investigations.

4.2.2.5 Electrode filter

With only one electrode being used for both injecting current and measuring voltage, the recorded traces (V_{rec}) become the sum of the true membrane voltage (V) and the voltage across the electrode (V_{el}). The latter, assumed to be a linearly filtered version of the input I(t), can be written as a convolution integral of the current with unknown electrode filter *f*(s).

$$V_{rec}(t) = V(t) + V_{el}(t) = V(t) + \int_0^\infty f(s)I(t-s)ds \quad (4.1)$$

The combined electrode and membrane filter is then determined using a variance minimisation procedure following *Badel et al. (2008)*. This combined filter is made from the sum of two exponentials; one with a fast time constant (0.2-0.5 ms) that is due to the electrode and one with a slow time constant (~15 ms) that is due to the membrane. The exponential with the slower decay is subtracted from the combined filter to yield the electrode filter. Using this electrode filter, the component of the voltage due to the electrode can be calculated and subtracted from V_{rec} to obtain V.

4.2.2.6 Data analysis for Dynamic I-V

It is well established that the electrical properties of a neuron can be represented by an equivalent RC circuit *(Piwkowska et al., 2009)* in which the capacitor represents the charge storing ability of the phospholipid bilayer and the single resistor in parallel is equivalent to the combined transmembrane current passing through various ion channels embedded in the membrane. Thus, any current injected into the neuron (I_{inj}) can be equated to the sum of current passing through the capacitor (I_{Cap}) and current passing through the resistor (I_{ion}), as shown in equation (4.2).

$$I_{inj}(t) = I_{Cap} + I_{ion}(V,t) + I_{noise} \quad (4.2)$$

Additional sources of high frequency variability gives the term I_{noise} which also accounts for weak background synaptic activity. The passing of current through the capacitor (I_{Cap}) can be represented as the resulting change in potential difference across the membrane multiplied by the cell capacitance; equation (4.3).

$$I_{inj}(t) = C\frac{dV}{dt} + I_{ion}(V,t) + I_{noise} \quad (4.3)$$

The injected current (I_{inj}) is known beforehand (noisy current traces), the derivative dV/dt can be calculated from recorded voltage response, and the capacitance can be calculated using a standard optimisation procedure based on the variance of the voltage (V) *(Badel et al., 2008)*. Therefore, the ionic transmembrane current (I_{ion}) can be calculated as shown below:

$$I_{ion}(V,t) + I_{noise} = I_{inj}(t) - C\frac{dV}{dt} \quad (4.4)$$

A scatter plot of the transmembrane current against voltage illustrates the dynamic relationship between the two (figure 4.8c), with the majority of variability coming from intrinsic noise (I_{noise}) *(Badel et al., 2008)*. The average transmembrane current in 1 mV bins removes the time dependence of I_{ion} (V,t) and defines the dynamic I-V curve (I_{dyn}).

$$I_{dyn}(V) = Mean[I_{ion}(V,t)] \quad (4.5)$$

The exponential integrate-and-fire model, from the class of single-variable neuron models, follows the general structure

$$\frac{dV}{dt} = F(V) + \frac{I_{inj}(t)}{C} \quad (4.6)$$

Where the forcing function F(V) for the EIF model is given below (equation 4.7) and is equivalent to the inverse of the dynamic I-V over capacitance (equation 4.8; found by merging equations 4.5 and 4.6)

$$F(V) = \frac{1}{\tau_m}\left(E_m - V + \Delta_T exp\left(\frac{V-V_T}{\Delta_T}\right)\right) = -\frac{I_{dyn}(V)}{C} \quad (4.7)$$

$$F(V) = \frac{-I_{dyn}(V)}{C} \quad (4.8)$$

The EIF model has four parameters: membrane time constant (τ_m), resting potential (E_m), spike-initiation threshold (V_T) and spike-onset sharpness (Δ_T), which describes the voltage range over which an action potential initiates. The refractory properties were generated by making E_m, $1/\tau_m$ and V_T dependent on the time since the last spike; thus constituting the rEIF model. A dynamic I-V curve was constructed from post-spike data in each of the following time windows: 5-10, 10-20, 20-30, 30-50, 50-100,

100-200 ms. The rEIF parameters relax back to the EIF parameters over time with either a single exponential ($1/\tau_m$ and V_T) or double exponential (E_m) relaxation (figure 4.9).

The pre and post-spike parameters calculated from the EIF and rEIF models were used to simulate a voltage response to the same noisy current inputs. The accuracy of these parameters was then tested by comparing the simulated response to the experimentally recorded voltage trace. The number of matching spikes, aligning to within ± 5 ms, was typically 60-90 %. Percentage spike match was compared across all time points for neurons filled with αSyn and vehicle.

4.2.3 Immunofluorescence

4.2.3.1 Immunostaining

After patch clamp recording, the patch electrode was carefully removed from the recorded cell and the integrity of the cell assessed. If the cell was still intact, then the slice was fixed immediately in PFA buffer for at least 1 hr at 4 °C, after which the slice was washed repeatedly with PBS (3 x 10 minutes). Slices were incubated for 1hr at room temperature in blocking buffer before being resuspended in either anti-αSyn or A11 antibodies (see western blot methods), 1/100 dilution in blocking buffer, for 1 hr at room temperature followed by overnight incubation at 4 °C. The primary antibodies were aspirated and the slices washed thoroughly in PBS (5 x 10 minutes) prior to the addition of secondary antibodies (1/100 in blocking buffer): Alexa Fluor® 568 goat anti-mouse IgG (H + L) for anti-αSyn staining or Alexa Fluor® 647 chicken anti-rabbit IgG (H + L) for A11 staining (molecular probes, #A11004 & #A21443 respectively).

Slices were incubated in secondary antibodies for 4 hours at room temperature and washed into PBS afterwards. For the purposes of background nuclear staining, slices were stained with DAPI (1 μg/ml in blocking buffer) for 4-8 minutes followed by repeated washes (5 x 4 minutes) with PBS.

Each slice was mounted onto a glass slide and excess liquid removed with filter paper. The slice was framed by a plastic coverslip and preserved with a drop of VECTASHIELD® mounting medium (Vector laboratories Ltd). A glass coverslip was placed on top and sealed down. Slices were stored at 4 °C before imaging on confocal microscopy.

4.2.3.2 Conjugation of Dylight-594 to αSyn

In addition to the immunostaining of fixed brain slices, monomeric αSyn was directly labelled with Dylight-594 to provide a quicker, more effective means of detecting αSyn intracellularly with confocal microscopy. The abundance of primary amine side chains in αSyn provide multiple covalent binding sites for N-hydroxysuccinimide (NHS) activated Dylight-594 esters. The protein was tagged using a Dylight labelling kit (Thermo Scientific) following the given instructions. In brief; monomeric αSyn stock was diluted to 1 mg/ml in PBS + 0.05 M Borate buffer (500 µl total volume) and added to 65 µg of lyophilised Dylight-594 NHS ester. The mixture was protected from light and left to stand for 4 hours at room temperature. Unbound ester was removed using the purification resin and microcentrifuge spin columns provided in the kit. The dye/protein ratio was calculated as described in the kit; by comparing the protein absorbance (A_{280}) to the absorbance at maximum excitation for Dylight-594 (A_{595}). Monomeric αSyn was found to be labelled at a ratio of 2.57 moles of dye per mole of protein. Labelled αSyn was aliquoted, flash frozen and stored at -20 °C until use. Attempts to label oligomeric αSyn directly were unsuccessful due to low protein concentrations. Labelled monomer did not readily aggregate into labelled oligomers and was not incorporated into aggregates when incubated in the presence of unlabelled αSyn (as determined by A_{595} absorbance).

4.2.3.3 Confocal microscopy

For all confocal experiments, the pinhole setting was 70 µm and scan speed was 400 Hz. Fluorescence antibodies were excited using multiple lasers in sequential scan mode; the gain and offset for each laser was held constant across all experiments. Control slices, incubated with secondary antibodies only, were imaged at the same confocal settings as those for recorded cells.

A drop of immersion oil was added on top of a mounted slice before positioning in an inverted microscope attached to a Leica SP5 confocal head (Leica Microsystems, Germany). Patched cells were located with an HCX PL APO lambda blue 40.0 x 1.25 OIL UV objective using epifluorescence from an EL6000 external light source. All images, z-stacks and tile scans were recorded and analysed in Leica acquisition software (LAS AF lite). Single images were the accumulative average of 3 frame scans and the optimal step size (0.5-0.13 µm) for z-stacks was determined by the software

depending on the objective being used. Neuron morphology was observed under 400 x magnification while studies of intracellular αSyn accumulation were recorded at 630 x and 1000 x magnification (HCX PL APO 62 x 1.40 OIL and HCX PL APO CS 100.0 x 1.40 OIL objectives respectively). All tile scans and z-stacks are presented as maximal projections.

4.3 Results

4.3.1 Preparation of oligomeric and monomeric αSyn in intracellular solution

Preliminary investigation showed that oligomeric αSyn preparations remained immunoreactive to the A11 antibody after several hours when diluted in intracellular solution and after being passaged out of the tip of patch pipettes (figure 4.1a). To prevent impurities from interfering with the formation of a tight seal in patch clamp recordings, the intracellular solution was passed through a standard filter (pore size 0.45 μm). However, A11 immunoreactivity was lost after passing the oligomer-containing intracellular solution through the filter; although samples still remained positive for anti-αSyn antibodies. It was thus deduced that oligomers, but not monomers, were removed by filtration. To prevent this from happening, the intracellular solution was filtered prior to the addition of oligomeric αSyn. However filtering the intracellular solution containing monomer ensured that any larger αSyn aggregates were removed during these experiments. A dilution series of αSyn oligomers (figure 4.1b) showed that the lower limit for A11 antibody detection was ~250 nM. The detection of monomer by anti-αSyn was more sensitive and remained positive at concentrations as low as 100 nM. Therefore, the concentration of αSyn species added to the intracellular solution for whole-cell patch clamp recordings was 500 nM; enough to allow diffusion into recorded cells and for immunofluorescence staining.

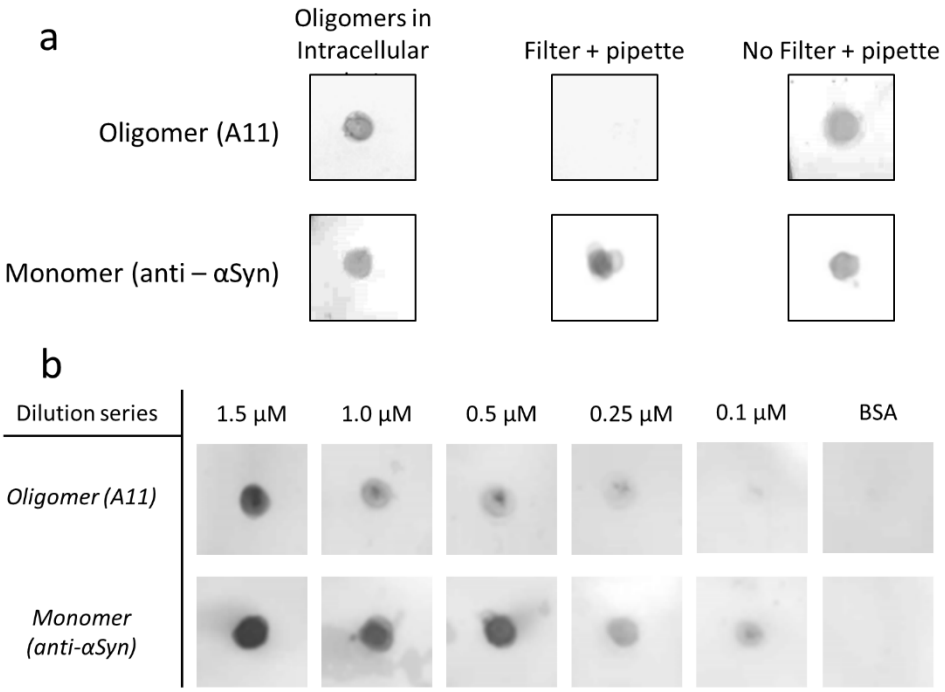

Figure 4.1 Oligomeric αSyn remains A11 positive after being added to intracellular solution but cannot pass through the filter. (a) Oligomers were tested with A11 (top) and anti-αSyn antibodies (bottom). Oligomers were stable in intracellular solution and passed out of the tip of the patch pipette, but were removed by the filter. Filtered αSyn remained positive for anti-αSyn indicating that monomers were able to pass through the filter. As such oligomers, but not monomers, were not filtered prior to patch clamping experiments. (b) Dilution series of αSyn oligomer and monomer to examine the strength of antibody immunoreactivity. Dot blots of oligomer become undetectable after ~0.25 µM while monomer remains positive at concenrations as low as 100 µM..

4.3.2 Introduction of αSyn into neurons via whole-cell patch clamp technique

To investigate the effects of αSyn species on neuronal electrophysiological properties, monomeric and oligomeric species were introduced into thick-tufted layer 5 (TTL5) pyramidal cells via the patch pipette during whole-cell patch clamp recordings. Including αSyn in the patch pipette, particularly without prior filtering, increased the risk of blockage at the tip of the electrode. The build-up of an αSyn aggregates in the electrode would increase the series resistance and thus worsen the voltage error during recordings. Therefore, the series resistance was carefully monitored at each time point (figure 4.2) and recordings were rejected if it exceeded 15.0 MΩ. In the data set (15 control recordings, 14 with monomer, 16 with *mOligomer* and 12 with *fOligomer*) there was no significant difference in the series resistance at time zero (breakthrough into whole cell, in MΩ: control 12.2 ± 0.28, monomer 12.1 ± 0.18, *mOligomer* 11.81

± 0.20, *fOligomer* 12.0 ± 0.18) and after 32 minutes of recording (in MΩ: control 13.1 ± 0.23, monomer 12.6 ± 0.19, *mOligomer* 12.38 ± 0.19, *fOligomer* 12.3 ± 0.14).

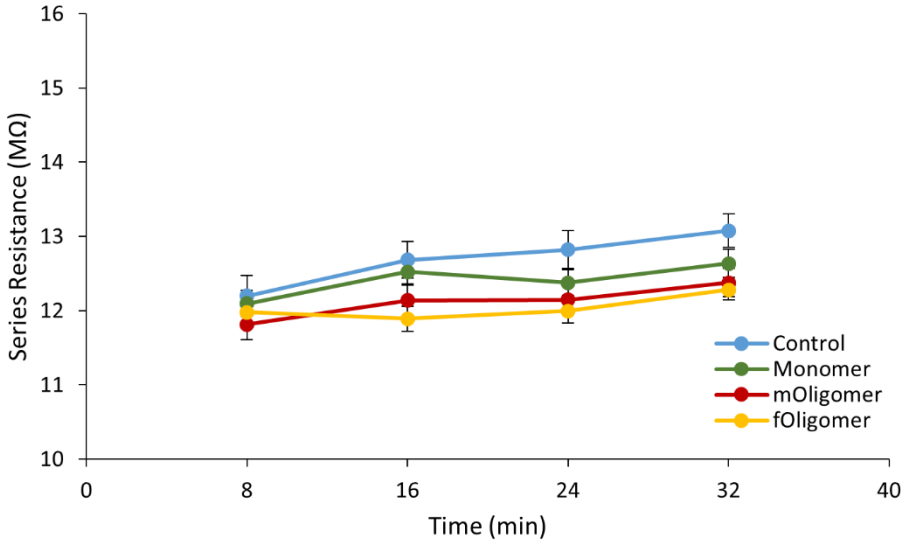

Figure 4.2 The series resistance of neurons was monitored over time to ensure that αSyn was not blocking the patch pipette. The series resistance did not significantly change throughout the duration of recordings for any of the experimental conditions. The cut-off point for series resistance was 15 MΩ; above which recordings were rejected.

In addition to αSyn, the intracellular solution in the patch pipette contained fluorescence dye (Alexa Fluor® 488) that rapidly diffused into cells so their morphology could be visualised (figure 4.3a). In the rare event of the pipette becoming blocked (fewer than 1 in 10 pipettes were blocked), the dye would also reveal this disruption (figure 4.3b) and the recordings would be disregarded.

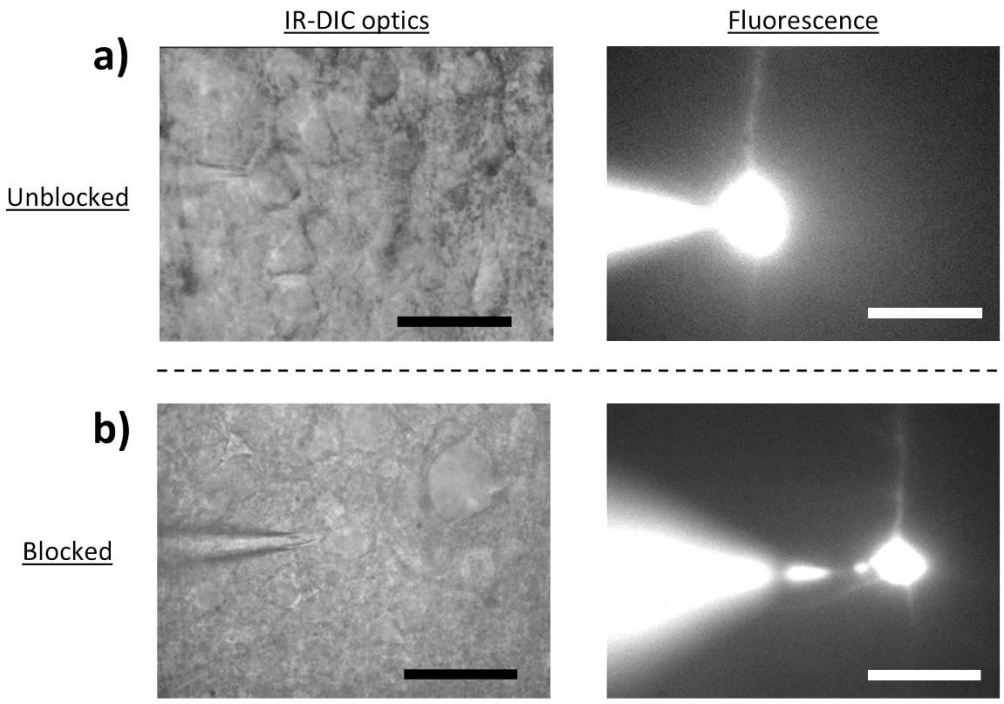

Figure 4.3 During whole-cell patch clamp recordings Alexa Fluor® 488 dye diffuses into the neuron so that its morphology can be visualised. The dye provides a way of monitoring blockages in the pipette tip. In the majority of experiments no blockage was seen (a), however, in a small number of cases a blocked tip (b) was revealed by the dye and the experiments were disregarded. Scale bars = 20 µm.

4.3.3 Identification of thick-tufted layer 5 (TTL5) pyramidal neurons

TTL5 pyramidal neurons are the largest of all the cortical cells and can be identified by their distinct morphology *(Larkman, 1991; Kasper et al., 1994)* (figure 4.4). TTL5 neurons characteristically display a long apical dendrite, which ascends to layer 1 bifurcating along the way, and thin basal dendrites that project outward from the base of the soma in all directions *(Markram, 1997; Ramaswamy et al., 2012)*. Slender-tufted pyramidal neurons are also found in layer 5 and are similar in size. However, their lack of bursting activity and reduced I_H current means that they could be distinguished from TTL5 pyramidal neurons *(Kasper et al., 1994)*.

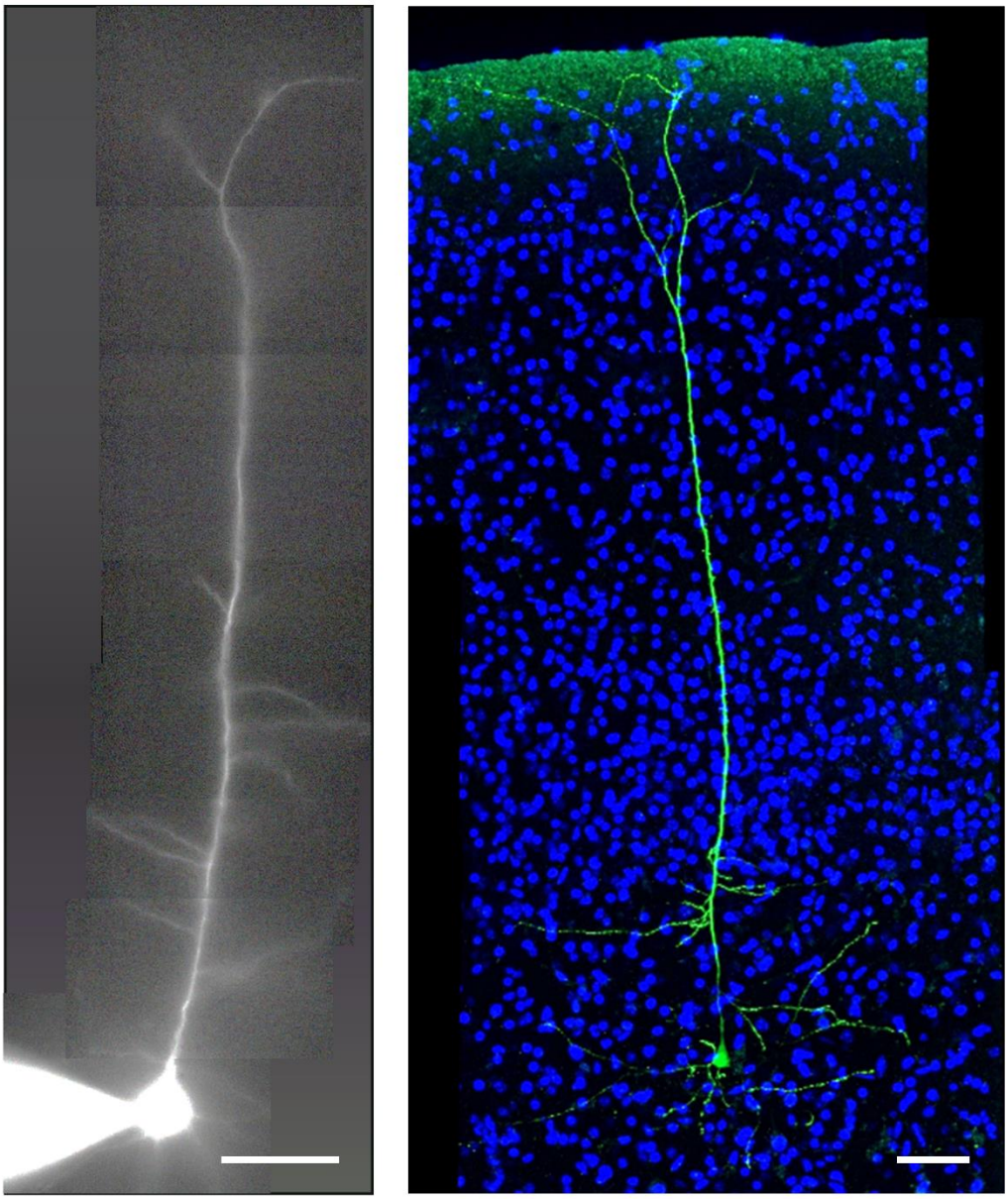

Figure 4.4 Thick-tufted layer 5 pyramidal neurons were identified by their size, distinct morphology and position within the neocortex. Neurons were visualised by fluorescence at 488 nm, both during whole-cell patch clamp recordings (left) and afterwards with confocal microscopy (right). NOTE; the two images presented here are separate examples of TTL5 pyramidal neurons. Green = Alexa Fluor® 488, blue = DAPI. Scale bars = 50 μm.

4.3.4 Endogenous expression of αSyn in the neocortex

In order to determine the effects of αSyn injected intracellularly into TTL5 neurons, it is necessary to show that protein in the patch pipette is able to diffuse into recorded cells. However, it was first important to examine the background expression of native αSyn so that it may be distinguished from the recombinant αSyn injected during recordings. Endogenous expression of αSyn in the CNS has been previously studied at a subcellular level *(Vivacqua et al., 2011)*. Here we investigated the varying expression levels of native αSyn in brain slices using an anti-αSyn antibody (figure 4.5), with particular focus on the layers of the neocortex (figure 4.6).

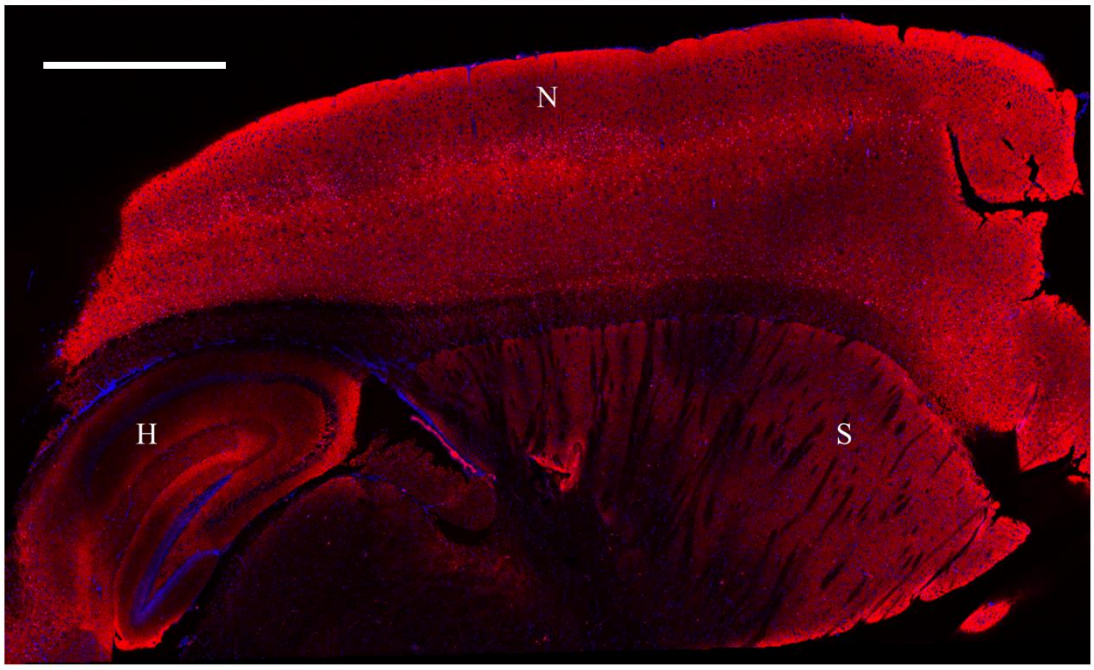

Figure 4.5 Endogenous expression of αSyn throughout the neocortex, hippocampus and striatum. A parasagittal section of mouse brain immunostained with anti-αSyn antibodies (red). N – neocortex, H – hippocampus, S – striatum. Scale bar = 1mm.

Similar to previous findings, αSyn was abundant in the hippocampus and striatum *(Vivacqua et al., 2011)*. For the majority of the cortical layers (1, 2/3 and 5) αSyn was not observed in the somata; thus creating a void pattern around the DAPI stained nuclei (figure 4.6). Some layer 4 neurons, however, showed distinctly strong levels of αSyn in both the nucleus and cytosol. Some neurons in layer 6 were also positive for intracellular αSyn though not as notably. Immunofluorescence staining also shows αSyn in other areas separate to the soma that may highlight its presynaptic localisation. Although this cannot be certain without additional markers, similar patterns of

immunofluorescence have been seen for αSyn localised to synaptic terminals *(Vivacqua et al., 2011)*. The finding that layer 5 pyramidal neurons have little endogenous αSyn in their soma and dendrites means that recombinant αSyn monomer and oligomer, applied intracellularly via the patch pipette, can easily be identified.

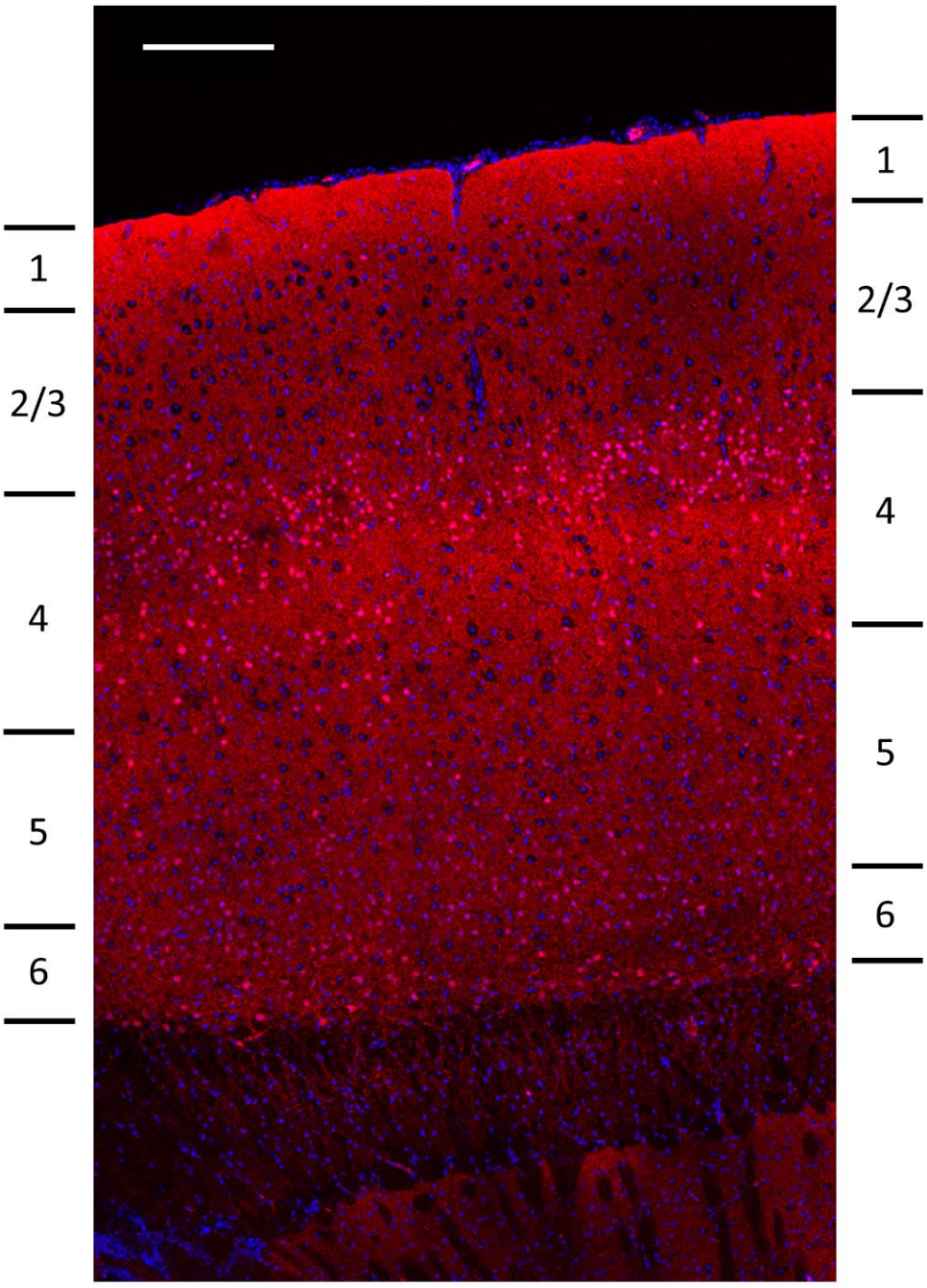

Figure 4.6 Endogenous expression of αSyn in the mouse somatosensory neocortex; magnified from figure 4.5. The layers of pyramidal neurons are labelled on each side. Layers 4 and 6 in particular show some expression of native αSyn within cell bodies while layers 1, 2/3 and 5 appear void of αSyn. Scale bar = 200 μm.

4.3.5 Detection of intracellularly injected αSyn species

Following whole cell patch clamp recording and slice fixation, αSyn species could be detected inside TTL5 pyramidal neurons. This was achieved by immunofluorescence staining with either A11 or anti-αSyn antibodies for cells filled with oligomer (figure 4.7a) or monomer (figure 4.7b) respectively. Oligomer was mainly detected in the soma of cells while monomer was detected in both the soma and going up the apical dendrite. Neither monomer nor oligomer were detected in the dendritic tufts, even after

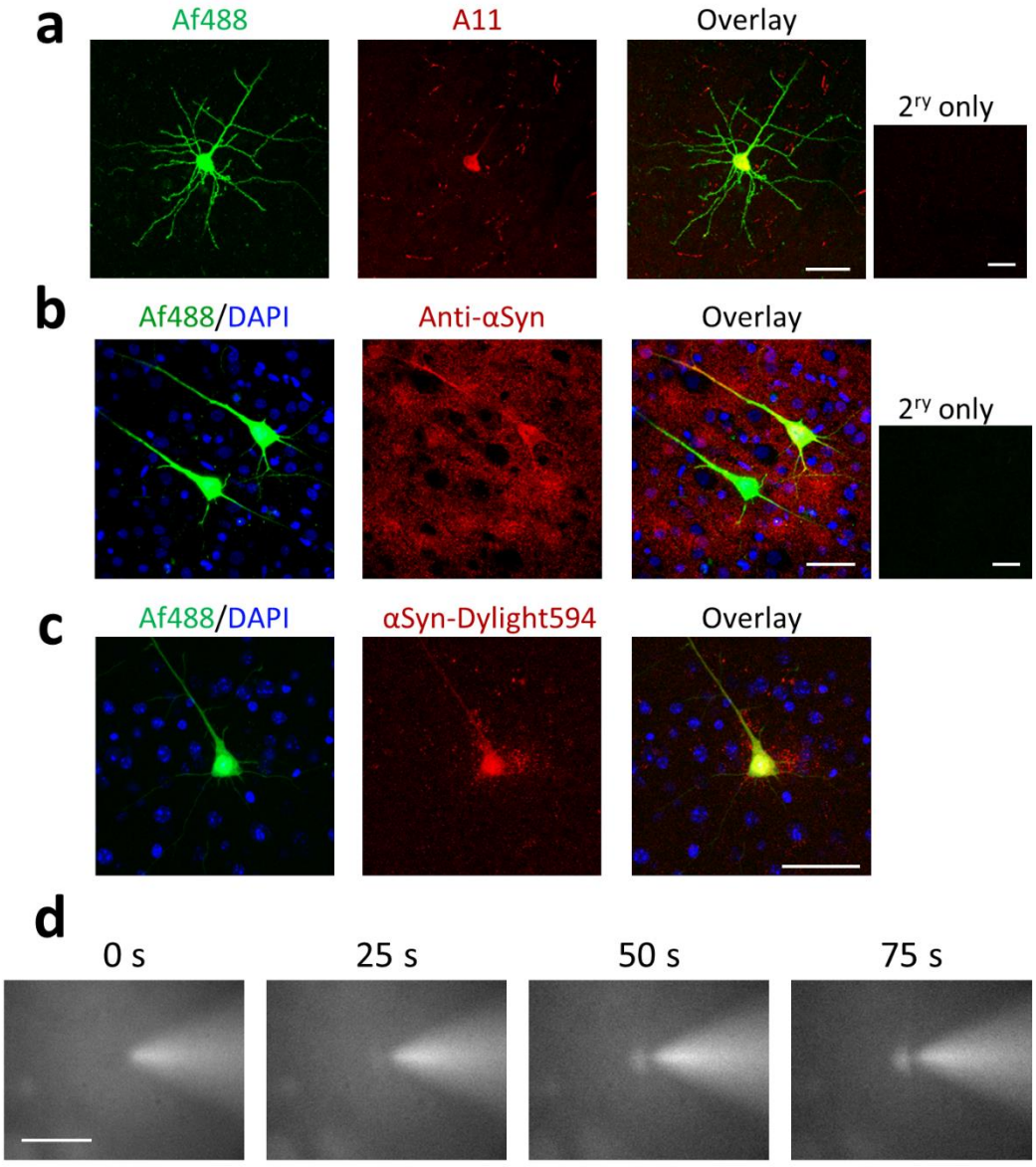

Figure 4.7 Immunofluorescence staining of neurons filled with αSyn species. During whole-cell patch clamp recordings, both oligomeric (a) and monomeric (b, right) αSyn diffused into the recorded neurons and was detected by immunofluorescence staining (red = A11 or anti-αSyn). In neurons injected with vehicle (b, left), immunostaining with anti-αSyn produced a void pattern indicating low native expression levels of αSyn in the soma. (c) Injecting conjugated αSyn-Dylight594 directly demonstrated αSyn diffusion into the recorded neuron and can be visualised in real time (d). Scale bars = 50 μm.

two hours of recording. Since only low background levels of αSyn were seen inside TTL5 neurons, it was possible to distinguish between vehicle filled neurons (figure 4.7b, left) and neurons filled with recombinant monomer (figure 4.7b, right). To further demonstrate protein diffusion out of the patch pipette and into the cell, αSyn monomer was conjugated to Dylight-594™ (figure 4.7c). With fluorescence labelling, αSyn could even be recorded live rapidly passing from the pipette into the cell (figure 4.7d).

4.3.6 Deriving electrophysiological parameters from neurons using the dynamic I-V method

A pair of naturalistic noisy currents with low and high variance (see methods) were injected, in series, into neurons at 8 minute (start-to-start) intervals following the injection of typical step current protocols (for standard I-V measurements). The voltage responses to these noisy currents were recorded using a single electrode setup with compensation to remove the electrode filter. To demonstrate the accuracy of the de-filtering process (see methods) a preliminary dual recording experiment was carried out in which both electrodes were attached to the soma of the same neuron; current was injected from one pipette and the voltage measured from both simultaneously. The differences in recorded voltage between the injecting electrode and the control electrode were removed by the filtering process (figure 4.8a) which is able to effectively separate the electrode voltage from the true membrane voltage. The dynamic I-V curve (I_{dyn}) is equivalent to the average transmembrane current (I_{ion}) (figure 4.8b), calculated from the difference between injected current (I_{inj}) and capacitive current (CdV/dt), at a given voltage (figure 4.8c) (see methods and *Badel et al. (2008)*). The forcing function for an exponential integrate-and-fire (EIF) model;

$$\frac{dV}{dt} = F(V) + \frac{I_{inj}(t)}{C}$$

equates to the inverse of I_{dyn} over capacitance (figure 4.8d), thus providing a rapid and accurate protocol for extracting neuron parameters. The refractory properties of neurons were found by modelling the post-spike data in subdivided time windows (figure 4.9a), giving EIF parameters that exponentially relax back to the pre-spike parameters (figure 4.9b).

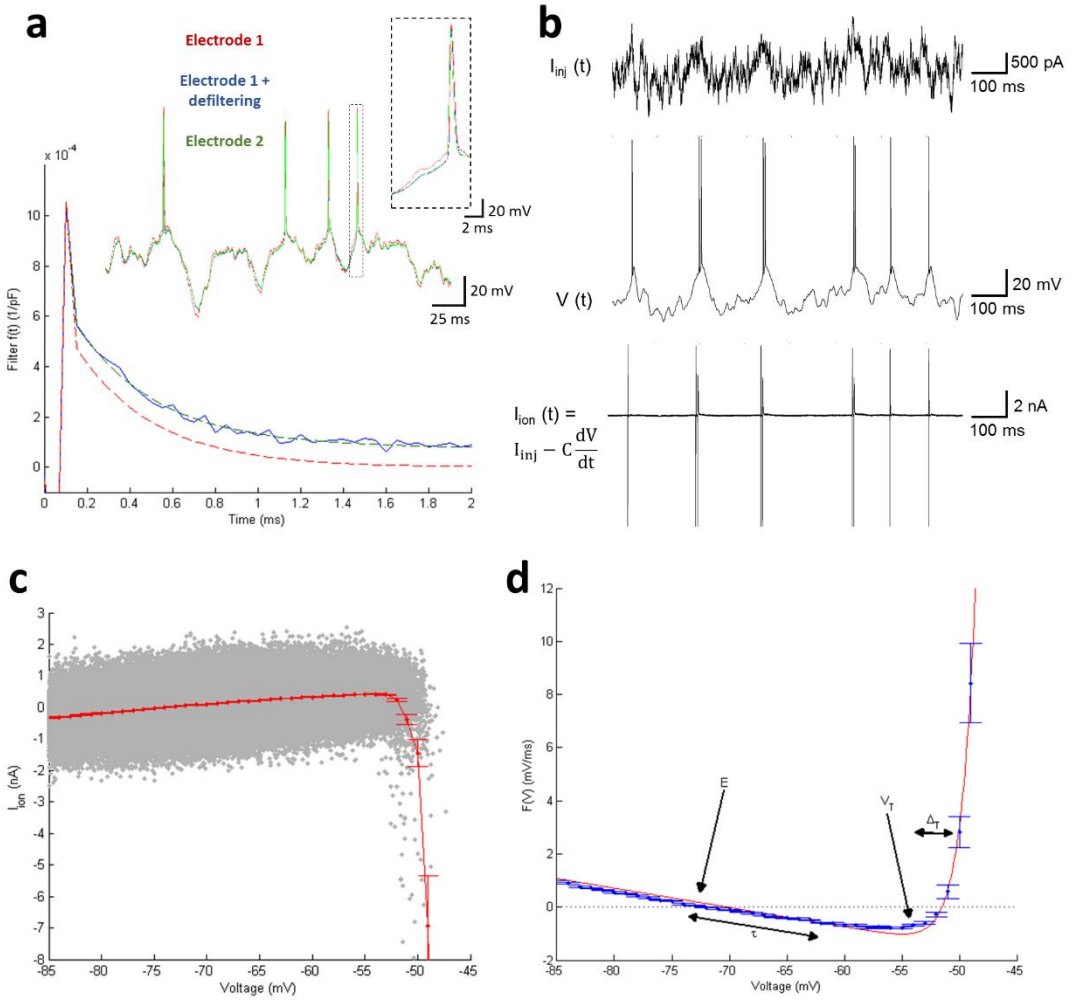

Figure 4.8 Generating the dynamic I-V curve and extracting parameters. (a) The optimal linear filter of the combined electrode and neuron. The sum of two exponentials (green dashed line) is fitted to the combined filter (blue). Removing the slower of the two exponentials, associated with the membrane response, provides the pure electrode filter (red dashed line). Inset: a control electrode (electrode 2, green) illustrates both the necessity and accuracy of defiltering when compared to the current – passing electrode (electrode 1; before (red) and after (blue) defiltering). (b) Neurons were stimulated with naturalistic current (I_{inj} (t), top) and the voltage response was recorded (V (t), middle). The ionic transmembrane current (I_{ion} (t), bottom) is calculated from the difference between stimulated current and capacitance current. (c) A scatter plot of I_{ion} (t) against V (t) (grey), with data 200ms after each spike excluded. The average I_{ion} in 1 mV bins constitutes the dynamic I-V curve I_{dyn} (red). (d) Thus, the experimentally derived data (blue points = inverse of I_{dyn} over capacitance) can be closely fitted to a computational neuron model (red = EIF model fit) from which electrophysiological parameters can be extracted; the roles of these various parameters are shown (E = resting membrane potential, τ = time constant, V_T = spike – initiation threshold and Δ_T = spike – onset sharpness)

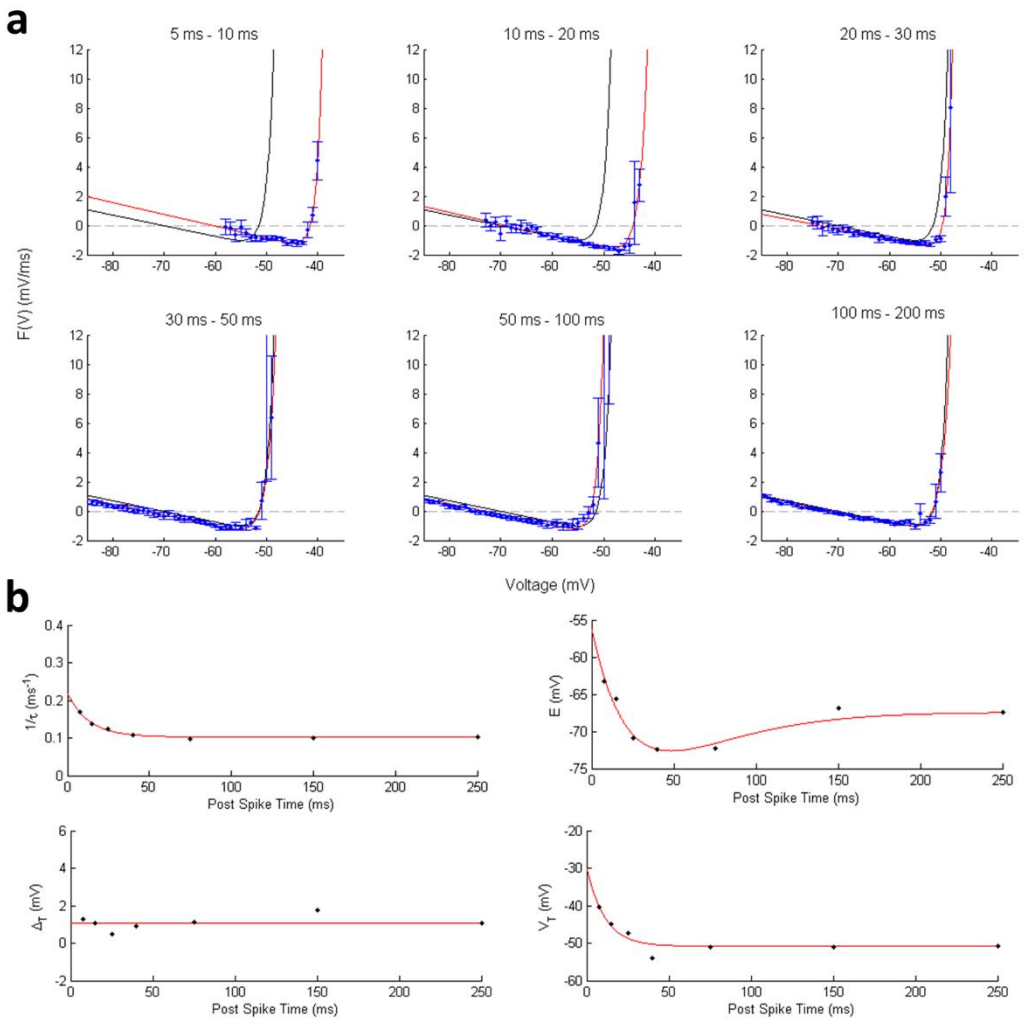

Figure 4.9 Measuring the refractory properties of neurons. (**a**) Dynamic I-V curves, generated from post – spike data in different time windows, show how neuron properties are shifted after firing but relax back over time to the pre-spike/subthreshold curve (black). (**b**) The relaxation of post-spike parameters over time: dots indicate parameters measured from EIF model fits in (a), red lines show relaxation with either a single ($1/\tau$ and V_T) or double (E) exponential. The spike-onset sharpness (Δ_T) did not consistently change during the post-spike time.

Figures 4.8 and 4.9 illustrate the dynamic I-V method in which experimental measurements may be used to parameterise EIF and rEIF neuron models. To assess the accuracy of this method parameters, extracted over time from neurons filled with either control or αSyn species, were used to simulate voltage responses *in silico* which were compared to the original experimentally recorded voltage traces (figure 4.10a-d). Both simulated and recorded voltage traces were produced from the same noisy current input. The percentage of matching spikes between recorded and simulated traces (± 5 ms), were above 70 % for all experimental conditions (vehicle, monomer, *mOligomer* and *fOligomer*) and did not significantly change over time (after 32 minutes, the percentage of correctly identified spikes was: control 79.1 ± 2.9 %, monomer 77.0 ± 3.6 %, *mOligomer* 72.4 ± 3.7 % and *fOligomer* 75.7 ± 5.5 %) (figure 4.10e). This degree of spike matching is similar to previously reported values for layer 5 pyramidal cells *(Badel et al., 2008).* Thus, the accuracy of parameter extraction is not compromised by perfusion of cells with either monomeric or oligomeric αSyn. Note that the spike matching will never be 100 %, due to spontaneous synaptic activity in experimental recordings which is absent in the simulations.

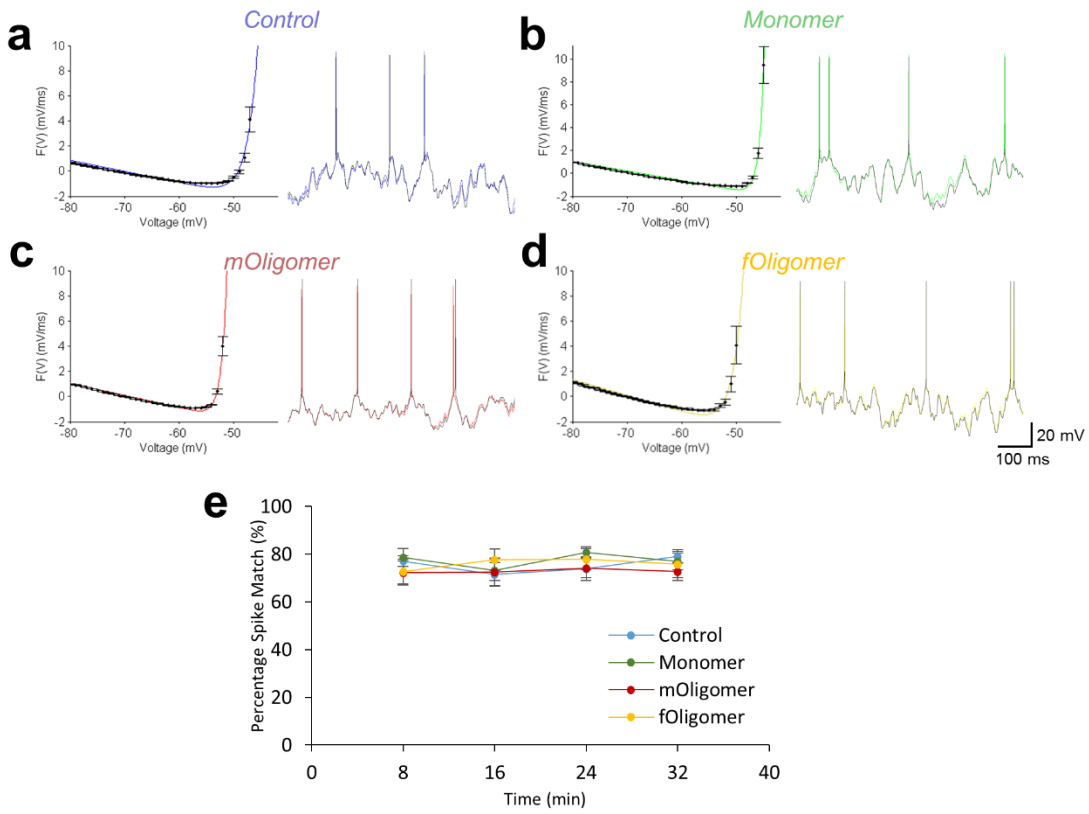

Figure 4.10 Percentage spike matching between recorded and simulated voltage responses in control and αSyn filled neurons. For control (a, blue), monomer (b, green), mOligomer (c, red) and fOligomer (d, yellow) filled neurons there is a consistently good fit of EIF model (line) to the F(V) derived from DIV curve (points). Next to each plot is a comparison of rEIF model simulation (black) to the experimentally recorded voltage (coloured); showing accurate spike prediction. Model fitting in this way means the reliability of the extracted parameters can be assessed. The percentage spike matches between experimentally recorded and rEIF simulated voltage traces (e) remain greater than 70% for all time points and for all αSyn populations, showing the dynamic IV method to be a consistently accurate approach to measuring neuronal changes in the presence of αSyn.

4.3.7 Standard I-V curves

Prior to injecting the noisy current at each time point, a short sequence of incrementing step currents were injected into neurons; the subthreshold response to which (figure 4.11a) was used to produce standard I-V curves (figure 4.11b). The standard I-V curve provides an alternative method for characterising neuron electrophysiology and can be constructed from the voltage response either before the sag due to inward rectifying current (I_H) or during the steady state that follows (V_{sag} or V_{steady} respectively). The gradient of the standard I-V curve around the resting potential equates to the neuron's input resistance.

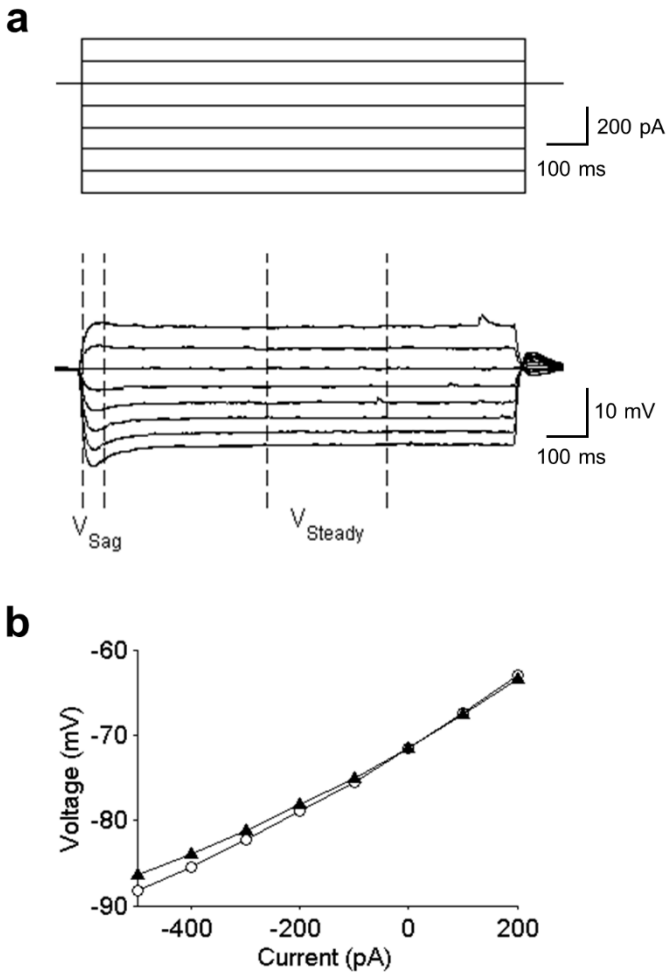

Figure 4.11 Generating the standard I-V curve. (a) Step currents (top) were injected into neurons and the subsequent voltage responses recorded (bottom). The standard I-V curve (b) was calculated from either the maximum voltage change during the initial sag (V_{Sag}; circles) and during steady state (V_{Steady}; triangles). The values of V_{Sag} and V_{steady} were the average voltage between the indicated dashed lines. The gradient of the standard I-V curve at 0 pA equates to the input resistance of the cell.

4.4 Discussion

The aim of the work outlined in this chapter was to develop a system whereby monomeric and oligomeric αSyn species could be injected into TTL5 pyramidal neurons and their electrophysiological properties monitored over time. To achieve this, I used the whole-cell patch clamp recording method in which αSyn was present in the intracellular recording solution. This novel approach allowed αSyn to pass via the pipette tip into the recorded cell and at the same time enabled electrophysiological measurements to be made using standard and dynamic I-V curves.

Oligomeric αSyn remained A11-positive after being diluted in intracellular solution. While figure 4.1 demonstrates that oligomers are indeed present after several hours, their dynamic nature could mean that a small fraction might have separated back into monomer. Therefore, the true concentration of oligomeric αSyn in the intracellular solution may be lower than the desired concentration of 500 nM. However, many studies have previously investigated αSyn toxicity and pore-like membrane permeabilisation activity using concentrations equivalent to or lower than 500 nM *(Huels et al., 2011; Diogenes et al., 2012; Martin et al., 2012; Tosatto et al., 2012; Mironov, 2015). Diogenes et al. (2012)* demonstrated impaired LTP action of αSyn oligomers in hippocampal neurons using concentrations lower than 100 nM. Similarly, amyloid-β peptides were shown to inhibit hippocampal LTP in a concentration dependent manner; reaching a maximal effect after 200 nM *(Ripoli et al., 2014).* A dilution series of A11 immunoreactivity (figure 4.1b) shows that concentrations lower than ~250 nM are too weak to be detected. Therefore, while the exact oligomer concentration in intracellular solution may change, the difference is likely to be small and far above the minimum concentration used in other studies to elicit toxic effects.

The stability of the series resistance of recordings over time (figure 4.2) and the continuous passage of Alexa Fluor® 488 dye (figure 4.3) into the recorded cell confirms that the pipettes did not become blocked at any point during experiments. The diffusion of αSyn out of the patch pipette and into the soma was confirmed by immunofluorescence staining. To identify injected αSyn it was first important to assess the levels of endogenous αSyn in the neocortex (figures 4.5 & 4.6). Endogenous αSyn is expressed in a wide range of neuronal cell types including dopaminergic, noradrenergic and cortical neurons, as well as non-neuronal cell types such as

endothelial cells and platelets *(Hashimoto et al., 1997; Abeliovich et al., 2000; Li et al., 2002; Tamo et al., 2002; Baltic et al., 2004)*. Interestingly, αSyn appeared to be differentially expressed in the various cortical layers, with some showing clear somatic expression (layers 4 and 6) while others were distinctly void of αSyn in their soma (layers 1, 2/3 and 5). The visualisation of endogenous αSyn is dependent on the choice of antibody. Monoclonal 2E3 antibodies, for example, detect αSyn in nerve cell fibers while 3D5 antibodies preferentially detect within nuclei *(Alim et al., 2004; Yu et al., 2007)*. Both these antibodies, however, have found that αSyn strongly associates with synaptic terminals in all the cortical layers *(Vivacqua et al., 2011)*. Nuclear localisation in the neocortex has been found to be absent from layers 1-3 and becomes increasingly abundant in layers 4-6 *(Vivacqua et al., 2011)*. The immunofluorescence presented here did not co-localise with DAPI suggesting cytoplasmic detection rather than specifically within the nucleus. In addition, immunofluorescence within each layer was not constant for every cell throughout the cortex, suggesting intra-layer variability that may highlight functional or area specificity. Pipette-to-soma diffusion was observed directly and in real time using conjugated αSyn-Dylight 594 (figure 4.7c-d). Attempts to incorporate labelled αSyn into oligomers were unsuccessful. Instead, A11 antibodies with conformational specificity *(Kayed et al., 2003)* were used to detect oligomeric αSyn inside recorded neurons.

TTL5 pyramidal neurons were identified by their morphological and electrophysiological properties. While the morphology of TTL5 pyramidal neurons are easily distinguishable from neurons in the other cortical layers, increasing evidence shows morphological variation within layer 5 that can be distinguished by differences in their subcortical projections *(Kasper et al., 1994; Hattox and Nelson, 2007; Oswald et al., 2013)*. However, the intrinsic morphological diversity of TTL5 neurons has also been shown *in silico* to have no effect on average synaptic properties and may provide a mechanism for robust microcircuit behaviour *(Ramaswamy et al., 2012)*. The precise morphology-physiology relationship of layer 5 pyramidal neurons is still not fully understood and is beyond the scope of this thesis. Therefore, the TTL5 pyramidal neurons described in this thesis were examined as a collective since it was not possible to determine the subcortical projection for each neuron. In addition to ensure that recordings were made consistently from the same region of the neocortex, only those

with distinct burst firing and I_H currents were selected; thus eliminating slender-tufted neurons from the analysis.

To examine the electrophysiological properties of TTL5 pyramidal neurons, both standard and dynamic I-V curves were constructed from the voltage responses to step and naturalistic currents respectively. As shown in this chapter, and previously in the literature *(Badel et al., 2008)*, dynamic I-V curves fit closely to the EIF model which can extract subthreshold parameters, show post-spike refractory properties and accurately predict spike times. Integrate-and-fire models have both a long history and a wide range of applications *(Burkitt, 2006a)*. They are especially important for developing our understanding of neural network dynamics and temporal responses *(Burkitt, 2006b)*. While the literature focuses on modelling the physiological properties of neurons, my work attempts to utilise these models to capture the pathological activity of αSyn. As shown by the consistently accurate spike predictions (figure 4.10), the effects of αSyn species can be captured within the parameters of these quantitative models. A thorough analysis of the impact of αSyn on a wide range of parameters over time is presented in chapter 5. These findings should promote the use of pathology modelling to further elucidate the electrophysiological changes underpinning neurodegenerative disorders.

5 Oligomeric alpha-Synuclein alters the electrophysiological properties of thick-tufted layer 5 pyramidal neurons in the neocortex

5.1 Introduction

The association between αSyn and cell death has been well established from expression models in yeast *(Outeiro and Lindquist, 2003)*, flies *(Park and Lee, 2006)*, nematode worms *(Kuwahara et al., 2006)* and rodents *(Winner et al., 2011)*. However, many of the symptoms of neurodegenerative diseases present themselves not necessarily as the direct result of cell death but rather through progressive neuronal dysfunction or network compensation *(Linazasoro, 2007; Nikolaus et al., 2009; Appel-Cresswell et al., 2010)*. Therefore, while it is important to develop our understanding of oligomer toxicity at the molecular level, investigating changes in neuronal function and electrophysiological properties may reveal how oligomer toxicity translates into pathological symptoms.

In the hippocampus, for example, αSyn oligomers have been shown to impede long term potentiation and modulate synaptic transmission; forming the basis for impaired memory and learning observed in disease patients *(Diogenes et al., 2012; Martin et al., 2012)*. In contrast to the hippocampus, however, much less is known about the toxicity of αSyn on pyramidal neurons in the neocortex; despite these regions being similarly afflicted neurodegenerative disorders.

Numerous theories exist surrounding the toxicity mechanisms through which αSyn oligomers act. Variations in toxicity can often be attributed to the structural and biophysical heterogeneity of the oligomers used *(Roberts and Brown, 2015)*. Soluble, annular oligomers of αSyn have been shown to form membrane-inserting pore complexes that allow the passage of cations in a non-selective manner *(Schmidt et al., 2012)*. Stepwise changes in membrane conductance have been observed after incubating αSyn with either planar bilayers *(Kim et al., 2009; Schmidt et al., 2012; Tosatto et al., 2012)*, or cell cultures *(Feng et al., 2010; Mironov, 2015)*. This action of αSyn oligomers has been compared to leak channels in neuronal membranes that promote excitability through distortions in ion homeostasis. While some have observed kinetic and pathological differences between oligomers applied to the

extracellular side of the membrane compared to insertion from the intracellular side *(Schmidt et al., 2012; Mironov, 2015)*, others have shown that internalisation and intracellular accumulation are vital for effecting changes in neuronal behaviour *(Ripoli et al., 2014)*.

Thus far, in chapter 3 two oligomeric species of αSyn were isolated from separate points along the aggregation pathway and structurally characterised. In chapter 4, using whole-cell patch clamping technique, monomeric and oligomeric αSyn was injected into TTL5 pyramidal neurons in the neocortex of mice. In this chapter, I use standard and dynamic I-V curves to examine the changes in electrophysiological parameters of neurons over time in the presence of αSyn oligomers. By employing an efficient method for neuronal model identification, described in chapter 4 *(Badel et al., 2008)*, I offer an in depth analysis of toxicity-induced changes in neuronal parameters to give insight into the mechanism through which oligomers act. Over time, neurons injected with these two oligomeric species displayed a similar reduction in input resistance compared to either control or monomer-injected neurons. Consequentially, the amount of current needed for spike initiation was significantly elevated and the firing rate markedly slower. These effects on neuron excitability could account for many of the cognitive symptoms prevalent throughout PD.

5.2 Methods of analysis

Using either the standard or dynamic I-V methods described in chapter 4, parameters were extracted from neurons with different treatments of αSyn and over a range of time points. Individual treatments were compared across different time points using repeated measures Analysis of Variance (ANOVA). At set time points, different αSyn treatments were analysed using two-tailed t tests with Bonferoni Correction for multiple comparisons. With the exception of threshold voltage, resting potential and spike amplitude, the parameters did not follow a normal distribution and, unless stated otherwise, are presented here as the mean value with bootstrap 95 % confidence intervals (made from 2000 bootstrap samples).

5.3 Results

Alpha Synuclein monomers and oligomers were injected into TTL5 pyramidal cells via the patch pipette (all at 0.5 μM). In control recordings, an equivalent volume of the buffer in which monomer and oligomer were dissolved (PBS 5 % V/V) was added to the intracellular solution. To monitor the changes in neuron parameters over time, both stepwise and naturalistic currents were injected in series at 8 minute (start-to-start) intervals, over a total period of 32 minutes. The resulting voltage responses were recorded, filtered and analysed by the standard and dynamic I-V methods outlined in chapter 4.

5.3.1 Impact of alpha-Synuclein on neuron parameters: marked reduction in input resistance

Dynamic I-V curves were generated for each αSyn treatment and at each time point (figure 5.1a). A number of parameters were extracted from the subthreshold and pre-spike data: membrane capacitance (C), membrane time constant (τ), input resistance (R_{in} = τ/C), resting membrane potential (E), spike threshold (V_T) and spike onset sharpness (Δ_T) (figure 5.1b).

In control cells (n = 18), the subthreshold parameters remained stable for the duration of experiments: values were not significantly different when measured at 8 minutes versus those measured at 32 minutes following whole cell breakthrough ($p > 0.05$ for all parameters). Since control parameters were unaltered after 32 minutes, I investigated whether parameters had changed at this point for neurons perfused with αSyn. A comparison of the effects of monomer (n=20) after 32 minutes showed no significant change ($p > 0.05$) in any of the parameters compared to control. There were, however, significant changes in parameters for both *mOligomer* (n = 19) and *fOligomer* (n = 13) filled neurons. After 32 minutes, there was a significant ($p < 0.005$) decrease in the input resistance (R_{in}) of recorded cells: from (mean ± std dev) 89.0 ± 22.3 MΩ in control cells to 55.1 ± 16.0 MΩ and 59.7 ± 18.6 MΩ in cells perfused with *mOligomers* and *fOligomers* respectively, a reduction of ~ 40 % (figure 5.1b). As expected, the membrane time constant was also significantly reduced ($p < 0.005$) from 16.1 ± 4.6 ms (control) to 11.8 ± 2.9 ms (*mOligomer*) and 13.1 ± 3.3 ms (*fOligomer*), a reduction of ~ 36 %. The membrane capacitance had significantly increased by ~20

% in oligomer perfused cells: from 183 ± 39.8 pF (control) to 219 ± 40.3 pF (*mOligomer*, $p < 0.005$) and 228 ± 56.1 pF (*fOligomer*, $p < 0.05$).

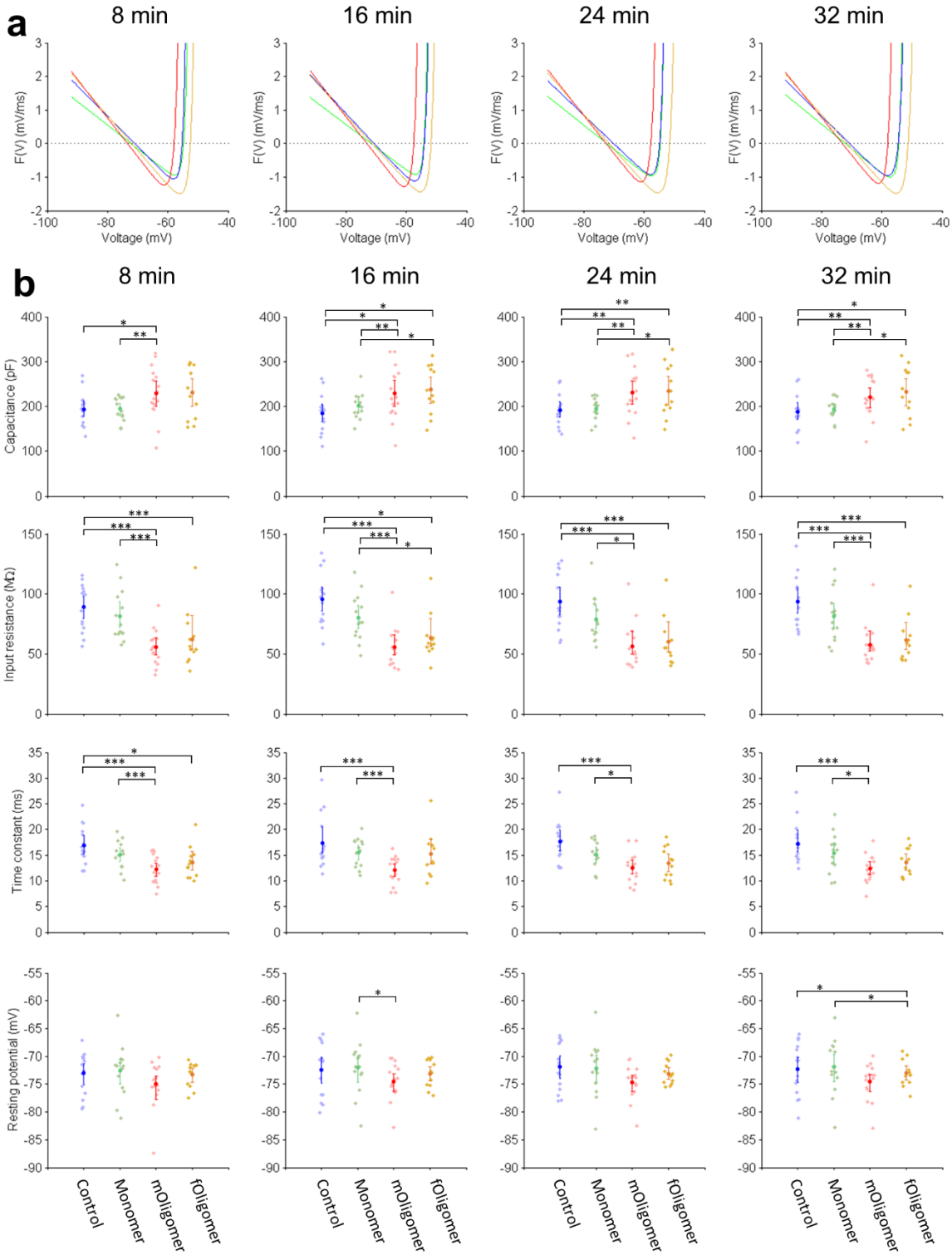

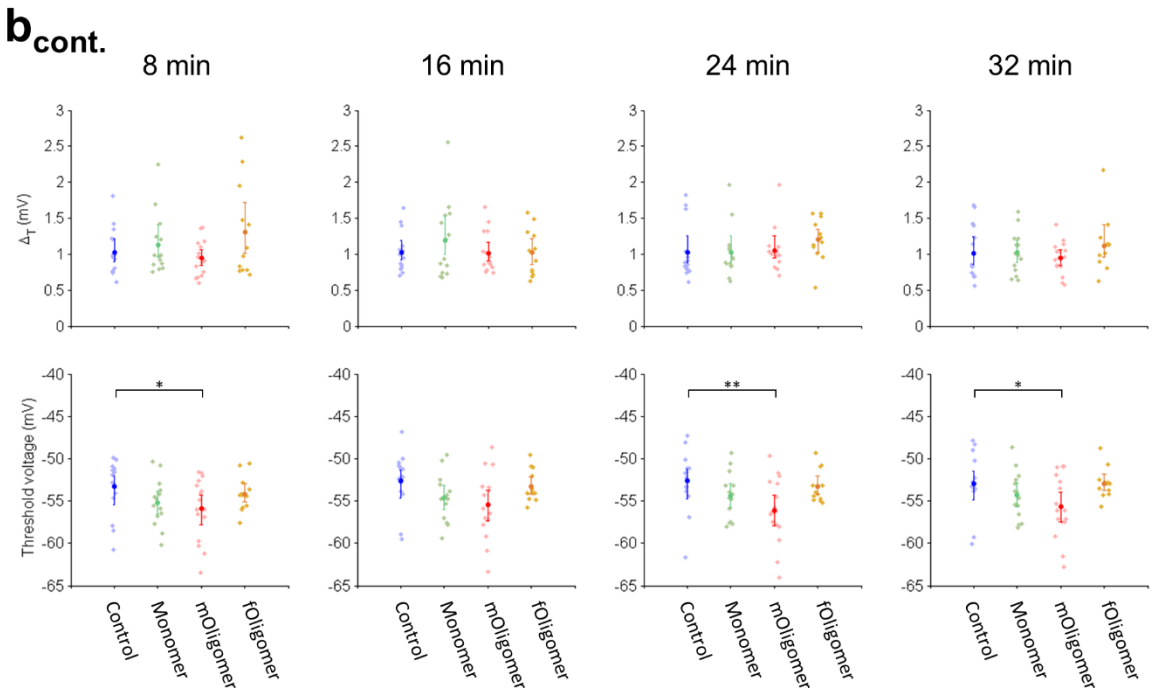

Figure 5.1 Time course of subthreshold parameters for TTL5 neurons filled with control (blue), αSyn monomer (green), *mOligomer* (red) or *fOligomer* (yellow). (a) The inverted dynamic I-V curves for each αSyn treatment and at each time point demonstrate the oligomer specific changes in parameters. Both oligomers have an increased slope (reduced input resistance) and the *mOligomer* is shifted left, giving a lower threshold voltage. (b) Quantification of subthreshold parameters: scatterplots show mean values (darker points) amongst all data (pale points) with error bars (95 % bootstrap confidence intervals). * $p < 0.05$, ** $p < 0.01$, *** $p < 0.005$.

To investigate the time course for changes in input resistance, membrane time constant and capacitance, I compared neuron parameters at earlier time points (8, 16 and 24 minutes) and found that oligomer perfused neurons remained significantly different from control. This suggests that the effects of the oligomers on these parameters occurred rapidly, within the first few minutes and then stabilised for the duration of the recordings. There was no significant difference between the effects of *mOligomers* and *fOligomers* on either input resistance, membrane time constant, or capacitance ($p > 0.05$).

The resting membrane potential and spike onset sharpness were unaffected by αSyn at any of the time points. The spike-threshold voltage, however, was significantly reduced in *mOligomer* filled neurons (mean ± standard deviation, 32 min, -56.0 ± 3.6 mV) compared to control (-52.6 ± 5.4 mV, P = 0.003), but not in *fOligomer* filled neurons (-54.91 ± 1.8 mV, P = 0.841).

The differential effects of *mOligomers* and *fOligomers* on subthreshold parameters are illustrated by their respectively shifted dynamic I-V curves from the control (figure 5.1a). In comparison the monomer dynamic I-V curves, and thereby monomer subthreshold parameters, align closely to those of the control. The qualities of the dynamic I-V curve in relation to each parameter are outline in chapter 4, figure 4.8d. The change in time constant with oligomers, for example, is seen as a steeper gradient for the linear portion of the dynamic I-V curve. Similarly, the change in V_T is conveyed by the leftward shift of the *mOligomer* curve that is not seen for the *fOligomer* (figure 5.1a). Although no significant change in resting membrane potential was found for either oligomer, their shifted curves both intersect with the control at approximately -80 mV, suggesting that αSyn oligomers have a reversal potential close to this voltage.

The effects of αSyn on the post-spike relaxation properties of TTL5 neurons were examined for each time point (figure 5.2). The post-spike dynamics of the membrane time constant, normalised to the pre-spike baseline, were unaffected by either monomer or oligomer. Similarly, changes in resting potential and threshold voltage showed no differences in their post-spike increase or exponential relaxation.

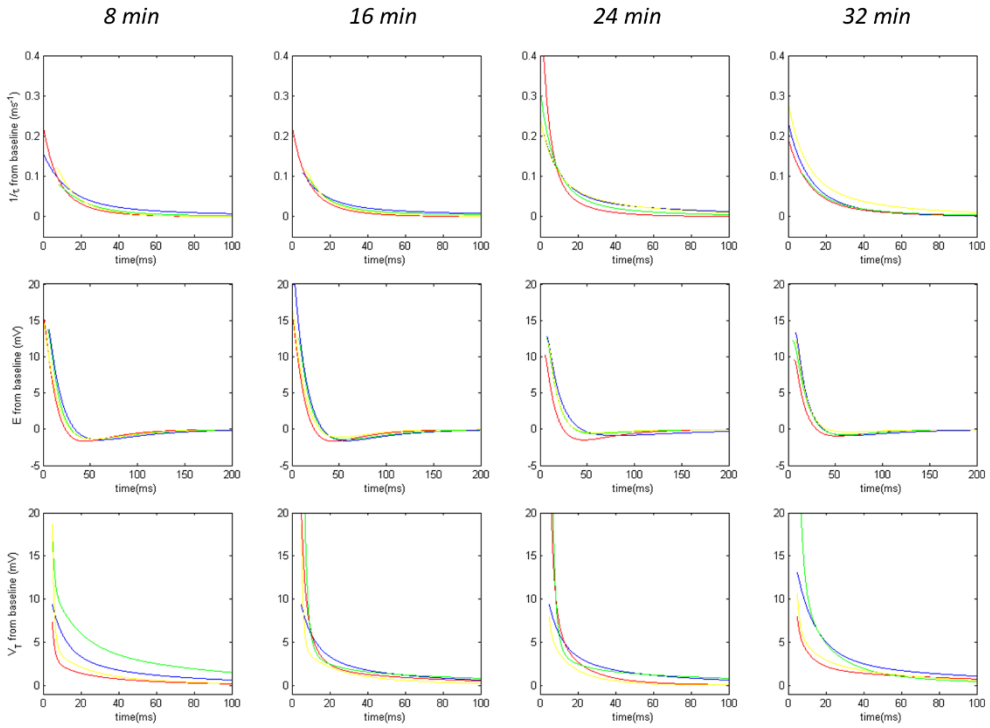

Figure 5.2 Time course of post spike parameters, normalised to baseline, for TTL5 neurons filled with control (blue), αSyn monomer (green), *mOligomer* (red) or *fOligomer* (yellow). Parameters show an immediate post-spike increase followed by either a single ($1/\tau$ & V_T) or double (E) exponential decay, but are unaltered by either monomeric or oligomeric αSyn.

Parameter	Control				Monomer				mOligomer				fOligomer			
	8 min		32 min		8 min		32 min		8 min		32 min		8 min		32 min	
	μ	σ	μ	σ	μ	σ	μ	σ	μ	σ	μ	σ	μ	σ	μ	σ
C (pF)	189	35.2	183	39.8	171	43.8	172	40.6	227*	53.3	219*	40.3	247	58.4	228*	56.1
R_{in} (MΩ)	85.7	19.5	89.0	22.3	81.4	18.6	79.8	19.7	52.3**	15.2	55.1**	16.0	60.5**	22.9	59.7**	18.6
τ (ms)	16.0	3.99	16.1	4.62	13.4	3.58	13.5	4.50	11.5**	3.10	11.8**	2.87	13.3*	3.08	13.1**	3.26
E (mV)	-73.4	3.60	-73.0	5.35	-72.4	4.33	-71.2	5.47	-75.1	4.26	-74.8	3.23	-73.3	2.20	-73.1	2.29
V_T (mV)	-52.9	3.25	-52.6	5.44	-55.3	2.59	-54.5	3.15	-56.0*	3.68	-56.0**	3.56	-54.3	1.98	-54.1	1.80
V_T – E (mV)	20.4	4.99	20.4	4.98	17.1	5.22	16.7	5.16	19.1	4.04	18.6	3.10	19.1	2.97	20.4	2.11
I_{spike} (pA)	249	78.6	243	87.8	220	76.0	225	89.9	385*	107.2	358**	95.1	343*	98.3	367**	104.7
Δ_T (mV)	1.04	0.33	1.00	0.35	1.20	0.42	1.02	0.27	1.17	0.92	1.00	0.28	1.38	0.69	1.11	0.38
A_{amp} (mV)	73.7	8.29	65.7	10.81	72.8	4.78	69.5	6.42	74.6	8.74	72.8	7.85	75.8	2.22	73.8	4.71
A_{dur} (ms)	1.30	0.30	1.29	0.29	1.32	0.39	1.24	0.32	1.00*	0.12	1.00*	0.12	0.95*	0.08	0.97*	0.10
A_{rise} (mV/ms)	26.9	5.62	24.0	6.58	25.1	4.31	22.2	5.35	23.9	7.22	22.4	6.17	26.9	2.69	25.4	4.06

Table 5.1 Extracted parameter values for neurons filled with αSyn monomer, *f* and *mOligomers* and vehicle. Values are means (μ) and standard deviations (σ) at 8 and 32 minutes after break through to whole-cell patch clamp recording. (*p<0.05; **p<0.005; versus control parameters at corresponding time points.)

To corroborate the findings from the dynamic I-V method, the input resistance was measured from the gradient, around rest, of the standard I-V curve either before or after the effects of the sag due to I_H activation had occurred (figure 5.3a-b). After 32 minutes, the input resistance was (mean ± SEM) 69.1 ± 3.8 MΩ in control compared to 45.4 ± 1.8 MΩ in *mOligomer* and 45.8 ± 3.4 MΩ in *fOligomer*. Thus a similar reduction in input resistance was observed to that measured by the dynamic I–V (~35% reduction, P < 0.005, figure 5.3c). Since the standard I-V curve could be generated from a much shorter stimulus than the dynamic I-V, this method was used to measure the input resistance at time zero. As shown in figure 5.3d-e, the input resistance was not significantly different between control cells (52.1 ± 6.3 MΩ) and *mOligomer* perfused cells (49.6 ± 5.4 MΩ) at time zero (P = 0.78) but became different after 16 minutes ($V_{Steady:}$ control R_{in} 58.7 ± 3.2 MΩ versus *mOligomer* R_{in} 44.2 ± 2.6 MΩ; P = 0.001) suggesting that the changes in input resistance do occur within a short period of recording.

In a small number of cells, the concentration of *mOligomer* in the intracellular solution was increased from 0.5 to 1.5 μM (n = 4) to see if the effects on parameters were concentration dependent. While a similar drop in input resistance was observed for *mOligomer* at this higher concentration (figure 5.3f), the change was not significantly greater than that observed with a lower concentration; suggesting that these effects are at a maximum. Conversely, increasing the monomer concentration from 0.5 to 1.5 μM (n = 7) did not significantly affect the input resistance compared to control cells.

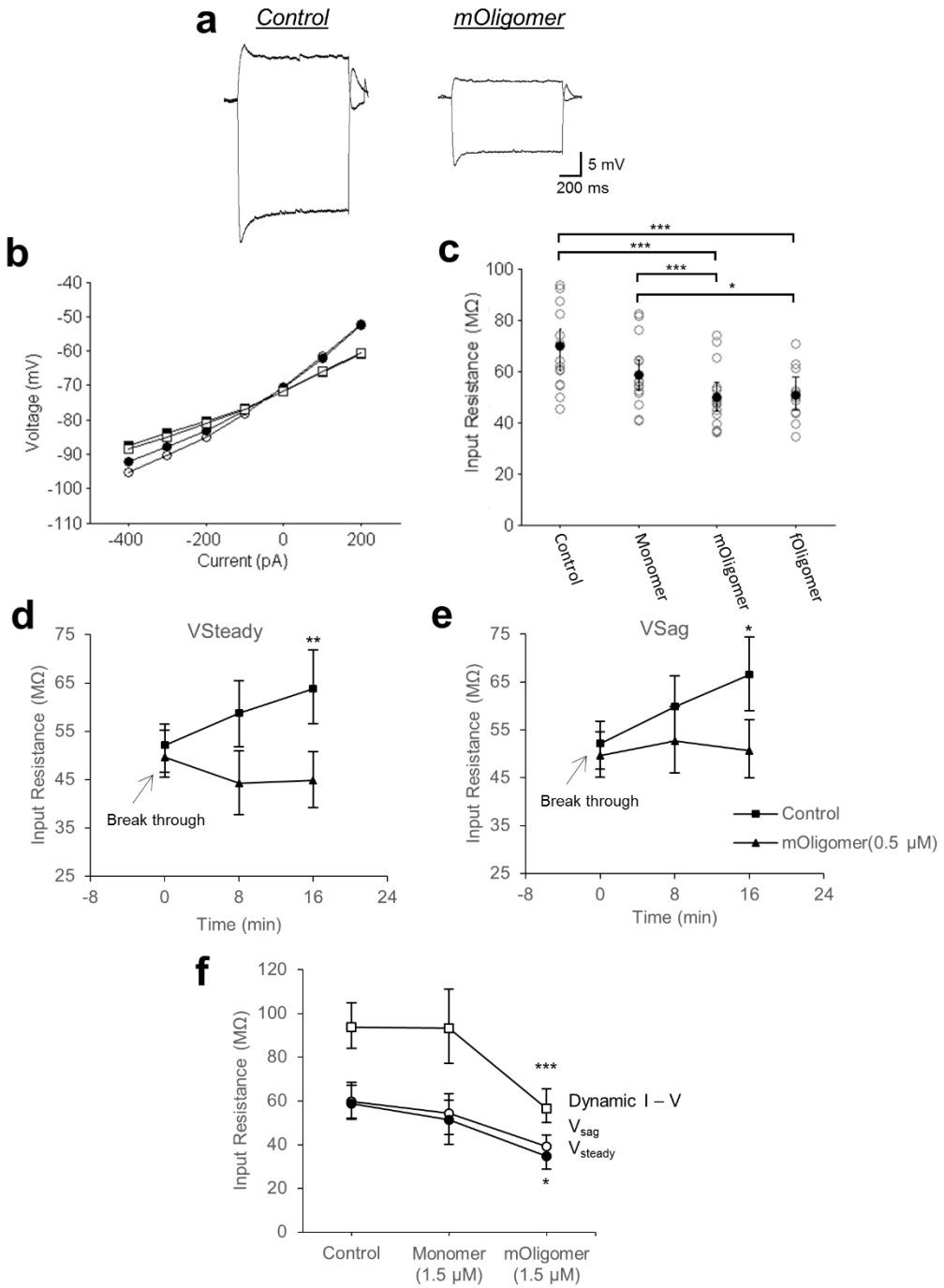

Figure 5.3 The oligomer induced fall in input resistance is observed in standard IV curves constructed from step currents. (a) Typical voltage responses of neurons filled with either vehicle (control) or *mOligomer* (input step currents were -400 & 100 pA). (b) The standard IV curve was generated from both the maximum voltage response during the initial sag (open points) and during the steady state (filled points). The shallower gradient at 0 mV for the *mOligomer* IV curve (squares) compared to control (circles) illustrates the reduction input resistance. (c) The standard IV input resistance at 32 minutes for control, monomer, *mOligomer* and *fOligomer*. (d-e) The standard IV curve was used to measure the input resistance immediately after whole-cell break through. At this early time point, the input resistance is the same for control and *mOligomer* but becomes significantly different over time. (f) The reduction in input resistance was still seen with higher concentrations of *mOligomer* (1.5 μM) but not with higher concentrations of monomer. This reduction was not significantly greater than that produced by lower concentrations of oligomer suggesting the effects are maximal. * $p < 0.05$, ** $p < 0.01$, *** $p < 0.005$.

5.3.2 Oligomeric αSyn impacts neuron excitability

With a reduction in input resistance the voltage response to a given current stimulus decreases, which would have a detrimental effect on neuron excitability. It would be predicted that a larger current is required to reach the action potential firing threshold for neurons perfused with oligomer compared to control cells. As seen from figure 5.4a, the potential difference between resting and threshold (V_T – E) is unaffected by αSyn treatments, despite the changes in V_T described earlier. Instead, changes in neuron excitability stem from a significant increase in the current required to trigger an action potential (I_{spike}) (figure 5.4b: over 60 % increase with either *mOligomer* or *fOligomer* compared to control; $p < 0.005$).

It would also be expected that the firing rate of oligomer perfused cells would be lower than control cells for a given current input. This was not directly observed in most recordings as the gain factor for the injected noisy currents was continually altered in order to maintain the firing rate. A higher gain factor, compared to control, was often required for oligomer filled cells to produce a 5-15 Hz firing rate. In a subset of recordings, however, the gain was set at the same level (400 pA) for both control cells and interleaved oligomer perfused cells to allow the firing rate to be fairly compared (figure 5.4c). After 32 minutes, the average firing rate was (mean ± SEM) 9.4 ± 0.54 Hz (n=5) in control neurons compared to 5.6 ± 1.14 Hz in *mOligomer* filled neurons (n=5), illustrating a significant ($p < 0.005$) decline in firing rate (figure 5.4d).

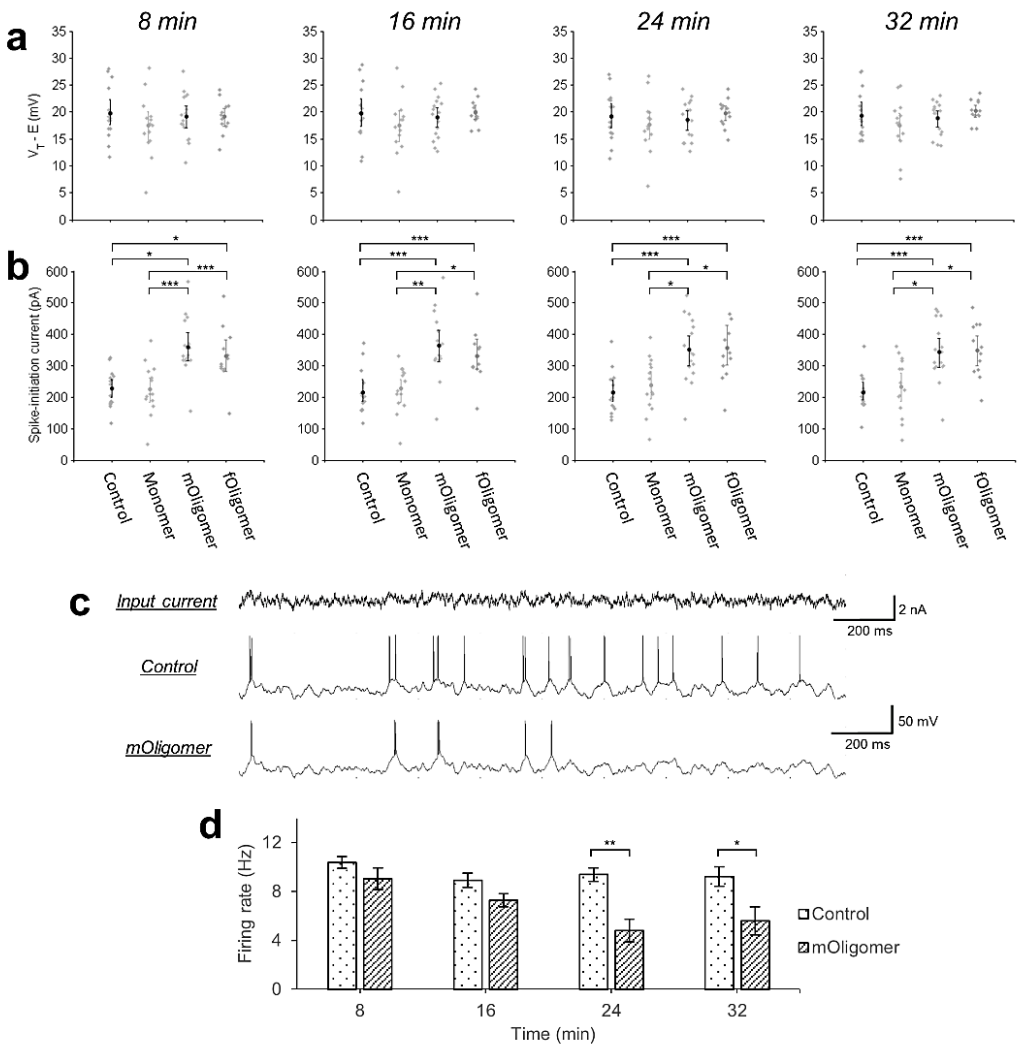

Figure 5.4 Oligomer perfused neurons have reduced excitability. (a) For a fixed current stimulus (-400 & 100 pA) a neuron with smaller input resistance (mOligomer) will produce a smaller voltage response. (b) Scatterplots of the voltage between resting and threshold (V_T - E) for control, monomer and oligomer perfused cells at different time points. (c) Scatterplots of spike initiation current (I_{Spike}), the amount of current needed for a resting neuron to reach threshold, show how oligomer-filled neurons require a much larger stimulus than control neurons in order to produce a similar voltage change. (d) Example voltage responses to a noisy current stimulus (gain = 400 pA) for a cell filled with vehicle (PBS, control) and a cell filled with mOligomer. (e) Bar chart plotting the mean firing rate for neurons perfused with mOligomer or vehicle against the time from whole-cell break through. * $p < 0.05$, ** $p < 0.01$, *** $p < 0.005$.

Furthermore, when parameters were simulated using the rEIF model, the linear increase in firing rate with input current gain factor (from 400 to 1000 pA in steps of 100) was significantly reduced (as determined by Analysis of Covariance) for both *fOligomer* ($p < 0.05$) and *mOligomer* ($p << 0.005$) filled neurons compared to either control or monomer (figure 5.5). Interestingly, the simulated firing rate for *mOligomer* was reduced after 8 minutes while the *fOligomer* only had an effect after 32 minutes. This later reduction was also significantly weaker than the *mOligomer* (the gradients of the linear regressions were significantly, $p < 0.005$, different from one another).

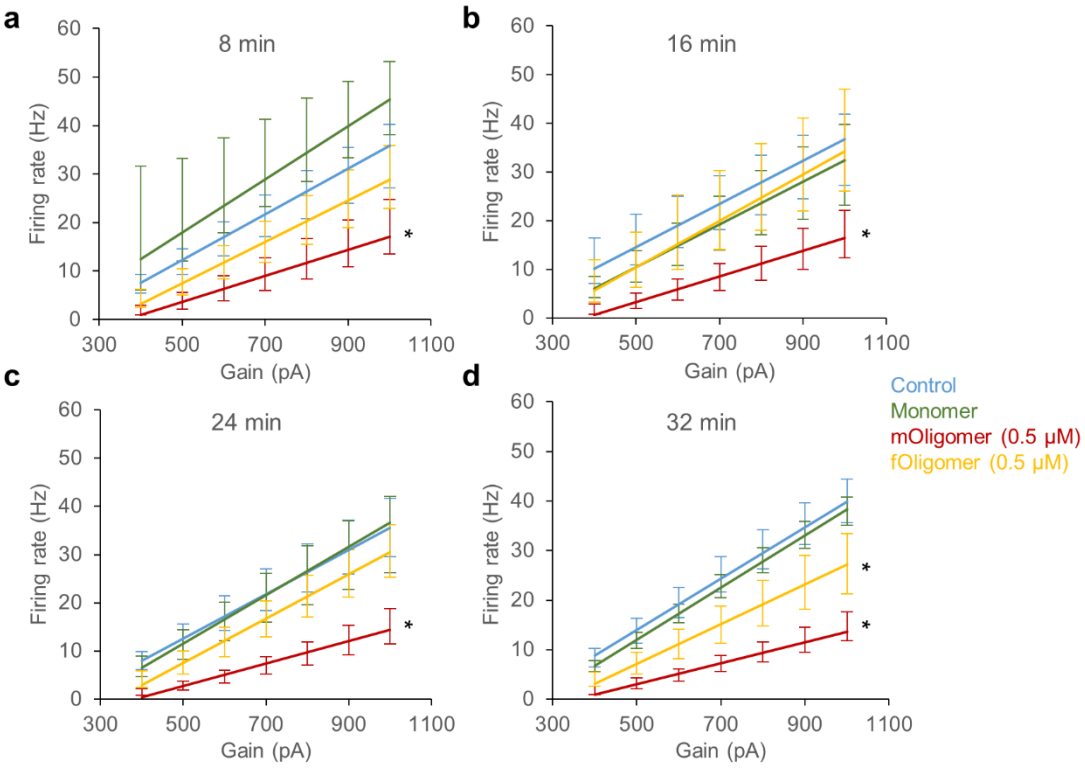

Figure 5.5 The linear relation between rEIF model firing rate and input current gain factor is reduced in oligomer, but not monomer, filled neurons. (a-d) The linear regressions at each time point were subject to Analysis of Covariance; those marked with * had significantly different intercept and slope than either control or monomer. This indicates that, for the *mOligomer* at all time points ($p << 0.005$) and *fOligomer* at 32 minutes ($p < 0.05$), both the overall firing rate (intercept) and the change in firing rate with increasing gain (slope) were significantly different.

5.3.3 Oligomeric αSyn impacts action potential duration

I investigated whether αSyn oligomers had any effect on the action potential by measuring a number of parameters that define the action potential waveform (figure 5.6a). There was no significant difference in action potential amplitude. However, action potential duration (A_{dur}) was significantly reduced by both *mOligomer* (8 minutes, $p < 0.005$) and *fOligomer* ($p < 0.005$) but not by monomer ($p = 0.606$) (figure 5.6b). This decrease in duration was not associated with an increase in the maximal rate of rise (A_{rise}) of the action potential but was instead associated with a faster rate of repolarisation.

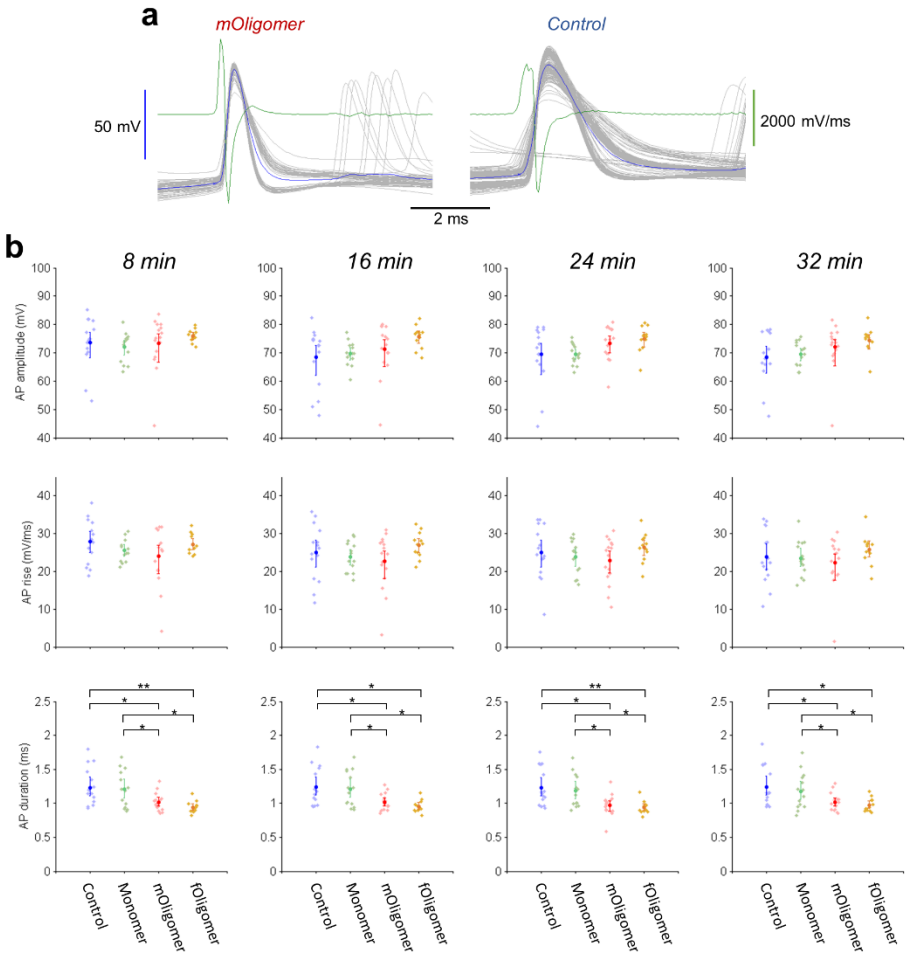

Figure 5.6 Action potential parameters were taken from responses to naturalistic current. (a) The average spike (blue) was generated from isolated spikes with an ISI greater than 200 ms (grey, overlaid). The spike initiation threshold (blue cross) was calculated using the peak second-derivative method (Sekerli et al., 2004), shown in green. (b) The action potential amplitude, maximum rate of rise and duration were measured at each time point. The AP duration was significantly shorter for oligomers than for either control or monomer. * $p < 0.05$, ** $p < 0.01$, *** $p < 0.005$.

5.4 Discussion

This chapter offers an in-depth analysis of the findings from the experimental methods outlined in chapter 4. After injecting αSyn monomer and oligomer species into TTL5 pyramidal neurons, parameters were extracted at regular intervals using both standard and dynamic I-V methods. The intracellular recording solution contained an ATP regenerating system (phosphocreatine) as well as 2 mM ATP. Such a system is important as it prevents the 'rundown' of many voltage gated and ligand gated ion channels during whole-cell dialysis *(Chen et al., 1990; Rosenmund and Westbrook, 1993)*. Thus the αSyn induced changes in electrophysiological properties were independent of a fall in ATP production due to the disruption of mitochondrial homeostasis.

	Monomer	mOligomer	fOligomer
Capacitance (C)	-	↑	↑
Input resistance (R_{in})	-	↓	↓
Membrane time constant (τ)	-	↓	↓
Resting potential (E)	-	-	-
Threshold voltage (V_T)	-	-	-
Voltage between resting and threshold ($V_T - E$)	-	-	-
Current to trigger action potential (I_{spike})	-	↑	↑
Spike onset sharpness (Δ_T)	-	-	-
Spike amplitude (A_{amp})	-	-	-
Spike width (A_{dur})	-	↓	↓
Spike rise (A_{rise})	-	-	-

Table 5.2 Summary of the trends in neuron parameters. Changes in the electrophysiological properties of neurons injected with monomer, *mOligomer* or *fOligomer*. Relative to the average value of control neurons after 30 minutes, parameters had either increased (↑), decreased (↓) or stayed the same (–).

Table 5.2 summarises the trends in parameters for neurons injected with monomer, *mOligomer* or *fOligomer*. Neurons filled with either species of oligomeric αSyn showed a markedly reduced input resistance (R_{in}), as calculated by both standard and dynamic I-V curves (figures 5.1 and 5.3 respectively), that was not seen for either monomer-filled or control neurons. The R_{in} values for control neurons (table 5.1) were similar to those determined elsewhere for TTL5 pyramidal neurons in mice *(Dani and Nelson, 2009; Oswald et al., 2013)*. The R_{in} of a neuron is a measure of how open

channels are in the membrane. Increasing evidence shows αSyn oligomers form pore complexes that are able to permeabilise lipid membranes both *in vitro (Volles and Lansbury, 2002; Kim et al., 2009; Schmidt et al., 2012)* and in cell cultures *(Feng et al., 2010; Tosatto et al., 2012; Mironov, 2015)*. By retracing the parameter's time course, it is clear that the oligomer-specific reduction in R_{in} appeared within the first 8 minutes of recording; the time zero values for R_{in} were not significantly different from control. Such rapid effects have been seen previously, with reports that αSyn pore formation can occur within as little time as 5 minutes *(Mironov, 2015)*. In complementation of the reduced R_{in}, many have reported increases in membrane conductance caused by the formation of leaky, non-selective cation channels by αSyn *(Feng et al., 2010; Schmidt et al., 2012; Tosatto et al., 2012)*. Others have shown cross – talk between αSyn and potassium channels *(Mironov, 2015)* which is supported by the -80 mV reversal potential observed here. It is possible therefore that with the intracellular application of αSyn, the R_{in} decreases as oligomers either directly insert into the membrane or activate channels already embedded. Sodium-potassium pumps (N^+/K^+-ATPase), responsible for maintaining the polarity of the membrane, would counter the effects oligomer channels and prevent rapid depolarisation. Over extended periods of time, however, the elevated activity of ion pumps could increase the energy demand on a cell and ultimately become unsustainable. Neurons with naturally high metabolic rates, such as dopaminergic neurons in the SNc, could be at greater risk of this and struggle to balance ionic concentrations across the membrane.

As one might expect, based on Ohm's law ($V = IR$), a fall in R_{in} means that for the same amount of input current the voltage response will be weaker. Inversely, the amount of current needed to push a PD-afflicted neuron up to firing threshold (I_{Spike}) will be greater than that of a healthy neuron (figure 5.4a-c). Thus, these results indicate that αSyn oligomers, but not monomers, have an inhibitory effect on neuron excitability and consequentially have a markedly reduced firing rate (figure 5.4d-e). Furthermore, these findings suggest that over the time period of the experiments (up to 120 minutes for some recordings) the introduced monomer does not oligomerise in the cell. This remained true when the concentration of monomer was markedly increased.

Despite their structural differences, the two oligomers (*mOligomers* and *fOligomers*) produced similar changes in the electrophysiological properties of TTL5 neurons. As

such, the specificity of αSyn to produce these effects is uncertain and may instead be due to the ring-like shape of the oligomer which has been described for other disease-associated proteins. In addition, an important control test would be to inject an oligomer made from randomised sequence, or to use a different protein such as amylin, to make sure that changes were specific to the disease protein of interest. Amylin has been used previously as a control to test whether membrane protein binding was a general property of amyloid fibrils or specific to amyloid-β *(Lorenzo et al., 2000)*. Previous studies on the effects amyloid-β oligomers on field EPSPs and LTP in hippocampal brain slices have used amylin oligomers for their control *(Kimura et al., 2012; Ripoli et al., 2014)*.

Since both oligomeric species of αSyn are ring-like in shape and of similar size, they may also share the pathological mechanism of forming pore-complexes in membranes. Subtle differences between oligomer species, however, in the shape of the dynamic I-V curve and in neuron excitability suggest that the *mOligomer* has a greater and faster effect than the *fOligomer*. The membrane permeabilising activity of oligomers is dependent on the structural flexibility of their hydrophobic core *(Campioni et al., 2010)*. Differences in tryptophan-39 fluorescence and CD spectra (chapter 3) may indicate differences in core rigidity between *mOligomers* and *fOligomers* that impact their ability to interact with membranes.

6 General Discussion

In this thesis, the aim was to combine in-depth structural characterisation of αSyn oligomers with detailed insight into their time-dependent effects on a wide range of electrophysiological parameters. This work was carried out to investigate two hypotheses. Firstly, that αSyn oligomers, but not monomers, produce changes in specific neuronal parameters. Secondly, that oligomers isolated from separate stages of the aggregation pathway display structural differences that alter their impact on neuron electrophysiology.

In chapter 3, recombinantly expressed human $\alpha Syn^{Y39W,\ E46K}$ was shown to form soluble, annular oligomers, referred to as *mOligomers*, under *in vitro* conditions during the early stages of aggregation. Insoluble, amyloid fibrils became the predominant structure in later stages of aggregation. When these fibrils were subjected to sonication, however, the resulting mixture of solubilised fragments were shown to include a separate species of A11-positive oligomer; *fOligomers*. In chapter 4, both monomeric and oligomeric αSyn were injected into TTL5 pyramidal neurons using the whole-cell patch clamp technique. Standard and dynamic I-V curves were generated at regular intervals to provide a time course of electrophysiological changes; presented in chapter 5. Neurons filled with either species of oligomer showed a reduced input resistance compared to either control or monomer-filled neurons. This translated into a reduction in neuron firing rate as a greater amount of input current was required for oligomer-filled neurons to reach their threshold voltage.

These effects could lead to circuit changes in the neocortex which might produce many of the cognitive symptoms experienced by patients suffering from PD and other related neurodegenerative disorders. The actions of oligomers specifically within TTL5 pyramidal neurons are likely to have major implications for the dynamics of network activity in the neocortex, signalling to subcortical areas and a number of physiological processes. Furthermore, the use of whole-cell patch clamp recordings and the extraction of parameters from dynamic I-V curves by EIF modelling presents a valid and reliable tool for studying the neuronal effects of disease-linked proteins such as αSyn.

The work presented in this thesis seeks to add electrophysiological context to current theories on oligomer toxicity and provides the groundwork for further investigations

into the influence of αSyn on the activity and functional properties of neurons. My findings support the first hypothesis that ring oligomers produce changes in neuronal electrophysiology. This supports previous work, both *in vitro* and in cell cultures, showing that ring oligomers may permeabilise membranes leading to an increase in conductance (decrease in resistance). The two species of ring oligomer investigated in this thesis showed differences in their secondary structure that may reflect their separate positions in the aggregation pathway. However, the electrophysiological impact of the oligomers was unaffected by their structural differences, thus nullifying the second hypothesis. This suggests that the conserved ring shape of the two species, resulting from the assembly of central hydrophobic regions into a pore complex, is enough to produce neuronal changes regardless of subtle differences in structure in the terminal regions. Since the general ring shape is not exclusive to αSyn, it is possible that oligomers formed from other proteins may also impact electrophysiology in a similar way.

6.1 The native structure of αSyn

Until recently, the native structure of αSyn was almost unanimously accepted as that of an unfolded monomer. However, recent findings of a physiologically occurring, helically folded αSyn tetramer have cast debate on the subject *(Bartels et al., 2011; Wang et al., 2011a; Fauvet et al., 2012)*. This tetrameric structure has been extracted from brain tissues and red blood cells *(Bartels et al., 2011)*, but has also been characterised from recombinantly expressed αSyn *(Wang et al., 2011a)*. The αSyn protein used throughout this thesis was found to exist predominantly as an unfolded monomer prior to aggregation experiments. Despite this, there are certain elements of my work that could support the theory of a physiological tetramer. Firstly, the detection of αSyn on western blots (figure 2.6, page 53) frequently produced small bands at higher molecular weights than the monomer. These bands were not strong enough to be detected by normal SDS-PAGE and did not appear on gel filtration chromatography, suggesting that they were only present in very low amounts. Secondly, analytical ultracentrifugation (AUC) of αSyn samples (figure 3.12, page 76) revealed a small peak with a sedimentation coefficient corresponding to a tetramer. Interestingly, this tetramer peak was observed in the *mOligomer* sample but not for the *fOligomer*; suggesting that sonication may remove it from the mixture.

The study of αSyn tetramer requires cross-linking and native gel electrophoresis *(Bartels et al., 2011; Wang et al., 2011a)* which were not carried out in this work. Therefore, it is uncertain whether the minor findings on western blot and AUC are linked to the physiological tetramer without further experimentation. Heat treatment of αSyn, a commonly used step in purification, has also been suggested to degrade the tetramer *(Bartels et al., 2011)* making it less likely to be present in the protein stock.

6.2 Structure of αSyn oligomers

The aggregation of αSyn into fibrils is a well-established feature of PD that has been extensively studied over the last few decades. Intermediate aggregates, formed prior to fibrils, include protofibrils and soluble oligomers, the latter of which represents a more pathologically active species compared to the relatively inert fibrils. The transient nature and inherent polydispersity of αSyn oligomers means that a variety of sizes, shapes and structures have been proposed; with many of the differences potentially stemming from the choice of oligomerisation protocol *(Uversky, 2010)*. In addition to structural heterogeneity, the toxicity mechanism through which αSyn oligomers act is the subject of numerous theories and ongoing debate *(Roberts and Brown, 2015).*

The *mOligomer*s characterised in this thesis are structurally similar to the soluble, annular oligomers shown previously to permeabilise vesicle membranes *(Volles et al., 2001; Lashuel et al., 2002b)* and impede fibril formation *(Lorenzen et al., 2014c)*. The *fOligomers* characterised in this thesis represent a potentially novel oligomeric species recovered from the fragmentation of αSyn fibrils.

Other species of annular oligomer, with varying diameters, have been formed by αSyn in the presence of different metal ions. Iron-induced oligomers, for example, were found to be 40-45 nm in diameter *(Danzer et al., 2007)*, whereas calcium produced annular oligomers 70-90 nm *(Lowe et al., 2004; Pountney et al., 2005)* and cobalt oligomers were 22-30 nm *(Pountney et al., 2005)*. There is also evidence for αSyn interactions with copper, lead, aluminium, magnesium, manganese, zinc and nickel ions *(Breydo et al., 2012)*, although the oligomers formed from such treatments are not necessarily annular in shape. The ability of αSyn to interact with such as array of metal ions is likely to be the result of low-affinity binding. The abundance of negative side chains in the exposed C-terminal allow metals to interact and neutralise the

Coulombic charge-charge repulsion; resulting in partial folding of αSyn *(Uversky et al., 2001b)*. Higher-affinity copper binding sites have also been located in both the N- and C-terminals *(Binolfi et al., 2008; Brown, 2009, 2010b)*. The increased amount of folding as a result of metal ion binding at either terminal region leads to the production of oligomers with varying properties and sizes.

Annular αSyn oligomers have been previously compared to the bacterial toxin; α-hemolysin *(Lashuel et al., 2002b)* that forms a cytolytic β-barrel structure. The central hydrophobic region of αSyn is vital in fibril formation *(Giasson et al., 2001)* and is likely to be involved in the formation of the hydrophobic core in ring-like oligomers *(van Rooijen et al., 2009a)*. As the hydrophobic regions of αSyn monomers align to form a β-sheet-rich oligomeric structure, the N- and C-terminal regions are more exposed for membrane, protein and small molecule interactions. Indeed, the membrane binding activity of the N-terminal region remains functional in the oligomeric state *(Lorenzen et al., 2014a)*, suggesting that this region is not hindered by αSyn oligomerisation. Therefore, it is possible for αSyn to form a wide range of annular oligomers that, although they share the same ring-like shape and hydrophobic core, are structurally diversified by the conformations and interactions in their terminals.

With this in mind, a comparison of *mOligomers* and *fOligomers* showed that both are similar in regard to size and shape, but differ in secondary structure characteristics. The structural differences reported in this thesis are likely to be located in the N-terminal region. This is because analysis of CD spectra for the two oligomers showed differences in α-helical content which is a structural feature exclusive to the N-terminal region. Furthermore, the fluorescence spectrum of the tryptophan-39 residue, located in the N-terminal, had a greater blue-shift in the *mOligomer* than the *fOligomer*. This suggests that the microenvironment surrounding this tryptophan is different within these two species.

The fact that the two oligomer species were isolated from different stages of the aggregation pathway is likely to be an important factor in understanding these conformational differences. The similarities between *fOligomers* and fibrils indicates that *fOligomers* may retain elements of the fibril structure that are not present in *mOligomers*. Alternatively, the fragmentation of fibrils might produce a mixture of

soluble fragments that could interfere with the specific structural characterisation of *fOligomers*. Nevertheless, the finding that annular *fOligomers* can be recovered from fibril fragmentation, could indicate that oligomers are able to directly insert into, and dissociate from, fibrillar structures.

6.3 Toxicity of αSyn oligomers

Lewy bodies were originally believed to be the most pathologically relevant form of αSyn as they predominated inside apoptotic neurons throughout the brain *(Wakabayashi et al., 2007)*. As a result, cell death was considered to play a principle role in the development of PD. However, attempts to correlate Lewy body density, in either cortical or brain stem neurons, with clinical symptoms have been unsuccessful. Many studies fail to correlate Lewy body density with neuron loss, the onset of symptoms, disease duration, disease severity or cognitive decline *(Gomez-Isla et al., 1999; Gomez-Tortosa et al., 1999; Gomez-Tortosa et al., 2000; Weisman et al., 2007; Jellinger, 2008; Schulz-Schaeffer, 2015)*. Instead, recent evidence has shown that neurodegeneration and cellular dysfunction precede Lewy pathology *(Milber et al., 2012)* and are caused by small oligomeric forms of αSyn *(Lashuel et al., 2013)*.

If the death of neurons is a secondary event in the pathology of PD *(Schulz-Schaeffer, 2015)* then the toxic action of oligomers must impact upon neuron function, i.e. synaptic activity and electrophysiology, in some manner. The physiological association of αSyn with synapses has made them the focus of current research in pathology *(Kramer and Schulz-Schaeffer, 2007; Schulz-Schaeffer, 2010)*. Oligomeric αSyn has been shown to modulate synaptic transmission and LTP by affecting glutamate receptors in the postsynaptic terminal *(Huels et al., 2011; Diogenes et al., 2012; Martin et al., 2012)*, as well as disrupt vesicle binding and neurotransmitter release in the presynaptic terminal *(Volles et al., 2001; Giehm et al., 2011; Choi et al., 2013; Spinelli et al., 2014)*. Previous electrophysiological investigations have led to the theory that αSyn oligomers are able to permeabilise membranes through the formation of a pore complex *(Butterfield and Lashuel, 2010)*. This concept is largely attributed to annular oligomers that are able to span membranes *(Zhang et al., 2013)* and produce discrete stepwise changes in membrane conductance reflecting the electrophysiology of a single channel opening and closing *(Kim et al., 2009; Feng et al., 2010; Schmidt et al., 2012; Tosatto et al., 2012; Mironov, 2015)*. Such pathological

activities would result in cellular dysfunction prior to death and are easily associated with disease symptoms; such as reduced LTP and memory loss.

Depending on the conditions for aggregation, oligomers have been characterised in a wide range of shapes and sizes, which alters their structural and functional properties. This heterogeneity only increases the complexity of the proposed mechanisms of oligomer toxicity *(Lashuel et al., 2013; Roberts and Brown, 2015)*. Other proposed mechanisms for the toxicity of αSyn oligomers include loss of cytoskeletal integrity *(Prots et al., 2013)*, endoplasmic reticulum stress *(Thayanidhi et al., 2010)*, impaired protein degradation systems *(Xilouri et al., 2013)* and mitochondrial dysfunction *(Devi et al., 2008)*. It is unclear whether many of these reported mechanisms produce an effect on neuron electrophysiology, or how these processes might interact with one another. Some toxicity mechanisms may not have a direct effect on electrophysiology but instead lead to changes in neuron structure that affect normal cell function. For example, changes to the cytoskeletal system with αSyn aggregation has been linked to dendritic spine retraction; reducing neuron connectivity *(Takahashi et al., 2003; Zaja-Milatovic et al., 2005)*. Protein degradation pathways, on the other hand, can be directly linked to synaptic activity as they are important for the turnover of glutamate receptors and their impairment by αSyn will affect neurotransmission *(Tai and Schuman, 2008)*. Mitochondrial dysfunction is known to play a central role in PD pathology and may be associated with electrophysiology as the oligomer pore complex can create an influx of calcium ions *(Danzer et al., 2007; Cali et al., 2012)* that leads to mitochondria-associated apoptosis *(Vila et al., 2008)*. Furthermore, the preferential insertion of αSyn into lipid-raft domains reveals subcellular targets that are linked to mitochondrial homeostasis *(Guardia-Laguarta et al., 2014)*.

The membrane permeabilising activity of oligomers has been proposed to be dependent on the compactness of their hydrophobic core *(Campioni et al., 2010)*. Despite their structural differences, the diameter of the central cavity was found to be similar for *mOligomers* and *fOligomers* which may indicate that they have a shared degree of permeabilising activity. This is reflected in the electrophysiological findings which showed that, while oligomers did alter the response properties of neurons, neither oligomer had a greater impact on neuronal electrophysiology than the other. In comparison, monomeric αSyn did not elicit a change in electrophysiological properties on the time scale of these experiments (some as long as two hours). Furthermore,

neurons filled with monomer were negative for A11 immunostaining; suggesting that the monomer did not noticeably oligomerise during the experiments. The fact that monomeric αSyn had no effect indicates that neuronal changes were not simply the result of the αSyn protein but rather the presence of a toxic, ring-like oligomeric structure. This oligomeric structure is not exclusive to αSyn and has also been reported for amyloid-β *(Lashuel et al., 2002a; Kayed et al., 2003; Haass and Selkoe, 2007; Faendrich, 2012)*. Therefore, the electrophysiological changes seen for αSyn oligomers may provide insight into the shared pathological mechanisms through which other proteins act *(Kayed et al., 2003; Yoshiike et al., 2007)*.

6.4 Endogenous αSyn in the neocortex

The differential expression of endogenous αSyn in the layers of the neocortex has been reported previously *(Vivacqua et al., 2011)* and was also observed in this work by immunostaining (figure 4.6, page 98). Interestingly, the high expression of αSyn in the somata of layer 4 neurons could indicate an important physiological role in the maintenance of the neocortical microcircuitry. Layer 4 neurons receive the strongest thalamic input of all cortical layers and send important excitatory signals to layer 2/3; which then relay an integrated signal to layer 5 *(Feldmeyer et al., 2002; Kampa et al., 2006)*. If specific neuron loss was to occur in layer 4 rather than in layer 5, then the pathology of αSyn in the neocortex might take place further upstream in the microcircuit. However, the resulting decrease in signal integration may still have downstream effects on the subcortical output from layer 5.

The purpose of differential expression of αSyn throughout the brain remains an unknown component for understanding its physiological function. With regard to neurodegenerative disease, elevated expression of αSyn has been reported in neurons under chronic oxidative stress *(Quilty et al., 2006)* and could therefore represent an indicator for neuron vulnerability. Neuron morphology and physiology are also believed to play an important role in the predisposition of specific cell types to neurodegeneration. Susceptible cells share two common properties. Firstly, they are projection neurons with disproportionally long and thin axons relative to the size of their somata *(Braak et al., 2003a)*. In contrast, local circuit neurons and projection neurons with short axons (such as the pyramidal neurons in layers 2 and 4) are more resistant *(Braak et al., 2004)*. Secondly, the long axon projections are typically

unmyelinated or poorly myelinated *(Braak et al., 2003b)*. Myelination potentially offers a neuroprotective function as the sheath thickness is directly proportional to axonal conduction speed. As a result, less energy is required for the transmission of impulses in neurons with myelinated axons *(Nieuwenhuys, 1998)*. The long projecting axons of TTL5 pyramidal neurons are unmyelinated in their primary collaterals and become progressively myelinated at the higher order axon branches *(Shu et al., 2007; Ramaswamy and Markram, 2015)*. These morphological properties, which are also found in DA neurons in the SNc, may put TTL5 pyramidal neurons at greater risk than other cortical layers in neurodegenerative diseases.

6.5 The pathological significance of oligomer-specific changes in electrophysiological properties

Increasing evidence points towards αSyn oligomers as being the most neurotoxic species. Therefore, it is possible that the significantly altered parameters observed for neurons perfused with oligomer, compared to neurons filled with vehicle (PBS) or monomer, may be the result oligomer toxicity. This allows one to theorise on the underlying mechanisms that would produce such electrophysiological changes and how they might affect physiological activity in a way that could elicit pathological symptoms.

Throughout the lifespan of rodents, for example, the input resistance of TTL5 neocortical neurons naturally decreases during maturation of the neocortex *(Zhu, 2000)*. This reduction is believed to be the result of increasing expression of ion channels that are open close to the resting membrane potential, such as I_H and other potassium conductances *(Zhu, 2000)*. As such, the insertion of αSyn oligomers into the membrane, forming pore complexes with reversal potentials close to -80 mV, or their activation of pre-existing potassium channels *(Mironov, 2015)* may add to the physiological age of the neocortex. This could explain the age dependence of many neurodegenerative disorders *(Niccoli and Partridge, 2012)* and why patients with familial mutations in αSyn experience early onset of symptoms *(Conway et al., 2000b)*.

A reduction in input resistance was accompanied by a change in excitation parameters that resulted in a lower firing rate for neurons filled with oligomer. In the microcircuit of the neocortex, TTL5 pyramidal neurons integrate signals from all neocortical layers

and are the primary output pathway for passing information to subcortical areas *(Romand et al., 2011; Ramaswamy and Markram, 2015)*. The loss of excitation specifically in these neurons would have a devastating impact on healthy cognitive function *(Winkler et al., 1995)*, emotional behaviour *(Hariri et al., 2000; Black et al., 2004)*, semantic memory *(Hodges and Patterson, 1995)* and sleep regulation *(Steriade et al., 2001)*. Disruption of all these processes, and many more, have all been characterised as secondary, non-motor symptoms for PD and other neurodegenerative disorders *(Chaudhuri et al., 2006)*.

6.6 Sleep regulation and αSyn

Sleep disturbances in PD have a reported prevalence ranging from 40 to 90 % *(Suzuki et al., 2011)*. The appearance of REM sleep behavioural disorder in early, presymptomatic stages of PD results from degeneration of the brainstem regulatory centres involved in sleep/wakefulness *(Boeve, 2010)*. However, other sleep disorders, involving slow-wave sleep, are commonly the result of impairments in thalamocortical activity *(Diederich and McIntyre, 2012)*. Slow-wave sleep duration naturally declines with age *(Doerr et al., 2010)* and is notably decreased in patients with PD *(Diederich et al., 2009)*; promoting symptoms of parasomnia. The onset of slow-wave sleep is characterised by low-frequency oscillations in neocortical neurons; rhythmically alternating between hyperpolarised (silent) and depolarised (active) phases *(Steriade et al., 1993; Contreras et al., 1996)*. These consistent fluctuations in membrane potential are accompanied by changes in input resistance; which effectively doubles during the hyperpolarising phase compared to the depolarising phase of slow-wave sleep *(Steriade et al., 2001)*. Furthermore, the input resistance of cortical neurons was found to be lowest during REM sleep and became highest in the waking state *(Steriade et al., 2001)*. Therefore, a pathological reduction in input resistance, as a result of αSyn oligomers, could potentially disrupt the pattern of slow-wave sleep and impede transitions between sleep and awake states.

6.7 Memory impairment and αSyn

At the end of oscillatory periods during slow-wave sleep, cortical neurons exhibit short-term, self-sustained activity that is believed to play an important role in declarative memory consolidation *(Steriade and Timofeev, 2003)*. The switching between silent and active states is mediated by an increase in firing rate in layer 5

neurons *(Timofeev et al., 2001; Chauvette et al., 2010)*. This physiological function may be affected by αSyn oligomer as neurons that are less able to regulate their firing rate might struggle to integrate memory during slow-wave sleep.

In addition to the neocortex, the hippocampus plays a principle role in the formation of memory and lesions in this area are implicated in neurodegenerative diseases as the source of amnesia and dementia *(Zolamorgan et al., 1986; Small et al., 2011)*. The hippocampus, therefore, has become the subject of many investigations into the electrophysiological effects of αSyn oligomers. Increasing evidence shows that synaptic transmission in hippocampal neurons is modulated by αSyn oligomers, which leads to a reduction in long-term potentiation (LTP) *(Diogenes et al., 2012; Martin et al., 2012)*. Both basal synaptic transmission and miniature synaptic currents were found to be enhanced by αSyn oligomers through a mechanism involving NMDA and AMPA receptor activation *(Huels et al., 2011; Diogenes et al., 2012)*. The activation of glutamatergic receptors by oligomeric αSyn is predicted to promote excitotoxicity by the accumulation of intracellular calcium in the postsynaptic terminal *(Danzer et al., 2007; Huels et al., 2011)*. Positive synaptic regulation through glutamatergic receptors has also been demonstrated for physiological levels of amyloid-β *(Puzzo et al., 2008; Abramov et al., 2009)*, although at abnormally high levels of amyloid-β synaptic transmission is markedly depressed along with LTP *(Palop and Mucke, 2010; Ripoli et al., 2014)*.

Overall, this suggests that pathological forms of αSyn (and amyloid-β) promote synaptic transmission and receptor activation but in doing so may weaken the effects of LTP. It is possible that the reduced input resistance observed for neurons filled with oligomers is the result of pre-existing or newly inserted ion channels opening in the membrane. However, which ion channels are involved and their effects on firing activity may be dependent on cell type and location in the brain. For example, cross-talk between αSyn and ATP-sensitive potassium channels has been reported previously in hippocampal cell cultures *(Mironov, 2015)*. On the other hand, the impairment of A-Type potassium channels by αSyn has led to an enhanced firing rate in dopaminergic SNc neurons *(Subramaniam et al., 2014)*.

While previous research shows that αSyn increases neuronal activity in the hippocampus and SNc, my findings suggest that neocortical neurons become less

active. It is possible, therefore, that the findings of oligomer toxicity in one brain region may not necessarily hold true for other regions. It is likely that αSyn has a varying effect in different brain regions; with the increased susceptibility of certain neurons contributing to the disease pathology.

6.8 Mitochondrial dysfunction and αSyn

The permeabilisation of membranes by annular oligomers has been associated with an influx of intracellular calcium *(Volles and Lansbury, 2002; Demuro et al., 2005; Furukawa et al., 2006; Danzer et al., 2007; Emmanouilidou et al., 2010)* that leads not only to post-synaptic dysfunction and excitotoxicity *(Danzer et al., 2007; Huels et al., 2011)* but would also contribute to mitochondrial-mediated cell death *(Henchcliffe and Beal, 2008; Vila et al., 2008; Nakamura, 2013; Chen et al., 2015)*. The pathological insertion of oligomers into lipid-raft domains within mitochondrial-associated ER membranes (MAM) has been linked to mitochondrial dysfunction *(Guardia-Laguarta et al., 2014)*. Furthermore, the accumulation of αSyn within mitochondria and its interaction with complex 1 activity leads to increased reactive oxygen species (ROS) production and mitophagy *(Devi et al., 2008; Chinta et al., 2010)*.

It is uncertain whether the toxicity effects of αSyn on mitochondria would present themselves through distinct electrophysiological changes. Nevertheless, the ATP regenerating system used for my whole-cell patch clamp recordings means that the changes in neuron parameters seen with intracellular oligomers were independent of a fall in ATP concentration.

6.9 Potential treatments of αSyn oligomers

There are newly emerging theories on treatment methods for αSyn that aim to disrupt the formation of annular oligomers and may also counter their neurotoxic effects. Several ligands that are known to bind to αSyn have been shown to form stable, non-toxic oligomers that are off pathway to fibril formation. The flavonoid baicalein, for example, inhibits oligomerisation of αSyn and amyloid-β and has also been shown to disaggregate existing fibrils *(Zhu et al., 2004; Jiang et al., 2010; Lu et al., 2011)*. The αSyn oligomers formed from baicalein are a compact globular species that do not permeabilise membranes as readily as annular oligomers *(Hong et al., 2008)*. Epigallocatechin gallate (EGCG), which has a structure similar to baicalein, is also

known to inhibit and disaggregate αSyn oligomers *(Bieschke et al., 2010; Caruana et al., 2011)*. EGCG binds to the C-terminal region of αSyn where it reduces membrane binding affinity *(Lorenzen et al., 2014b)*. These ligands present a possible treatment method for PD as they are able to prevent the formation of toxic, ring-like oligomers.

Another treatment method involves antibodies that have a structural epitope that is able to recognise oligomeric, but not monomeric or fibrillar, species. The A11 antibody used throughout this thesis has been shown previously to effectively target αSyn oligomers in membranes and inhibit their permeabilising activity *(Schmidt et al., 2012)*. The use of A11 antibodies might be able to reverse the electrophysiological effects of αSyn by blocking the conductance channels formed by pore-complex insertion. Animals that have been immunised with other antibodies, which target the C-terminal of αSyn, have shown attenuated neurodegeneration in PD-like models *(Masliah et al., 2011; Games et al., 2013; Games et al., 2014)* and are currently in phase 1 clinical trials (PRX002 – *Prothena/Roche*).

7 Conclusions and future research

7.1 Conclusions

Protein aggregation is a shared pathological trait for many neurodegenerative diseases. In synucleinopathies such as Parkinson's disease, multiple system atrophy and dementia with Lewy bodies, the accumulation of αSyn in specific regions of the brain remains a clinical hallmark for the stages of pathology. The molecular mechanism(s) through which αSyn aggregates and exerts its toxicity remains unknown. Increasing evidence, however, supports the hypothesis that oligomeric αSyn species, that are formed prior to the appearance of large amyloid fibrils, play a central role in the pathogenesis of disease. Fibrillar αSyn, the main component of Lewy bodies, is thought to play a neuroprotective role by removing potentially toxic soluble aggregates from the cytosol. The fragmentation of fibrils is believed to present an additional stage of the protein aggregation pathway in which smaller aggregates are released back into the cytosol where they enhance toxicity and act as seeds for new fibril formation.

In this thesis, I examined the occurrence of soluble oligomers during the *in vitro* aggregation of αSyn. In addition to purifying *mOligomers* formed during the early stages of aggregation, I found that *fOligomers* were a key component in the solubilised mixture recovered from fibril fragmentation. Despite their isolation from separate points on the aggregation pathway, the two oligomeric species were similar in size and shape, although structural analysis suggested that *fOligomers* may retain elements of the fibril structure that are not present in *mOligomers*.

A leading hypothesis for αSyn oligomer toxicity is through the formation of a pore complex in lipid membranes. This activity has been mainly ascribed to ring-like oligomers, similar to those presented in this work, that are able to produce changes in membrane conductance similar to leak channels. Therefore, understanding the electrophysiological impact of αSyn oligomers could not only further our understanding of their toxicity mechanism, but also reveal their impact upon the functional output of neurons and how this in turn translates into the pathological symptoms of disease. To this endeavour, I investigated the effects of αSyn oligomers on TTL5 pyramidal neurons. I used dynamic I-V curves and reliable mathematical models to examine the changes in neuronal parameters over time. My findings are

consistent with the theory of oligomer insertion or channel opening in the membrane. The fact that monomeric αSyn did not alter neuronal properties supports the mounting evidence that αSyn toxicity stems from a gain-of-function mechanism in the oligomer. However, it is uncertain whether the changes in neuronal properties are specific to the αSyn protein or to the annular structure of the oligomers. The characterisation of annular oligomers produced by other disease-linked proteins highlights the possibility that the electrophysiological changes observed for αSyn may apply to other proteins and indeed have relevance in other neurodegenerative diseases.

Overall, this thesis sought to better our understanding of the electrophysiological impact of structurally characterised αSyn oligomers in the neocortex. By acting on the input resistance and excitability of neurons, we see how oligomers exhibit their pathology on healthy cortical activity and may theorise how these effects give way to the plethora of non-motor symptoms associated with neurodegenerative diseases.

7.2 Future research

Investigating the toxicity-induced changes in electrophysiology for cortical neurons provides insight into the pathology surrounding cognitive impairments in PD. However, the underlying cause of motor dysfunction in PD is the specific loss of dopamine (DA) containing neurons in the substantia nigra pars compacta (SNc) region of the basal ganglia. The selective vulnerability of these neurons is believed to be the result of their combined morphological and physiological traits. In addition to their long, unmyelinated axonal projections, that are orders of magnitude larger than other neuronal types *(Pissadaki and Bolam, 2013)*, their perpetual DA metabolism produces an abnormal build-up of free radicals that puts greater strain on their energy costs *(Jenner et al., 1992; Bolam and Pissadaki, 2012; Hwang, 2013)*. Furthermore, the expression of αSyn in disease models has been shown to cause specific neurodegeneration in DA neurons of the SNc *(Winner et al., 2011)*. A useful extension of my research would be to characterise the electrophysiological impact of αSyn in these neurons to further elucidate their inherent susceptibility to degeneration. Preliminary work to this effect as already been carried out by myself with successful identification of and recording from DA neurons in the SNc (figure 7.1a). However, the prominent I_H current displayed by these neurons (figure 7.1b) is currently unaccounted for in the EIF models (figure 7.1c) which results in a poor prediction of

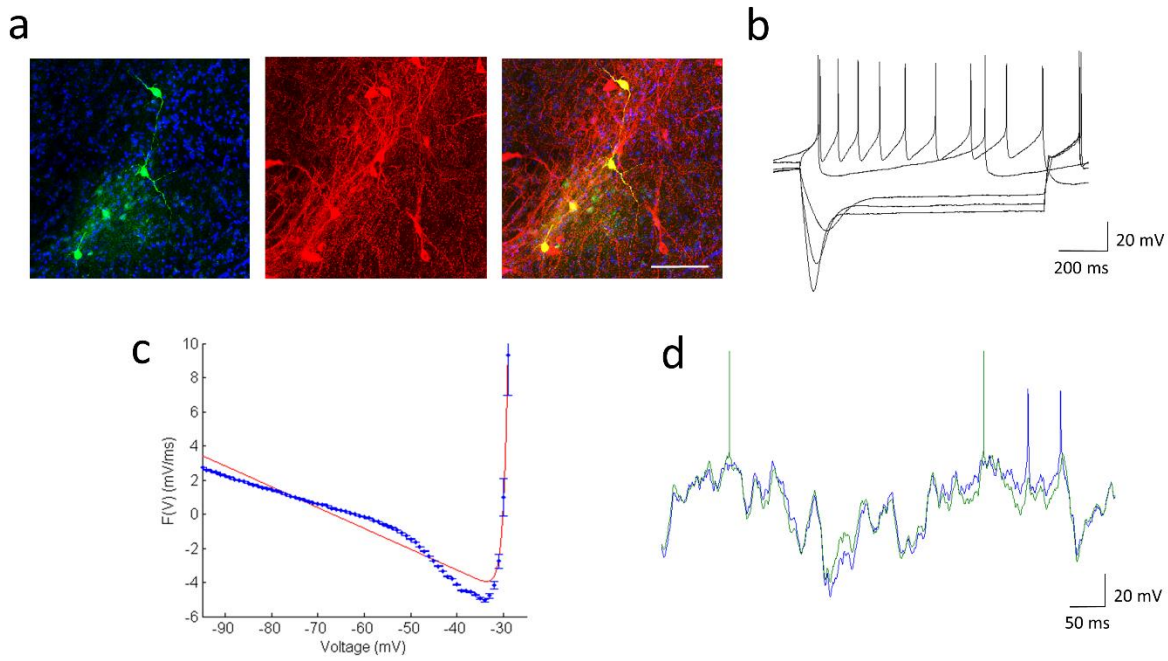

Figure 7.1 Dopaminergic neurons in the substantia nigra pars compacta (SNc) region show prominent I_H current that is unaccounted for in the EIF model. (a) Recorded neurons in the SNc were labelled with Alexa Fluor® 488 (green) and confirmed to be dopaminergic by staining for tyrosine hydroxylase (red); nuclei were stained with DAPI (blue) (scale bar = 100 µm). (b) The typical voltage response of DA SNc neurons to step currents (-300 to 100 pA in steps of 100 pA). Note the prominent I_H current with hyperpolarising step current and continuous firing pattern at rest. (c) The EIF fit (red line) to an inverted dynamic I-V curve (blue points) taken from the voltage response to naturalistic currents. The accentuated curvature of the dynamic I-V (as a result of I_H current) means that these neurons cannot be reliably parameterised by the EIF model. (d) Simulation of EIF parameters (green) does not accurately replicate the firing pattern from experimentally recorded DA SNc neurons (blue).

spike times (figure 7.1d). Therefore, a first step would be to develop the EIF model to account for the physiological properties of SNc neurons.

The structural characterisation of oligomeric αSyn species, shown in chapter 3, involved spectroscopy analysis of their size and secondary structure and imaging under transmission electron microscopy. To gain further insight into the structure of αSyn oligomers would require more powerful analytical tools such as nuclear magnetic resonance (NMR), atomic force microscopy (AFM), cryo-electron microscopy or X-ray crystallography. However, many of these techniques require highly purified and homogenous protein samples which may present a difficulty due to the range of oligomer sizes produced during aggregation. Heavy metal ions and cross-linking agents have been previously used to stabilise the oligomeric structure *(Dettmer et al., 2013)*, although such structures are likely to have altered properties from those formed in the absence of inducers *(Pountney et al., 2005)*. Low resolution

3D models of annular αSyn oligomers have been generated based on single angle X-ray scattering *(Giehm et al., 2011)* and NMR paramagnetic relaxation enhancement *(Bertoncini et al., 2005)*. It is possible therefore that these methods may be used in the future to provide more detail on the differences between *mOligomers* and *fOligomers*.

Both species of αSyn oligomer described in this thesis produced similar effects on neuronal parameters. The fact that monomeric αSyn did not produce the same effects as the oligomers indicates that unfolded and un-aggregated αSyn was not inherently toxic over this time course. However, these findings alone cannot confirm whether toxicity is a specific function of the αSyn protein or if it is derived from the generic ring-like conformation of the oligomer. Similar ring-like oligomers have been found for the amyloid-β peptide which suggests a shared mechanism for aggregation *(Lashuel et al., 2002a; Kayed et al., 2003)*. Amylin, a protein that differs from amyloid-β and αSyn in its primary sequence but shares the ability to oligomerise *(Lorenzo et al., 2000)*, has been used previously as a control to demonstrate the specific toxicity of amyloid-β oligomers *(Kimura et al., 2012; Ripoli et al., 2014)*. In addition, investigating whether the non-toxic αSyn oligomers induced by flavonoids are able to reverse the electrophysiological changes would strengthen the theory of oligomer toxicity. Thus, comparing the electrophysiological impact of other proteins that are able to form toxic or non-toxic oligomers would be important for conclusively assigning toxicity to αSyn but may also demonstrate a shared pathology for disease-associated proteins.

The methods detailed in chapter 4 provide a way for toxic αSyn oligomers to be directly injected into neurons for studying their intracellular effects. However, increasing evidence shows extracellular αSyn to have an important role in toxicity and the spreading of pathology *(Lee, 2008)*. Previous investigations have applied extracellular αSyn oligomers to brain slices and recorded changes in neuronal properties and synaptic transmission *(Huels et al., 2011; Diogenes et al., 2012; Martin et al., 2012)*. Importantly, the membrane interacting and permeabilising properties of αSyn have been found to be different when inserting from the extracellular side compared to the intracellular side *(Mironov, 2015)*. Extracellular oligomers were not used in this thesis as the amounts need for continuous circulation in aCSF were greater than those available from purification of *mOligomers* or *fOligomers*. However, the pre-incubation of brain slices or cell cultures in solutions containing oligomers,

followed by patch clamp recordings, could present a plausible approach as the amount of oligomer required would be more reasonable.

The elevated expression of αSyn found in layer 4 pyramidal neurons, compare to layer 5, may highlight the differences in their functional role within the neocortical microcircuit and could indicate differences in their susceptibility to disease. Investigating the electrophysiological effects of αSyn in layer 4 could provide an interesting contrast to layer 5 and may help us understand the role of endogenous αSyn in the neocortex. The electrophysiological impact of oligomers may be accentuated in cells expressing higher levels of endogenous αSyn and monomer-injected cells may also reveal a delayed onset of changes as they might be more likely to oligomerise intracellularly.

The work presented in this thesis shows that the electrophysiological impact of αSyn oligomers can be accurately captured within the parameters of EIF models. As such the altered electrophysiological properties of TTL5 neurons may be applied to previously established network models *(Harrison et al., 2015)* to investigate how αSyn toxicity may impact upon the dynamic connections within the neocortical microcircuit. The development of pathological models based on experimental data presents a useful, ethically viable approach to furthering our understanding of neurodegenerative diseases.

8 References

Abeliovich A, Schmitz Y, Farinas I, Choi-Lundberg D, Ho WH, Castillo PE, Shinsky N, Verdugo JMG, Armanini M, Ryan A, Hynes M, Phillips H, Sulzer D, Rosenthal A (2000) Mice lacking alpha-synuclein display functional deficits in the nigrostriatal dopamine system. Neuron 25:239-252.

Abramov E, Dolev I, Fogel H, Ciccotosto GD, Ruff E, Slutsky I (2009) Amyloid-beta as a positive endogenous regulator of release probability at hippocampal synapses. Nature Neuroscience 12:1567-U1120.

Albani D, Peverelli E, Rametta R, Batelli S, Veschini L, Negro A, Forloni G (2004) Protective effect of TAT-delivered alpha-synuclein: relevance of the C-terminal domain and involvement of HSP70. Faseb Journal 18:1713-+.

Alim MA, Ma QL, Takeda K, Aizawa T, Matsubara M, Nakamura M, Asada A, Saito T, Kaji H, Yoshii M, Hisanaga S, Ueda K (2004) Demonstration of a role for alpha-synuclein as a functional microtubule-associtated protein. Journal of Alzheimers Disease 6:435-442.

Apetri MM, Maiti NC, Zagorski MG, Carey PR, Anderson VE (2006) Secondary structure of alpha-synuclein oligomers: Characterization by Raman and atomic force microscopy. Journal of Molecular Biology 355:63-71.

Appel-Cresswell S, de la Fuente-Fernandez R, Galley S, McKeown MJ (2010) Imaging of compensatory mechanisms in Parkinson's disease. Current Opinion in Neurology 23:407-412.

Ariesandi W, Chang C-F, Chen T-E, Chen Y-R (2013) Temperature-Dependent Structural Changes of Parkinson's Alpha-Synuclein Reveal the Role of Pre-Existing Oligomers in Alpha-Synuclein Fibrillization. Plos One 8.

Armstrong RA, Lantos PL, Cairns NJ (2005) Multiple system atrophy: laminar distribution of the pathological changes in frontal and temporal neocortex - a study in ten patients. Clinical Neuropathology 24:230-235.

Auluck PK, Caraveo G, Lindquist S (2010) alpha-Synuclein: Membrane Interactions and Toxicity in Parkinson's Disease. Annual Review of Cell and Developmental Biology, Vol 26 26:211-233.

Auluck PK, Chan HYE, Trojanowski JQ, Lee VMY, Bonini NM (2002) Chaperone suppression of alpha-synuclein toxicity in a Drosophila model for Parkinson's disease. Science 295.

Baba M, Nakajo S, Tu PH, Tomita T, Nakaya K, Lee VMY, Trojanowski JQ, Iwatsubo T (1998) Aggregation of alpha-synuclein in Lewy bodies of sporadic Parkinson's disease and dementia with lewy bodies. American Journal of Pathology 152:879-884.

Badel L, Lefort S, Brette R, Petersen CCH, Gerstner W, Richardson MJE (2008) Dynamic I-V curves are reliable predictors of naturalistic pyramidal-neuron voltage traces. Journal of Neurophysiology 99:656-666.

Baltic S, Perovic M, Mladenovic A, Raicevic N, Ruzdijic S, Rakic L, Kanazir S (2004) alpha-synuclein is expressed in different tissues during human fetal development. Journal of Molecular Neuroscience 22:199-203.

Bartels T, Choi JG, Selkoe DJ (2011) alpha-Synuclein occurs physiologically as a helically folded tetramer that resists aggregation. Nature 477:107-U123.

Barz S, Hummel T, Pauli E, Majer M, Lang CJG, Kobal G (1997) Chemosensory event-related potentials in response to trigeminal and olfactory stimulation in idiopathic Parkinson's disease. Neurology 49:1424-1431.

Beraud D, Hathaway HA, Trecki J, Chasovskikh S, Johnson DA, Johnson JA, Federoff HJ, Shimoji M, Mhyre TR, Maguire-Zeiss KA (2013) Microglial Activation and Antioxidant Responses Induced by the Parkinson's Disease Protein alpha-Synuclein. Journal of Neuroimmune Pharmacology 8:94-117.

Bertler A, Rosengren E (1959) Occurrence and distribution of dopamine in brain and other tissues. Experientia 15:10-11.

Bertoncini CW, Jung YS, Fernandez CO, Hoyer W, Griesinger C, Jovin TM, Zweckstetter M (2005) Release of long-range tertiary interactions potentiates aggregation of natively unstructured alpha-synuclein. Proceedings of the National Academy of Sciences of the United States of America 102:1430-1435.

Betarbet R, Sherer TB, MacKenzie G, Garcia-Osuna M, Panov AV, Greenamyre JT (2000) Chronic systemic pesticide exposure reproduces features of Parkinson's disease. Nature Neuroscience 3:1301-1306.

Biere AL, Wood SJ, Wypych J, Steavenson S, Jiang YJ, Anafi D, Jacobsen FW, Jarosinski MA, Wu GM, Louis JC, Martin F, Narhi LO, Citron M (2000) Parkinson's disease-associated alpha-sylnuclein is more fibrillogenic than beta- and gamma-synuclein and cannot cross-seed its homologs. Journal of Biological Chemistry 275:34574-34579.

Bierer LM, Hof PR, Purohit DP, Carlin L, Schmeidler J, Davis KL, Perl DP (1995) Neocortical neurofibrillary tangles correlate with dementia severity in Alzheimer's disease. Archives of Neurology 52:81-88.

Bieschke J, Russ J, Friedrich RP, Ehrnhoefer DE, Wobst H, Neugebauer K, Wanker EE (2010) EGCG remodels mature alpha-synuclein and amyloid-beta fibrils and reduces cellular toxicity. Proceedings of the National Academy of Sciences of the United States of America 107:7710-7715.

Binolfi A, Rasia RM, Bertoncini CW, Ceolin M, Zweckstetter M, Griesinger C, Jovin TM, Fernandez CO (2006) Interaction of alpha-synuclein with divalent metal ions reveals key differences: A link between structure, binding specificity and fibrillation enhancement. Journal of the American Chemical Society 128.

Binolfi A, Lamberto GR, Duran R, Quintanar L, Bertoncini CW, Souza JM, Cervenansky C, Zweckstetter M, Griesinger C, Fernandez CO (2008) Site-specific interactions of Cu(II) with alpha and beta-synuclein: Bridging the molecular gap between metal binding and aggregation. Journal of the American Chemical Society 130:11801-11812.

Bisaglia M, Tessari I, Mammi S, Bubacco L (2009) Interaction Between alpha-Synuclein and Metal Ions, Still Looking for a Role in the Pathogenesis of Parkinson's Disease. Neuromolecular Medicine 11:239-251.

Bitan G, Lomakin A, Teplow DB (2001) Amyloid beta-protein oligomerization - Prenucleation interactions revealed by photo-induced cross-linking of unmodified proteins. Journal of Biological Chemistry 276:35176-35184.

Bjorkblom B, Adilbayeva A, Maple-Grodem J, Piston D, Okvist M, Xu XM, Brede C, Larsen JP, Moller SG (2013) Parkinson Disease Protein DJ-1 Binds Metals and Protects against Metal-induced Cytotoxicity. Journal of Biological Chemistry 288:22809-22820.

Black JE, Kodish IM, Grossman AW, Klintsova AY, Orlovskaya D, Vostrikov V, Uranova N, Greenough WT (2004) Pathology of layer v pyramidal neurons in the prefrontal cortex of patients with schizophrenia. American Journal of Psychiatry 161:742-744.

Boeve BF (2010) REM sleep behavior disorder Updated review of the core features, the REM sleep behavior disorder-neurodegenerative disease association, evolving concepts, controversies, and future directions. Year in Neurology 2 1184:15-54.

Bohnen NI, Albin RL (2011) The cholinergic system and Parkinson disease. Behavioural Brain Research 221:564-573.

Bolam JP, Pissadaki EK (2012) Living on the edge with too many mouths to feed: Why dopamine neurons die. Movement Disorders 27:1478-1483.

Bonifati V, Rizzu P, van Baren MJ, Schaap O, Breedveld GJ, Krieger E, Dekker MCJ, Squitieri F, Ibanez P, Joosse M, van Dongen JW, Vanacore N, van Swieten JC, Brice A, Meco G, van Duijn CM, Oostra BA, Heutink P (2003) Mutations in the DJ-1 gene associated with autosomal recessive early-onset parkinsonism. Science 299:256-259.

Braak H, Rub U, Gai WP, Del Tredici K (2003a) Idiopathic Parkinson's disease: possible routes by which vulnerable neuronal types may be subject to neuroinvasion by an unknown pathogen. Journal of Neural Transmission 110:517-536.

Braak H, Del Tredici K, Bohl J, Bratzke H, Braak E (2000) Pathological changes in the parahippocampal region in select non-Alzheimer's dementias. Parahippocampal Region: Implications for Neurological and Psychiatric Diseases 911:221-239.

Braak H, Ghebremedhin E, Rub U, Bratzke H, Del Tredici K (2004) Stages in the development of Parkinson's disease-related pathology. Cell and Tissue Research 318:121-134.

Braak H, Rub U, Steur E, Del Tredici K, de Vos RAI (2005) Cognitive status correlates with neuropathologic stage in Parkinson disease. Neurology 64:1404-1410.

Braak H, Del Tredici K, Bratzke H, Hamm-Clement J, Sandmann-Keil D, Rueb U (2002) Staging of the intracerebral inclusion body pathology associated with idiopathic Parkinson's disease (preclinical and clinical stages). Journal of Neurology 249:III.1-III.5.

Braak H, Del Tredici K, Rub U, de Vos RAI, Steur E, Braak E (2003b) Staging of brain pathology related to sporadic Parkinson's disease. Neurobiology of Aging 24:197-211.

Breydo L, Wu JW, Uversky VN (2012) α-Synuclein misfolding and Parkinson's disease. Biochimica et Biophysica Acta (BBA) - Molecular Basis of Disease 1822:261-285.

Brissaud É (1899) Leçons sur les maladies nerveuses: Masson.

Brown DR (2009) Metal binding to alpha-synuclein peptides and its contribution to toxicity. Biochemical and Biophysical Research Communications 380.

Brown DR (2010a) Metalloproteins and neuronal death. Metallomics 2:186-194.

Brown DR (2010b) Oligomeric Alpha-synuclein and Its Role in Neuronal Death. Iubmb Life 62:334-339.

Brown DR (2013) alpha-Synuclein as a ferrireductase. Biochemical Society Transactions 41:1513-1517.

Burkitt AN (2006a) A review of the integrate-and-fire neuron model: I. Homogeneous synaptic input. Biological Cybernetics 95:1-19.

Burkitt AN (2006b) A review of the integrate-and-fire neuron model: II. Inhomogeneous synaptic input and network properties. Biological Cybernetics 95:97-112.

Burre J, Sharma M, Tsetsenis T, Buchman V, Etherton MR, Suedhof TC (2010) alpha-Synuclein Promotes SNARE-Complex Assembly in Vivo and in Vitro. Science 329:1663-1667.

Bush AI (2000) Metals and neuroscience. Current Opinion in Chemical Biology 4.

Bussell R, Eliezer D (2003) A structural and functional role for 11-mer repeats in alpha-synuclein and other exchangeable lipid binding proteins. Journal of Molecular Biology 329:763-778.

Butterfield SM, Lashuel HA (2010) Amyloidogenic Protein Membrane Interactions: Mechanistic Insight from Model Systems. Angewandte Chemie-International Edition 49:5628-5654.

Cabin DE, Shimazu K, Murphy D, Cole NB, Gottschalk W, McIlwain KL, Orrison B, Chen A, Ellis CE, Paylor R, Lu B, Nussbaum RL (2002) Synaptic vesicle depletion correlates with attenuated synaptic responses to prolonged repetitive stimulation in mice lacking alpha-synuclein. Journal of Neuroscience 22:8797-8807.

Cali T, Ottolini D, Negro A, Brini M (2012) alpha-Synuclein Controls Mitochondrial Calcium Homeostasis by Enhancing Endoplasmic Reticulum-Mitochondria Interactions. Journal of Biological Chemistry 287:17914-17929.

Campioni S, Mannini B, Zampagni M, Pensalfini A, Parrini C, Evangelisti E, Relini A, Stefani M, Dobson CM, Cecchi C, Chiti F (2010) A causative link between the structure of aberrant protein oligomers and their toxicity. Nature Chemical Biology 6:140-147.

Cappai R, Leck SL, Tew DJ, Williamson NA, Smith DP, Galatis D, Sharples RA, Curtain CC, Ali FE, Cherny RA, Culvenor JG, Bottomley SP, Masters CL, Barnham KJ, Hill AF (2005) Dopamine promotes alpha-synuclein aggregation into SDS-resistant soluble oligomers via a distinct folding pathway. Faseb Journal 19:1377-+.

Carlsson A (1959) The occurrence, distribution and physiological role of catecholamines in the nervous system. Pharmacological reviews 11:490-493.

Carlsson A, Lindqvist M, Magnusson T (1957) 3,4-Dihydroxyphenylalanine and 5-hydroxytryptophan as reserpine antagonists. Nature 180:1200-1200.

Carlsson A, Lindqvist M, Magnusson T, Waldeck B (1958) On the presence of 3-hydroxytyramine in brain. Science (New York, NY) 127:471-471.

Caruana M, Hoegen T, Levin J, Hillmer A, Giese A, Vassallo N (2011) Inhibition and disaggregation of alpha-synuclein oligomers by natural polyphenolic compounds. Febs Letters 585:1113-1120.

Cauller L (1995) Layer I of primary sensory neocortex: Where top-down converges upon bottom-up. Behavioural Brain Research 71:163-170.

Cauller LJ, Connors BW (1994) Synaptic physiology of horizontal afferents to layer-I in slices of rat SI neocortex. Journal of Neuroscience 14:751-762.

Chandra S, Chen XC, Rizo J, Jahn R, Sudhof TC (2003) A broken alpha-helix in folded alpha-synuclein. Journal of Biological Chemistry 278:15313-15318.

Chandra S, Fornai F, Kwon HB, Yazdani U, Atasoy D, Liu XR, Hammer RE, Battaglia G, German DC, Castillo PE, Sudhof TC (2004) Double-knockout mice for alpha- and beta-synucleins: Effect on synaptic functions. Proceedings of the National Academy of Sciences of the United States of America 101:14966-14971.

Charcot J (1877) On Parkinson's disease. In *Lectures on diseases of the nervous system delivered at the Salpêtrière*. London: New Sydenham Society.

Chartier-Harlin MC, Kachergus J, Roumier C, Mouroux V, Douay X, Lincoln S, Levecque C, Larvor L, Andrieux J, Hulihan M, Waucquier N, Defebvre L, Amouyel P, Farrer M, Destee A (2004) alpha-synuclein locus duplication as a cause of familial Parkinson's disease. Lancet 364:1167-1169.

Chaudhuri KR, Yates L, Martinez-Martin P (2005) The non-motor symptom complex of Parkinson's disease: a comprehensive assessment is essential. Current neurology and neuroscience reports 5:275-283.

Chaudhuri KR, Healy DG, Schapira AHV (2006) Non-motor symptoms of Parkinson's disease: diagnosis and management. The Lancet Neurology 5:235-245.

Chauvette S, Volgushev M, Timofeev I (2010) Origin of Active States in Local Neocortical Networks during Slow Sleep Oscillation. Cerebral Cortex 20:2660-2674.

Checkoway H, Powers K, Smith-Weller T, Franklin GM, Longstreth WT, Swanson PD (2002) Parkinson's disease risks associated with cigarette smoking, alcohol consumption, and caffeine intake. American Journal of Epidemiology 155:732-738.

Chen C-C, Abrams S, Pinhas A, Brumerg JC (2009) Morphological Heterogeneity of Layer VI Neurons in Mouse Barrel Cortex. Journal of Comparative Neurology 512:726-746.

Chen L, Xie Z, Turkson S, Zhuang X (2015) A53T Human alpha-Synuclein Overexpression in Transgenic Mice Induces Pervasive Mitochondria Macroautophagy Defects Preceding Dopamine Neuron Degeneration. The Journal of neuroscience : the official journal of the Society for Neuroscience 35:890-905.

Chen PE, Specht CG, Morris RGM, Schoepfer R (2002) Spatial learning is unimpaired in mice containing a deletion of the alpha-synuclein locus. European Journal of Neuroscience 16:154-158.

Chen QX, Stelzer A, Kay AR, Wong RKS (1990) GABAA receptor function is regulated by phosphorylation in acutely dissociated guinea-pig hippocampal neurons. Journal of Physiology-London 420:207-221.

Chen XH, Desilva HAR, Pettenati MJ, Rao PN, Stgeorgehyslop P, Roses AD, Xia Y, Horsburgh K, Ueda K, Saitoh T (1995) The human NACP/alpha-synuclein gene - chromosome assignment to 4q21.3-q22 and TAQI RFLP analysis. Genomics 26:425-427.

Cherny D, Hoyer W, Subramaniam V, Jovin TM (2004) Double-stranded DNA stimulates the fibrillation of alpha-synuclein in vitro and is associated with the mature fibrils: An electron microscopy study. Journal of Molecular Biology 344:929-938.

Chinta SJ, Mallajosyula JK, Rane A, Andersen JK (2010) Mitochondrial alpha-synuclein accumulation impairs complex I function in dopaminergic neurons and results in increased mitophagy in vivo. Neuroscience Letters 486:235-239.

Choi B-K, Choi M-G, Kim J-Y, Yang Y, Lai Y, Kweon D-H, Lee NK, Shin Y-K (2013) Large alpha-synuclein oligomers inhibit neuronal SNARE-mediated vesicle docking. Proceedings of the National Academy of Sciences of the United States of America 110:4087-4092.

Choi W, Zibaee S, Jakes R, Serpell LC, Davletov B, Crowther RA, Goedert M (2004) Mutation E46K increases phospholipid binding and assembly into filaments of human alpha-synuclein. Febs Letters 576:363-368.

Clayton DF, George JM (1998) The synucleins: a family of proteins involved in synaptic function, plasticity, neurodegeneration and disease. Trends in Neurosciences 21:249-254.

Clayton DF, George JM (1999) Synucleins in synaptic plasticity and neurodegenerative disorders. Journal of Neuroscience Research 58:120-129.

Contreras D, Timofeev I, Steriade M (1996) Mechanisms of long lasting hyperpolarizations underlying slow sleep oscillations in cat corticothalamic networks. Journal of Physiology-London 494:251-264.

Conway KA, Harper JD, Lansbury PT (1998) Accelerated in vitro fibril formation by a mutant alpha-synuclein linked to early-onset Parkinson disease. Nature Medicine 4:1318-1320.

Conway KA, Harper JD, Lansbury PT (2000a) Fibrils formed in vitro from alpha-synuclein and two mutant forms linked to Parkinson's disease are typical amyloid. Biochemistry 39:2552-2563.

Conway KA, Lee SJ, Rochet JC, Ding TT, Williamson RE, Lansbury PT (2000b) Acceleration of oligomerization, not fibrillization, is a shared property of both alpha-synuclein mutations linked to early-onset Parkinson's disease: Implications for pathogenesis and therapy. Proceedings of the National Academy of Sciences of the United States of America 97:571-576.

Cotzias GC, Van Woert MH, Schiffer LM (1967) Aromatic amino acids and modification of parkinsonism. The New England journal of medicine 276:374-379.

Cotzias GC, Papavasiliou PS, Gellene R (1969) Modification of Parkinsonism chronic treatment with L-DOPA. New England Journal of Medicine 280:337-350.

Crowther RA, Jakes R, Spillantini MG, Goedert M (1998) Synthetic filaments assembled from C-terminally truncated alpha-synuclein. Febs Letters 436:309-312.

Dani VS, Nelson SB (2009) Intact Long-Term Potentiation but Reduced Connectivity between Neocortical Layer 5 Pyramidal Neurons in a Mouse Model of Rett Syndrome. Journal of Neuroscience 29:11263-11270.

Danzer KM, Krebs SK, Wolff M, Birk G, Hengerer B (2009) Seeding induced by alpha-synuclein oligomers provides evidence for spreading of alpha-synuclein pathology. Journal of Neurochemistry 111:192-203.

Danzer KM, Ruf WP, Putcha P, Joyner D, Hashimoto T, Glabe C, Hyman BT, McLean PJ (2011) Heat-shock protein 70 modulates toxic extracellular alpha-synuclein oligomers and rescues trans-synaptic toxicity. Faseb Journal 25.

Danzer KM, Haasen D, Karow AR, Moussaud S, Habeck M, Giese A, Kretzschmar H, Hengerer B, Kostka M (2007) Different species of alpha-synuclein oligomers induce calcium influx and seeding. Journal of Neuroscience 27:9220-9232.

Dauer W, Przedborski S (2003) Parkinson's disease: Mechanisms and models. Neuron 39:889-909.

Dauer W, Kholodilov N, Vila M, Trillat AC, Goodchild R, Larsen KE, Staal R, Tieu K, Schmitz Y, Yuan CA, Rocha M, Jackson-Lewis V, Hersch S, Sulzer D, Przedborski S, Burke R, Hen R (2002) Resistance of alpha-synuclein null mice to the parkinsonian neurotoxin MPTP. Proceedings of the National Academy of Sciences of the United States of America 99:14524-14529.

Davidson WS, Jonas A, Clayton DF, George JM (1998) Stabilization of alpha-synuclein secondary structure upon binding to synthetic membranes. Journal of Biological Chemistry 273:9443-9449.

Davies P, Moualla D, Brown DR (2011a) Alpha-Synuclein Is a Cellular Ferrireductase. Plos One 6.

Davies P, Wang XY, Sarell CJ, Drewett A, Marken F, Viles JH, Brown DR (2011b) The Synucleins Are a Family of Redox-Active Copper Binding Proteins. Biochemistry 50:37-47.

de Lau LML, Breteler MMB (2006) Epidemiology of Parkinson's disease. Lancet Neurology 5:525-535.

de Lau LML, Bornebroek M, Witteman JCM, Hofman A, Koudstaal PJ, Breteler MMB (2005) Dietary fatty acids and the risk of Parkinson disease - The Rotterdam study. Neurology 64:2040-2045.

Del Tredici K, Rub U, de Vos RAI, Bohl JRE, Braak H (2002) Where does Parkinson disease pathology begin in the brain? Journal of Neuropathology and Experimental Neurology 61:413-426.

DeLong MR, Wichmann T (2007) Circuits and circuit disorders of the basal ganglia. Archives of Neurology 64:20-24.

Demuro A, Mina E, Kayed R, Milton SC, Parker I, Glabe CG (2005) Calcium dysregulation and membrane disruption as a ubiquitous neurotoxic mechanism of soluble amyloid oligomers. Journal of Biological Chemistry 280.

Desplats P, Lee H-J, Bae E-J, Patrick C, Rockenstein E, Crews L, Spencer B, Masliah E, Lee S-J (2009) Inclusion formation and neuronal cell death through neuron-to-neuron transmission of alpha-synuclein. Proceedings of the National Academy of Sciences of the United States of America 106.

Dettmer U, Newman AJ, Luth ES, Bartels T, Selkoe D (2013) In Vivo Cross-linking Reveals Principally Oligomeric Forms of alpha-Synuclein and beta-Synuclein in Neurons and Non-neural Cells. Journal of Biological Chemistry 288:6371-6385.

Dettmer U, Newman AJ, Soldner F, Luth ES, Kim NC, von Saucken VE, Sanderson JB, Jaenisch R, Bartels T, Selkoe D (2015) Parkinson-causing alpha-synuclein missense mutations shift native tetramers to monomers as a mechanism for disease initiation. Nature Communications 6.

Devi L, Raghavendran V, Prabhu BM, Avadhani NG, Anandatheerthavarada HK (2008) Mitochondrial import and accumulation of alpha-synuclein impair complex I in human dopaminergic neuronal cultures and Parkinson disease brain. Journal of Biological Chemistry 283:9089-9100.

Dexter DT, Wells FR, Lees AJ, Agid F, Agid Y, Jenner P, Marsden CD (1989) Increased nigra iron content and alterations in other metal-ions occuring in brain in Parkinson's disease. Journal of Neurochemistry 52.

Dexter DT, Carayon A, Javoyagid F, Agid Y, Wells FR, Daniel SE, Lees AJ, Jenner P, Marsden CD (1991) Alterations in the levels of iron, ferritin and other trace-metals in Parkinson's disease and other neurodegenerative diseases affecting the basal ganglia. Brain 114.

Dickson DW, Ruan D, Crystal H, Mark MH, Davies P, Kress Y, Yen SH (1991) Hippocampal degeneration differentiates diffuse Lewy body disease (DLBD)from Alzheimer's disease - light and electron-microscopic immunocytochemistry of CA2-3 neurites specific to DLBD. Neurology 41:1402-1409.

Diederich NJ, McIntyre DJ (2012) Sleep disorders in Parkinson's disease: Many causes, few therapeutic options. Journal of the Neurological Sciences 314:12-19.

Diederich NJ, Paolini V, Vaillant M (2009) Slow wave sleep and dopaminergic treatment in Parkinson's disease: a polysomnographic study. Acta Neurologica Scandinavica 120:308-313.

Diogenes MJ, Dias RB, Rombo DM, Miranda HV, Maiolino F, Guerreiro P, Nasstrom T, Franquelim HG, Oliveira LMA, Castanho MARB, Lannfelt L, Bergstrom J, Ingelsson M, Quintas A, Sebastiao AM, Lopes LV, Outeiro TF (2012) Extracellular Alpha-Synuclein Oligomers Modulate Synaptic Transmission and Impair LTP Via NMDA-Receptor Activation. Journal of Neuroscience 32.

Divac I (1975) Magnocellular nuclei of basal forebrain project to neocortex, brain-stem, and olfactory bulb - review of some functional correlates. Brain Research 93:385-398.

Doerr JP, Hirscher V, Riemann D, Voderholzer U (2010) Disturbances of slow-wave sleep and psychiatric disorders. Nervenarzt 81:347-353.

Drolet RE, Behrouz B, Lookingland KJ, Goudreau JL (2004) Mice lacking alpha-synuclein have an attenuated loss of striatal dopamine following prolonged chronic MPTP administration. Neurotoxicology 25:761-769.

Dusa A, Kaylor J, Edridge S, Bodner N, Hong DP, Fink AL (2006) Characterization of oligomers during alpha-synuclein aggregation using intrinsic tryptophan fluorescence. Biochemistry 45:2752-2760.

Ehringer H, Hornykiewicz O (1960) Distribution of noradrenaline and dopamine (3-hydroxytyramine) in the human brain and their behavior in diseases of the extrapyramidal system. Klinische Wochenschrift 38:1236-1239.

El-Agnaf OMA, Salem SA, Paleologou KE, Curran MD, Gibson MJ, Court JA, Schlossmacher MG, Allsop D (2006) Detection of oligomeric forms of alpha-synuclein protein in human plasma as a potential biomarker for Parkinson's disease. Faseb Journal 20.

El-Agnaf OMA, Salem SA, Paleologou KE, Cooper LJ, Fullwood NJ, Gibson MJ, Curran MD, Court JA, Mann DMA, Ikeda S, Cookson MR, Hardy J, Allsop D (2003) alpha-synuclein implicated in Parkinson's disease is present in extracellular biological fluids, including human plasma. Faseb Journal 17:1945-+.

Eliezer D, Kutluay E, Bussell R, Browne G (2001) Conformational properties of alpha-synuclein in its free and lipid-associated states. Journal of Molecular Biology 307:1061-1073.

Emmanouilidou E, Melachroinou K, Roumeliotis T, Garbis SD, Ntzouni M, Margaritis LH, Stefanis L, Vekrellis K (2010) Cell-Produced alpha-Synuclein Is Secreted in a Calcium-Dependent Manner by Exosomes and Impacts Neuronal Survival. Journal of Neuroscience 30.

Engert F, Bonhoeffer T (1999) Dendritic spine changes associated with hippocampal long-term synaptic plasticity. Nature 399.

Eriksen N, Stark AK, Pakkenberg B (2009) Age and Parkinson's Disease-Related Neuronal Death in the Substantia Nigra Pars Compacta. Journal of Neural Transmission-Supplement:203-213.

Faendrich M (2012) Oligomeric Intermediates in Amyloid Formation: Structure Determination and Mechanisms of Toxicity. Journal of Molecular Biology 421:427-440.

Fahn S, Parkinson Study G (2005) Does levodopa slow or hasten the rate of progression of Parkinson's disease? Journal of Neurology 252:37-42.

Fauvet B, Mbefo MK, Fares M-B, Desobry C, Michael S, Ardah MT, Tsika E, Coune P, Prudent M, Lion N, Eliezer D, Moore DJ, Schneider B, Aebischer P, El-Agnaf OM, Masliah E, Lashuel HA (2012) alpha-Synuclein in Central Nervous System and from Erythrocytes, Mammalian Cells, and Escherichia coli Exists Predominantly as Disordered Monomer. The Journal of biological chemistry 287:15345-15364.

Feany MB, Bender WW (2000) A Drosophila model of Parkinson's disease. Nature 404.

Feldmeyer D, Lubke J, Silver RA, Sakmann B (2002) Synaptic connections between layer 4 spiny neurone-layer 2/3 pyramidal cell pairs in juvenile rat barrel cortex: physiology and anatomy of interlaminar signalling within a cortical column. Journal of Physiology-London 538:803-822.

Feng LR, Maguire-Zeiss KA (2011) Dopamine and Paraquat Enhance alpha-Synuclein-Induced Alterations in Membrane Conductance. Neurotoxicity Research 20.

Feng LR, Federoff HJ, Vicini S, Maguire-Zeiss KA (2010) alpha-Synuclein mediates alterations in membrane conductance: a potential role for alpha-synuclein oligomers in cell vulnerability. European Journal of Neuroscience 32:10-17.

Findley L, Aujla M, Bain PG, Baker M, Beech C, Bowman C, Holmes J, Kingdom WK, MacMahon DG, Peto V, Playfer JR (2003) Direct economic impact of Parkinson's disease: A research survey in the United Kingdom. Movement Disorders 18:1139-1145.

Fortin DL, Troyer MD, Nakamura K, Kubo S, Anthony MD, Edwards RH (2004) Lipid rafts mediate the synaptic localization of alpha-synuclein. Journal of Neuroscience 24:6715-6723.

Fourcaud-Trocme N, Hansel D, van Vreeswijk C, Brunel N (2003) How spike generation mechanisms determine the neuronal response to fluctuating inputs. Journal of Neuroscience 23:11628-11640.

Fredenburg RA, Rospigliosi C, Meray RK, Kessler JC, Lashuel HA, Eliezer D, Lansbury PT, Jr. (2007) The impact of the E46K mutation on the properties of alpha-synuclein in its monomeric and oligomeric states. Biochemistry 46:7107-7118.

Fuchs J, Nilsson C, Kachergus J, Munz M, Larsson EM, Schuele B, Langston JW, Middleton FA, Ross OA, Hulihan M, Gasser T, Farrer MJ (2007) Phenotypic variation in a large Swedish pedigree due to SNCA duplication and triplication. Neurology 68:916-922.

Furukawa K, Matsuzaki-Kobayashi M, Hasegawa T, Kikuchi A, Sugeno N, Itoyama Y, Wang Y, Yao PJ, Bushlin I, Takeda A (2006) Plasma membrane ion permeability induced by mutant alpha-synuclein contributes to the degeneration of neural cells. Journal of Neurochemistry 97.

Galvan A, Wichmann T (2008) Pathophysiology of parkinsonism. Clinical Neurophysiology 119:1459-1474.

Games D, Seubert P, Rockenstein E, Patrick C, Trejo M, Ubhi K, Ettle B, Ghassemiam M, Barbour R, Schenk D, Nuber S, Masliah E (2013) Axonopathy in an alpha-Synuclein Transgenic Model of Lewy Body Disease Is Associated with Extensive Accumulation of C-Terminal Truncated alpha-Synuclein. American Journal of Pathology 182:940-953.

Games D, Valera E, Spencer B, Rockenstein E, Mante M, Adame A, Patrick C, Ubhi K, Nuber S, Sacayon P, Zago W, Seubert P, Barbour R, Schenk D, Masliah E (2014) Reducing C-Terminal-Truncated Alpha-Synuclein by Immunotherapy Attenuates Neurodegeneration and Propagation in Parkinson's Disease-Like Models. Journal of Neuroscience 34:9441-9454.

Gasser T (2007) Update on the genetics of Parkinson's disease. Movement Disorders 22:S343-S350.

George JM (2002) The synucleins. Genome Biology 3:reviews3002.3001-reviews3002.3006.

George JM, Jin H, Woods WS, Clayton DF (1995) Characterization of a novel protein regulated during the cirtical period of song learning in zebra finch. Neuron 15:361-372.

Gerfen CR, Engber TM, Mahan LC, Susel Z, Chase TN, Monsma FJ, Sibley DR (1990) D1 and D2 dopamine receptor regulated gene-expression of striatonigral and striatopallidal neurons. Science 250:1429-1432.

Giasson BI, Murray IVJ, Trojanowski JQ, Lee VMY (2001) A hydrophobic stretch of 12 amino acid residues in the middle of alpha-synuclein is essential for filament assembly. Journal of Biological Chemistry 276:2380-2386.

Giasson BI, Forman MS, Higuchi M, Golbe LI, Graves CL, Kotzbauer PT, Trojanowski JQ, Lee VMY (2003) Initiation and synergistic fibrillization of tau and alpha-synuclein. Science 300:636-640.

Giehm L, Svergun DI, Otzen DE, Vestergaard B (2011) Low-resolution structure of a vesicle disrupting alpha-synuclein oligomer that accumulates during fibrillation. Proceedings of the National Academy of Sciences of the United States of America 108:3246-3251.

Glabe CG (2004) Conformation-dependent antibodies target diseases of protein misfolding. Trends in Biochemical Sciences 29:542-547.

Gluck MR, Youngster SK, Ramsay RR, Singer TP, Nicklas WJ (1994) Studies on the characterization of the inhibitory mechanism of 4'-alkylated 1-methyl-4-phenylpyridinium and phenylpyridine analogs in mitochondria and electron-transport particles. Journal of Neurochemistry 63:655-661.

Goers J, Uversky VN, Fink AL (2003a) Polycation-induced oligomerization and accelerated fibrillation of human alpha-synuclein in vitro. Protein Science 12:702-707.

Goers J, Manning-Bog AB, McCormack AL, Millett IS, Doniach S, Di Monte DA, Uversky VN, Fink AL (2003b) Nuclear localization of alpha-synuclein and its interaction with histones. Biochemistry 42:8465-8471.

Goetz CG, Stebbins GT (1993) Risk factors for nursing home placement in advanced Parkinson's disease. Neurology 43:2227-2229.

Golbe LI (1991) Young-onset Parkinson's disease - a clinical review. Neurology 41:168-173.

Gomez-Isla T, Growdon WB, McNamara M, Newell K, Gomez-Tortosa E, Hedley-Whyte ET, Hyman BT (1999) Clinicopathologic correlates in temporal cortex in dementia with Lewy bodies. Neurology 53:2003-2009.

Gomez-Tortosa E, Irizarry MC, Gomez-Isla T, Hyman BT (2000) Clinical and neuropathological correlates of dementia with Lewy bodies. Molecular Basis of Dementia 920:9-15.

Gomez-Tortosa E, Newell K, Irizarry MC, Albert M, Growdon JH, Hyman BT (1999) Clinical and quantitative pathologic correlates of dementia with Lewy bodies. Neurology 53:1284-1291.

Gorell JM, Rybicki BA, Johnson CC, Peterson EL (1999) Occupational metal exposures and the risk of Parkinson's disease. Neuroepidemiology 18.

Gosavi N, Lee HJ, Lee JS, Patel S, Lee SJ (2002) Golgi fragmentation occurs in the cells with prefibrillar alpha-synuclein aggregates and precedes the formation of fibrillar inclusion. Journal of Biological Chemistry 277:48984-48992.

Gowers WR (1888) *A Manual of Diseases of the Nervous System*. Philadelphia: Blakiston & Son.

Greenamyre JT, Hastings TG (2004) Parkinson's - Divergent causes, convergent mechanisms. Science 304:1120-1122.

Greenbaum EA, Graves CL, Mishizen-Eberz AJ, Lupoli MA, Lynch DR, Englander SW, Axelsen PH, Giasson BI (2005) The E46K mutation in alpha-synuclein increases amyloid fibril formation. Journal of Biological Chemistry 280:7800-7807.

Greenfield JG, Bosanquet FD (1953) The brain-stem lesions in Parkinsonism. Journal of neurology, neurosurgery, and psychiatry 16:213-226.

Greten-Harrison B, Polydoro M, Morimoto-Tomita M, Diao L, Williams AM, Nie EH, Makani S, Tian N, Castillo PE, Buchman VL, Chandra SS (2010) alpha beta gamma-Synuclein triple knockout mice reveal age-dependent neuronal dysfunction. Proceedings of the National Academy of Sciences of the United States of America 107:19573-19578.

Guardia-Laguarta C, Area-Gomez E, Rueb C, Liu Y, Magrane J, Becker D, Voos W, Schon EA, Przedborski S (2014) alpha-Synuclein Is Localized to Mitochondria-Associated ER Membranes. Journal of Neuroscience 34:249-259.

Gulati A, Alison F, Frauke S, Linda K, Chris C, Chaudhuri KR (2004) A clinical observational study of the pattern and occurrence of non-motor symptoms in Parkinson's disease ranging from early to advanced disease. Movement Disorders 19:S406-S406.

Gur M, Snodderly DM (2008) Physiological differences between neurons in layer 2 and layer 3 of primary visual cortex (V1) of alert macaque monkeys. Journal of Physiology-London 586:2293-2306.

Guttman M, Slaughter PM, Theriault ME, DeDoer DP, Naylor CD (2003) Burden of parkinsonism: A population-based study. Movement Disorders 18:313-319.

Haass C, Selkoe DJ (2007) Soluble protein oligomers in neurodegeneration: lessons from the Alzheimer's amyloid beta-peptide. Nature Reviews Molecular Cell Biology 8:101-112.

Haaxma CA, Bloem BR, Borm GF, Oyen WJG, Leenders KL, Eshuis S, Booij J, Dluzen DE, Horstink MWIM (2007) Gender differences in Parkinson's disease. Journal of Neurology Neurosurgery and Psychiatry 78:819-824.

Haehner A, Hummel T, Hummel C, Sommer U, Junghanns S, Reichmann H (2007) Olfactory loss may be a first sign of idiopathic Parkinson's disease. Movement Disorders 22:839-842.

Hallman H, Lange J, Olson L, Stromberg I, Jonsson G (1985) Neurochemical and histochemical characterization of neurotoxic effects of 1-methyl-4-phenyl-1,2,3,6-tetrahydropyridine on brain catecholamine neurons in the mouse. Journal of Neurochemistry 44:117-127.

Hansen C, Angot E, Bergstrom A-L, Steiner JA, Pieri L, Paul G, Outeiro TF, Melki R, Kallunki P, Fog K, Li J-Y, Brundin P (2011) alpha-Synuclein propagates from mouse brain to grafted dopaminergic neurons and seeds aggregation in cultured human cells. Journal of Clinical Investigation 121:715-725.

Hardy J (2006) No definitive evidence for a role for the environment in the etiology of Parkinson's disease. Movement Disorders 21:1790-1791.

Hardy J, Cookson MR, Singleton A (2003) Genes and parkinsonism. Lancet Neurology 2:221-228.

Hariri AR, Bookheimer SY, Mazziotta JC (2000) Modulating emotional responses: effects of a neocortical network on the limbic system. Neuroreport 11:43-48.

Harper JD, Lansbury PT (1997) Models of amyloid seeding in Alzheimier's disease and scrapie: Mechanistic truths and physiological consequences of the time-dependent solubility of amyloid proteins. Annual Review of Biochemistry 66:385-407.

Harris KD, Mrsic-Flogel TD (2013) Cortical connectivity and sensory coding. Nature 503:51-58.

Harrison PM, Badel L, Wall MJ, Richardson MJE (2015) Experimentally Verified Parameter Sets for Modelling Heterogeneous Neocortical Pyramidal-Cell Populations. PLoS Comput Biol 11:e1004165.

Hashimoto M, Yoshimoto M, Sisk A, Hsu LJ, Sundsmo M, Kittel A, Saitoh T, Miller A, Masliah E (1997) NACP, a synaptic protein involved in Alzheimer's disease, is differentially regulated during megakaryocyte differentiation. Biochemical and Biophysical Research Communications 237:611-616.

Hassler R (1938) The pathology of paralysis agitans and post-encephalitic Parkinson's. Journal Fur Psychologie Und Neurologie 48:387-476.

Hattox AM, Nelson SB (2007) Layer V neurons in mouse cortex projecting to different targets have distinct physiological properties. Journal of Neurophysiology 98:3330-3340.

Hay E, Schuermann F, Markram H, Segev I (2013) Preserving axosomatic spiking features despite diverse dendritic morphology. Journal of Neurophysiology 109:2972-2981.

Hay E, Hill S, Schuermann F, Markram H, Segev I (2011) Models of Neocortical Layer 5b Pyramidal Cells Capturing a Wide Range of Dendritic and Perisomatic Active Properties. Plos Computational Biology 7.

Heise H, Hoyer W, Becker S, Andronesi OC, Riedel D, Baldus M (2005) Molecular-level secondary structure, polymorphism, and dynamics of full-length alpha-synuclein fibrils studied by solid-state NMR. Proceedings of the National Academy of Sciences of the United States of America 102:15871-15876.

Hely MA, Morris JGL, Reid WGJ, Trafficante R (2005) Sydney multicenter study of Parkinson's disease: non-L-dopa-responsive problems dominate at 15 years. Movement Disorders 20:190-199.

Henchcliffe C, Beal MF (2008) Mitochondrial biology and oxidative stress in Parkinson disease pathogenesis. Nature Clinical Practice Neurology 4:600-609.

Hernan MA, Takkouche B, Caamano-Isorna F, Gestal-Otero JJ (2002) A meta-analysis of coffee drinking, cigarette smoking, and the risk of Parkinson's disease. Annals of Neurology 52:276-284.

Hernan MA, Chen HL, Schwarzschild MA, Ascherio A (2003) Alcohol consumption and the incidence of Parkinson's disease. Annals of Neurology 54:170-175.

Hindle JV (2010) Ageing, neurodegeneration and Parkinson's disease. Age and Ageing 39:156-161.

Hines ML, Carnevale NT (1997) The NEURON simulation environment. Neural Computation 9:1179-1209.

Hodges JR, Patterson K (1995) Is semantic memory consistently impaired early in the course of Alzheimer's disease neuroanatomical and diagnostic implications. Neuropsychologia 33:441-459.

Hodgkin AL, Huxley AF (1952a) Currents carried by sodium and potassium ions through the membrane of the giant axon of Loligo. The Journal of physiology 116:449-472.

Hodgkin AL, Huxley AF (1952b) A quantitative description of membrane current and its application to conduction and excitation in nerve. The Journal of physiology 117:500-544.

Hodgkin AL, Huxley AF (1952c) The components of membrane conductance in the giant axon of Loligo. The Journal of physiology 116:473-496.

Hodgkin AL, Huxley AF, Katz B (1952) Measurement of current-voltage relations in the membrane of the giant axon of Loligo. The Journal of physiology 116:424-448.

Hong D-P, Fink AL, Uversky VN (2008) Structural Characteristics of alpha-Synuclein Oligomers Stabilized by the Flavonoid Baicalein. Journal of Molecular Biology 383:214-223.

Hong D-P, Han S, Fink AL, Uversky VN (2011) Characterization of the Non-Fibrillar alpha-Synuclein Oligomers. Protein and Peptide Letters 18:230-240.

Hooks BM, Hires SA, Zhang Y-X, Huber D, Petreanu L, Svoboda K, Shepherd GMG (2011) Laminar Analysis of Excitatory Local Circuits in Vibrissal Motor and Sensory Cortical Areas. Plos Biology 9.

Hornykiewicz O (1963) The tropical localization and content of noradrenalin and dopamine (3-hydroxytyramine) in the substantia nigra of normal persons and patients with Parkinson's disease. Wiener klinische Wochenschrift 75:309-312.

Hoyer W, Antony T, Cherny D, Heim G, Jovin TM, Subramaniam V (2002) Dependence of alpha-synuclein aggregate morphology on solution conditions. Journal of Molecular Biology 322:383-393.

Hsu LJ, Sagara Y, Arroyo A, Rockenstein E, Sisk A, Mallory M, Wong J, Takenouchi T, Hashimoto M, Masliah E (2000) alpha-synuclein promotes mitochondrial deficit and oxidative stress. American Journal of Pathology 157:401-410.

Huels S, Hoegen T, Vassallo N, Danzer KM, Hengerer B, Giese A, Herms J (2011) AMPA-receptor-mediated excitatory synaptic transmission is enhanced by iron-induced alpha-synuclein oligomers. Journal of Neurochemistry 117:868-878.

Hurtig HI, Trojanowski JQ, Galvin J, Ewbank D, Schmidt ML, Lee VMY, Clark CM, Glosser G, Stern MB, Gollomp SM, Arnold SE (2000) Alpha-synuclein cortical Lewy bodies correlate with dementia in Parkinson's disease. Neurology 54:1916-1921.

Hwang O (2013) Role of oxidative stress in Parkinson's disease. Experimental neurobiology 22:11-17.

Ibanez P, Bonnet AM, Debarges B, Lohmann E, Tison F, Pollak P, Agid Y, Durr A, Brice A, French Parkinson's Disease G (2004) Causal relation between alpha-synuclein gene duplication and familial Parkinson's disease. Lancet 364:1169-1171.

Illes-Toth E, Dalton CF, Smith DP (2013) Binding of Dopamine to Alpha-Synuclein is Mediated by Specific Conformational States. Journal of the American Society for Mass Spectrometry 24:1346-1354.

Iwai A, Masliah E, Yoshimoto M, Ge NF, Flanagan L, Desilva HAR, Kittel A, Saitoh T (1995) The precursor protein of non-A-beta component of Alzheimer's disease amyloid is a presynaptic protein of the central nervous system. Neuron 14:467-475.

Jakes R, Spillantini MG, Goedert M (1994) Identification of 2 distinct synucleins from human brain. Febs Letters 345:27-32.

Jellinger KA (2008) A critical reappraisal of current staging of Lewy-related pathology in human brain. Acta Neuropathologica 116:1-16.

Jenner P, Dexter DT, Sian J, Schapira AHV, Marsden CD (1992) Oxidative stress as a cause of nigral cell-death in Parkinson's disease and incidental Lewy body disease. Annals of Neurology 32:S82-S87.

Jensen PH, Hager H, Nielsen MS, Hojrup P, Gliemann J, Jakes R (1999) alpha-synuclein binds to tau and stimulates the protein kinase A-catalyzed tau phosphorylation of serine residues 262 and 356. Journal of Biological Chemistry 274:25481-25489.

Jiang M, Porat-Shliom Y, Pei Z, Cheng Y, Xiang L, Sommers K, Li Q, Gillardon F, Hengerer B, Berlinicke C, Smith WW, Zack DJ, Poirier MA, Ross CA, Duan W (2010) Baicalein reduces E46K alpha-synuclein aggregation in vitro and protects cells against E46K alpha-synuclein toxicity in cell models of familiar Parkinsonism. Journal of Neurochemistry 114:419-429.

Jo EJ, McLaurin J, Yip CM, St George-Hyslop P, Fraser PE (2000) alpha-synuclein membrane interactions and lipid specificity. Journal of Biological Chemistry 275:34328-34334.

Junn E, Mouradian MM (2002) Human alpha-synuclein over-expression increases intracellular reactive oxygen species levels and susceptibility to dopamine. Neuroscience Letters 320:146-150.

Kampa BM, Letzkus JJ, Stuart GJ (2006) Cortical feed-forward networks for binding different streams of sensory information. Nature Neuroscience 9:1472-1473.

Kanda S, Bishop JF, Eglitis MA, Yang Y, Mouradian MM (2000) Enhanced vulnerability to oxidative stress by alpha-synuclein mutations and C-terminal truncation. Neuroscience 97:279-284.

Kasper EM, Larkman AU, Lubke J, Blakemore C (1994) Pyramidal neurons in layer 5 of the rat visual cortex .1. correlation among cell morphology, intrinsic electrophysiological properties, and axon targets. Journal of Comparative Neurology 339:459-474.

Katsuse O, Iseki E, Marui W, Kosaka K (2003) Developmental stages of cortical Lewy bodies and their relation to axonal transport blockage in brains of patients with dementia with Lewy bodies. Journal of the Neurological Sciences 211.

Kayed R, Head E, Thompson JL, McIntire TM, Milton SC, Cotman CW, Glabe CG (2003) Common structure of soluble amyloid oligomers implies common mechanism of pathogenesis. Science 300:486-489.

Keeler JF, Pretsell DO, Robbins TW (2014) Functional implications of dopamine D1 vs D2 receptors: a 'prepare and select' model of the striatal direct vs indirect pathways. Neuroscience 282:156-175.

Kessler JC, Rochet JC, Lansbury PT (2003) The N-terminal repeat domain of alpha-synuclein inhibits beta-sheet and amyloid fibril formation. Biochemistry 42:672-678.

Kim H-Y, Cho M-K, Kumar A, Maier E, Siebenhaar C, Becker S, Fernandez CO, Lashuel HA, Benz R, Lange A, Zweckstetter M (2009) Structural Properties of Pore-Forming Oligomers of alpha-Synuclein. Journal of the American Chemical Society 131:17482-17489.

Kim HJ, Chatani E, Goto Y, Paik SR (2007) Seed-dependent accelerated fibrillation of alpha-synuclein induced by periodic ultrasonication treatment. Journal of Microbiology and Biotechnology 17:2027-2032.

Kim J, Matney CJ, Blankenship A, Hestrin S, Brown SP (2014) Layer 6 Corticothalamic Neurons Activate a Cortical Output Layer, Layer 5a. Journal of Neuroscience 34:9656-9664.

Kim TD, Paik SR, Yang CH (2002) Structural and functional implications of C-terminal regions of alpha-synuclein. Biochemistry 41:13782-13790.

Kim TD, Paik SR, Yang CH, Kim J (2000) Structural changes in alpha-synuclein affect its chaperone-like activity in vitro. Protein Science 9:2489-2496.

Kimura R, MacTavish D, Yang J, Westaway D, Jhamandas JH (2012) Beta Amyloid-Induced Depression of Hippocampal Long-Term Potentiation Is Mediated through the Amylin Receptor. Journal of Neuroscience 32:17401-17406.

Kirik D, Rosenblad C, Burer C, Lundberg C, Johansen TE, Muzyczka N, Mandel RJ, Bjorklund A (2002) Parkinson-like neurodegeneration induced by targeted overexpression of alpha-synuclein in the nigrostriatal system. Journal of Neuroscience 22:2780-2791.

Kitada T, Asakawa S, Hattori N, Matsumine H, Yamamura Y, Minoshima S, Yokochi M, Mizuno Y, Shimizu N (1998) Mutations in the parkin gene cause autosomal recessive juvenile parkinsonism. Nature 392:605-608.

Ko LW, Mehta ND, Farrer M, Easson C, Hussey J, Yen S, Hardy J, Yen SHC (2000) Sensitization of neuronal cells to oxidative stress with mutated human alpha-synuclein. Journal of Neurochemistry 75:2546-2554.

Kokhan VS, Afanasyeva MA, Van'kin GI (2012) alpha-Synuclein knockout mice have cognitive impairments. Behavioural Brain Research 231:226-230.

Kozloski J, Hamzei-Sichani F, Yuste R (2001) Stereotyped position of local synaptic targets in neocortex. Science 293:868-872.

Kramer ML, Schulz-Schaeffer WJ (2007) Presynaptic alpha-synuclein aggregates, not Lewy bodies, cause neurodegeneration in dementia with Lewy bodies. In: J Neurosci, pp 1405-1410. United States.

Kruger R, Kuhn W, Muller T, Woitalla D, Graeber M, Kosel S, Przuntek H, Epplen JT, Schols L, Riess O (1998) Ala30Pro mutation in the gene encoding alpha-synuclein in Parkinson's disease. Nature Genetics 18:106-108.

Kuwahara T, Koyama A, Gengyo-Ando K, Masuda M, Kowa H, Tsunoda M, Mitani S, Iwatsubo T (2006) Familial Parkinson mutant alpha-synuclein causes dopamine neuron dysfunction in transgenic Caenorhabditis elegans. Journal of Biological Chemistry 281:334-340.

Lai BCL, Marion SA, Teschke K, Tsui JKC (2002) Occupational and environmental risk factors for Parkinson's disease. Parkinsonism & Related Disorders 8:297-309.

Langston JW, Ballard P, Tetrud JW, Irwin I (1983) Chronic parkinsonism in humans due to a product of meperidine analog synthesis. Science 219:979-980.

Larkman AU (1991) Dendritic morphology of pyramidal neurons of the visual cortex of the rat .1. branching patterns. Journal of Comparative Neurology 306:307-319.

Lashuel HA, Overk CR, Oueslati A, Masliah E (2013) The many faces of alpha-synuclein: from structure and toxicity to therapeutic target. Nature Reviews Neuroscience 14:38-48.

Lashuel HA, Hartley D, Petre BM, Walz T, Lansbury PT (2002a) Neurodegenerative disease - Amyloid pores from pathogenic mutations. Nature 418:291-291.

Lashuel HA, Petre BM, Wall J, Simon M, Nowak RJ, Walz T, Lansbury PT (2002b) alpha-synuclein, especially the Parkinson's disease-associated mutants, forms pore-like annular and tubular protofibrils. Journal of Molecular Biology 322:1089-1102.

Lee H-J, Suk J-E, Bae E-J, Lee S-J (2008a) Clearance and deposition of extracellular alpha-synuclein aggregates in microglia. Biochemical and Biophysical Research Communications 372.

Lee H-J, Suk J-E, Patrick C, Bae E-J, Cho J-H, Rho S, Hwang D, Masliah E, Lee S-J (2010) Direct Transfer of alpha-Synuclein from Neuron to Astroglia Causes

Inflammatory Responses in Synucleinopathies. Journal of Biological Chemistry 285.

Lee HJ, Choi C, Lee SJ (2002) Membrane-bound alpha-synuclein has a high aggregation propensity and the ability to seed the aggregation of the cytosolic form. Journal of Biological Chemistry 277:671-678.

Lee M, Hyun DH, Halliwell B, Jenner P (2001) Effect of the overexpression of wild-type or mutant alpha-synuclein on cell susceptibility to insult. Journal of Neurochemistry 76:998-1009.

Lee S-J (2008) Origins and effects of extracellular alpha-synuclein: Implications in Parkinson's disease. Journal of Molecular Neuroscience 34:17-22.

Lee S-J, Jeon H, Kandror KV (2008b) alpha-Synuclein is localized in a subpopulation of rat brain synaptic vesicles. Acta Neurobiologiae Experimentalis 68:509-515.

Lees AJ (2007) Unresolved issues relating to the shaking palsy on the celebration of James Parkinson's 250th birthday. Movement Disorders 22:S327-S334.

Lees AJ, Tolosa E, Olanow CW (2015) Four pioneers of L-dopa treatment: Arvid Carlsson, Oleh Hornykiewicz, George Cotzias, and Melvin Yahr. Movement Disorders 30:19-36.

Lehmensiek V, Tan EM, Schwarz J, Storch A (2002) Expression of mutant alpha-synucleins enhances dopamine transporter-mediated MPP+ toxicity in vitro. Neuroreport 13:1279-1283.

Lesage S, Anheim M, Letournel F, Bousset L, Honoré A, Rozas N, Pieri L, Madiona K, Dürr A, Melki R, Verny C, Brice A, for the French Parkinson's Disease Genetics Study G (2013) G51D α-synuclein mutation causes a novel Parkinsonian–pyramidal syndrome. Annals of Neurology 73:459-471.

Lewy FH (1912) Die Lehre vom Tonus und der Bewegung: Zugleich Systematische Untersuchungen Zur Klinik, Physiologie, Pathologie und Pathogenese der Paralysis Agitans: Julius Springer.

Li J, Uversky VN, Fink AL (2001) Effect of familial Parkinson's disease point mutations A30P and A53T on the structural properties, aggregation, and fibrillation of human alpha-synuclein. Biochemistry 40:11604-11613.

Li JY, Jensen PH, Dahlstrom A (2002) Differential localization of alpha-, beta- and gamma-synucleins in the rat CNS. Neuroscience 113:463-478.

Li NY, Ragheb K, Lawler G, Sturgist J, Rajwa B, Melendez JA, Robinson JP (2003) Mitochondrial complex I inhibitor rotenone induces apoptosis through enhancing mitochondrial reactive oxygen species production. Journal of Biological Chemistry 278:8516-8525.

Linazasoro G (2007) Classical Parkinson disease versus Parkinson complex - Reflections against staging and in favour of heterogeneity. European Journal of Neurology 14.

Lo Bianco C, Ridet JL, Schneider BL, Deglon N, Aebischer P (2002) alpha-Synucleinopathy and selective dopaminergic neuron loss in a rat lentiviral-based model of Parkinson's disease. Proceedings of the National Academy of Sciences of the United States of America 99.

Lorenzen N, Lemminger L, Pedersen JN, Nielsen SB, Otzen DE (2014a) The N-terminus of alpha-synuclein is essential for both monomeric and oligomeric interactions with membranes. Febs Letters 588:497-502.

Lorenzen N, Cohen SIA, Nielsen SB, Herling TW, Christiansen G, Dobson CM, Knowles TPJ, Otzen D (2012) Role of Elongation and Secondary Pathways in S6 Amyloid Fibril Growth. Biophysical Journal 102:2167-2175.

Lorenzen N, Nielsen SB, Yoshimura Y, Vad BS, Andersen CB, Betzer C, Kaspersen JD, Christiansen G, Pedersen JS, Jensen PH, Mulder FAA, Otzen DE (2014b) How Epigallocatechin Gallate Can Inhibit alpha-Synuclein Oligomer Toxicity in Vitro. Journal of Biological Chemistry 289:21299-21310.

Lorenzen N, Nielsen SB, Buell AK, Kaspersen JD, Arosio P, Vad BS, Paslawski W, Christiansen G, Valnickova-Hansen Z, Andreasen M, Enghild JJ, Pedersen JS, Dobson CM, Knowles TPJ, Otzen DE (2014c) The Role of Stable alpha-Synuclein Oligomers in the Molecular Events Underlying Amyloid Formation. Journal of the American Chemical Society 136:3859-3868.

Lorenzo A, Yuan ML, Zhang ZH, Paganetti PA, Sturchler-Pierrat C, Staufenbiel M, Mautino J, Sol Vigo F, Sommer B, Yankner BA (2000) Amyloid beta interacts with the amyloid precursor protein: a potential toxic mechanism in Alzheimer's disease. Nature Neuroscience 3:460-464.

Lotharius J, Brundin P (2002a) Pathogenesis of Parkinson's disease: Dopamine, vesicles and alpha-synuclein. Nature Reviews Neuroscience 3:932-942.

Lotharius J, Brundin P (2002b) Impaired dopamine storage resulting from alpha-synuclein mutations may contribute to the pathogenesis of Parkinson's disease. Human Molecular Genetics 11:2395-2407.

Lotharius J, Barg S, Wiekop P, Lundberg C, Raymon HK, Brundin P (2002) Effect of mutant alpha-synuclein on dopamine homeostasis in a new human mesencephalic cell line. Journal of Biological Chemistry 277:38884-38894.

Lowe R, Pountney DL, Jensen PH, Gai WP, Voelcker NH (2004) Calcium(II) selectively induces alpha-synuclein annular oligomers via interaction with the C-terminal domain. Protein Science 13:3245-3252.

Lu J-H, Ardah MT, Durairajan SSK, Liu L-F, Xie L-X, Fong W-FD, Hasan MY, Huang J-D, El-Agnaf OMA, Li M (2011) Baicalein Inhibits Formation of alpha-Synuclein Oligomers within Living Cells and Prevents A beta Peptide Fibrillation and Oligomerisation. Chembiochem 12:615-624.

Lyons KE, Hubble JP, Troster AI, Pahwa R, Koller WC (1998) Gender differences in Parkinson's disease. Clinical Neuropharmacology 21:118-121.

Maries E, Dass B, Collier TJ, Kordower JH, Steece-Collier K (2003) The role of [alpha]-synuclein in Parkinson's disease: insights from animal models. Nat Rev Neurosci 4:727-738.

Markram H (1997) A network of tufted layer 5 pyramidal neurons. Cerebral Cortex 7:523-533.

Maroteaux L, Campanelli JT, Scheller RH (1988) Synuclein - A neuron-specific protein localized to the nucleus and presynaptic nerve-terminal. Journal of Neuroscience 8:2804-2815.

Martin ZS, Neugebauer V, Dineley KT, Kayed R, Zhang W, Reese LC, Taglialatela G (2012) a-Synuclein oligomers oppose long-term potentiation and impair memory through a calcineurin-dependent mechanism: relevance to human synucleopathic diseases. Journal of Neurochemistry 120:440-452.

Masliah E, Rockenstein E, Veinbergs I, Mallory M, Hashimoto M, Takeda A, Sagara Y, Sisk A, Mucke L (2000) Dopaminergic loss and inclusion body formation in alpha-synuclein mice: Implications for neurodegenerative disorders. Science 287:1265-1269.

Masliah E, Rockenstein E, Mante M, Crews L, Spencer B, Adame A, Patrick C, Trejo M, Ubhi K, Rohn TT, Mueller-Steiner S, Seubert P, Barbour R, McConlogue L, Buttini M, Games D, Schenk D (2011) Passive Immunization Reduces Behavioral and Neuropathological Deficits in an Alpha-Synuclein Transgenic Model of Lewy Body Disease. Plos One 6.

Mattila PM, Rinne JO, Helenius H, Dickson DW, Roytta M (2000) Alpha-synuclein-immunoreactive cortical Lewy bodies are associated with cognitive impairment in Parkinson's disease. Acta Neuropathologica 100:285-290.

Mayeux R, Denaro J, Hemenegildo N, Marder K, Tang MX, Cote LJ, Stern Y (1992) A population based investigation of Parkinson's disease with and without dementia - relationship to age and gender. Archives of Neurology 49:492-497.

McNaught KSP, Olanow CW (2006) Protein aggregation in the pathogenesis of familial and sporadic Parkinson's disease. Neurobiology of Aging 27.

Milber JM, Noorigian JV, Morley JF, Petrovitch H, White L, Ross GW, Duda JE (2012) Lewy pathology is not the first sign of degeneration in vulnerable neurons in Parkinson disease. Neurology 79:2307-2314.

Mironov SL (2015) alpha-Synuclein forms non-selective cation channels and stimulates ATP-sensitive potassium channels in hippocampal neurons. Journal of Physiology-London 593:145-159.

Morens DM, Grandinetti A, Waslien CI, Park CB, Ross GW, White LR (1996) Case-control study of idiopathic Parkinson's disease and dietary vitamin E intake. Neurology 46:1270-1274.

Morgan DG, Finch CE (1988) Dopaminergic changes in the basal ganglia - a generalized phenomenon of aging in mammals. Annals of the New York Academy of Sciences 515:145-160.

Murayama M, Perez-Garci E, Luescher H-R, Larkum ME (2007) Fiberoptic system for recording dendritic calcium signals in layer 5 neocortical pyramidal cells in freely moving rats. Journal of Neurophysiology 98:1791-1805.

Murphy DD, Rueter SM, Trojanowski JQ, Lee VMY (2000) Synucleins are developmentally expressed, and alpha-synuclein regulates the size of the presynaptic vesicular pool in primary hippocampal neurons. Journal of Neuroscience 20:3214-3220.

Muthane UB, Swamy HS, Satishchandra P, Subhash MN, Rao S, Subbakrishna D (1994) Early-onset Parkinson's disease - are juvenile-onset and young-onset different. Movement Disorders 9:539-544.

Müller MLTM, Bohnen NI (2013) Cholinergic Dysfunction in Parkinson's Disease. Current neurology and neuroscience reports 13:377-377.

Nakamura K (2013) alpha-Synuclein and Mitochondria: Partners in Crime? Neurotherapeutics 10:391-399.

Narhi L, Wood SJ, Steavenson S, Jiang YJ, Wu GM, Anafi D, Kaufman SA, Martin F, Sitney K, Denis P, Louis JC, Wypych J, Biere AL, Citron M (1999) Both familial Parkinson's disease mutations accelerate alpha-synuclein aggregation. Journal of Biological Chemistry 274:9843-9846.

Nelson R, Sawaya MR, Balbirnie M, Madsen AO, Riekel C, Grothe R, Eisenberg D (2005) Structure of the cross-beta spine of amyloid-like fibrils. Nature 435:773-778.

Niccoli T, Partridge L (2012) Ageing as a Risk Factor for Disease. Current Biology 22:R741-R752.

Nicklas WJ, Youngster SK, Kindt MV, Heikkila RE (1987) MPTP, MPP+ and mitochondrial function. Life Sciences 40:721-729.

Nicola SM, Surmeier DT, Malenka RC (2000) Dopaminergic modulation of neuronal excitability in the striatum and nucleus accumbens. Annual Review of Neuroscience 23:185-215.

Nieuwenhuys R (1998) Structure and Organisation of Fibre Systems. In: The Central Nervous System of Vertebrates, pp 113-157: Springer Berlin Heidelberg.

Nikolaus S, Antke C, Mueller H-W (2009) In vivo imaging of synaptic function in the central nervous system I. Movement disorders and dementia. Behavioural Brain Research 204.

Oswald MJ, Tantirigama MLS, Sonntag I, Hughes SM, Empson RM (2013) Diversity of layer 5 projection neurons in the mouse motor cortex. Frontiers in Cellular Neuroscience 7.

Outeiro TF, Lindquist S (2003) Yeast cells provide insight into alpha-synuclein biology and pathobiology. Science 302:1772-1775.

Outeiro TF, Putcha P, Tetzlaff JE, Spoelgen R, Koker M, Carvalho F, Hyman BT, McLean PJ (2008) Formation of Toxic Oligomeric alpha-Synuclein Species in Living Cells. Plos One 3.

Pacheco CR, Morales CN, Ramírez AE, Muñoz FJ, Gallegos SS, Caviedes PA, Aguayo LG, Opazo CM (2015) Extracellular α-synuclein alters synaptic transmission in brain neurons by perforating the neuronal plasma membrane. Journal of Neurochemistry:n/a-n/a.

Paik SR, Shin HJ, Lee JH, Chang CS, Kim J (1999) Copper(II)-induced self-oligomerization of alpha-synuclein. Biochemical Journal 340:821-828.

Paleologou KE, Kragh CL, Mann DMA, Salem SA, Al-Shami R, Allsop D, Hassan AH, Jensen PH, El-Agnaf OMA (2009) Detection of elevated levels of soluble -synuclein oligomers in post-mortem brain extracts from patients with dementia with Lewy bodies. Brain 132.

Palop JJ, Mucke L (2010) Amyloid-beta-induced neuronal dysfunction in Alzheimer's disease: from synapses toward neural networks. Nature Neuroscience 13:812-818.

Park SS, Lee D (2006) Selective loss of dopaminergic neurons and formation of Lewy body-like aggregations in alpha-synuclein transgenic fly neuronal cultures. European Journal of Neuroscience 23:2908-2914.

Parkinson J (1817) An essay on the shaking palsy. London: Whittingham and Rowland for Sherwood, Needly and Jones.

Pearce JMS (1989) Armand Trousseau and Parkinson's disease. Journal of Neurology, Neurosurgery, and Psychiatry 52:274-274.

Perez RG, Waymire JC, Lin E, Liu JJ, Guo FL, Zigmond MJ (2002) A role for alpha-synuclein in the regulation of dopamine biosynthesis. Journal of Neuroscience 22:3090-3099.

Perrin RJ, Woods WS, Clayton DF, George JM (2000) Interaction of human alpha-synuclein and Parkinson's disease variants with phospholipids - Structural analysis using site-directed mutagenesis. Journal of Biological Chemistry 275:34393-34398.

Petreanu L, Gutnisky DA, Huber D, Xu N-l, O'Connor DH, Tian L, Looger L, Svoboda K (2012) Activity in motor-sensory projections reveals distributed coding in somatosensation. Nature 489:299-+.

Pfefferkorn CM, Lee JC (2010) Tryptophan Probes at the a-Synuclein and Membrane Interface. Journal of Physical Chemistry B 114:4615-4622.

Pham CLL, Cappai R (2013) The interplay between lipids and dopamine on alpha-synuclein oligomerization and membrane binding. Bioscience Reports 33:807-814.

Pissadaki EK, Bolam JP (2013) The energy cost of action potential propagation in dopamine neurons: clues to susceptibility in Parkinson's disease. Frontiers in Computational Neuroscience 7.

Piwkowska Z, Destexhe A, Bal T (2009) Associating living cells and computational models: an introduction to dynamic clamp principles and its applications. In: Dynamic-Clamp from principles to applications (Destexhe A, Bal T, eds), pp 1 - 30: Springer.

Poewe W (2008) Non-motor symptoms in Parkinson's disease. European Journal of Neurology 15:14-20.

Polymeropoulos MH, Lavedan C, Leroy E, Ide SE, Dehejia A, Dutra A, Pike B, Root H, Rubenstein J, Boyer R, Stenroos ES, Chandrasekharappa S, Athanassiadou A, Papapetropoulos T, Johnson WG, Lazzarini AM, Duvoisin RC, DiIorio G, Golbe LI, Nussbaum RL (1997) Mutation in the alpha-synuclein gene identified in families with Parkinson's disease. Science 276:2045-2047.

Porras G, Li Q, Bezard E (2012) Modeling Parkinson's Disease in Primates: The MPTP Model. Cold Spring Harbor perspectives in medicine 2:a009308.

Pospischil M, Toledo-Rodriguez M, Monier C, Piwkowska Z, Bal T, Fregnac Y, Markram H, Destexhe A (2008) Minimal Hodgkin-Huxley type models for different classes of cortical and thalamic neurons. Biological Cybernetics 99:427-441.

Pountney DL, Voelcker NH, Gai WP (2005) Annular alpha-synuclein oligomers are potentially toxic agents in alpha-synucleinopathy. Hypothesis. Neurotoxicity Research 7:59-67.

Prots I, Veber V, Brey S, Campioni S, Buder K, Riek R, Boehm KJ, Winner B (2013) alpha-Synuclein Oligomers Impair Neuronal Microtubule-Kinesin Interplay. Journal of Biological Chemistry 288:21742-21754.

Proukakis C, Dudzik CG, Brier T, MacKay DS, Cooper JM, Millhauser GL, Houlden H, Schapira AH (2013) A novel alpha-synuclein missense mutation in Parkinson's disease. Neurology 80:1062-1064.

Przedborski S, Jackson-Lewis V, Naini AB, Jakowec M, Petzinger G, Miller R, Akram M (2001) The parkinsonian toxin 1-methyl-4-phenyl-1,2,3,6-tetrahydropyridine (MPTP): a technical review of its utility and safety. Journal of Neurochemistry 76:1265-1274.

Puzzo D, Privitera L, Leznik E, Fa M, Staniszewski A, Palmeri A, Arancio O (2008) Picomolar Amyloid-beta Positively Modulates Synaptic Plasticity and Memory in Hippocampus. Journal of Neuroscience 28:14537-14545.

Quik M, Perez XA, Bordia T (2012) Nicotine as a potential neuroprotective agent for Parkinson's disease. Movement Disorders 27:947-957.

Quilty MC, King AE, Gai WP, Pountney DL, West AK, Vickers JC, Dickson TC (2006) Alpha-synuclein is upregulated in neurones in response to chronic oxidative stress and is associated with neuroprotection. Experimental Neurology 199:249-256.

Ramaswamy S, Markram H (2015) Anatomy and Physiology of the Thick-tufted Layer 5 Pyramidal Neuron. Frontiers in Cellular Neuroscience 9.

Ramaswamy S, Hill SL, King JG, Schuermann F, Wang Y, Markram H (2012) Intrinsic morphological diversity of thick-tufted layer 5 pyramidal neurons ensures robust and invariant properties of in silico synaptic connections. Journal of Physiology-London 590:737-752.

Rasia RM, Bertoncini CW, Marsh D, Hoyer W, Cherny D, Zweckstetter M, Griesinger C, Jovin TM, Fernandez CO (2005) Structural characterization of copper(II) binding to alpha-synuclein: Insights into the bioinorganic chemistry of Parkinson's disease. Proceedings of the National Academy of Sciences of the United States of America 102:4294-4299.

Reimann MW, Anastassiou CA, Perin R, Hill SL, Markram H, Koch C (2013) A Biophysically Detailed Model of Neocortical Local Field Potentials Predicts the Critical Role of Active Membrane Currents. Neuron 79:375-390.

Ripoli C, Cocco S, Li Puma DD, Piacentini R, Mastrodonato A, Scala F, Puzzo D, D'Ascenzo M, Grassi C (2014) Intracellular Accumulation of Amyloid-beta (A beta) Protein Plays a Major Role in A beta-Induced Alterations of Glutamatergic Synaptic Transmission and Plasticity. Journal of Neuroscience 34:12893-12903.

Roberts HL, Brown DR (2015) Seeking a mechanism for the toxicity of oligomeric alpha-synuclein. Biomolecules 5:282-305.

Romand S, Wang Y, Toledo-Rodriguez M, Markram H (2011) Morphological development of thick-tufted layer V pyramidal cells in the rat somatosensory cortex. Frontiers in Neuroanatomy 5.

Rosenmund C, Westbrook GL (1993) Rundown of N-methyl-D-aspartate channels during whole-cell recording in rat hippocampal neurons - role of Ca^{2+} and ATP. Journal of Physiology-London 470:705-729.

Rosensweig C, Ono K, Murakami K, Lowenstein DK, Bitan G, Teplow DB (2012) Preparation of Stable Amyloid beta-Protein Oligomers of Defined Assembly Order. Amyloid Proteins: Methods and Protocols, Second Edition 849:23-31.

Ross CA, Poirier MA (2004) Protein aggregation and neurodegenerative disease. Nature Medicine 10:S10-S17.

Ross GW, Petrovitch H, Abbott RD, Tanner CM, Popper J, Masaki K, Launer L, White LR (2008a) Association of olfactory dysfunction with risk for future Parkinson's disease. Annals of Neurology 63:167-173.

Ross OA, Braithwaite AT, Skipper LM, Kachergus J, Hulihan MM, Middleton FA, Nishioka K, Fuchs J, Gasser T, Maraganore DM, Adler CH, Larvor L, Chartier-Harlin M-C, Nilsson C, Langston JW, Gwinn K, Hattori N, Farrer MJ (2008b) Genomic investigation of alpha-synuclein multiplication and parkinsonism. Annals of Neurology 63:743-750.

Royer CA (2006) Probing protein folding and conformational transitions with fluorescence. Chemical Reviews 106:1769-1784.

Ruiz PJG (2004) Prehistory of Parkinson's disease. Neurologia 19:735-737.

Rybicki BA, Johnson CC, Uman J, Gorell JM (1993) Parkinson's disease mortality and the industrial use of heavy-metals in Michigan. Movement Disorders 8:87-92.

Saiki S, Sato S, Hattori N (2012) Molecular pathogenesis of Parkinson's disease: update. Journal of neurology, neurosurgery, and psychiatry 83:430-436.

Samii A, Nutt JG, Ransom BR (2004) Parkinson's disease. Lancet 363:1783-1793.

Sandberg A, Luheshi LM, Sollvander S, de Barros TP, Macao B, Knowles TPJ, Biverstal H, Lendel C, Ekholm-Petterson F, Dubnovitsky A, Lannfelt L, Dobson CM, Hard T (2010) Stabilization of neurotoxic Alzheimer amyloid-beta oligomers by protein engineering. Proceedings of the National Academy of Sciences of the United States of America 107:15595-15600.

Scherzer CR, Grass JA, Liao Z, Pepivani I, Zheng B, Eklund AC, Ney PA, Ng J, McGoldrick M, Mollenhauer B, Bresnick EH, Schlossmacher MG (2008) GATA transcription factors directly regulate the Parkinson's disease-linked gene alpha-synuclein. Proceedings of the National Academy of Sciences of the United States of America 105:10907-10912.

Schmidt F, Levin J, Kamp F, Kretzschmar H, Giese A, Boetzel K (2012) Single-Channel Electrophysiology Reveals a Distinct and Uniform Pore Complex Formed by alpha-Synuclein Oligomers in Lipid Membranes. Plos One 7.

Schulz-Schaeffer WJ (2010) The synaptic pathology of alpha-synuclein aggregation in dementia with Lewy bodies, Parkinson's disease and Parkinson's disease dementia. Acta Neuropathologica 120.

Schulz-Schaeffer WJ (2015) Is Cell Death Primary or Secondary in the Pathophysiology of Idiopathic Parkinson's Disease? Biomolecules 5:1467-1479.

Senior SL, Ninkina N, Deacon R, Bannerman D, Buchman VL, Cragg SJ, Wade-Martins R (2008) Increased striatal dopamine release and hyperdopaminergic-like behaviour in mice lacking both alpha-synuclein and gamma-synuclein. European Journal of Neuroscience 27:947-957.

Serpell LC, Berriman J, Jakes R, Goedert M, Crowther RA (2000) Fiber diffraction of synthetic alpha-synuclein filaments shows amyloid-like cross-beta conformation. Proceedings of the National Academy of Sciences of the United States of America 97:4897-4902.

Sharon R, Goldberg MS, Bar-Josef I, Betensky RA, Shen J, Selkoe DJ (2001) alpha-synuclein occurs in lipid-rich high molecular weight complexes, binds fatty acids, and shows homology to the fatty acid-binding proteins. Proceedings of the National Academy of Sciences of the United States of America 98:9110-9115.

Shepherd GMG (2009) Intracortical cartography in an agranular area. Frontiers in neuroscience 3:337-343.

Sherer TB, Betarbet R, Testa CM, Seo BB, Richardson JR, Kim JH, Miller GW, Yagi T, Matsuno-Yagi A, Greenamyre JT (2003) Mechanism of toxicity in rotenone models of Parkinson's disease. Journal of Neuroscience 23:10756-10764.

Sherman SM (2012) Thalamocortical interactions. Current Opinion in Neurobiology 22:575-579.

Shorter J, Lindquist S (2004) Hsp104 catalyzes formation and elimination of self-replicating Sup35 prion conformers. Science 304:1793-1797.

Shu Y, Duque A, Yu Y, Haider B, McCormick DA (2007) Properties of action-potential initiation in neocortical pyramidal cells: Evidence from whole cell axon recordings. Journal of Neurophysiology 97:746-760.

Shulman LM (2007) Gender differences in Parkinson's disease. Gender Medicine 4:8-18.

Silberberg G, Gupta A, Markram H (2002) Stereotypy in neocortical microcircuits. Trends in Neurosciences 25:227-230.

Silveira-Moriyama L, Petrie A, Williams DR, Evans A, Katzenschlager R, Barbosa ER, Lees AJ (2009) The Use of a Color Coded Probability Scale to Interpret Smell Tests in Suspected Parkinsonism. Movement Disorders 24:1144-1153.

Singleton AB et al. (2003) alpha-synuclein locus triplication causes Parkinson's disease. Science 302:841-841.

Small SA, Schobel SA, Buxton RB, Witter MP, Barnes CA (2011) A pathophysiological framework of hippocampal dysfunction in ageing and disease. Nature Reviews Neuroscience 12:585-601.

Smith CJ, Clarke AR, Chia WN, Irons LI, Atkinson T, Holbrook JJ (1991) Detection and characterization of intermediates in the folding of large proteins by the use of genetically inserted tryptophan probes. Biochemistry 30:1028-1036.

Smith Y, Wichmann T, Factor SA, DeLong MR (2012) Parkinson's Disease Therapeutics: New Developments and Challenges Since the Introduction of Levodopa. Neuropsychopharmacology 37:213-246.

Sommer U, Hummel T, Cormann K, Mueller A, Frasnelli J, Kropp J, Reichmann H (2004) Detection of presymptomatic Parkinson's disease: Combining smell tests, transcranial sonography, and SPECT. Movement Disorders 19:1196-1202.

Soto C (2003) Unfolding the role of protein misfolding in neurodegenerative diseases. Nature Reviews Neuroscience 4:49-60.

Souza JM, Giasson BI, Lee VMY, Ischiropoulos H (2000) Chaperone-like activity of synucleins. Febs Letters 474:116-119.

Spillantini MG, Crowther RA, Jakes R, Hasegawa M, Goedert M (1998) alpha-synuclein in filamentous inclusions of Lewy bodies from Parkinson's disease and dementia with Lewy bodies. Proceedings of the National Academy of Sciences of the United States of America 95:6469-6473.

Spillantini MG, Schmidt ML, Lee VMY, Trojanowski JQ, Jakes R, Goedert M (1997) alpha-synuclein in Lewy bodies. Nature 388:839-840.

Spinelli KJ, Taylor JK, Osterberg VR, Churchill MJ, Pollock E, Moore C, Meshul CK, Unni VK (2014) Presynaptic Alpha-Synuclein Aggregation in a Mouse Model of Parkinson's Disease. Journal of Neuroscience 34:2037-2050.

Sreerama N, Woody RW (1993) A self-consistent method for the analysis of protein secondary structure from circular dichroism. Analytical Biochemistry 209:32-44.

Steriade M, Timofeev I (2003) Neuronal plasticity in thalamocortical networks during sleep and waking oscillations. Neuron 37:563-576.

Steriade M, Nunez A, Amzica F (1993) A novel slow (less then 1 Hz) oscillation of neocortical neurons *in vivo* - depolarizing and hyperpolarizing components. Journal of Neuroscience 13:3252-3265.

Steriade M, Timofeev I, Grenier F (2001) Natural waking and sleep states: A view from inside neocortical neurons. Journal of Neurophysiology 85:1969-1985.

Stockl MT, Zijlstra N, Subramaniam V (2013) alpha-Synuclein oligomers: an amyloid pore? Insights into mechanisms of alpha-synuclein oligomer-lipid interactions. Molecular neurobiology 47:613-621.

Stuart GJ, Dodt HU, Sakmann B (1993) Patch-clamp recordings from the soma and dendrites of neurons in brain slices using infrared video microscopy. Pflugers Archiv-European Journal of Physiology 423:511-518.

Studier FW, Moffatt BA (1986) Use of bacteriophage-T7 RNA-polymerase to direct selective high level expression of cloned genes. Journal of Molecular Biology 189:113-130.

Subramaniam M, Althof D, Gispert S, Schwenk J, Auburger G, Kulik A, Fakler B, Roeper J (2014) Mutant alpha-Synuclein Enhances Firing Frequencies in

Dopamine Substantia Nigra Neurons by Oxidative Impairment of A-Type Potassium Channels. Journal of Neuroscience 34:13586-13599.

Sugiyama H, Hainfellner JA, Yoshimura M, Budka H (1994) Neocortical changes in Parkinson's disease, revisited. Clinical Neuropathology 13:55-59.

Surmeier DJ, Ding J, Day M, Wang Z, Shen W (2007) D1 and D2 dopamine-receptor modulation of striatal glutamatergic signaling in striatal medium spiny neurons. Trends in Neurosciences 30:228-235.

Suzuki K, Miyamoto M, Miyamoto T, Iwanami M, Hirata K (2011) Sleep disturbances associated with Parkinson's disease. Parkinson's disease 2011:219056-219056.

Swadlow HA (1989) Efferent neurons and suspected interneurons in S1 vibrissa cortex of the awake rabbit - receptive fields and axonal properties. Journal of Neurophysiology 62:288-308.

Swensen AM, Marder E (2000) Multiple peptides converge to activate the same voltage-dependent current in a central pattern-generating circuit. Journal of Neuroscience 20:6752-6759.

Szymusiak R (1995) Magnocellular nuclei of the basal forebrain - substrates of sleep and arousal regulation. Sleep 18:478-500.

Tai H-C, Schuman EM (2008) Ubiquitin, the proteasome and protein degradation in neuronal function and dysfunction. Nature Reviews Neuroscience 9:826-838.

Takahashi H, Sekino Y, Tanaka S, Mizui T, Kishi S, Shirao T (2003) Drebrin-dependent actin clustering in dendritic filopodia governs synaptic targeting of postsynaptic density-95 and dendritic spine morphogenesis. Journal of Neuroscience 23.

Tamo W, Imaizumi T, Tanji K, Yoshida H, Mori F, Yoshimoto M, Takahashi H, Fukuda I, Wakabayashi K, Satoh K (2002) Expression of alpha-synuclein, the precursor of non-amyloid beta component of Alzheimer's disease amyloid, in human cerebral blood vessels. Neuroscience Letters 326:5-8.

Tanaka M, Collins SR, Toyama BH, Weissman JS (2006) The physical basis of how prion conformations determine strain phenotypes. Nature 442:585-589.

Tanner CM (1989) The role of environmental toxins in the etiology of Parkinson's disease. Trends in Neurosciences 12:49-54.

Terry RD, Masliah E, Salmon DP, Butters N, Deteresa R, Hill R, Hansen LA, Katzman R (1991) Physical basis of cognitive alterations in Alzheimer's disease - synapse loss is the major correlate of cognitive impairment. Annals of Neurology 30:572-580.

Thayanidhi N, Helm JR, Nycz DC, Bentley M, Liang Y, Hay JC (2010) alpha-Synuclein Delays Endoplasmic Reticulum (ER)-to-Golgi Transport in Mammalian Cells by Antagonizing ER/Golgi SNAREs. Molecular Biology of the Cell 21:1850-1863.

Thomson AM (2010) Neocortical layer 6, a review. Frontiers in Neuroanatomy 4.

Thomson AM, Lamy C (2007) Functional maps of neocortical local circuitry. Frontiers in neuroscience 1:19-42.

Tieu K (2011) A guide to neurotoxic animal models of Parkinson's disease. Cold Spring Harbor perspectives in medicine 1:a009316.

Timofeev I, Grenier F, Steriade M (2001) Disfacilitation and active inhibition in the neocortex during the natural sleep-wake cycle: An intracellular study. Proceedings of the National Academy of Sciences of the United States of America 98:1924-1929.

Tosatto L, Andrighetti AO, Plotegher N, Antonini V, Tessari I, Ricci L, Bubacco L, Dalla Serra M (2012) Alpha-synuclein pore forming activity upon membrane association. Biochimica Et Biophysica Acta-Biomembranes 1818:2876-2883.

Trousseau A (1867) Lectures on Clinical Medicine, Delivered at the Hôtel-Dieu, Paris. The British Journal of Psychiatry 13:197-207.

Trétiakoff C (1919) Contribution à l'étude de l'anatomie pathologique du locus niger de Soemmering avec quelques déductions relatives à la pathogénie des troubles du tonus musculaire et de la maladie de Parkinson.

Tsigelny IF, Bar-On P, Sharikov Y, Crews L, Hashimoto M, Miller MA, Keller SH, Platoshyn O, Yuan JXJ, Masliah E (2007) Dynamics of alpha-synuclein aggregation and inhibition of pore-like oligomer development by beta-synuclein. Febs Journal 274.

Ueda K, Fukushima H, Masliah E, Xia Y, Iwai A, Yoshimoto M, Otero DAC, Kondo J, Ihara Y, Saitoh T (1993) Molecular cloning of cDNA encoding an unrecognized component of amyloid in Alzheimer's disease. Proceedings of the National Academy of Sciences of the United States of America 90:11282-11286.

Uhlenbeck GE, Ornstein LS (1930) On the Theory of the Brownian Motion. Physical Review 36:823-841.

Ulmer TS, Bax A, Cole NB, Nussbaum RL (2005) Structure and dynamics of micelle-bound human alpha-synuclein. Journal of Biological Chemistry 280:9595-9603.

Uversky VN (2010) Mysterious oligomerization of the amyloidogenic proteins. Febs Journal 277:2940-2953.

Uversky VN, Li J, Fink AL (2001a) Evidence for a partially folded intermediate in alpha-synuclein fibril formation. Journal of Biological Chemistry 276:10737-10744.

Uversky VN, Li J, Fink AL (2001b) Metal-triggered structural transformations, aggregation, and fibrillation of human alpha-synuclein - A possible molecular

link between Parkinson's disease and heavy metal exposure. Journal of Biological Chemistry 276:44284-44296.

Uversky VN, Lee HJ, Li J, Fink AL, Lee SJ (2001c) Stabilization of partially folded conformation during alpha-synuclein oligomerization in both purified and cytosolic preparations. Journal of Biological Chemistry 276:43495-43498.

Uversky VN, Cooper EM, Bower KS, Li J, Fink AL (2002) Accelerated alpha-synuclein fibrillation in crowded milieu. Febs Letters 515.

Valente EM et al. (2004) Hereditary early-onset Parkinson's disease caused by mutations in PINK1. Science 304:1158-1160.

Vamvaca K, Volles MJ, Lansbury PT, Jr. (2009) The First N-terminal Amino Acids of alpha-Synuclein Are Essential for alpha-Helical Structure Formation In Vitro and Membrane Binding in Yeast. Journal of Molecular Biology 389:413-424.

Van Den Eeden SK, Tanner CM, Bernstein AL, Fross RD, Leimpeter A, Bloch DA, Nelson LM (2003) Incidence of Parkinson's disease: Variation by age, gender, and Race/Ethnicity. American Journal of Epidemiology 157:1015-1022.

van Rooijen BD, Claessens MMAE, Subramaniam V (2009a) Lipid bilayer disruption by oligomeric alpha-synuclein depends on bilayer charge and accessibility of the hydrophobic core. Biochimica Et Biophysica Acta-Biomembranes 1788:1271-1278.

van Rooijen BD, van Leijenhorst-Groener KA, Claessens MMAE, Subramaniam V (2009b) Tryptophan Fluorescence Reveals Structural Features of alpha-Synuclein Oligomers. Journal of Molecular Biology 394:826-833.

Vila M, Ramonet D, Perier C (2008) Mitochondrial alterations in Parkinson's disease: new clues. Journal of Neurochemistry 107:317-328.

Vivacqua G, Casini A, Vaccaro R, Fornai F, Yu S, D'Este L (2011) Different sub-cellular localization of alpha-synuclein in the C57BL\6J mouse's central nervous system by two novel monoclonal antibodies. Journal of Chemical Neuroanatomy 41:97-110.

Volles MJ, Lansbury PT (2002) Vesicle permeabilization by protofibrillar alpha-synuclein is sensitive to Parkinson's disease-linked mutations and occurs by a pore-like mechanism. Biochemistry 41.

Volles MJ, Lee SJ, Rochet JC, Shtilerman MD, Ding TT, Kessler JC, Lansbury PT (2001) Vesicle permeabilization by protofibrillar alpha-synuclein: Implications for the pathogenesis and treatment of Parkinson's disease. Biochemistry 40:7812-7819.

Wakabayashi K, Tanji K, Mori F, Takahashi H (2007) The Lewy body in Parkinson's disease: Molecules implicated in the formation and degradation of alpha-synuclein aggregates. Neuropathology 27:494-506.

Wallace BA, Lees JG, Orry AJW, Lobley A, Janes RW (2003) Analyses of circular dichroism spectra of membrane proteins. Protein Science 12:875-884.

Wang W, Perovic I, Chittuluru J, Kaganovich A, Nguyen LTT, Liao J, Auclair JR, Johnson D, Landeru A, Simorellis AK, Ju S, Cookson MR, Asturias FJ, Agar JN, Webb BN, Kang C, Ringe D, Petsko GA, Pochapsky TC, Hoang QQ (2011a) A soluble alpha-synuclein construct forms a dynamic tetramer. Proceedings of the National Academy of Sciences of the United States of America 108:17797-17802.

Wang X, Moualla D, Wright JA, Brown DR (2010) Copper binding regulates intracellular alpha-synuclein localisation, aggregation and toxicity. Journal of Neurochemistry 113:704-714.

Wang XJ, Buzsaki G (1996) Gamma oscillation by synaptic inhibition in a hippocampal interneuronal network model. Journal of Neuroscience 16:6402-6413.

Wang Y-Q, Buell AK, Wang X-Y, Welland ME, Dobson CM, Knowles TPJ, Perrett S (2011b) Relationship between Prion Propensity and the Rates of Individual Molecular Steps of Fibril Assembly. Journal of Biological Chemistry 286.

Wang ZF, Kai L, Day M, Ronesi J, Yin HH, Ding J, Tkatch T, Lovinger DM, Surmeier DJ (2006) Dopaminergic control of corticostriatal long-term synaptic depression in medium spiny neurons is mediated by cholinergic interneurons. Neuron 50:443-452.

Watakabe A, Hirokawa J, Ichinohe N, Ohsawa S, Kaneko T, Rockland KS, Yamamori T (2012) Area-specific substratification of deep layer neurons in the rat cortex. Journal of Comparative Neurology 520:3553-3573.

Weinreb PH, Zhen WG, Poon AW, Conway KA, Lansbury PT (1996) NACP, a protein implicated in Alzheimer's disease and learning, is natively unfolded. Biochemistry 35:13709-13715.

Weisman D, Cho M, Taylor C, Adame A, Thal LJ, Hansen LA (2007) In dementia with Lewy bodies, Braak stage determines phenotype, not Lewy body distribution. Neurology 69:356-359.

Whitmore L, Wallace BA (2004) DICHROWEB, an online server for protein secondary structure analyses from circular dichroism spectroscopic data. Nucleic Acids Research 32:W668-W673.

Whitmore L, Wallace BA (2008) Protein secondary structure analyses from circular dichroism spectroscopy: Methods and reference databases. Biopolymers 89:392-400.

Wingfield P (2001) Protein precipitation using ammonium sulfate. Current protocols in protein science / editorial board, John E Coligan [et al] Appendix 3:3F-Appendix 3F.

Winkler J, Suhr ST, Gage FH, Thal LJ, Fisher LJ (1995) Essential role of neocortical acetylcholine in spatial memory. Nature 375:484-487.

Winner B, Jappelli R, Maji SK, Desplats PA, Boyer L, Aigner S, Hetzer C, Loher T, Vilar M, Campionic S, Tzitzilonis C, Soragni A, Jessberger S, Mira H, Consiglio A, Pham E, Masliah E, Gage FH, Riek R (2011) In vivo demonstration that alpha-synuclein oligomers are toxic. Proceedings of the National Academy of Sciences of the United States of America 108:4194-4199.

Withers GS, George JM, Banker GA, Clayton DF (1997) Delayed localization of synelfin (synuclein, NACP) to presynaptic terminals in cultured rat hippocampal neurons. Developmental Brain Research 99:87-94.

Wood SJ, Wypych J, Steavenson S, Louis JC, Citron M, Biere AL (1999) alpha-synuclein fibrillogenesis is nucleation-dependent - Implications for the pathogenesis of Parkinson's disease. Journal of Biological Chemistry 274:19509-19512.

Wright JA, Wang X, Brown DR (2009) Unique copper-induced oligomers mediate alpha-synuclein toxicity. Faseb Journal 23:2384-2393.

Wu Y, Le W, Jankovic J (2011) Preclinical Biomarkers of Parkinson Disease. Archives of Neurology 68:22-30.

Xilouri M, Brekk OR, Stefanis L (2013) Alpha-synuclein and Protein Degradation Systems: a Reciprocal Relationship. Molecular Neurobiology 47:537-551.

Xu J, Kao SY, Lee FJS, Song WH, Jin LW, Yankner BA (2002) Dopamine-dependent neurotoxicity of alpha-synuclein: A mechanism for selective neurodegeneration in Parkinson disease. Nature Medicine 8:600-606.

Xue W-F, Hellewell AL, Hewitt EW, Radford SE (2010) Fibril fragmentation in amyloid assembly and cytotoxicity When size matters. Prion 4:20-25.

Xue W-F, Hellewell AL, Gosal WS, Homans SW, Hewitt EW, Radford SE (2009) Fibril Fragmentation Enhances Amyloid Cytotoxicity. Journal of Biological Chemistry 284:34272-34282.

Yagi H, Kusaka E, Hongo K, Mizobata T, Kawata Y (2005) Amyloid fibril formation of alpha-synuclein is accelerated by preformed amyloid seeds of other proteins - Implications for the mechanism of transmissible conformational diseases. Journal of Biological Chemistry 280:38609-38616.

Yahr MD, Duvoisin RC, Schear MJ, Barrett RE, Hoehn MM (1969) Treatment of parkinsonism with levodopa. Archives of neurology 21:343-354.

Yoshiike Y, Kayed R, Milton SC, Takashima A, Glabe CG (2007) Pore-forming proteins share structural and functional homology with amyloid oligomers. Neuromolecular Medicine 9:270-275.

Yu S, Li X, Liu G, Han J, Zhang C, Li Y, Xu S, Liu C, Gao Y, Yang H, Ueda K, Chan P (2007) Extensive nuclear localization of alpha-synuclein in normal rat brain neurons revealed by a novel monoclonal antibody. Neuroscience 145:539-555.

Yu Y, Hill AP, McCormick DA (2012) Warm Body Temperature Facilitates Energy Efficient Cortical Action Potentials. Plos Computational Biology 8.

Zaja-Milatovic S, Keene CD, Montine KS, Leverenz JB, Tsuang D, Montine TJ (2006) Selective dendritic degeneration of medium spiny neurons in dementia with Lewy bodies. Neurology 66.

Zaja-Milatovic S, Milatovic D, Schantz AM, Zhang J, Montine KS, Samii A, Deutch AY, Montine TJ (2005) Dendritic degeneration in neostriatal medium spiny neurons in Parkinson disease. Neurology 64.

Zarranz JJ, Alegre J, Gomez-Esteban JC, Lezcano E, Ros R, Ampuero I, Vidal L, Hoenicka J, Rodriguez O, Atares B, Llorens V, Tortosa EG, del Ser T, Munoz DG, de Yebenes JG (2004) The new mutation, E46K, of alpha-synuclein causes Parkinson and Lewy body dementia. Annals of Neurology 55:164-173.

Zhang H, Griggs A, Rochet J-C, Stanciu LA (2013) In Vitro Study of alpha-Synuclein Protofibrils by Cryo-EM Suggests a Cu2+-Dependent Aggregation Pathway. Biophysical Journal 104:2706-2713.

Zhang SM, Hernan MA, Chen H, Spiegelman D, Willett WC, Ascherio A (2002) Intakes of vitamins E and C, carotenoids, vitamin supplements, and PD risk. Neurology 59:1161-1169.

Zhu JJ (2000) Maturation of layer 5 neocortical pyramidal neurons: amplifying salient layer 1 and layer 4 inputs by Ca2+ action potentials in adult rat tuft dendrites. Journal of Physiology-London 526:571-587.

Zhu M, Rajamani S, Kaylor J, Han S, Zhou FM, Fink AL (2004) The flavonoid baicalein inhibits fibrillation of alpha-synuclein and disaggregates existing fibrils. Journal of Biological Chemistry 279:26846-26857.

Zimprich A et al. (2004) Mutations in LRRK2 cause autosomal-dominant Parkinsonism with pleomorphic pathology. Neuron 44:601-607.

Zolamorgan S, Squire LR, Amaral DG (1986) Human amnesia and the medial temporal region - enduring memory impairment following a bilateral lesion limited to field CA1 of the hippocampus. Journal of Neuroscience 6:2950-2967.